The potential of QEMSCAN in predicting washability of Mpumalanga coals

Shinelka Singh

10270842

Masters in Geology – GLY890

15th December 2015

Department of Geology

University of Pretoria

ABSTRACT

Traditional float and sink analyses are undertaken to determine the washability of coal. Float and sink analyses are costly, require toxic heavy organic liquids and the procedure to wash and dry the float and discard fractions is lengthy. QEMSCAN has the ability to characterise particle density based on the mineralogical composition of the particle. The objective of this research is to determine if QEMSCAN is a viable alternative to float and sink analysis. Float and sink analysis typically requires coarse size fractions while QEMSCAN analysis requires samples to be crushed down to 1mm. Any crushing will liberate minerals, which will alter the particle density distribution. Crushing a large particle generates 'puzzle pieces' of the original particle. The smaller 'puzzle pieces' have densities frequently different to the original particle. A mineralogical based particle density prediction model confirms that the float and sink analysis data used in this study is valid. The measured ash contents for the different float and discard fractions were within the expected limits. It is observed that there are a set of controls over the liberation of particles when crushed. Particles in the low float fractions (<1.6g/cm^3) predominantly comprise vitrinite rich coal with fine lamellae of kaolinite. The higher float fractions (>1.6-2.0g/cm^3) comprise bright and dull coal incorporated into an 'inertodetrinite' texture. Cleats and kaolinite laminae serve as preferential cleavage planes in the lower density fractions, while bright and dull coal serve as preferential breakage planes in the higher float fractions. As a result, these phases are liberated and there is evidence to support that liberation of minerals have controls that can be identified and corrected for. Thus, washability can be determined using QEMSCAN since the significant effect of liberation can be calculated and corrected, for a specific coal type.

Declaration

I, Shinelka Singh declare that the thesis/dissertation, which I hereby submit for the degree

Masters in Geology at the University of Pretoria, is my own work and has not previously been submitted by me for a degree at this or any other tertiary institution.

SIGNATURE: 

DATE: 15th December 2015

Contents

List of tables

List of figures

1. Introduction

Float and sink analysis allows for washability determination. The analysis involves the separation of coal into density fractions using heavy organic liquids with densities between that of coal and coal-associated minerals. Washability data is integral for coal resource assessments, production-phase planning, coal preparation plant design and day-to-day plant control. Washability curves demonstrate a relationship between density, ash and calorific value. As density fraction increases, ash content increases and calorific value decreases. Most importantly, washability curves indicate the relative density at which the coal must be separated in order to obtain specified ash content at a known yield. Improved beneficiation processes/workflows can be implemented for optimal coal efficiency (SACPS, 2011).

Currently the motivation for finding alternate processes to generate washability data is due to the toxic, costly, heavy organic liquids used and the lengthy procedure of washing and drying products and discards. Due to heavy reliance of toxic organic liquids used in float and sink testing, the 2004 newsletter for the Queensland Branch of the Australian Coal Preparation Society declared that the Standards Australian committee MN-001-02 (Coal Preparation) was deliberating the withdrawal of AS 4156.1 (Coal preparation – Higher Rank Coals – Float and Sink Testing) (Galvin, 2006). The committee pushed to find an alternative means to float and sink testing within 5 years.

Alternative means of obtaining washability data was explored by Galvin (2006) and includes dense medium suspensions, magnetized fluids, gas pycnometry and using salt solutions like zinc chloride to replace organic liquids. Salt solutions, although advantageous over heavy organic liquids, require rigorous washing to remove the solution from the coal, are expensive to recover once made into a dilute solution and some solutions are hazardous in high concentrations, like zinc chloride (Callen et al., 2008). Replacing organic liquids with aqueous solutions introduces the problem of clay breakdown (Galvin, 2006).

A water fluidization column technique was first developed by Galvin and Pratten (1999) for a narrow size range. As illustrated by Moritomi et al., (1982), particles segregating at different densities are supported further using a high suspension density and low fluidization velocity. This allows for small dense particles to dwell below larger low-density particles that have higher terminal velocity at infinite dilution.

Galvin and Pratten (1999) demonstrate that the density distribution of a coal sample could either be obtained by fluidising narrow particle size ranges (Method 1) or fluidizing a broad size range and the subsamples sized into smaller fractions for analysis (Method 2). A disadvantage of water-based techniques is that clays and other composite particles break down in water (Galvin, 2006).

Method 1 would allow for particle size reduction as there is no sieving after fluidization resulting in a fluidized bed comprising fine mineral matter occurring with large coal particles (Galvin, 2006). Method 2 sieves the sample after analysis, resulting in negligible particle size

changes, although fine particles will be lost from the fluidizing bed (Galvin, 2006). Losses can be overcome by first wet screening the sample at the lowest screen size available (Galvin, 2006). Method 2 is a simplified analytical technique that generates washability data by water fluidization and was later further enhanced by Callen et al. (2002), to generate washability data for a broader size range of coal and associated mineral impurities (-4+0.045mm).

The study derived yield-ash data for a variety of Australian coal samples to validate the robustness and accuracy of the technique (Callen et al., 2008). The study concluded fluidization to be an effective, rapid and accurate method, although inconsistencies occurred at low ash density fractions when comparing the cumulative yield-ash results to those produced by float and sink analysis. A discrepancy was present between the yield-ash curve generated in the low ash/density region which is due to dispersion and is corrected by means of a correction factor (Callen et al., 2002).

The study was further pursued by Callen et al. (2008) to investigate alternate water-based methods for attaining the washability of coal covering -50+0.0045mm diameter particles. Results acquired from a mechanical Boner Jig, a Hydraulic Mintek Jig and a water fluidization based Reflux Classifier was compared to results obtained from float and sink analysis. The study concluded that the Boner Jig performed best for the -16+0.25mm particles, the Mintek MDS Jig for the -50+16mm fraction and the Reflux Classifier worked well for the entire -50+0.0045mm size range. Additionally, an algorithm was developed to enhance accuracy of washability data produced by the Reflux Classifier. The Boner Jig and Mintek MDS Jig generated data that deviated towards the low ash end of the curve due to particle dispersion (Callen et al., 2008).

An automated washability monitor for coal providing near-real time analysis was developed to determine washability utilizing both x-ray transmission and image processing of individual coal particles. The three main objectives of the study were achieved, which were; easy operation, to reduce the manual effort significantly and to have an on-line approach. Tests carried out on the prototype were reported to be promising (Bachmann et al., 2011).

QEMSCAN is a scanning electron microscope (SEM) based analytical system configured to automatically determine the mineralogical characteristics of particles (van Alphen, 2009). QEMSCAN technology incorporates an automated image analysis system that utilizes Back Scatter Electron (BSE) intensity and Energy Dispersive (EDS) X-ray Signals in its analysis. QEMSCAN coal analysis determines elemental proportions, textural data and particle sizes (of the bulk sample or of individual mineralogical phases). The technology has also proven successful in predicting slagging propensity and abrasive characteristics, which previously required costly equipment and processes to determine (van Alphen, 2009).

A study by Singh (2010) proved that QEMSCAN can identify and quantify bright coal (vitrinite and reactive semifusinite) from dull coal (fusinite, inertinite and secretinite) based on the composition of carbon, organically bound sulphur, and oxygen. Samples were sent for

petrographic analysis to determine maceral identity and proportion, and for chemical analysis. In order to try to establish a textural relationship in macerals, petrographic images were correlated to BSE images from maceral standards set in mounting medium. Results from comparisons of the images show that maceral identification would be challenging using maceral textures under BSE imaging, as significantly less detail is observed compared to petrographic images (Singh, 2010).

X-ray spectra of the macerals were acquired to characterise reactive from less reactive coal based on elemental proportions of carbon, oxygen and organically bound sulphur. Analysis of the spectral results revealed that the sulphur-rich carbon bearing phase is vitrinite or reactive inertinite, whereas the carbon rich phases with low levels of sulphur are inertinite and secretinite (Singh, 2010).

The research undertaken for this project determines if QEMSCAN can predict yield and ash data as float and sink analysis currently achieves to predict the washability of coal. Float and sink testing achieves gravity separation of coal by placing the coal in organic liquids with a range of pre-set densities. Washability curves are determined from the yield derived per float fraction, as well as from ash values of the density separated fractions. The density of QEMSCAN analysed particles are determined using iDiscover software, version 4.2 (FEI QEMSCAN®, 2007). A corresponding ash and yield value is calculated and compared to those derived from float and sink testing.

2. Background information

2.1 QEMSCAN

QEMSCAN was developed to automatically identify minerals of most ore and rock-forming minerals of a sample at 450 000 points per hour (8 milliseconds per point). Minerals are identified based on the elements identified in a 1000 count X-ray spectrum, while each of these X-ray spectrum are interpreted on-line. Each pixel value stored for analyzed points are individual chemical compositions that correspond to pre-defined mineral identification rules. Chemical composition is used to discriminate between mineralogical phases, while the backscatter electron intensity represents the atomic weight variation within the sample (van Alphen, 2005).

2.1.1 QEMSCAN evolution

In the early 1970's, manually operated scanning electron microscopes were beginning to be more extensively used in coal research by the combined introduction of the first commercial Noran SEM by Noran Instruments with a digital electron beam control system and the introduction of the Particle Recognition and Characteristic (PRC) software developed by U.S. Steel Research Laboratories (Galbreath et al., 1996). A SEM could now automatically locate, identify and measure morphological characteristics of minerals in coal. Computer controlled or coal characterisation SEM (CCSEM), otherwise known as SEM-based automatic image analysis system (SEM-AIA) was considered to be an important method to quantitatively analyse coals and their associated mineral contents. The CCSEM determines the centroid of a bright phase and collects a single x-ray spectrum at the centroid position (van Alphen, 2005).

The first CCSEM utilized two independent routines controlled by the PRC and coal mineral analysis (CMA) software (Lee, 1978) (Huggins et al., 1982). The PRC software locates and measures morphological features of grains while the CMA software (Nissen and Gruelich, 1987) positions the electron beam at the centre of the grain to obtain X-ray spectra (van Alphen, 2005). The Quantitative Mineral Analysis (QMA) routine is similar to that of PRC and CMA as the QMA routine processes backscattered electron images to determine the position of mineral grains (van Alphen, 2005).

Later CCSEM investigations expanded to describing inorganic-organic associations, instead of being limited to measuring minerals in coal (van Alphen, 2005). Two backscattered electron thresholds were used in order to distinguish between the carnauba wax mounting medium, organic coal and minerals in coal (Straszheim and Markuszewski, 1990) (van Alphen, 2005). The Energy and Environmental Research Centre of the University of North Dakota developed the particle-by-particle scanning electron microscope programme (PBPSEM) to automatically quantify included and excluded minerals in coal (Steadman et al., 1991). The Analysis of Mineral and Coal Associations (AMCA) developed by Brigham

Young University uses the same principles as PBPSEM to differentiate between mounting medium, coal and minerals (Yu et al., 1993).

The Quantitative Evaluation of Materials using a Scanning Electron Microscope (QEM*SEM, later renamed to QEMSCAN), developed by CSIRO, Australia is similar to the CCSEM (Skorupska and Couch, 1993). Unlike CCSEM that determines the centroid of a bright phase and collects a spectrum, QEM*SEM sets a raster of adjacently-spaced points over a particle and determines the chemical composition of the phase at each point (Gottlieb et al., 1991). Data acquisition is rapid (16-50 micro-seconds) due to combined x-ray spectra from four x-ray detectors. QEMSCAN uses a scanning electron microscope, four energy dispersive X-ray spectrometers, a micro-analyser and the latest electronic processing unit to obtain quantitative mineralogical data (van Alphen, 2009).

The ASCAN system developed by Anglo Research Laboratories in South Africa utilizes the raster of points over a particle similar to QEMSCAN, instead of the centroid method used by CCSEM (van Alphen and Falcon, 2000). ASCAN utilizes a single energy dispersive detector, it is not an integrated system, mineral identification is done offline and depends on the principles of fuzzy logic to identify minerals. ASCAN was previously installed at Eskom to characterise coal, fly ash and clinkers (van Alphen, 2005).

2.1.2 Uses in industry and coal-related research

QEMSCAN is used in the minerals industry to obtain quantitative mineralogical data to measure ore quality at the exploration stage, to design mineral processing plants and to assess and optimise existing process plant performance. Coal and its by-products are similar to metalliferous ores in that they are composed of complex multi-component material with intricate interlayering of coal macerals and minerals on a macro to micro-scale. It is important to understand the chemistry and textural relationship between macerals and mineral phases so that the behavior of coal during preparation and combustion can be predicted. Coal can be used more efficiently if there is more importance placed on understanding how the individual components of coal react to preparation methods, and how they interact during combustion. A better understanding of the interaction of coal components during combustion to produce ash and emissions allow for new strategies to be developed to better manage these coal by-products (French et al., 2008).

QEMSCAN's primary use in the coal industry is to quantify mineral/phase proportions and the morphological features (size, liberation, particle characterization and texture) in any particular coal and ash sample. Eskom currently uses QEMSCAN data to determine the nature and proportion of stone contamination, to predict the abrasive characteristics, to predict slagging propensity of coal and to quantify the phase proportions in ash samples (van Alphen, 2009). Coal samples could be borehole core, pulverized fuel or crushed coal. The QEMSCAN

EVO50 instrument used at ESKOM Research, Testing and Development Centre in Rosherville, Cleveland is shown in Figure 1.

Figure 1. QEMSCAN comprising Zeiss EVO 50 SEM with four silicon drifted detectors based at ESKOM Research and Innovation Centre.

2.1.3 Data acquisition

Figure 2 is a schematic displaying the functioning of a scanning electron microscope. An electron gun acts as a source of electrons. A potential difference of 25kV is used to accelerate the electrons to form a high energy beam. Either tungsten filaments or lanthanum hexaboride are used as cathodes due to their highest melting points and lowest vapour pressure in comparison to other types of metals. As the electrons are aimed at a prepared sample, the electron beam passes through a vacuum and hits the sample. Back scattered electrons and X-ray signals are produced. The electrons in the beam interact with the atoms in the sample to produce a difference in energy that is lost by the electron due to interaction with the atoms in the sample. The energy difference is detected by the energy dispersive (EDS) detector used for both quantitative and qualitative X-ray analysis (French et al., 2008).

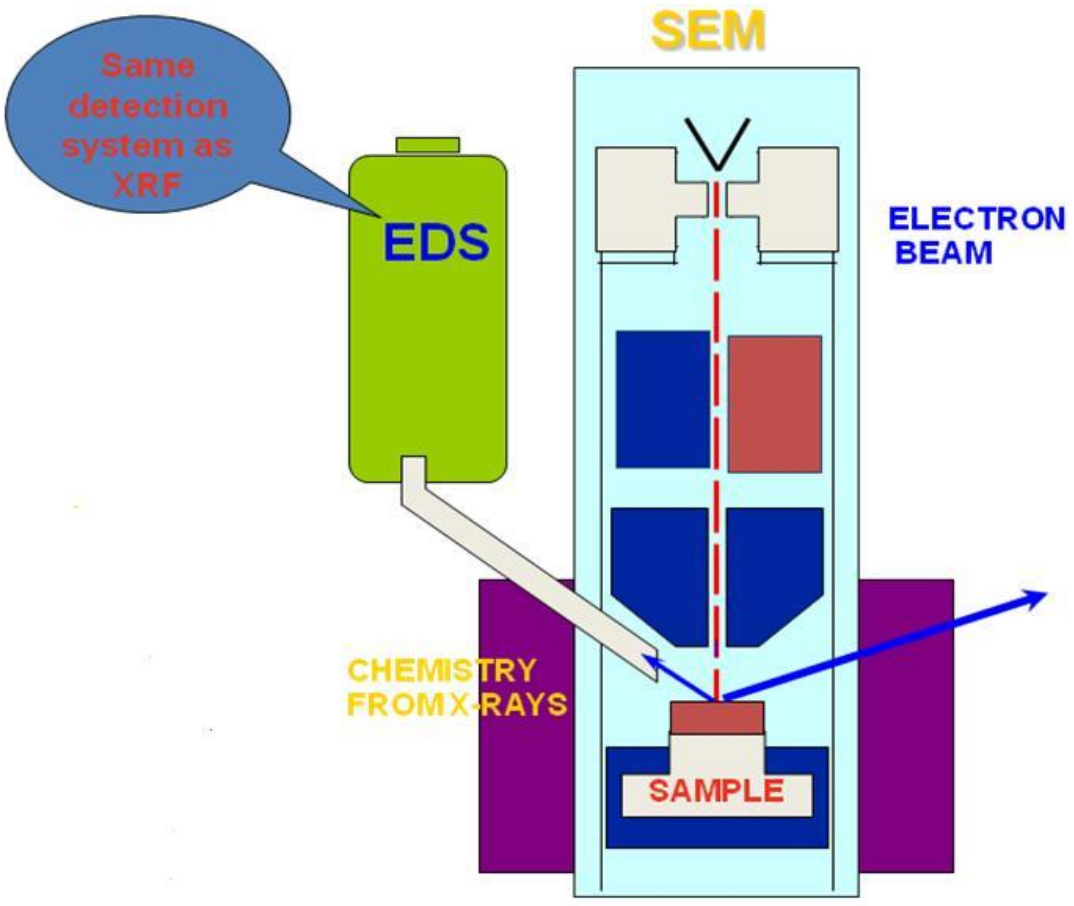

Figure 2. Schematic illustrating the functioning of the scanning electron microscope (van Alphen, 2009).

Figure 3 illustrates the interaction of the electron beam with the sample, and the resulting detection of electrons. As the beam interacts with the sample, a range of signals are produced. The variety of signals produced from the interaction of the primary beam with the sample can be seen in Figure 3. The most commonly used signals used are back-scattered electrons and X-ray signals, which are generated within the specimen interaction volume of the sample. The specimen interaction volume is the volume within the sample in which atomic interactions occur, due to interaction of the primary electron beam with the sample atoms. The interaction

volume is dependent on the atomic number of the sample being analysed, applied accelerating voltage, angle of incident beam and beam diameter (French et al., 2008).

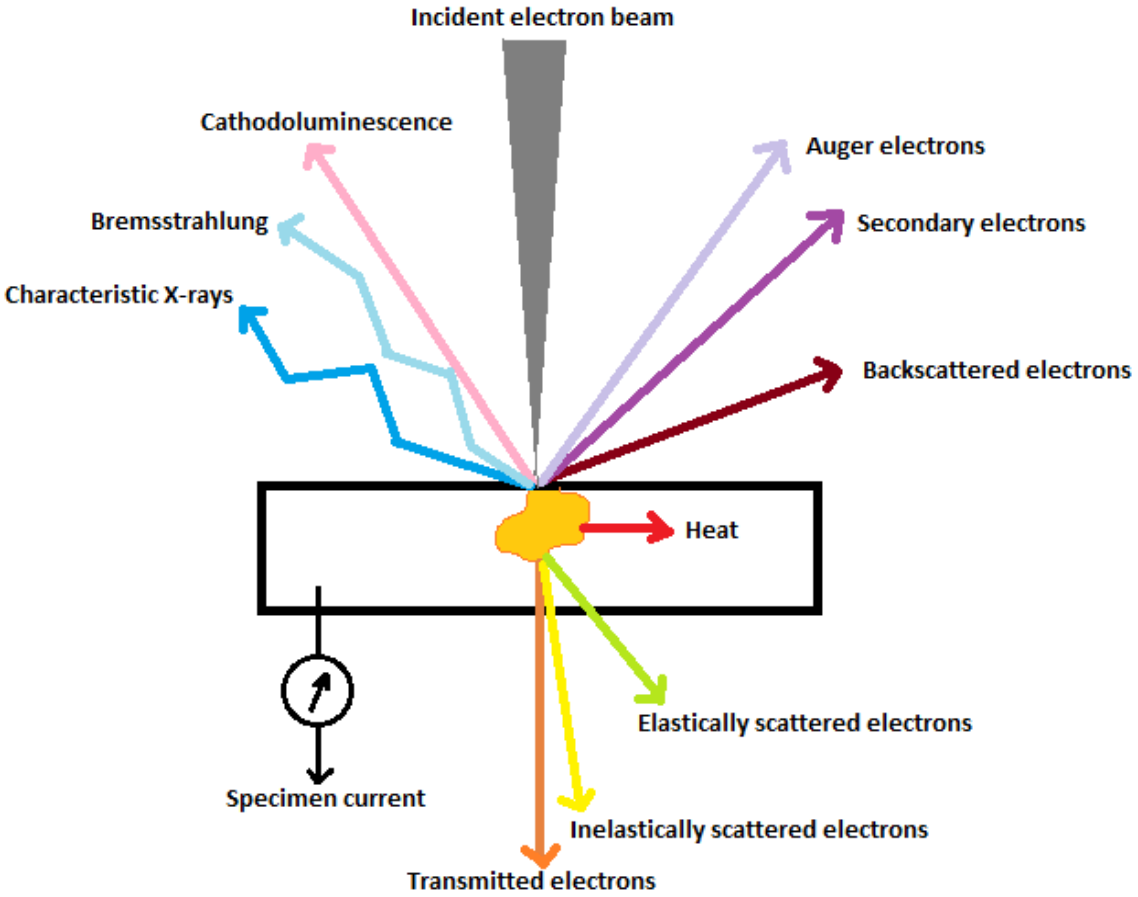

Figure 3. Illustration of the primary electron beam interacting with the sample to form various signals. (Adapted from French et al., 2008)

X-ray signals provide in depth compositional information of the sample while backscatter electron intensity represents the atomic weight variation within the sample (French et al., 2008). When a primary beam electron collides with an electron from the sample atom, substantial energy is lost to that atom (Postek et al., 1980). The energy gained by the specimen atom causes it to ionize and electrons emitted as a part of this ionization are observed as secondary electrons (Postek et al., 1980). The secondary electron signal provides topographic information of the sample surface. Other signals produced that are used more commonly in other areas of specialized study are cathodoluminescence, Bremsstrahlung and auger electrons (Figure 3) (French et al., 2008).

Primary beam electrons interact with the nucleus of atoms in the sample with minimal energy loss allowing these electrons to escape from the sample and are detected as back-scatter electrons (BSE). The BSE have higher energy than secondary electrons due to being sourced from greater depths in the sample (French et al., 2008).

The beryllium window of the energy-dispersive X-ray detectors limit the detection of elements to sodium and above although a thin window system allows for the detection of

carbon and elements with higher atomic numbers than carbon. QEMSCAN has four silicon drift detectors which allow for high count rates (250 000 counts/sec) without a loss in resolution. This allows for exploring analysis using higher counting times and the silicon drift detectors would accommodate either shorter analysis time, or better quality data acquired in a longer time period (French et al., 2008).

Bremsstrahlung is X-ray radiation formed as a result of primary electrons losing some energy through collision with the sample surface causing inelastic scattering. The energy distribution of X-rays formed is continuous and forms the continuum (background) of the X-ray signal. The inner shells of the atoms eject electrons to a ground state due to collision of primary beam electrons, resulting in an ion in an excited state to return to ground state. Energy is released when an electron drops from an outer shell to an inner shell, and this energy is seen as a characteristic X-ray that is unique to that specific element. The characteristic X-rays are used to identify and quantify elements. When an electron drops from the outer shell to occupy an inner shell, a special nomenclature is used to describe the electron movements from shell to shell. The first letter is representative of the shell from which the electron originates, while a Greek symbol is used to represent the shell the electron moves to. Kα x-ray lines are the most commonly used and are formed due to the ejection of an electron from the K shell, which then moved to occupy the L shell (French et al., 2008).

Prepared samples are loaded into the instrument and the analysis is set up in iMeasure software, version 4.2 (FEI QEMSCAN®, 2007). The back scattered electrons are used to generate an image from which the particles to be analysed are defined. The backscattered brightness profile (Figure 4) represents the atomic weight variation within the sample. It follows from observation of the BSE acquired image in Figure 4, that the lighter components of the image are high density minerals, while the darker components would be the less dense coal matter. The darkest component (lowest density) is the carnauba wax which serves as a mounting medium for coal sample preparation. Using epoxy resin as a coal sample preparation medium is not as good as carnauba wax because epoxy resin and coal has a similar backscatter electron response signal, i.e. it is difficult to differentiate between coal and epoxy (van Alphen, 2009).

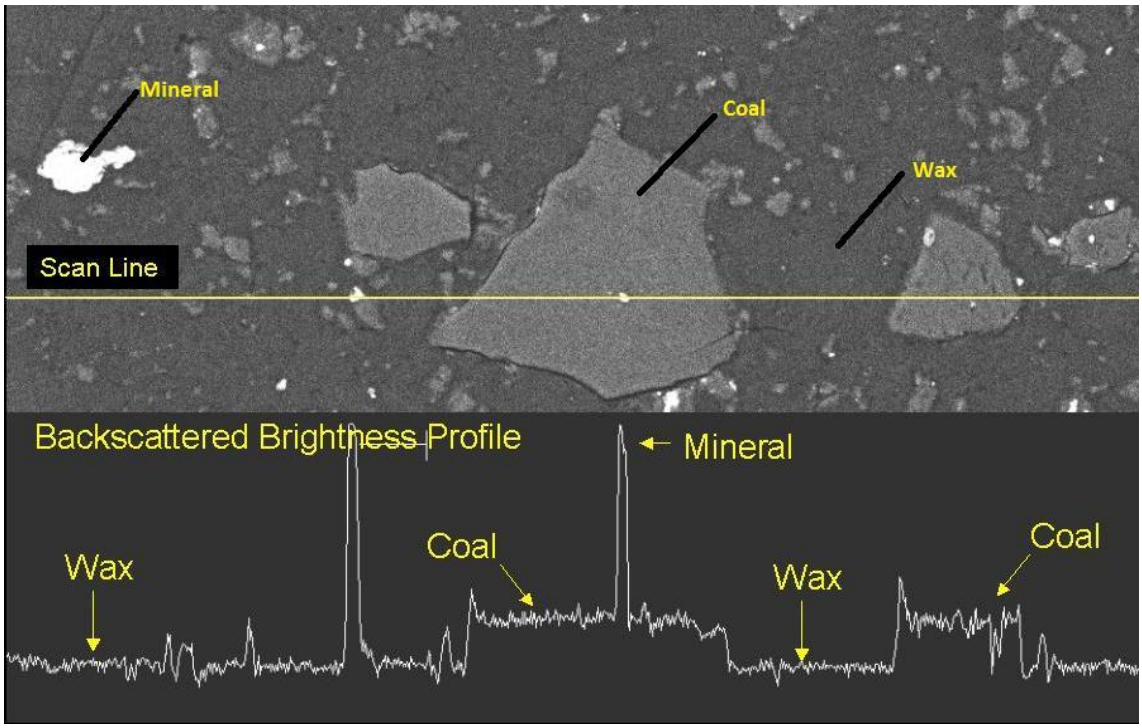

Figure 4. Back scatter electron image of coal samples in carnauba wax (modified from van Alphen, 2009).

Once the particles to be analysed have been identified utilising BSE, x-ray spectra are acquired to determine the mineralogical composition of the analysed particles (van Alphen, 2005). X-ray spectra are taken and represented as a pixel in a user-defined grid after the particles have been chosen for measurement (French et al., 2008). A measurement is created for each sample. Each measurement setting describes the mode of measurement selected, target minerals, number of particles required, particle size and shape (Intellection, 2007). There are four types of scan modes that are determined using line spacing and points within the line.

A Bulk Mineral Analysis (BMA), based on the line scan is a one dimension analysis with each block being scanned in the x direction and the y spacing as such that most particles are intersected once (Intellection, 2007). Points are closely spaced in the X-direction along widely spaced lines. The distance between selected lines in the Y-direction is to be greater than the largest particle size to ensure that each particle is not intersected more than once (French et al., 2008). BMA scans are used to obtain quantitative modal mineralogy, grain sizes and mineral association data (Intellection, 2007).

A Particle Mineral Analysis (PMA) is a two directional analysis where the area of each particle is measured (Intellection, 2007). The points are closely spaced and are of equal values in the X and Y directions (French et al., 2008). PMA scans are used to obtain particle images, quantitative modal mineralogy, grain sizes and mineral association data (Intellection, 2007). The PMA mode has previously been the most commonly utilized mode for coal mineral analysis (French et al., 2008).

A Specific Mineral Search (SMS) is a variation of the PMA analysis mode and is used to acquire better statistics on phases that occur between 0.1-1.0 vol.% (French et al., 2008). The SMS mode of analysis utilizes BSE intensity to locate particles falling within a stipulated BSE range (French et al., 2008). Only particles containing the target phase/s are located and analysed (Intellection, 2007). The Trace Mineral Search (TMS) is analogous to the SMS mode of analysis and is used to locate phases present in very low quantities (French et al., 2008).

The Field Scan Mode analyses a full image per field and is used to analyse textural associations between phases. The fields can later be stitched to produce a complete image of the sample surface analysed (Intellection, 2007). All samples analysed in this research project were set to Field Scan Mode.

2.1.4 Data processing

Once the samples are analysed, the data is processed in iDiscover software version 4.2 (FEI QEMSCAN®, 2007). Each pixel represents a separate analysis, utilising the elemental proportion derived from the X-ray spectrum together with the BSE information to identify the mineral. A mineral identification standard, known as the Species Identification Protocol (SIP) file assigns each mineral a specific colour to help highlight the relative mineral proportions, textural characteristics, size and shape of particles (van Alphen, 2009).

A false colour image, as seen in Figure 5, is the final outcome of minerals identified using x-ray spectra and BSE data. The sample can be further processed to correct for field stitching, touching particles, as well as a number of other available particle processing options. Once the samples have been thoroughly processed, information such as particle size distribution and textural associations within individual particles can be acquired (van Alphen, 2009).

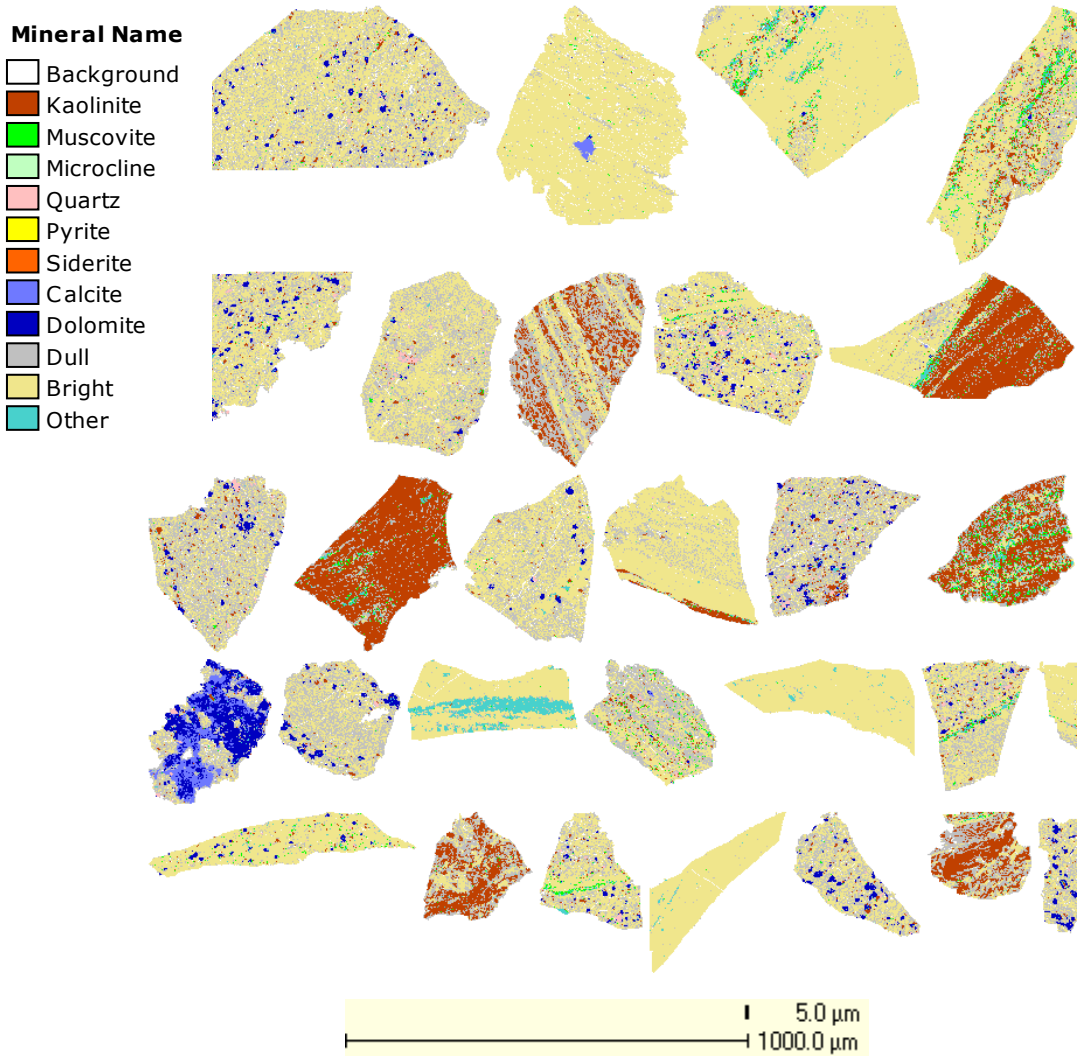

Figure 5. False colour image of coal particles.

2.2 South African coal

South African coal-bearing strata are part of the Karoo Supergroup, which is a sequence of Early Carboniferous to Early Jurassic age glacial, marine and terrestrial sediments. Coal from these ages can be found in a similar geological setting surrounding South Africa, such as in Botswana, Zimbabwe, Zambia and Mozambique. The majority of coal in the Karoo Basin is found in the Early to Middle Permian Ecca Group, overlying the glacial sequences of the Dwyka Formation that are Carboniferous in age. Late Triassic age coal is found in the Molteno area in the south of the Karoo Basin (Ward, 1984).

The coal in the Southern Hemisphere (Gondwana) is distinctly different from that of the Northern Hemisphere (Laurasia) due to the varying vegetation and climate conditions predominating at the time of coal formation, as well as the ensuing geological events (SACPS, 2011).

Coal in the Northern hemisphere formed in the hot and humid coastal Carboniferous swamps in a slowly subsiding basin (SACPS, 2011). Coals originating from in the Permian swamps of the Southern hemisphere were formed in temperatures that changed from cold, increasing to warm conditions relating to the waning of an ice age (SACPS, 2011). The Southern Hemisphere had an active environment, with flowing rivers that frequently flooded, causing deposition of sediments into surrounding swamps (van Alphen, 2009). The cycle was truncated by rising sea levels, which resulted in flooding of the swamps. The cycle of flooding and sediment deposition into swamps were repeated five times (van Alphen, 2009).

Crushed coal from the Northern hemisphere produces narrow density ranges of particles, i.e. high quality low density particles and high ash, high density stone. Southern hemisphere coal produces a wide range of density particles, due to the introduction of mineral matter during fluvial activity in the coal forming process. Thus, coal from the Southern hemisphere has a higher proportion of near density particles compared to coal from the Northern hemisphere (van Alphen, 2009).

Coal in South Africa is predominantly sourced from the Mpumalanga coal fields and the Waterberg coal fields in Limpopo (Figure 6). Northern hemisphere coal is predominantly bright, vitrinite-rich coal with a lower proportion of minerals, whereas Southern hemisphere Gondwana coal is dull, inertinite-rich coal with a higher proportion of included minerals and in-seam partings (van Alphen, 2009).

In general, South African coal and coal from similar Gondwana provinces, results in coal that is more difficult/expensive to beneficiate than Northern hemisphere coal (Falcon and Ham, 1988).

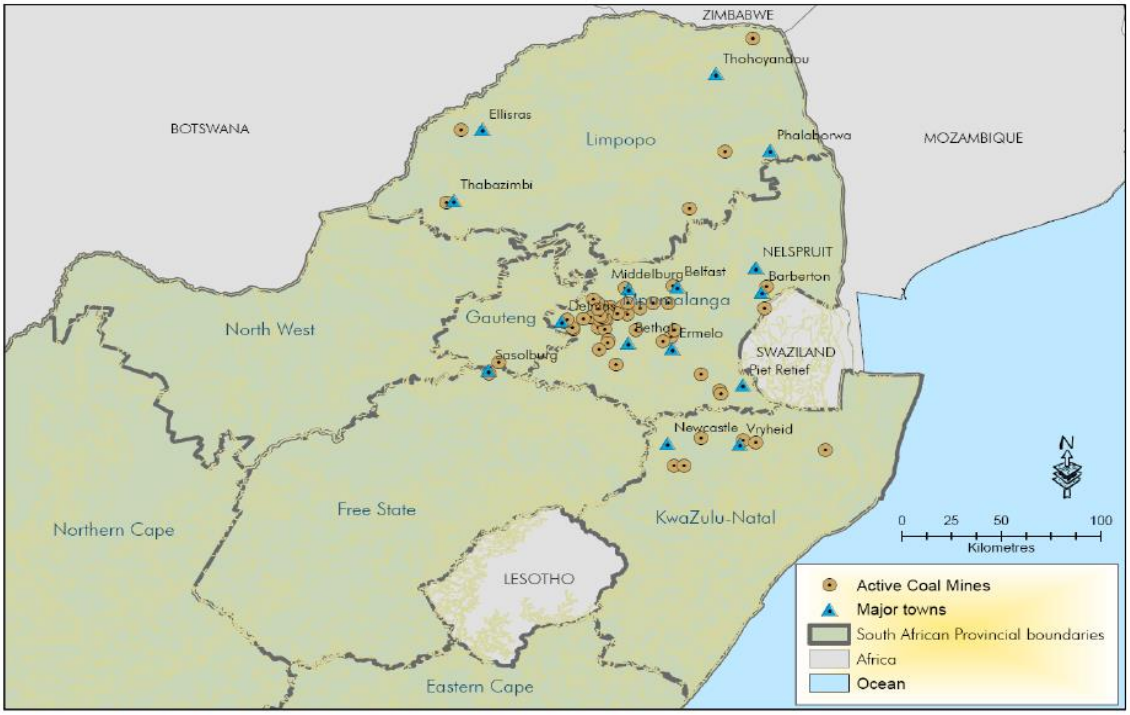

Figure 6. Map illustrating the active coal mines in South Africa (SSA, 2012)

2.2.1 Maceral formation

Macerals are formed due to fossilization of plant remains that have been subjected to physical and chemical alteration through geological time. The macerals differ in chemistry and physical characteristics due to their origin being from different parts of the plant, which have since undergone primary accumulation, early phases of biochemical degradation and early coalification. The nature of plant population, climatic controls, acidity (pH) and redox (Eh) values greatly influences the formation of macerals during the initial phases of peat accumulation. The most important factor controlling degradation of plant matter is the redox value (Falcon and Snyman, 1986).

As illustrated in Figure 7 below, aerobic conditions providing unlimited oxygen allows for almost complete disintegration of plant matter, while limited oxygen (sub-aerobic) conditions (such as undercover leaf mould) allows for mouldering to occur. The process of mouldering involves aerobic bacteria producing humic-poor substances, the dissipation of the cellular contents and plant tissues, drying out of the cell walls, the vegetable matter is reduced to detrital grains and bands of wood resembling charcoal. Fusinization occurs if the process is continued to the final result, creating fusinite (Falcon and Snyman, 1986).

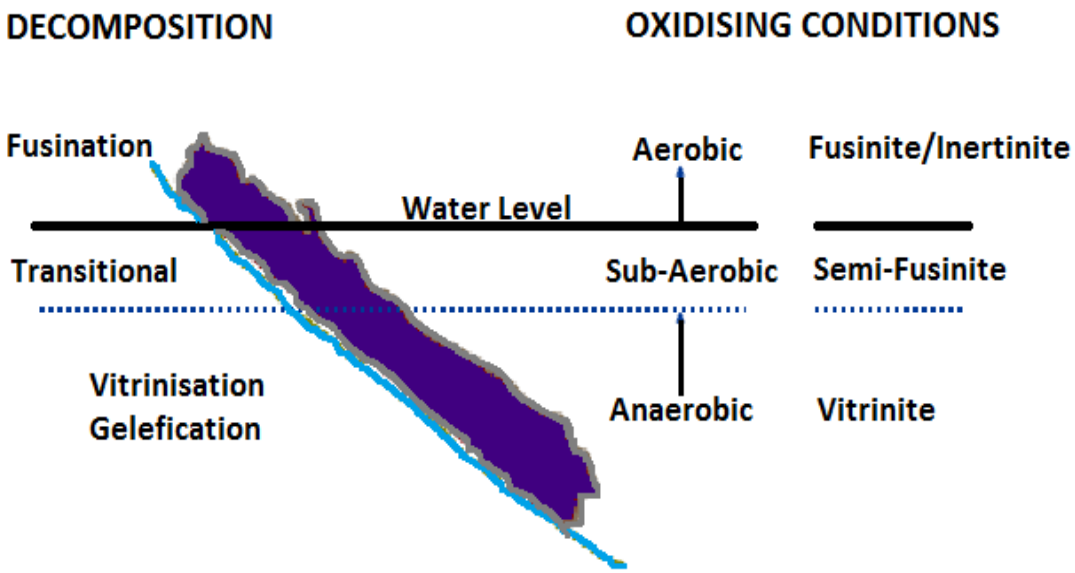

Figure 7. Maceral formation and the effects of oxidation (Eh). (van Alphen, 2012).

Plants growing in swamp conditions partially decay (biochemically alter) and if they do not completely disintegrate, peat is formed (SACPS, 2011). Partially submerged peat with restricted oxygen supply (sub-aerobic) provides ideal conditions for peatification to take place (Falcon and Snyman, 1986).

Peatification produces humic acids and partial or full gelification of the woody plant tissue occurs. A dopplerite gel is produced as a result of precipitation of humic acids in solution. Extreme gelification/vitrinization makes it difficult to determine cell structures (Falcon and Snyman, 1986).

Fermentation (otherwise known as putrefaction) occurs when peat is subjected to reducing conditions (anaerobic) resulting in anaerobic bacteria producing hydrogen-rich matter through consumption of oxygen (Falcon and Snyman, 1986).

Biochemical degradation processes discontinue after the accumulating plant matter has been buried more than one meter and maturation processes take over. Coalification occurs when peat swamp metamorphoses to phases of lignite, bituminous coal and anthracite as temperature and pressure conditions are increased with time. Coal rank describes which phase the coal has reached in the coalification series. The type of coal is described by the proportions of organic matter formed during biochemical degradation in the peat phase (Falcon and Snyman, 1986).

Thick beds of peat are buried by coarse and/or fine grained sediments. The repetition of the cycle results in compaction of layers of peat separated by layers of sandstone and/or shale respectively. Deposition of sediment over the peat layers increases the pressure and temperature conditions. Coal is the final product after the moisture content of the organic matter is reduced as pressure and temperature conditions increase over time (SACPS, 2011).

The organic material comprising coal is divided into three maceral groups, which are vitrinite, inertinite and liptinite (SACPS, 2011). The macerals in the vitrinite group were formed predominantly from well-preserved cell walls and cell fillings of woody plant tissue from the trunks, branches, stems, twigs, leaves and roots (Appendix A, Table A.3.). The well preserved cells may be filled with fine clay and/or a mixture of vitrinite macerals and fine minerals (Falcon and Snyman, 1986).

Inertinite macerals are formed from the same plant material as vitrinite macerals, but have been oxidized and significantly altered during the peat stage of formation (Appendix A, Table A.4.). The inertinite macerals decompose under aerobic or sub-aerobic conditions allowing for oxidation and carbon-enrichment/fusinitization (Figure 7). Liptinite macerals are formed from the chemically resistant parts of plants, such as the spores, cuticles, suberine cell walls, resins, polymerized waxes, fats and oils from vegetable material (Appendix A, Table A.5.), (Falcon and Snyman, 1986).

2.2.2 Classification

2.2.2(a) Traditional maceral and microlithotype classifications

When looking at a piece of coal in hand specimen, the bright brittle bands are vitrinite rich, while the dull bands comprise inertinite and mineral matter. The recognised lithotypes are vitrain, clarain, durain and fusain. The most common minerals found in South African coal are clays, quartz, carbonates, pyrite, glauconite, rutile, apatite and gypsum. Coal-associated minerals are further divided into intrinsic inorganic material (present in the original plant material) and extrinsic inorganic material (introduced at a later stage to organic material) (Falcon and Snyman, 1986).

Maceral and microlithotype classifications are based on petrographic analysis of coal. Maceral analyses carried out under oil immersion requires an automatic point counter at traverse intervals of 0.4mm and spacing between traverses of 0.5mm. A minimum of 500 points are counted for a maceral analysis (Falcon and Snyman, 1986).

Microlithotype analyses utilise a 50x50 µm graticule, within which the proportions of macerals and minerals in a 50x50 µm graticule are determined. The proportions could include a single maceral (monomaceral), a combination of two macerals (bimaceral) or a combination of three macerals (trimaceral) (Appendix A, Table A.1) (Falcon and Snyman, 1986).

A carbominerite particle is defined as an association of coal with a specific proportion of mineral or mineral grouping. Carbominerite particles comprise of groupings which are classified with the following proportions of coal to mineral: carbargillate (20-60vol.% clay minerals), carbosilicate (20-60vol.% quartz), carbopyrite (5-20vol.% sulphides), carbankerite (20-60vol.% carbonates) and carbopolyminerite (20-60vol.% mineral matter) within a coal particle. Carbominerite has a density range of 1.55-1.95g.cm^{-3} (Falcon and Snyman, 1986).

The microlithotypes (mono-, bi-, tri-) are classified as mineral free if mineral proportions are <20%, or <5% volume for pyrite. The mineral rich microlithotypes are further subdivided into the types of minerals which are predominant (Appendix A, Table A.2) (Falcon and Snyman, 1986).

2.2.2(b) QEMSCAN maceral and microlithotype classification

In a study conducted in 2010 by Singh, it was established that QEMSCAN could differentiate between bright and dull coal due to variances in their elemental composition (a QEMSCAN maceral classification system). Although carbon/oxygen ratios vary for different macerals, the dominant discriminator used by QEMSCAN to differentiate reactive from unreactive macerals was organically bound sulphur (French et al., 2008) (Harrison, 1990) (Singh, 2010). A test data set (CNCC and Masuka) was used to determine a relationship between petrographically derived vitrite content to QEMSCAN derived vitrite content (Singh, 2010).

Randomly selected coal particles were set in epoxy resin. An oil immersion petrographic microscope was used to characterise the macerals and to acquire a light reflectance image.

The same standards were loaded in QEMSCAN. Correlative microscopy was used to find easily identifiable features (Cracks, holes and minerals) to acquire X-ray spectra from each maceral (Figure 8 and Figure 9). The sulphur, carbon and oxygen proportions were utilized to distinguish between bright and dull coal particles (Singh, 2010).

Oxygen content is in general higher for more reactive macerals. It can be seen from spectral results that the sulphur-rich carbon bearing phase is vitrinite or reactive inertinite (bright), whereas the carbon rich phases with low levels of sulphur is inertinite and secretinite (dull) (Figure 11). Figure 11 also illustrates the variance of carbon concentrations for various macerals. Of the macerals, vitrinite has the lowest carbon concentration, while sclerotinite has the highest amount of elemental carbon. It is important to note that in the vitrinite spectrum in Figure 10, low aluminium and silica is evidence of 'intrinsic ash', which is later assumed to be a 2% intrinsic ash value for the purpose of QEMSCAN ash% calculations (Singh, 2010).

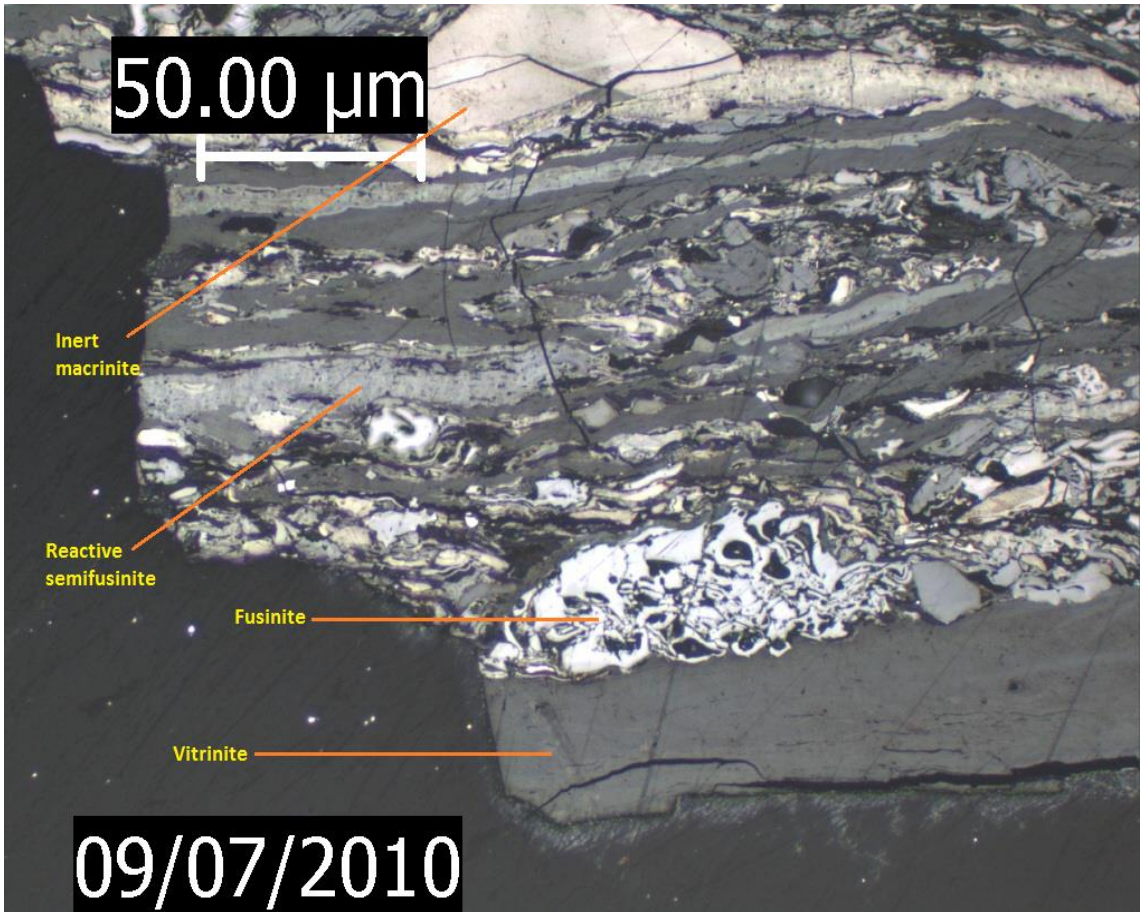

Figure 8. Petrographic image of various macerals and maceral groups present in sample 5b3 (Singh, 2010).

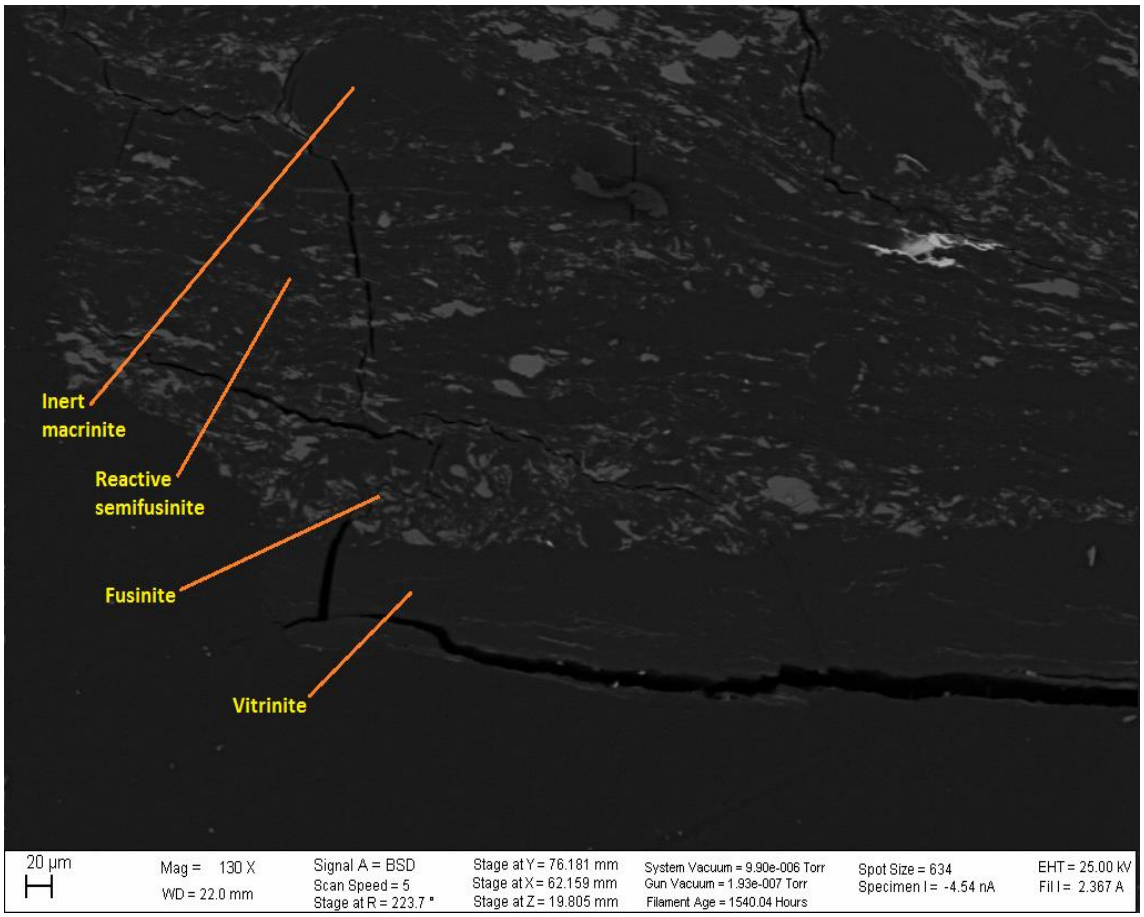

Figure 9. QEMSCAN acquired BSE image of various macerals and maceral groups present in sample 5b3 (Singh, 2010).

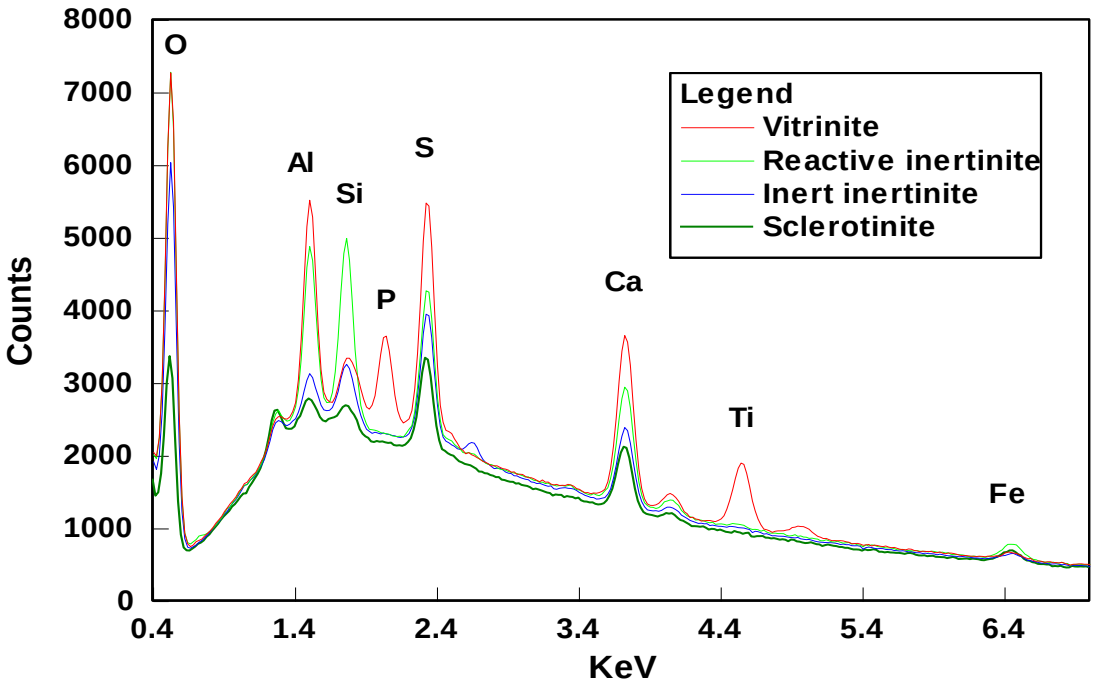

Figure 10. A million count X-ray spectrum of vitrinite, reactive inertinite, inert inertinite and sclerotinite (secretinite) (Singh, 2010). Low counts of aluminium and silica are evidence of 'intrinsic ash'.

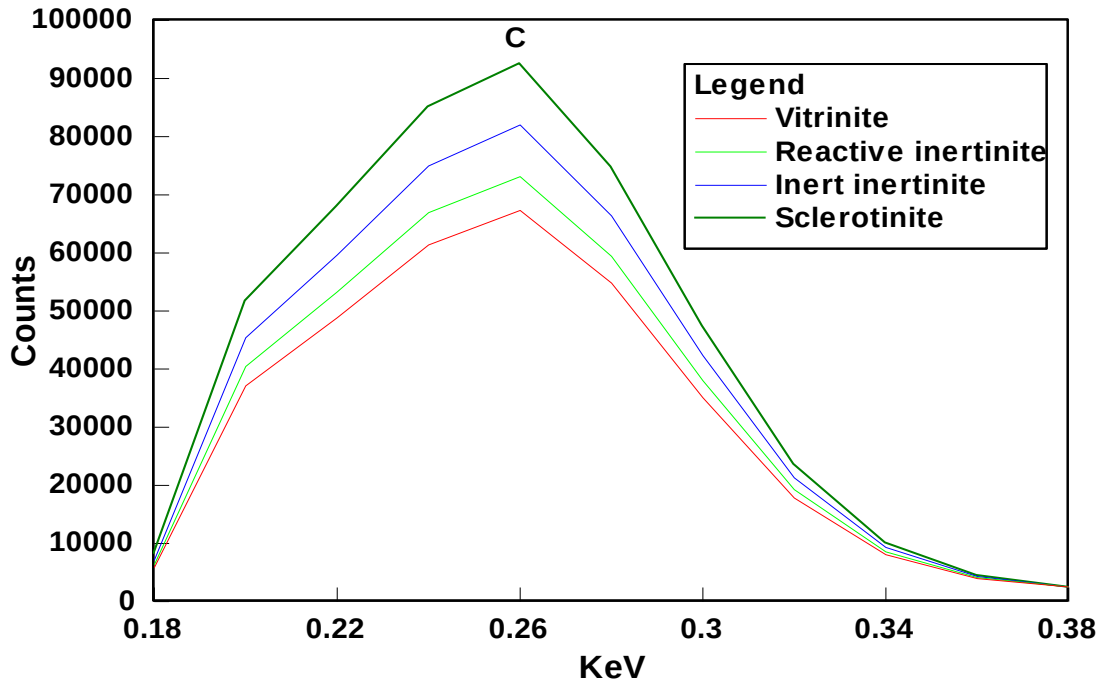

Figure 11: Different in carbon peaks (Singh, 2010)

The microlithotype classification utilized on QEMSCAN is analogous to the petrographic microlithotype classification. The QEMSCAN-based "microlithotype" categoriser was defined by varying proportions of bright coal (vitrinite and reactive inertinite), dull coal (inert inertinite and secretinite) and mineral matter (Singh, 2010). BSE cannot be used to distinguish between the different macerals, which is in contrast to petrographic analysis which is based on light reflectance and texture to discriminate the macerals.

Vitrite has >95% of a single maceral, and is therefore termed a 'monomaceral'. The density range for the maceral groups and their respective macerals are known. Using this information, QEMSCAN was calibrated to detect and quantify vitrite content (Singh, 2010). QEMSCAN was then calibrated to detect and quantify vitrite content. Six different ratios of vitrite content were programmed to be analysed by QEMSCAN to compare to petrographic results. The vitrite ratio that best fit the petrographic results on a 1:1 ratio would then be used by QEMSCAN to measure vitrite (Singh, 2010).

The six different theoretical proportions (vitrite80, vitrite80+60 ,vitrite60+40 , vitrite40+20, vitrite20+10 and vitrite10+5) of vitrinite content were programmed to be analysed by QEMSCAN to compare to petrographic results (Singh, 2010). Vitrite80 was used to describe a particle that had 80-100% of the particle comprise a volume of vitrinite. Vitrite80+60 included all vitrite80 particles, as well as all particles detected by QEMSCAN to have 80-60% of each particle comprise a volume of vitrinite. Thus all size fractions were calculated (Singh, 2010).

The vitrite80+60 fraction best fit the petrographically derived vitrite due to the 1000 count time used (Figure 12). In a 1000 count spectrum, sulphur was only detected 60-80% of the time, representing its correlation to vitrite (Singh, 2010). A linear relationship indicates that the QEMSCAN derived vitrite correlated well with the petrographic results. An average vitrite density of 1.3g.cm^{-3} was assumed when calculating the proportions.

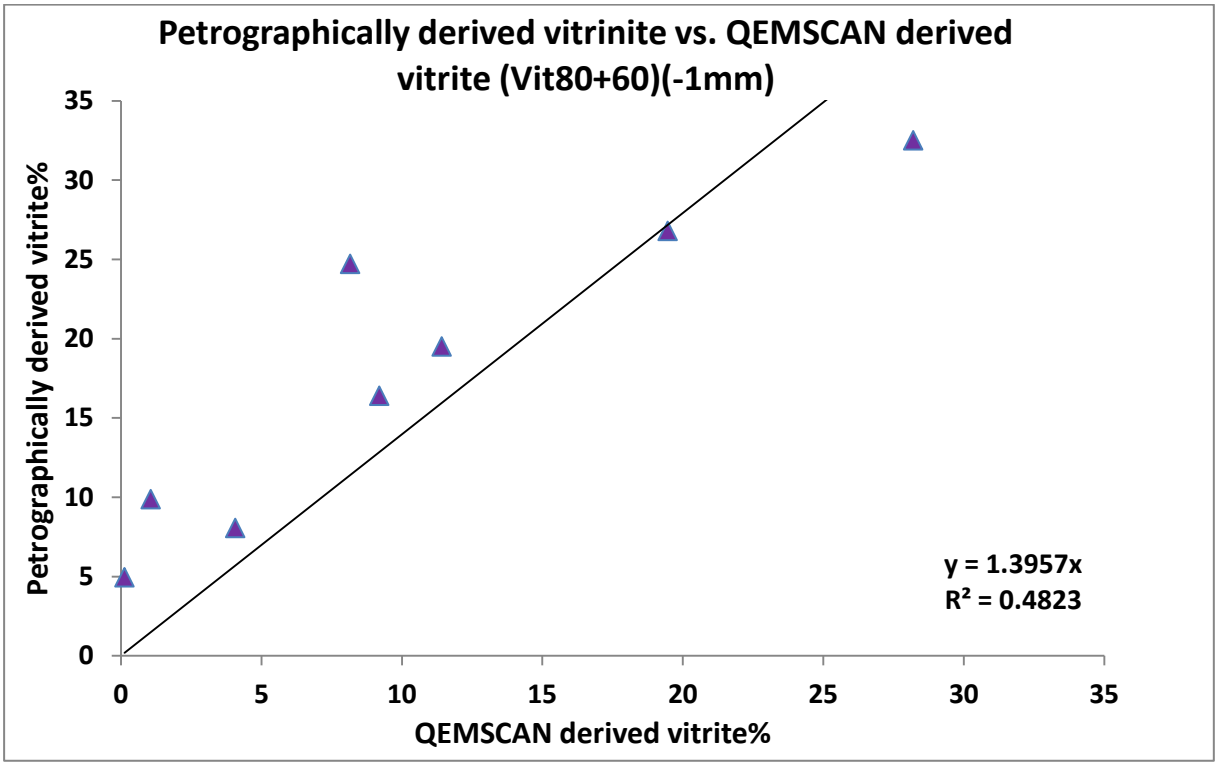

Figure 12: Petrographically derived vitrite content plotted against QEMSCAN derived vitrite (Singh, 2010)

Randomly selected coarse bright and dull particles were crushed down to 1mm, the false colour image results of which are shown in Figure13a and Figure13b. The crushed particles were analysed to validate the maceral discrimination and the QEMSCAN particle microlithotype classification (Singh, 2010).

The microlithotype categoriser developed on QEMSCAN is based on the ratio of bright to dull macerals and the proportion of mineral matter. QEMSCAN analysis confirms that the "bright" coal is predominantly "vitrinite" particles with minor kaolinite layers, calcite/dolomite cleats and included pyrite, whereas "dull" coal was predominantly carbominerite particles consisting of fine maceral and mineral matter grains (Singh, 2010). Dull coal has an inertodentrite texture. Each particle analysed in the dull coal is texturally similar. This clearly highlighted QEMSCAN's ability to characterise particles.

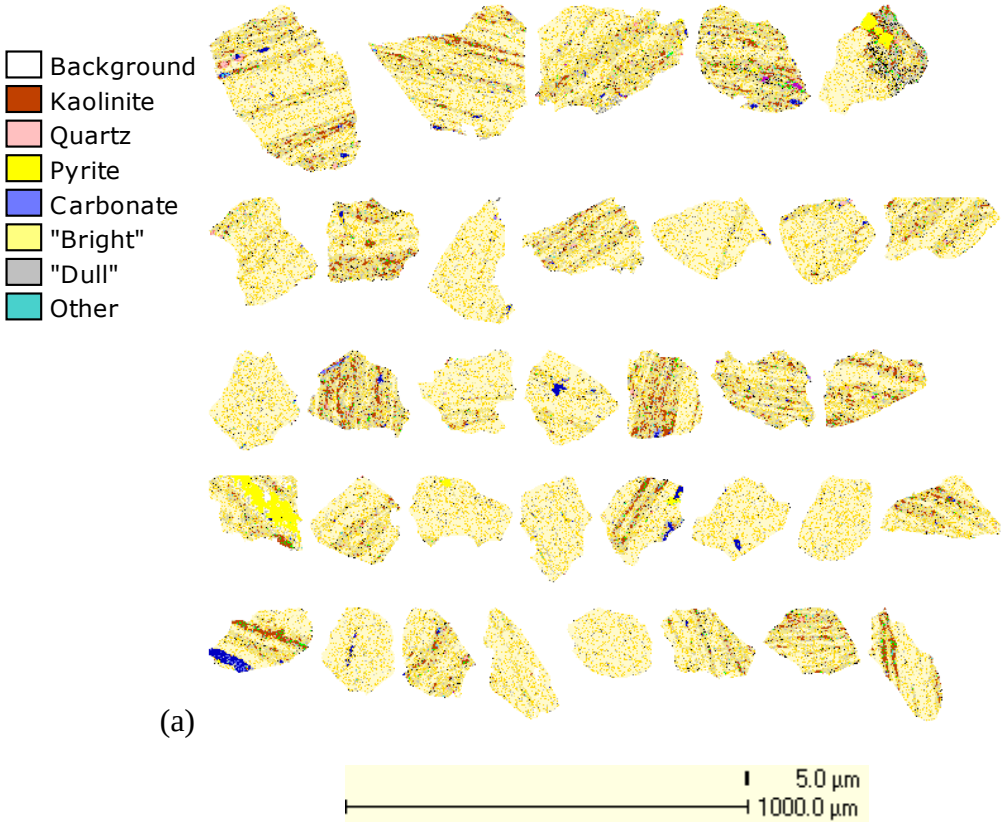

(a)

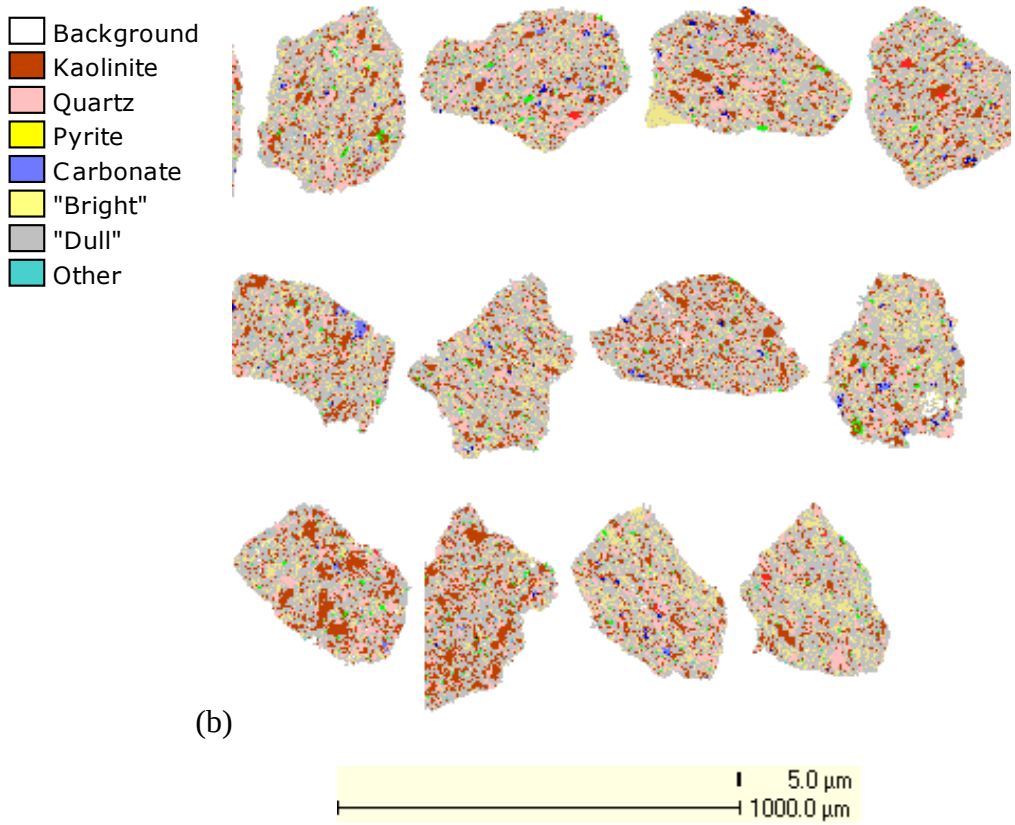

(b)

Figure 13: False colour image of bright coal (a) and dull coal (b) (Singh, 2010).

2.2.3 Maceral properties – physical and chemical characteristics

Each maceral group is defined by a set of physical and chemical characteristics (SACPS, 2011). The exact density of each maceral group is not known but an approximate range has been defined (Figure 14). Macerals are not crystalline nor do they have a fixed elemental composition. It is therefore difficult to define their elemental and physical properties (Falcon and Snyman, 1986).

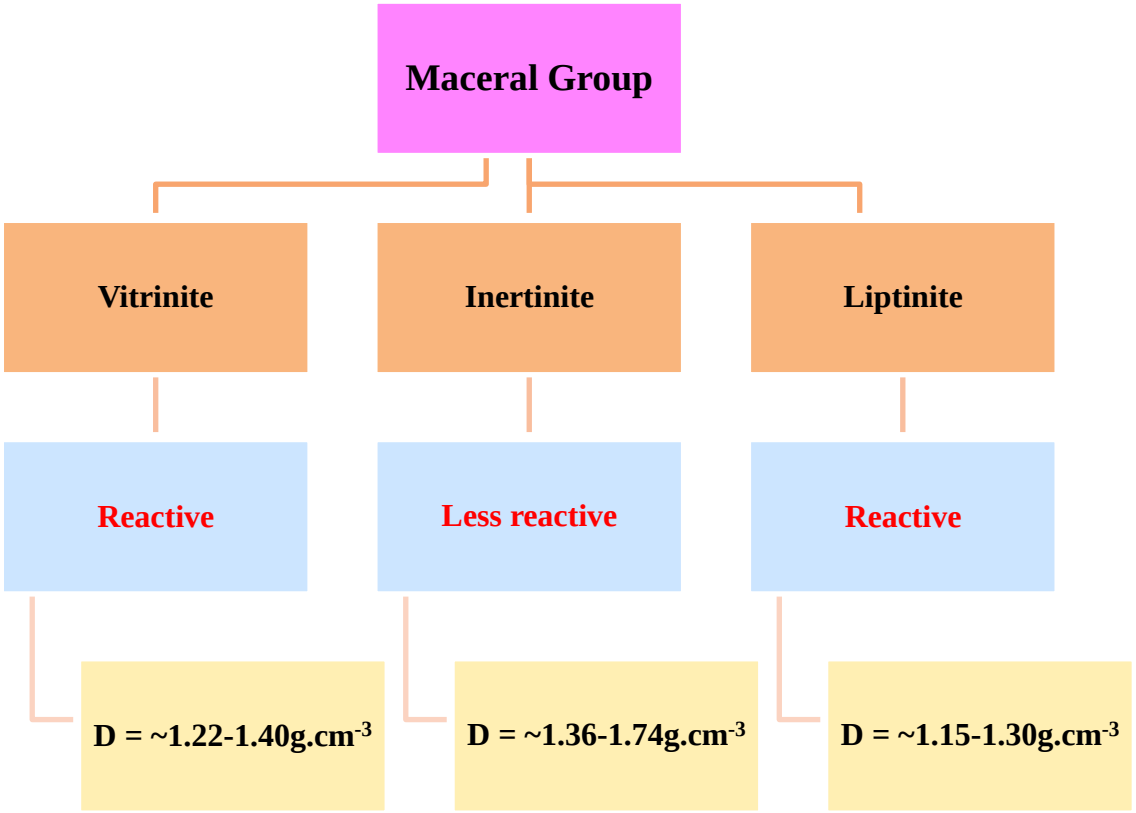

Figure 14: Density ranges for maceral groups. (Falcon and Snyman, 1986).

The maceral groups have a range of densities, ranging according to their rank, which represents the stage of maturation/metamorphosis of a coal. The rank influences the density of vitrinite, but not necessarily the density of inertinite. In addition, a coal's chemistry changes with rank. The approximate relative densities of vitrinite, inertinite and liptinite are 1.3g.cm^{-3}, 1.5g.cm^{-3} and 1.25g.cm^{-3} respectively (Figure 14). The range of each of these maceral groups present in different types of coal varies (Falcon and Snyman, 1986).

2.3 Coal washability

Float and sink analysis involves the separation of coal into different density fractions using toxic liquids. The density ranges from pure coal (~1.2g.cm^{-3}) to the density of minerals associated with coal (Speight, 2005). Float and sink analyses are used for determining washability characteristics of a coal, to evaluate the efficiency of separators and for plant control (SACPS, 2011).

Density is the measure of the mass per unit volume of a material, measured in grams per cubic centimetre (g.cm^{-3}). The relative density (RD), or specific gravity of a material is the density of a material, divided by the density of water. RD has no units because it is a ratio of how many more times dense a material is than water. Since the density of water is 1.0g.cm^{-3}, the RD is numerically the same as its density (SACPS, 2011).

Carbon tetrachloride (CCl_4) is commonly used as an organic liquid for float and sink analysis, which has a density of ~1.6g.cm^{-3}. Due to the toxicity of carbon tetrachloride and its vapours, perchloroethylene is an acceptable replacement as it has a density of ~1.62g.cm^{-3}. Perchloroethylene can be diluted with benzene to obtain lower densities or bromoform can be used to achieve higher densities (SACPS, 2011). Even higher densities are reached in other industries by utilizing methyl iodide (3.31g.cm^{-3}) and clerici (3.8 - 4.25g.cm^{-3}) (Galvin, 2006). Organic liquids are used for finer size fractions due to their low viscosity, low volatility and non-reactivity to shale (SANS7936, 2010).

Other common organic liquids used for float and sink testing include white spirit, lead free petroleum spirit, toluene, acetylene tetrabromide, perchloroethylene, o-xylene, m-xylene, p-xylene and certigrav (SACPS, 2011)(SANS7936, 2010). Using organic liquids as a separating medium is expensive but preferred over aqueous solutions as the products are easier to deal with and the process of washing and drying products are unnecessary due to the solvents being highly volatile (SANS7936, 2010). It is important that the organic solutions do not react with or alter the coal sample in any way, although particle contamination commonly occurs due to chlorine absorption (Speight, 2005).

The floats are separated out and dried, while the sink is subjected to immersion in a separating liquid with higher density. The process is continued until a range of float fractions and a sink fraction are obtained. The final sink fraction is the material that sinks in the highest density liquid available. If the equipment is situated indoors, such as in a laboratory environment, it is essential that a fume extraction system be present above the tanks to extract the toxic fumes (Galvin, 2006).

In each density fraction, the particles are separated according to the density per particle. The lowest density particles contain the least ash and highest calorific value (CV), while as the density increases, ash increases and CV decreases. Washability curves illustrate the relationship between ash content and the quantity of the float or sink generated per density fraction (SACPS, 2011).

A full set of washability curves can be determined if the ash% is acquired for each density fraction (SANS, 2010). Sulphur content and calorific values can also be assessed, recorded and presented in washability curves (SANS, 2010). Washability curves plot density, yield% and ash% against each other in order to establish float, sink, characteristic ash and yield gravity curves (Speight, 2005). By close study of the washability curves, the coal can be beneficiated in the most profitable way (SACPS, 2011). Washability curve analysis can be used to interpret plant efficiency, reserve estimation, daily plant control, determination of plant design and for determining the potential recovery and quality of coal reserves (Speight, 2005). The washability curves for each coal size range for this project is included in Appendix D.

2.4 Alternative solutions

2.4.1 Inorganic solutions

Traditional float and sink analysis involves density separation of material in an organic liquid. Inorganic solutions provide an alternate density separation medium, but the technique involving the separation of material in a medium of known density is the same. Aqueous salt solutions (e.g., calcium chloride, zinc chloride, sodium metatungstate) have a higher density than water, allowing for them to be a possible nontoxic alternative to toxic organic liquids (Galvin, 2006). Care is taken not to use salt solutions with sample that easily disintegrates in water i.e. weathered coal (SANS7936, 2010). Particle breakdown commonly occurs with water-based systems, allowing clays to break down to smaller particles (Galvin, 2006).

A salt solution such as zinc chloride is usually used for large scale work and has a density range of ~1.3g.cm^{-3} to ~1.75g.cm^{-3} (SACPS, 2011). Salt solutions have high viscosities and this becomes a problem for small particle sizes as particle settling velocity will decrease (Galvin, 2006). The high viscosity solution requires that smaller particles, thus particles with larger surface area, be in contact with the liquid for a longer period to ensure adequate liquid-uptake (Galvin, 2006). The results will be sensitive to particle size and the residence time of particles in the liquid (Galvin, 2006).

Aqueous salt solutions require that the solution be washed from the recovered density fraction before the fractions are dried (Galvin, 2006). Most salts are expensive and need to be recovered from the washed solids using a counter current washing operation (Galvin, 2006). Zinc chloride presents contamination issues (salt dries in pores) due to the high concentrations required and should not be used on coal that is being analysed for its chlorine content (SACPS, 2011). If zinc chloride is used, it is integral that the density fractions be rinsed thoroughly and air-dried in an open space (SACPS, 2011).

The coal ash comparison may be compromised due to coal reacting with the salt solution as exchange of and adsorption of ions takes place (Galvin, 2006). Salt solutions require periodic

filtering for dispersed clays (Galvin, 2006). Solution recovery and periodic cleaning make this a costly washing procedure (Galvin, 2006). Zinc chloride is corrosive, penetrates coal (SACPS, 2011) and should not be allowed to touch the skin (SANS7936, 2010). The disposal of zinc chloride is an environmental hazard (SACPS, 2011).

Caesium formate solutions overcome both the toxicity issues associated with organic liquids and the high viscosities of salt solutions. It is possible to generate densities of 1.1g.cm^{-3} - 2.2g.cm^{-3} with viscosities similar to organic liquids, allowing for similar separation times. Absorption increases as particle size decreases, but the final results are not adversely affected. Although caesium formate is expensive, recovery is good. Potassium formate solutions have a higher viscosity that that of caesium formate, but it is a tenth the cost (Galvin, 2006).

A mix of potassium and caesium formate solutions has the advantage of an acceptable lowered viscosity but the disadvantages include a complex recovery process and lower maximum density. Tungstate solutions such as sodium polytungstate (sodium metatungstate) and lithium metatungstate (LMT) are an alternative to organic liquids, although they are expensive and unsuitable for commercial use. The formate and tungstate solutions avoid particle dispersion as predominant with salt solutions (Galvin, 2006).

2.4.2 Suspensions

Suspensions provide an alternate density separation medium, but the technique involving the separation of material in a medium of known density is the same as traditional float and sink analysis. Solids in aqueous suspension may be used to create a stable suspension with low viscosity if the solid is an insoluble material and the correct particle size distribution is used (SANS7936, 2010). A suspension is created by dispersing fine particles in a liquid medium, usually water (Galvin, 2006). For relatively dense particles, the density of the system increases as per equation 1 (Galvin, 2006):

$$\rho_s = \rho(1 - \phi) + \rho_p\phi \qquad (1)$$

Where:

ρ_s = *density of suspension (g.cm^{-3})*

ρ = *density of liquid (g.cm^{-3})*

ρ_p = *density of the particles and (g.cm^{-3}),*

ϕ = *volume fraction of solids (cm^3).*

Particles with a higher density than the suspension settle to form a dense layer of sediment on the bottom of the tank. Settling velocity is calculated per particle with a unique size and density. If fine particles are used, the settling rate decreases in agreement with Stoke's Law as per equation 2 (Galvin, 2006):

$U_T = \Delta\rho g D2/18\mu$ (2)

Where:

U_T = *settling rate (mm.s^{-1})*

$\Delta\rho$ = *density difference between particles and the fluid (g.cm^{-3})*

g = *gravitational acceleration (m.s^{-2})*

D = *diameter of particle (m) and,*

μ = *viscosity (kg.ms).*

As particle size decreases, the surface area/surface energy increases, leading to aggregation of particles forming larger, less stable particles that will settle at a higher rate. Adjusting the surface charge utilizing a pH adjustment corrects for agglomeration as it forces the particles to repel each other, and stability is once again achieved. Aggregation is determined by the field of colloidal stability. Aggregation increases as the volume of the solid increases, due to the increased number of collisions. The use of high density particles to prepare a suspension allows for a minimum volume fraction of solids and therefore minimum aggregation (Galvin, 2006).

Suitable solids for aqueous suspensions include finely ground shale, froth floatation tailings, hematite, magnetite and ferrosilicon (SANS7936, 2010). Solids may be mixed and bentonite added to stabilize the suspension (SANS7936, 2010). Aqueous solutions require constant mixing to maintain mixture homogeneity and to prevent settling (SANS7936, 2010). Hematite suspensions form very dense sediments that are difficult to re-suspend (Galvin, 2006). Hematite suspensions are opaque, making it difficult to see if a separation has been made (Galvin, 2006). The resulting required washing of the hematite from the coal leads to clay breakdown (Galvin, 2006).

The Erickson Cone has an open cylinder connected to a lower conical vessel and a screen in between a support and sink fraction. The suspension medium is carefully pumped into the conical opening and then to the cylindrical bath to allow the suspension of fine material in the medium. The second vessel collects the medium and overflow floats. The density of the medium can be increased by the addition of high density particles or decreased by diluting with water. The separation density is higher than the suspension density due to the medium being pumped up the vessel. Density tracers are used to establish separation density. If the medium comprises magnetic particles, a magnetic separator is needed to remove particles (Galvin, 2006).

Magnetized suspensions such as the use of a ferrofluid consist of 10nm magnetite particles and surfactant (water or kerosene) is added to stabilize the solution (Galvin, 2006). The particles remain in suspension due to thermal energies being higher than that of sedimentation energies (Galvin, 2006). Magnetised ferrofluids subjected to a magnetic field gradient allows

for an increase in effective weight of the fluid per unit volume (Galvin, 2006). As a result, a nonmagnetic particle present in the fluid will experience substantial effective buoyancy force and will float, even though the particle density is higher than the fluid density (Galvin, 2006). The Ferro Hydrostatic Separator (FHS) produced by De Beers, utilizes magnetic suspensions (Galvin, 2006). Magnetic separation has proven to work for high density material such as diamonds, but little work has been conducted on coal (Galvin, 2006). Solids in suspensions are non-toxic and non-volatile (SANS7936, 2010). Generally, suspensions should not be used on size fractions less than 4mm (SANS7936, 2010).

2.4.3 Autogenous separations

Autogenous separations occur when the particles undergoing separation achieve a suspension density. A suspended state is accomplished by water fluidization, allowing minimal mixing and even segregation of the particles. Autogenous separation is the principle on which the Teetered Bed Separator and jigs operate. Autogenous fluidization does not achieve density separation fractions as current float and sink analysis achieves. Instead, the density fractions are inconsistent and are indicative of the density distribution of the material. A continuous mathematical function is employed to relate the cumulative yield to the separation density, and the cumulative yield to the cumulative ash. A set of yields and ash values can then be calculated for specific density fractions by interpolation (Galvin, 2006).

2.4.4 Water fluidization and jigging

A water fluidization column technique was first developed by Galvin and Pratten (1999) for a narrow size range. Ash-yield relationships were investigated in later papers by Callen et al. (2002) and Callen et al. (2008) as discussed below. Galvin and Pratten (1999) demonstrate that the density distribution of a coal sample could either be obtained by fluidising narrow particle size ranges or fluidizing a broad size range and the subsamples sized into smaller fractions for analysis. The latter technique is a simplified analytical technique that generates washability data by water fluidization and was later further enhanced by Callen et al. (2002), to generate washability data for a broader size range of coal and associated mineral impurities (-4+0.045mm). Particle segregation is independent of whether the input material is sized into smaller size fractions or when fluidizing a broad size range (Callen et al., 2002). The study derived yield-ash data for a variety of Australian coal samples to validate the robustness and accuracy of the technique (Callen et al., 2008).

The study concluded fluidization to be an effective, rapid and accurate method, although inconsistencies occurred at low ash density fractions when comparing the cumulative yield-ash results to those produced by traditional float and sink analysis (Callen et al., 2002). A discrepancy was present between the yield-ash curve generated in the low ash/density region

(Callen et al., 2002). The discrepancy is due to the effects of dispersion (causing particle mixing) and corrected by means of a correction factor (Callen et al., 2002). The effects of dispersion increase when fluidization velocity increases and when suspension density decreases (Callen et al., 2002). The study was further pursued by Callen et al. (2008) to investigate alternate water-based methods for attaining the washability of coal covering -50+0.0045mm diameter particles. It is preferable to use narrow size fractions to ensure efficient density separations, but fluidizing a larger particle size range is feasible when minimal sample is available (Callen et al., 2008).

As per Callen et al., (2008) a reflux classifier was constructed from Perspex, with the vertical column connected to a channel inclined at 70° to the horizontal. The study compared the reflux classifier, Boner jig and Mintek jig to float and sink data. The inclined portion was modified to allow for five channels. An internal cycle is developed by the upward fluidization of particles into channels between the plates, while there is downward segregation of particles through the inclined plates. Particles are prevented from misplacement during segregation due to this self-recycling effect enhancing separation (Callen et al., 2008).

The reflux classifier developed in the study utilized long, closely spaced channels to generate a shear-induced lift-force. These conditions provide for low density particles to be hydraulically transported to the overflow while the high density particles separate out of the flow and slide down the inclined plates. The inclined plates are an additional separation mechanism providing density based separation. The reflux classifier and Boner jig were in better agreement with the float and sink data than the Mintek jig. The Boner Jig and Mintek MDS Jig generated data that deviated towards the low ash end of the curve due to particle dispersion (Callen et al., 2008).

The study concluded that the Boner Jig performed best for the -16+0.25mm particles, the Mintek MDS Jig for the -50+16mm fraction and the Reflux Classifier worked well for the entire -50+0.0045mm size range. Separation of particles is reliant on plate length, degree of inclination, array spacing and rate of fluidization. Generally, the reflux classifier is suitable for processing coal 2mm or less in size fraction. Additionally, an algorithm was developed to enhance accuracy of washability data produced by the Reflux Classifier. Although the reflux classifier has the advantage of analysing process streams with small quantities of misplaced particles, the disadvantages include required additional size fractionation and separation is dependent on input and handling of the operator (Callen et al., 2008).

2.4.5 Direct measurement of particle density

A direct measure of particle density is accomplished by measuring the mass and volume of a particle. The volume of a particle is established by placing it in a vessel of known volume and determining the quantity of fluid required to fill pore spaces and to fill spaces between particles. Liquid entering the pores of particles are not counted as a part of the particle,

although it is assumed that the liquid enters all the particle pores. Major errors can result due to this assumption. A gas can also be used, where a gas is injected to a set pressure to determine particle volume. The density obtained is the true particle density. Both the liquid and gas measurements are compared to calculate the pore volume and the apparent particle density for all possible conditions. Varying temperature will adversely affect the results (Galvin, 2006).

Water pycnometry requires the dry mass of the sample to be obtained, after which the sample is loaded into a vessel of known volume and filled with a fluid of known density. The liquid must thoroughly wet the particles and fill the pore spaces. The apparent density is calculated by dividing the dry mass by the volume of the solid and non-wetted pores. The apparent density value should be close to that of the true density and to that of gas pycnometry if the volume of non-wetted pores is insignificant. Apparent density relevant to coal preparation is obtained by weighing and then placing the particles in the pycnometer in the wet state (Galvin, 2006).

Errors can occur when measuring wet particles due to water existing between particles and the initial wet mass of particles would be erroneous if the surface moisture of the particles is significant. The air dried approach is preferred and the air dry apparent density is converted to the wet/in situ density. Displacement pycnometry requires a particle to be weighed in air and in water. The apparent density of a particle in a wet state weighed in air will be the same to that of a particle submerged in water in a coal preparation plant (Galvin, 2006).

Gas pycnometry allows for determination of the true particle density (to be corrected to apparent particle density to determine behaviour in a coal preparation plant) and has been commercialized by UltraSort Pty Ltd Australia. A particle range of 4-40mm is required and analysis takes place at a rate of 30 particles per minute. The device comprises of a particle feeder, weigher, pycnometer and a sorter, requiring thousands of particles to be analysed to obtain a statistically adequate data set (Galvin, 2006).

2.4.6 Washability monitor for coal

A new method investigated to determine washability uses both x-ray transmission and image processing of coal particles. The result is an automated washability monitor able to provide near real-time analysis. The particle size distribution in float and sink analysis is based on sieve analysis. Errors in sieve analysis are due to sieve meshes having inconsistent shapes, sieved particles not being uniformly equant in habit and due to larger but acicular/columnar particles passing through small mesh sizes. The new test method uses the particle volume (measuring length, width and height) rather than the sieve size to describe size distribution, serving to eradicate errors that are currently present in sieving (Bachmann et al., 2011).

The volume is determined using the principles of laser triangulation. Laser triangulation utilizes a laser projecting a focused dot onto a flat surface, after which the laser image is projected using a lens onto a detector (CCD line or position sensing device to determine distance). The lens is situated at an angle to the surface on which the dot is projected. The analysis is converted from a single dimension to two dimensions by substituting the spot laser by a line laser and the detector by a camera linked to a high-end computer (Bachmann et al., 2011).

As the coal particle moves on the conveyor belt, several height lines are recorded and the volume of each particle is summed up (Bachmann et al., 2011). A second laser is mounted on the other side of the laser to scan the other side of the particle and the data from the two cameras are correlated to eliminate/minimise errors (Bachmann et al., 2011). The mass of the material is determined using the fundamental principles of the application of x-rays (Zou et al., 2008). The density is calculated by dividing the mass by the volume of the particle (Bachmann et al., 2011). The calculation of the particle density is almost immediate, allowing for sorting of the particles using a robotic arm right after they have undergone the x-ray measurement (Bachmann et al., 2011). The washability curves, density and volume distribution of the sample can be calculated (Bachmann et al., 2011).

3. Research design

The purpose of this study is to determine if QEMSCAN analysis of coal can be used to predict the washability of a coal as determined by traditional float and sink analyses. Crushing the sample down to an acceptable size (<2mm) is required for QEMSCAN analyses. A major concern is liberation of minerals that can occur during crushing. Liberation will alter the density distribution of the particles and will therefore adversely affect the ability of QEMSCAN to determine the true particle density distribution of the original coarse size fraction.

Float and sink analysis is essentially the density distribution of particles in the coal sample on a mass basis. QEMSCAN can determine the density of individual particles and therefore can determine the mass % density distribution of a coal. If the density of a texturally homogenous coal particle is crushed, smaller particles with similar density are generated. Conversely, if a particle has many cleats or kaolinite laminae and is crushed, the smaller particles generated will have densities in a larger range (between that of coal and the cleats/minerals liberated during crushing).

The QEMSCAN categoriser uses proportions of mineral to macerals as per the original microlithotype classification system to categorise particles (Appendix A). Petrographic analysis classifies microlithotypes by the proportions of macerals and minerals present in a 50x50micron graticule microscopic observation by a petrographer. QEMSCAN classifies microlithotypes by the proportions of macerals and minerals present in individual particles analysed by the automated QEMSCAN sample analysis procedure.

Screened size fractions and its relation to liberation of particles were investigated. Figure 15 illustrates the processes and tests conducted on the original coal sample. The coal was screened into eight size fractions in preparation for float and sink analyses. Each screened fraction underwent float and sink analysis and were typically separated into eight density fractions. The 0.5+12mm and +150mm screened fractions were exceptions with five and seven density separation fractions obtained, respectively.

Float and sink density separation of coal requires the coal particles to undergo testing at a coarse size fraction of >2mm, primarily because coarse size fractions are typically the feed to coal processing plants. Additionally, smaller size fractions have a higher surface area resulting in a greater volume of organic liquid being in direct contact with the coal, therefore coarse size fractions are required because fine size fractions would be difficult to separate out of the organic liquid, wash and dry after testing. When the tested samples are dried, they are then crushed down to the size of the client's request.

QEMSCAN analysis requires samples to be crushed down to a size fraction of ≤2mm because the samples are set in Teflon moulds with a 30mm diameter. Each prepared sample block contains a representative sample with a statistically adequate number of particles available for analysis. Each float and sink fraction was crushed down to 100% passing 0.5mm, 1.0mm and

2.0mm from the original size fractions for QEMSCAN analysis and pulverised fuel (PF) is prepared to 100% passing 212 microns for chemical proximate analysis (Figure 15).

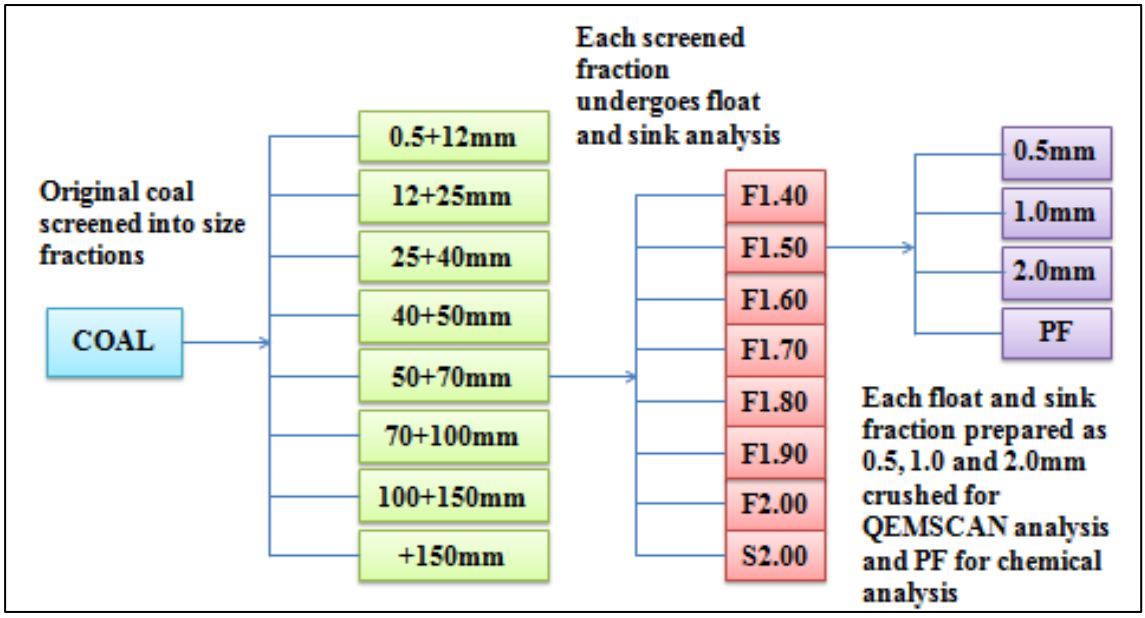

Figure 15. Analytical processes and tests conducted on the coal – each float and sink fraction was crushed down to 100% passing 0.5mm, 1mm and 2mm for QEMSCAN analysis and PF (pulverised fuel) with 100% passing 212microns for chemical analysis.

Crushing down the original size fraction allows for liberation of cleat material, finely dispersed clay and coal, as these phases serve as planes of preferential cleavage. It is presumed that coal particles preferentially cleave along calcite, dolomite and pyrite cleats, as well as parallel to the kaolinite bedding plane in the lower density fractions. For higher density fractions and sink fractions, the particles (now predominantly stone) cleave along the beds of coal. Size distribution graphs of these phases were investigated. Liberation of cleat/clay material at a smaller size range on the size distribution graph would indicate preferential cleavage planes, sizes of liberated particles, and estimations of the thickness of cleats may be made.

The QEMSCAN calculated ash was compared to the proximate analysis dry base ash percentage in order to verify QEMSCAN results (Appendix B.2). The QEMSCAN calculated ash value is determined by measuring the volume of minerals in the coal sample and converting to a mass percentage using known densities. The theoretical mass% of mineral hosted volatiles is subtracted and an assumed 2mass% ‘intrinsic ash’ is added (Figure 11).

Float and sink data was validated in two ways. The first is the mineralogically based ash density validation model that was developed using ratios of the most common macerals and minerals present in South African coal. The second is the minimum number of particles present per size fraction undergoing float and sink analysis (Appendix C).

Yields experimentally determined in float and sink analyses were generated utilizing QEMSCAN iDiscover processing software. Densities were assigned to macerals and inorganic minerals in the iDiscover software.

The densities of individual particles were calculated. The density of the particle is calculated by multiplying the relative volume proportion of minerals to macerals in the particle, to the respective mineral and maceral density. Although a prepared sample block analyses the coal and mineral particles in cross section, the 'area' of each measured mineral/maceral can be related to the volume proportion as per stereological principals. The principle of stereology relates to the interpretation of three-dimensional structures by analysing/measuring their two-dimensional structures (Appendix B).

The model generates theoretical particles by varying the volume proportion of the most common macerals to minerals. Volume proportions of vitrinite to kaolinite, vitrinite to quartz, inertinite to kaolinite and inertinite to quartz were calculated.

Densities of theoretical particles were calculated using volume percent and the relative density:

$$\rho_p = \left(\frac{v_{min}}{100}\right) \times \rho_{min} + \left(\frac{v_{mac}}{100}\right) \times \rho_{mac} \qquad (3)$$

Where,

ρ_p = *density of theoretical particle (g.cm^{-3})*

v_{min} = *volume percent of mineral in particle (vol.%)*

ρ_{min} = *density of mineral in particle (g.cm^{-3})*

v_{mac} = *volume percent of maceral in particle (vol.%)*

ρ_{mac} = *density of maceral in particle (g.cm^{-3}).*

The volume proportions were converted to mass percentages for comparison with ash values from proximate analysis (reported in mass %):

$$m_{mac} = \frac{(v_{mac} \times \rho_{mac})}{(v_{mac} \times \rho_{mac}) + (v_{min} + \rho_{min})} \times 100 \qquad (4)$$

$$m_{mac} = \frac{(v_{min} \times \rho_{min})}{(v_{mac} \times \rho_{mac}) + (v_{min} + \rho_{min})} \times 100 \qquad (5)$$

Where,

m_{mac} = *mass percent maceral in theoretical particle (g.cm^{-3})*

m_{min} = *mass percent mineral in theoretical particle (g.cm^{-3})*

v_{min} = *volume percent of mineral in particle (vol.%)*

ρ_{min} = *density of mineral in particle (g.cm^{-3})*

v_{mac} = *volume percent of maceral in particle (vol.%)*

ρ_{mac} = *density of maceral in particle (g.cm^{-3}).*

The mass proportion is used to calculate the ash content of the artificial particle. A 2% by mass intrinsic ash value is assumed for vitrinite and inertinite, while 98% mass percent organic material is assumed to have combusted. Kaolinite comprises 13.96% H_2O by mass, which is released as volatiles during combustion. Plotting the resulting calculated ashes of the theoretical particles to relative density generates a number of curves. A number of curves were generated to cover a variety of coals.

The float and sink data is used to validate the model. The ash density model predicts the ash percentage range of a set particle density, as well as the density range of particles falling outside the defined ranges of the validation model for a specified ash. If the float and sink data is not within the expected modelled ranges, then the results obtained can be questioned.

The ash density validation model could alternately be created using volume proportions, but the proximate ash values would have to be converted to volume percentages for comparison. Due to the range in fly ash densities, an accurate volume may be difficult to calculate/obtain physically (and unnecessary).

In summary, QEMSCAN data can be used to calculate the mass percent density fraction distribution. This is analogous to float and sink analyses. A comparison between QEMSCAN particle density distribution relative to float and sink density distribution will indicate if QEMSCAN can be used to predict the washability of a coal. Any deviations between the QEMSCAN derived particle density distribution and float and sink density distribution is indicative of liberation, analytical errors (QEMSCAN and float and sink data) and the reliability of QEMSCAN data.

4. Methodology

The most significant aspect of empirical studies is accurate sample preparation which ensures accurate raw data (Mouton, 2006). The data set comprises of coal that had been screened into specific size fractions before undergoing float and sink analysis. Samples were prepared according to a standard sample preparation method designed for each size fraction and were analysed using QEMSCAN technology. The samples were processed electronically to obtain raw data. The pulverised fuel (PF) samples were sent for proximate analysis at the coal laboratories based at Eskom Research, Testing and Development Centre in Rosherville.

4.1 Float and sink analysis procedure

A coal is sampled and screened into specific size ranges. Float and sink analysis separates each size fraction into density fractions. The quantity of sample used for a test is related to the degree of accuracy required and is dependent on the purpose for the test. Generally a minimum of 2000 particles are required per sample in order for float and sink analysis to be carried out (SANS7936, 2010). Detailed explanations of the float and sink test procedure are included in Appendix B.

4.2 Chemical analysis – proximate analysis

The samples underwent proximate analysis, which is one of the routine analyses carried out to reveal how the coal will perform in industrial use (Ward, 1984). The proximate analysis determines the inherent moisture in the coal, the ash value (measure of inorganic matter remaining when the coal and volatiles are burned off) and the volatile matter (VM) content (Ward, 1984) (SANS17426, 2011).

The fixed carbon content is calculated by difference (Appendix B.2, SANS17426, 2011). All values for proximate analysis are reported as mass percent fractions to the nearest 0.1% (SANS17426, 2011). Proximate analysis requires that the sample be prepared to 100% --- passing 212 μm (van Alphen, 2011). Detailed explanations of the proximate analysis test procedure are included in Appendix B.

4.3 QEMSCAN sample preparation and instrument operation

Traditional float and sink analysis requires coarse size fractions (typically ≥2mm) while QEMSCAN analysis requires that the samples be crushed down to ≤2mm. The samples are split using a rotary micro-splitter to obtain a smaller quantity of sample that is representative of the entire sample received. Duplicate samples were not used due to the large quantity of samples, and thus time constraints in terms of analysis time involved in this project. The samples are then potted in carnauba wax and polished to a 3micron finish.

The standard QEMSCAN polished block of coal in carnauba wax is 30mm in diameter, and analyses are conducted on 45 fields of view, each field of view has an area of 1200 um^2. The polished samples are carbon coated to avoid the sample charging in the chamber when struck by the electron beam. The samples are loaded into the instrument, the system is calibrated and the samples are analysed. Detailed explanations of QEMSCAN sample preparation and instrument operation procedures are included in Appendix B.

5. Results

5.1 Validation of data sets: QEMSCAN data and Float and Sink data

5.1.1 QEMSCAN data validated by chemical proximate analyses.

The procedure to experimentally determine an ash value by proximate analysis is given in Appendix B.2. The QEMSCAN calculated ash value is determined by measuring the volume of minerals in the coal sample and converting to a mass percentage using known densities. The theoretical mass% of mineral hosted volatiles is subtracted and an assumed 2mass% 'intrinsic ash' is added (Figure 10).

An example would be that of kaolinite ($Al_2[Si_2O_5](OH)_4$), which comprises 13.96 mass% water (Nesse, 2000). Quartz is a form of silicon dioxide (SiO_2) and does not have a volatile component (Nesse, 2000). If 1g of quartz is combusted in a boiler, 1g of ash is produced, whereas if 1g of kaolinite is combusted, 0.86g ash is produced. The volume % data output by QEMSCAN is converted to mass % using the known densities of minerals and coal macerals.

Table 1 displays the samples received in the float and sink data set. Size fraction -12+0.5mm was only floated at 1.50, 1.80 and 2.0g.cm^{-3}, while the +150mm size fraction did not have a 1.40 float fraction. In addition, 3 samples were not present for QEMSCAN analysis as they were misplaced at the chemical laboratory (Float 1.9 and 2.0 from the -40+25mm size fraction and float 1.6 from the +150mm size fraction, highlighted in Table 1). A box plot calculation was used to determine outliers (Appendix E). Data points outside of the outer fences were regarded as outliers while data points falling between the inner and outer fence were termed 'suspected outliers' but included in the test data set.

Table 1: Data set comprising float and sink fractions available per size fraction. Missing samples are highlighted in bold font and outliers are highlighted in bold italic font.

Size fraction (mm)	Float and sink fractions
-12+0.5	F1.50, F1.80, F2.00, S2.00
-25+12	F1.40, ***F1.50, F1.60, F1.70,*** F1.80, F1.90, F2.00, S2.00
-40+25	F1.40, F1.50, F1.60, F1.70, F1.80, **F1.90, F2.00**, S2.00
-50+40	F1.40, F1.50, F1.60, F1.70, F1.80, F1.90, F2.00, S2.00
-70+50	F1.40, F1.50, F1.60, F1.70, F1.80, F1.90, F2.00, S2.00
-100+70	F1.40, F1.50, F1.60, F1.70, F1.80, F1.90, F2.00, S2.00
-150+100	***F1.40, F1.50***, F1.60, F1.70, F1.80, F1.90, F2.00, S2.00
+150	***F1.50,*** **F1.60**, F1.70, F1.80, F1.90, ***F2.00, S2.00***

Figure 16 and 17 illustrates the relationship between ash values calculated by QEMSCAN and the chemically obtained proximate ash mass %. The good relationship (linear) between these values validates QEMSCAN results. It is observed that the coarser fraction deviates slightly more from the trend than the finer fraction.

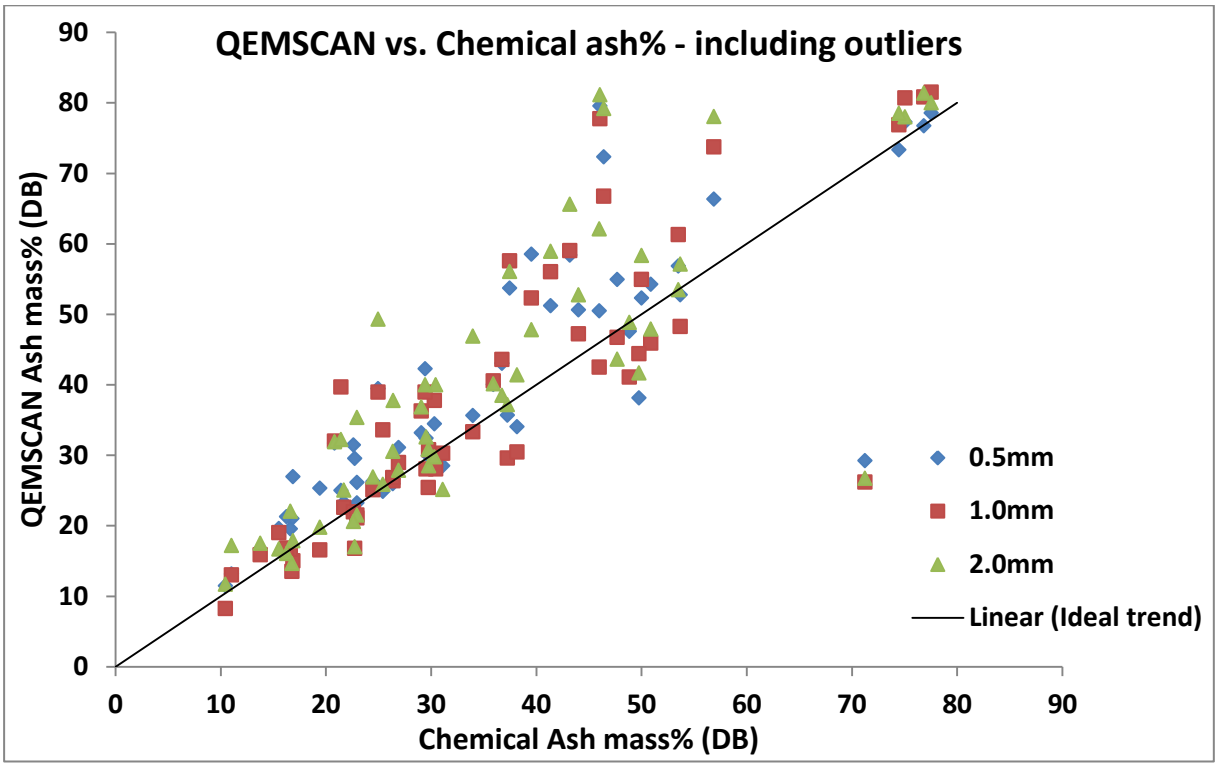

Figure 16: Ash% calculated by QEMSCAN vs. ash% determined using chemical analysis (outliers included

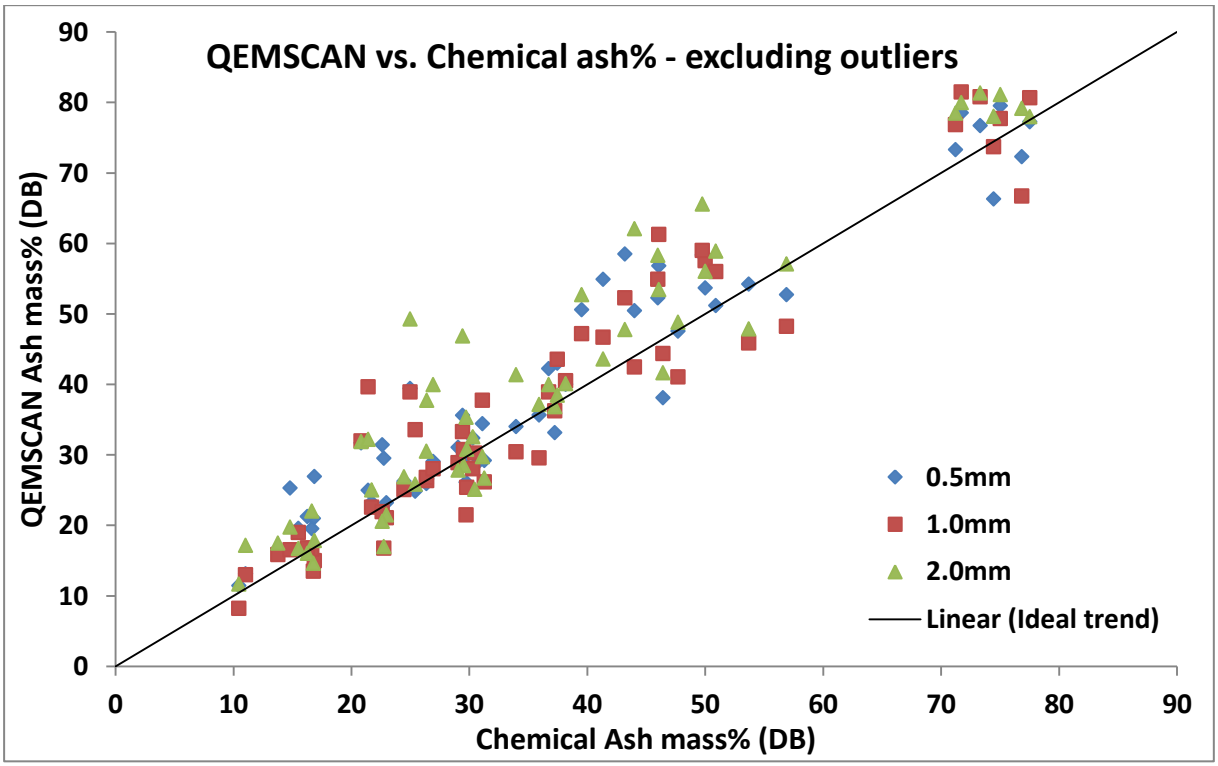

Figure 17. Ash% calculated by QEMSCAN vs. ash% determined using chemical analysis (outliers excluded as determined by box plot in Appendix E).

The coefficient of determination value (R^2) follows a linear trend more closely for the 0.5mm fraction (R^2 = 0.9215), while the 1.0mm (R^2 = 0.9027) and 2.0mm (R^2 = 0.9004) fractions

with similar R^2 values deviate more from a linear trend. This serves as an indication that variance in the data set is greater for larger size fractions.

5.1.2 Float and sink data validated by (a) minimum yield received per density fraction/size fraction and (b) mineralogical ash density based validation model

5.1.2(a) Mass received per density fraction/size fraction to undergo float and sink analysis.

The float and sink dataset was compared against both the SANS7936, 2010 and SACPS, 2011 guidelines to calculate minimum mass of sample required for float and sink analysis. The size fractions pertaining to this project were different from the general SANS guidelines, while the SACPS procedure allowed for calculation of a minimum mass of any given size range.

The SANS7936, 2010 procedure for determination of float and sink characteristics for hard coal provides a general guideline of masses per size fraction that would ensure a minimum of 2000 particles present per size fraction. The size ranges in this project varied from the ranges stipulated in the guidelines. As an absolute minimum requirement, at least 20grams and 10 particles per relative density fraction is required (SANS7936, 2010).

Table 2 displays the total mass received per density fraction of each size fraction, as well as total mass per size fraction. The floats 1.4g.cm^{-3} and 2.0g.cm^{-3} from the -150+100mm size fraction and the floats 1.5g.cm^{-3} and 2.0g.cm^{-3} from the +150mm size fraction contained less than 10 particles per relative density fraction, while all other density fractions contained more than 10 particles (Table 2).

Table 2: Mass of samples received per relative density per size fraction. Samples highlighted in bold contain less than 10 particles.

	Mass sampled (g)							
Size fraction (mm)	**-12+0.5**	**-25+12**	**-40+25**	**-50+40**	**-70+50**	**-100+70**	**-150+100**	**+150**
F1.40		1760	3080	3640	17040	15800	**780**	
F1.50	11400	2660	9860	19080	46260	57000	14740	**5900**
F1.60		5500	18080	44440	125740	182520	107120	47900
F1.70		7400	19060	50960	152260	169480	74580	54120
F1.80	21160	3100	7000	11980	31000	50020	11340	24220
F1.90		1400	3980	8360	20360	35420	15880	25620
F2.00	5160	1020	3020	6480	20400	30120	**2760**	**5580**
S2.00	19440	9220	25700	43420	145180	147600	70560	104020
Total	57160	32060	89780	188360	558240	687960	297760	267360

As a general rule from the SACPS guideline, a minimum of 1000 particles per size fraction is acceptable to conduct float and sink testing (SACPS, 2011). A calculation determining minimum sample size was established assuming that the coal is fairly closely graded and that the average relative density of the coal is 1.5g.cm^{-3} (SACPS, 2011).

The minimum mass required per size fraction is calculated as per equation 6 (SACPS, 2011):

$$M = 5.24D \quad (6)$$

Where:

M = *mass of sample (kg)*

D = *average diameter of particles (mm).*

Table 3 confirms that according to SACPS 2011 guidelines, there was insufficient sample present for reliable float and sink data for the -12+25mm, -40+25mm, -50+40mm, -150+100mm and +150mm size fractions. The total mass per size fraction is greater than the calculated minimum masses required for the -12+0.5mm, -70+50mm and -100+70mm size fractions (SACPS, 2011).

Table 3: Mass of each size fraction and minimum masses required per size fraction. Masses highlighted in bold fall short of the minimum mass as calculated by SACPS 2011 guideline.

Size fraction (mm)	-12+0.5	-25+12	-40+25	-50+40	-70+50	-100+70	-150+100	+150
Mean particle diameter (mm)	6.25	18.50	32.50	45.00	60.00	85.00	125.00	150.00
Minimum mass required (Kg)	32.75	96.94	170.30	235.80	314.40	445.40	655.00	786.00
Mass present per size fraction (Kg)	57.16	**32.06**	**89.78**	**188.36**	558.24	687.96	**297.76**	**267.36**

5.1.2(b) Mineralogical ash density based validation model

A mineralogical density validation model was developed in order to validate the results of float and sink analysis. The density of a particle is the weighted average density of the individual minerals and macerals in the particle. The weighting factor is the mass percentage proportion of the individual minerals and macerals in the particle. The ash content of the particle can be calculated by subtracting the total mass percentage of mineral derived volatiles from the total mass percentage mineral matter in the particle. The mineralogical density based ash validation model assumes that the four major components of coal are vitrinite (1.30g.cm^{-3}), inertinite (1.55g.cm^{-3}), kaolinite (2.65g.cm^{-3}), and quartz (2.65g.cm^{-3}). It is also assumed that vitrinite and inertinite have 2% intrinsic ash (Figure 10).

By varying the proportion of these four mineralogical phases, it is possible to calculate the ash content and the density of the individual particles. The model is a plot of density and calculated dry base ash for different combinations and proportions of coal and minerals in particles (Figure 18). Once developed, any float and sink data can be superimposed onto the model to determine if the float and sink results are within calculated limits. If a point falls out of the range, then either there is a problem with the float and sink data or the mineralogy of the particles contain alternate minerals other than the four main components.

A 2% ash value was assumed for both vitrinite and inertinite as both contain a small amount of intrinsic, organically bound inorganic elements (Figure 11). An ash value for each of the combinations of minerals to macerals was theoretically determined as calculated in Chapter 3: Research Design.

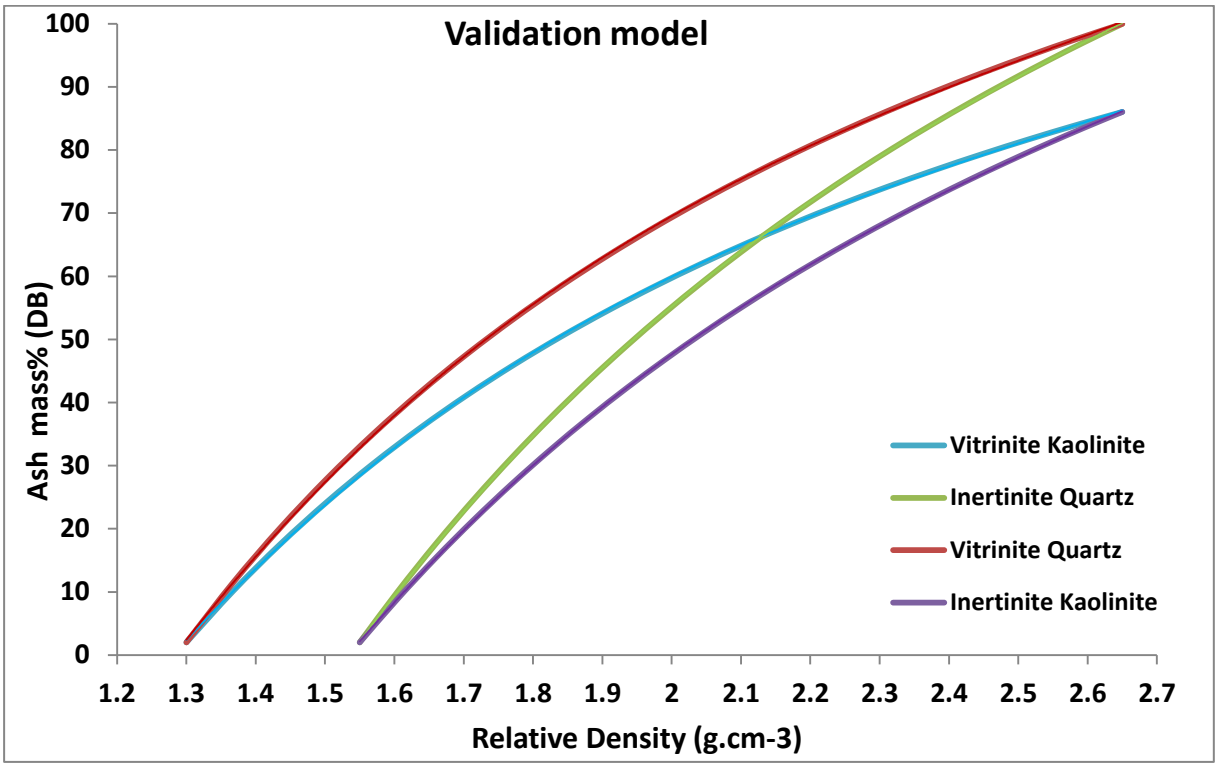

Figure 18. Mineralogical density based ash validation model.

The 1.4 float fraction was physically acquired by collecting the floating coal off an organic liquid with a density of 1.4g.cm^{-3}, resulting in the coal particles comprising the 1.4 float fraction all being less than a density of 1.4g.cm^{-3}. Similarly, the 1.5 float fraction will comprise particles of a density between 1.4 and 1.5g.cm^{-3}. For this reason, the 1.4 float fraction was allocated a density of 1.35g.cm^{-3}, the 1.5 float fraction was allocated as 1.45cm^{-3}, and so forth for preceding floats on the validation models.

The average chemical proximate ash values for the data set, the average QEMSCAN ash values for the data set (to include the average 0.5mm, 1.0mm and 2.0mm QEMSCAN analysed samples per density fraction) and historical data per relative density fraction are included with the mineralogical density validation model as per Figure 19 for comparative purposes. The historical data included in Figure 19 is an average of all washability data available to Eskom up to date.

The historical data fits the validation curve well for densities 1.35g.cm^{-3} and above. The historical data set initially follows a vitrinite/kaolinite trend in the lower density fractions (1.35-1.6g.cm^{-3}), moving towards a kaolinite/inertinite trend in the lower-to-middle (1.6-

1.8g.cm^{-3}) density fractions and shifts over to an inertinite/quartz trend at higher densities (>1.8g.cm^{-3}).

It is observed that the QEMSCAN data follows the same trend as the float and sink data. The average QEMSCAN and chemical data sets fit into the range determined by the model, except at the 1.4 float fractions, some of the 1.5 float fractions and the sink fraction. The elevated ash values at the lower density fractions are due to kaolinite laminations, while the low ash values for the sink are due to liberated coal laminations (Figure 19).

It is expected that density fractions lower than 1.6g.cm^{-3} have ash values that deviate from the model due to kaolinite occurring as laminations within bright coal. Once the sample is crushed, smaller particles with a wide range of densities are generated (illustrated in sub-chapter 5.3. Density categoriser). The range calculated for the model exclusively used the ratios of four predominant phases within coal, and does not include the cleat phases.

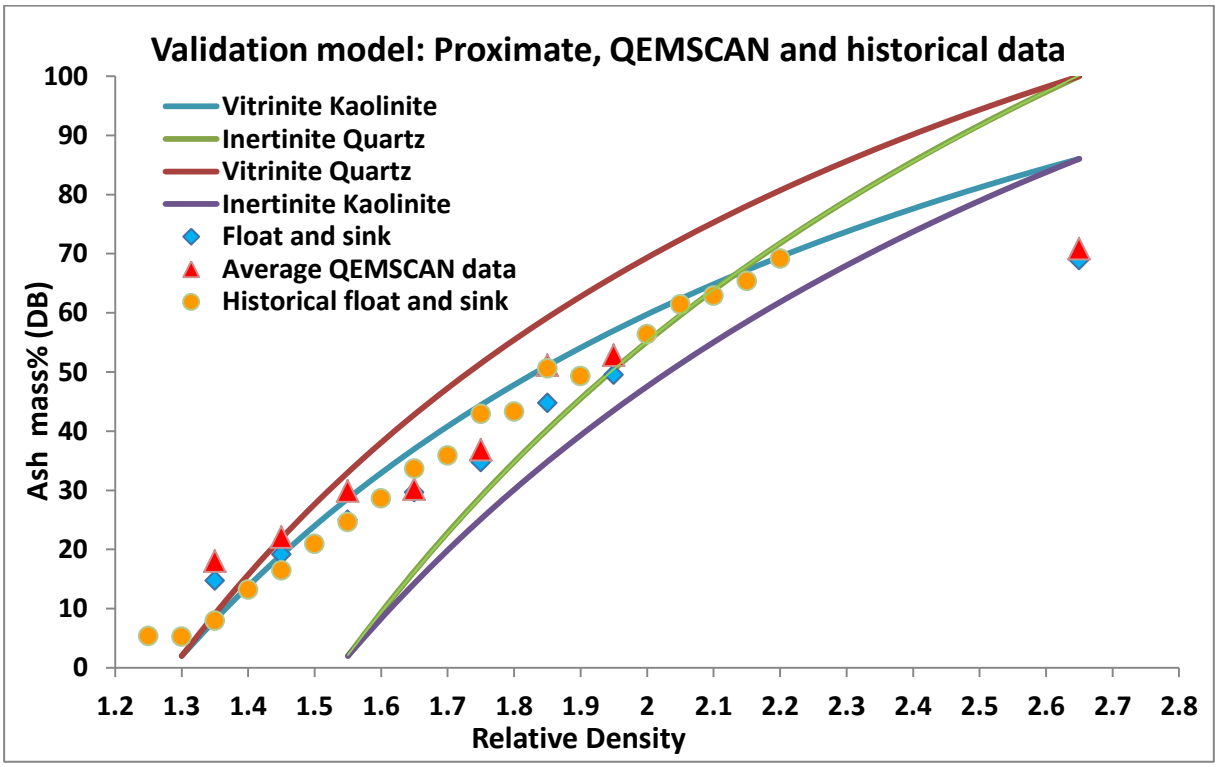

Figure 19. Mineralogical density validation model with average chemical proximate, QEMSCAN (0.5mm, 1.0mm and 2.0mm) and historical ash values.

In Figure 20, Figure 21, Figure 22 and Figure 23, “good fit” data is a reference to data points falling within the mineralogical model, while “poor fit” is a reference to data points falling outside the range as determined by the mineralogical model. Figure 20 and Table 4 shows that the float and sink data ash values acquired using proximate analysis fits the model better than the 0.5mm data (Figure 21 and Table 5), the 1.0mm data (Figure 22 and Table 6) or the 2.0mm data (Figure 23 and Table 7). As expected, the lower float fractions (1.4 and 1.5 floats) have ashes higher than predicted by the model, due to the presence of kaolinite

laminations and cleat material. The mid to higher float fractions (1.6-2.0 floats) mostly fit the model within the QEMSCAN calculated ranges for the 0.5mm, 1.0mm and 2.0mm crushed fractions.

The ash values for the 1.4 float in the -150+100mm size range and 2.0 sink from the +150mm deviate significantly from the trend of the validation model. Additionally, the 1.6 float from the -25+12mm size fraction has significantly deviated from the model for the 0.5mm, 1.0mm and 2.0mm QEMSCAN crushed samples. The 1.5 float fraction of the -150+100mm size fraction deviated significantly from the model for the 1.0mm and 2.0mm QEMSCAN crushed samples.

Both the 1.4 float from the -150+100mm size fraction and the 1.5 float from the +150mm had less than 10 particles in the size fraction, thus accuracy may have been adversely affected by poor particle statistics. Density fractions with less than 10 particles present and the 1.6 float anomaly/deviation from the -25+12mm size fractions in the 1.0mm and 2.0mm crushed samples will be investigated further in the next sub-chapter (particle characteristics).

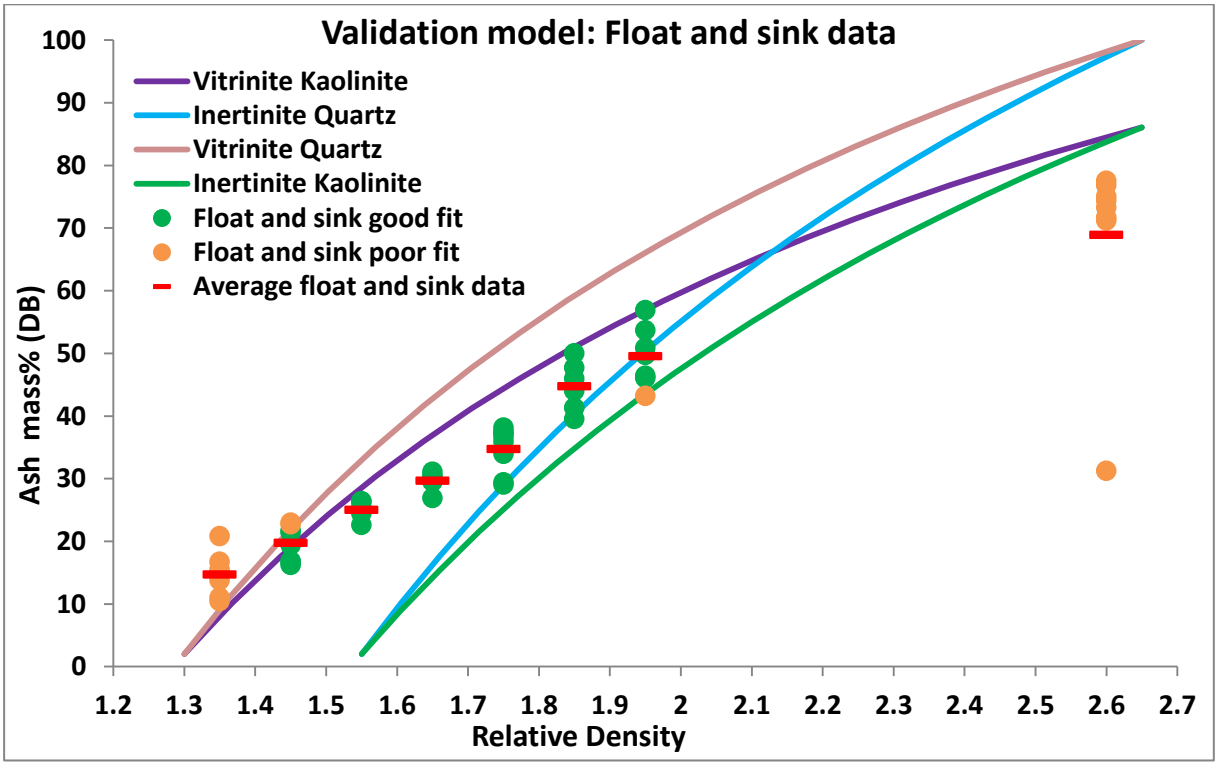

Figure 20. Mineralogical density validation model with proximate ash% for float and sink data set.

Table 4: Dry base ash% as determined by proximate analysis for the float and sink data (shaded cells indicate poorly fit data).

	-12+0.5mm	-25+12mm	-40+25mm	-50+40mm	-70+50mm	-100+70mm	-150+100mm	+150mm
	Ash% (DB)	Ash% (DB)	Ash% (DB)	Ash% (DB)	Ash% (DB)	Ash% (DB)	Ash% (DB)	Ash% (DB)
F1.40		10.45	11.03	13.78	15.52	16.77	20.83	
F1.50	19.41	16.86	16.64	16.26	22.96	21.72	22.75	21.42
F1.60		24.97	24.47	25.42	26.41	26.37	22.61	
F1.70		29.74	29.78	29.52	30.31	31.11	30.45	26.92
F1.80	29.06	37.26	35.93	38.18	33.96	29.43	36.74	37.47
F1.90		50.00		45.99	47.70	44.02	41.35	39.53
F2.00	50.89	43.20		53.69	49.77	46.06	56.89	46.43
S2.00	75.04	74.46	76.84	77.53	71.24	73.32	71.72	31.29

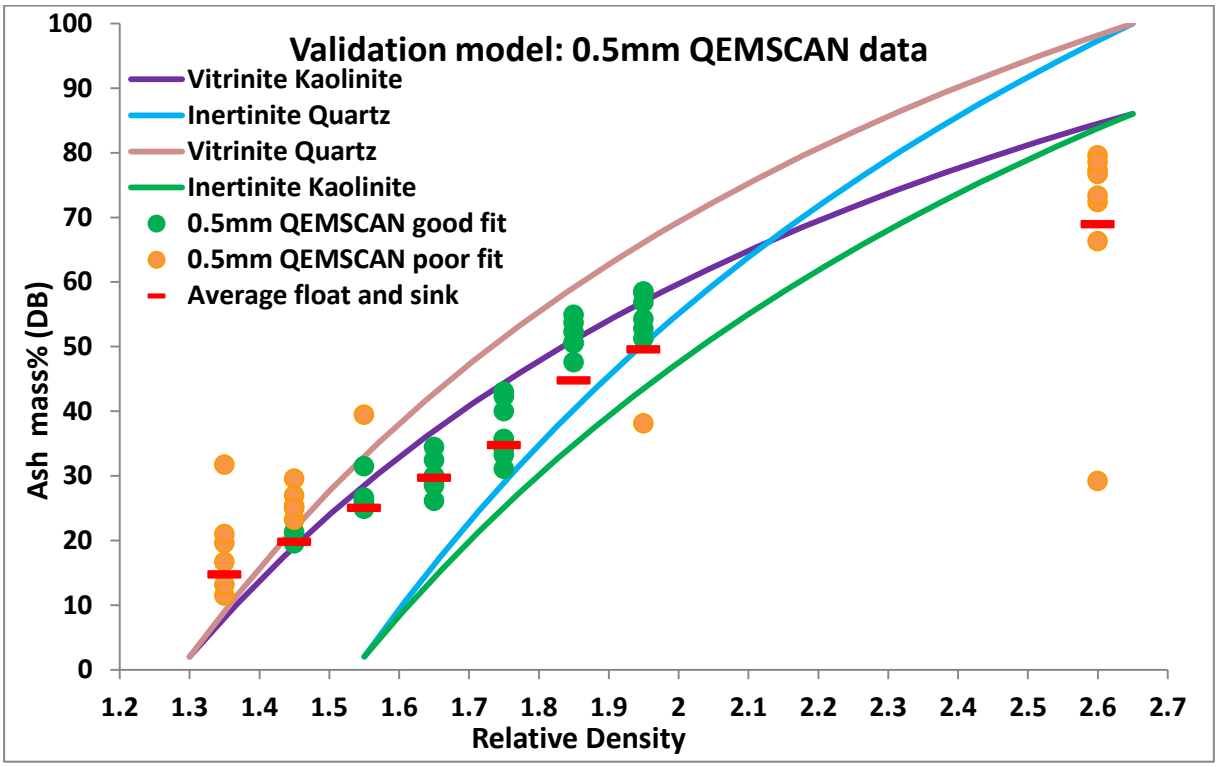

Figure 21. Mineralogical density validation model with QEMSCAN 0.5mm ash values.

Table 5: Dry base ash% as determined by QEMSCAN for the 0.5mm samples (shaded cells indicate poorly fit data).

	-12+0.5mm	-25+12mm	-40+25mm	-50+40mm	-70+50mm	-100+70mm	-150+100mm	+150mm
	Ash% (DB)	Ash% (DB)	Ash% (DB)	Ash% (DB)	Ash% (DB)	Ash% (DB)	Ash% (DB)	Ash% (DB)
F1.40		11.47	13.15	16.66	19.58	20.98	31.7	
F1.50	25.32	26.94	19.54	21.25	23.21	23.25	29.51	24.99
F1.60		39.45	26.27	24.86	26.59	25.96	31.45993	
F1.70		26.10551	29.93	30	32.39	34.42	28.4755	29.08017
F1.80	31.08	33.18	35.67	40.01	34.02	35.62	42.26371	43.00547
F1.90		53.7		52.27	47.56	50.48	54.91588	50.59166
F2.00	51.21	58.51		54.26	58.36	56.83	52.7545	38.1
S2.00	79.55	66.31	72.31	77.25	73.31	76.71	78.53802	29.2

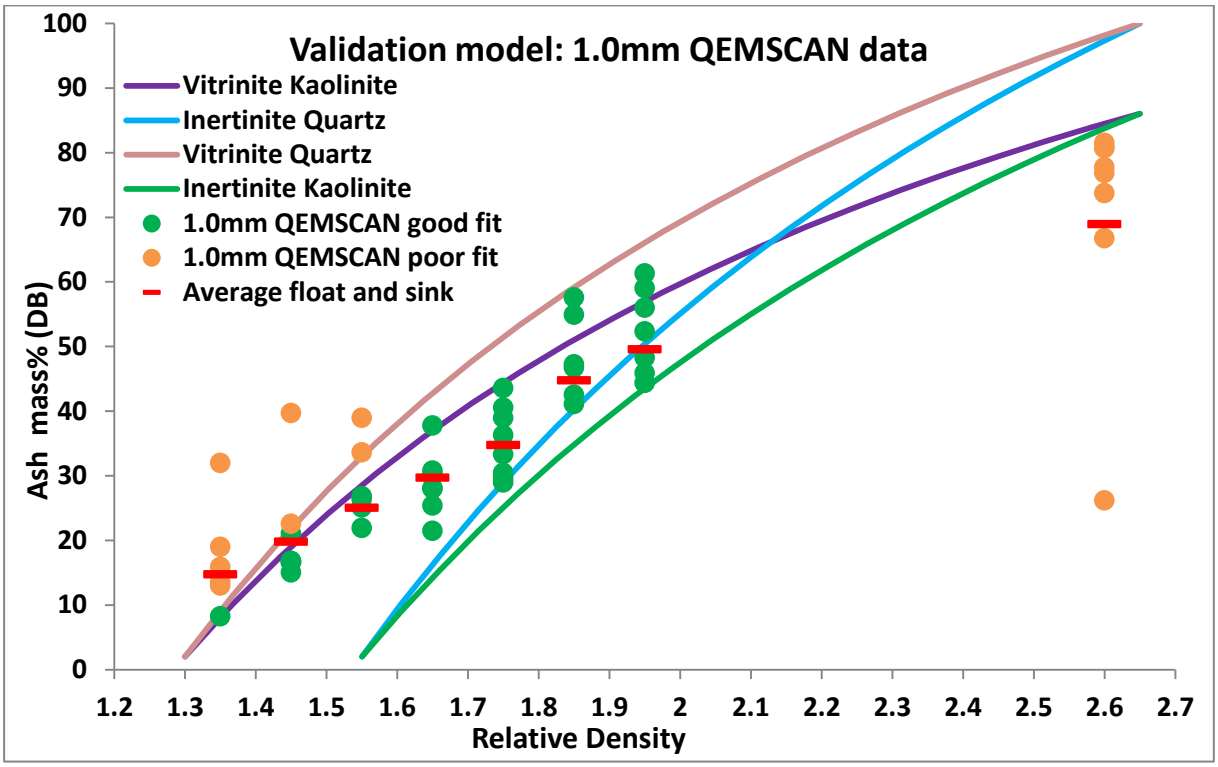

Figure 22. Mineralogical density validation model with QEMSCAN 1.0mm ash values.

Table 6: Dry base ash% as determined by QEMSCAN for the 1.0mm samples (shaded cells indicate poorly fit data).

	-12+0.5mm	-25+12mm	-40+25mm	-50+40mm	-70+50mm	-100+70mm	-150+100mm	+150mm
	Ash% (DB)	Ash% (DB)	Ash% (DB)	Ash% (DB)	Ash% (DB)	Ash% (DB)	Ash% (DB)	Ash% (DB)
F1.40		8.23	13.01	15.87	19.00	13.52	31.97	
F1.50	16.54	15.01	16.63	16.82	21.08	22.57	16.76	39.68
F1.60		38.95	25.09	33.59	26.34	26.81	21.93	
F1.70		21.47	25.39	30.77	28.02	37.77	30.26	28.04
F1.80	28.92	36.27	29.59	40.54	30.43	33.30	38.94	43.57
F1.90		57.57		54.90	41.09	42.49	46.70	47.19
F2.00	55.99	52.30		45.90	59.00	61.30	48.26	44.37
S2.00	77.73	73.71	66.73	80.66	76.86	80.81	81.50	26.16

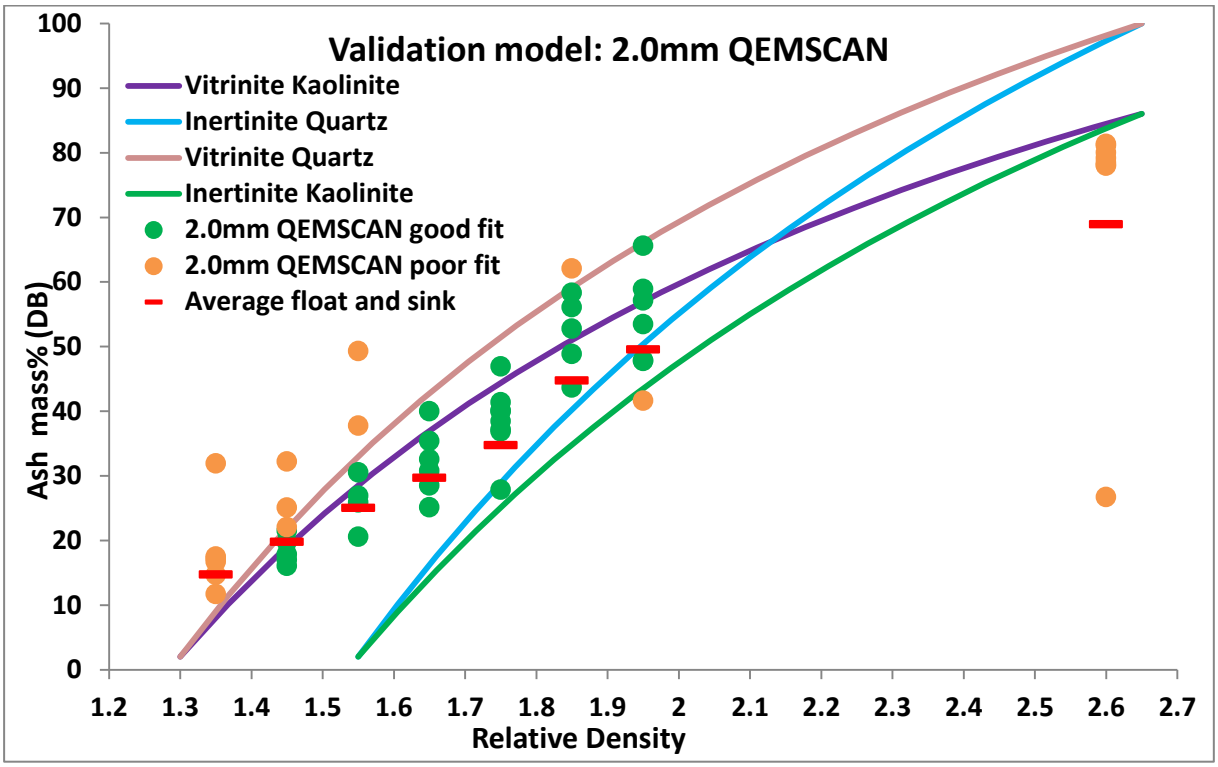

Figure 23. Mineralogical density validation model with QEMSCAN 2.0mm ash values.

Table 7: Dry base ash% as determined by QEMSCAN for the 2.0mm samples (shaded cells indicate poorly fit data).

	-12+0.5mm	-25+12mm	-40+25mm	-50+40mm	-70+50mm	-100+70mm	-150+100mm	+150mm
	Ash% (DB)	Ash% (DB)	Ash% (DB)	Ash% (DB)	Ash% (DB)	Ash% (DB)	Ash% (DB)	Ash% (DB)
F1.40		11.68	17.19	17.49	16.70	14.65	31.89	
F1.50	19.78	17.84	22.04	16.04	21.50	25.05	16.98	32.20
F1.60		49.31	26.92	25.87	37.76	30.53	20.57	
F1.70		35.36	30.79	28.48	32.56	29.77	25.12	39.96
F1.80	27.87	36.84	37.14	40.11	41.39	46.90	39.96	38.46
F1.90		56.06		58.32	48.84	62.08	43.63	52.76
F2.00	58.92	47.78		47.87	65.58	53.47	57.11	41.64
S2.00	81.12	78.05	79.18	77.99	78.49	81.36	80.00	26.71

Across the float and sink data set, the QEMSCAN acquired 0.5mm, 1.0mm and 2.0mm crushed size fractions, the range in ash per density fraction is large for the 1.4 and 1.5 float fractions, smaller for the 1.6 float fraction, smallest for the 1.7 float fraction and again larger for float fractions higher than 1.7. The ranges in ash values per density fractions are smallest for the 0.5mm samples, larger for the 1.0mm samples and largest for the 2.0mm samples. Ash values for floats 1.4, 1.5 and 1.6 deviate more from the validation model as the crushed sample particle size is increased from pulverised fuel (100% passing 212microns) used for the chemical analysis to the 0.5mm, 1.0mm and 2.0mm QEMSCAN analysis.

5.2 Particle characterization

The particle characterisation graph is unique to Eskom and represents the quantities of the most common components present in coal i.e. pyrite, carbonates, sandstone, siltstone, mudstone, carbominerite, dull and bright coal. A dull/bright particle comprises alternating bands/laminations of dull and bright coal, which would therefore have a density between that of dull and bright coal. The graph quantifies particles observed in false colour images generated by QEMSCAN. The particle characterization graph is usually used to compare coal qualities from various sources. The mineralogical proportions of particles in each float fraction, as well as liberation in each float fraction are revealed in the particle characterisation graphs.

The particle characterisation histogram is arranged to have the highest density component (pyrite and carbonate cleats) to the left of the graph, high density phases in the middle (stone) and mid-to-lowest density phases occurring on the right (carbominerite and coal). The dry based ash values are given for the samples analysed per relative density fraction. As observed from the mineralogical ash density based validation model, the ash value increases as the relative density increases (and CV decreases). The proportion of coal to mineral has a direct impact on the ash%. The proportion of coal decreases and mineral increases as relative density increases.

The dry base ash% to relative density trend is observed as a general movement of the predominant phases from the right to the left of the particle characterisation histogram as the relative density increases. The false colour images placed below each particle characterization graph are from the various size fractions from the 0.5mm crushed samples.

5.2.1 Particle characteristics – 1.4g.cm^{-3} floats

The 1.4g.cm^{-3} float fraction predominantly comprises an average of ~58.62% bright, 11.63% dull/bright and 15.67% carbominerite particles across the 0.5mm, 1.0mm and 2.0mm samples (Figure 24, Figure 25 and Figure 26). The 0.5mm sample has almost double the quantity of cleats as the 1.0mm and 2.0mm samples. This would make sense as the 0.5mm crushed fraction would liberate more cleats than the 1.0mm or 2.0mm samples.

It would be expected that the larger size fractions that have undergone float and sink tests would have a higher liberation effect than the smaller size fractions. Figure 24, Figure 25 and Figure 26 reveals that this is not the case as the liberation varying between size fractions appears somewhat random, but may be a function of particle statistics. A logical trend may emerge if a greater number of particles were analysed. Mudstone, siltstone, cleats and carbominerite are the main contributors to ash. The particle characterization plot allows for quantification of liberation phases across density fractions.

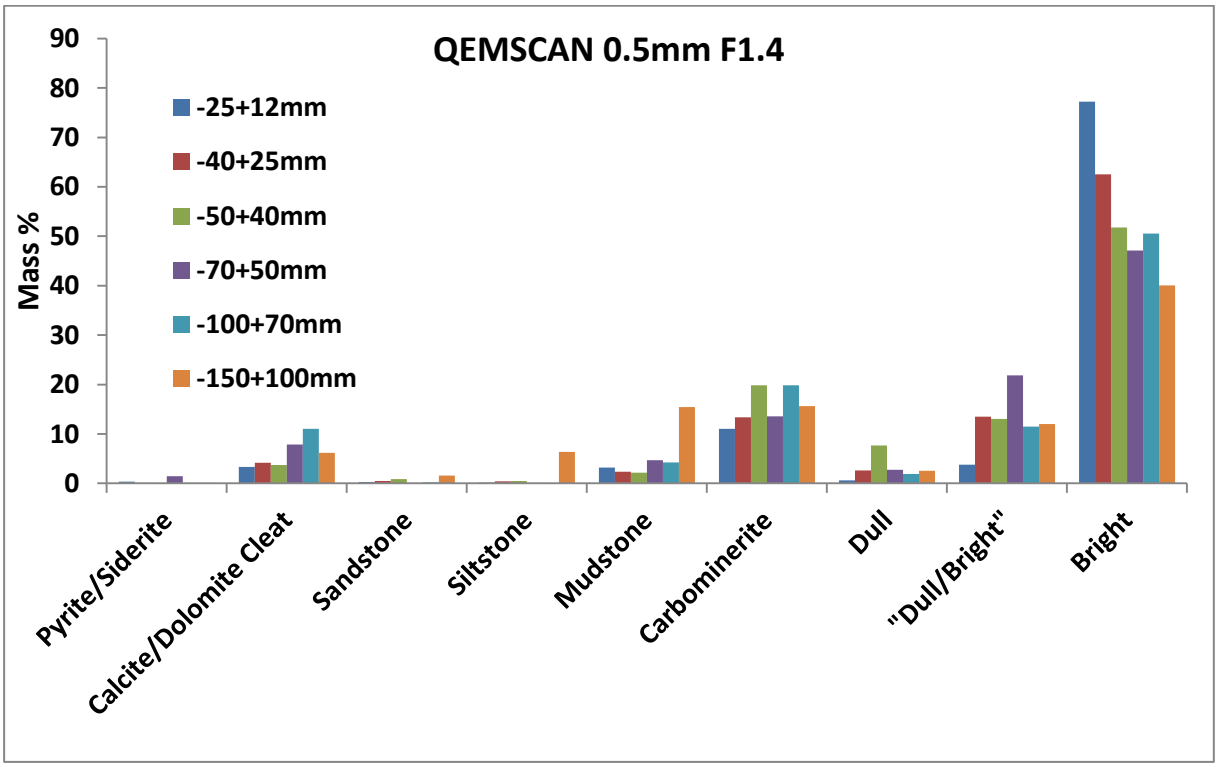

Figure 24. Particle characterisation graph for the 0.5mm crushed 1.4g.cm^{-3} float fractions.

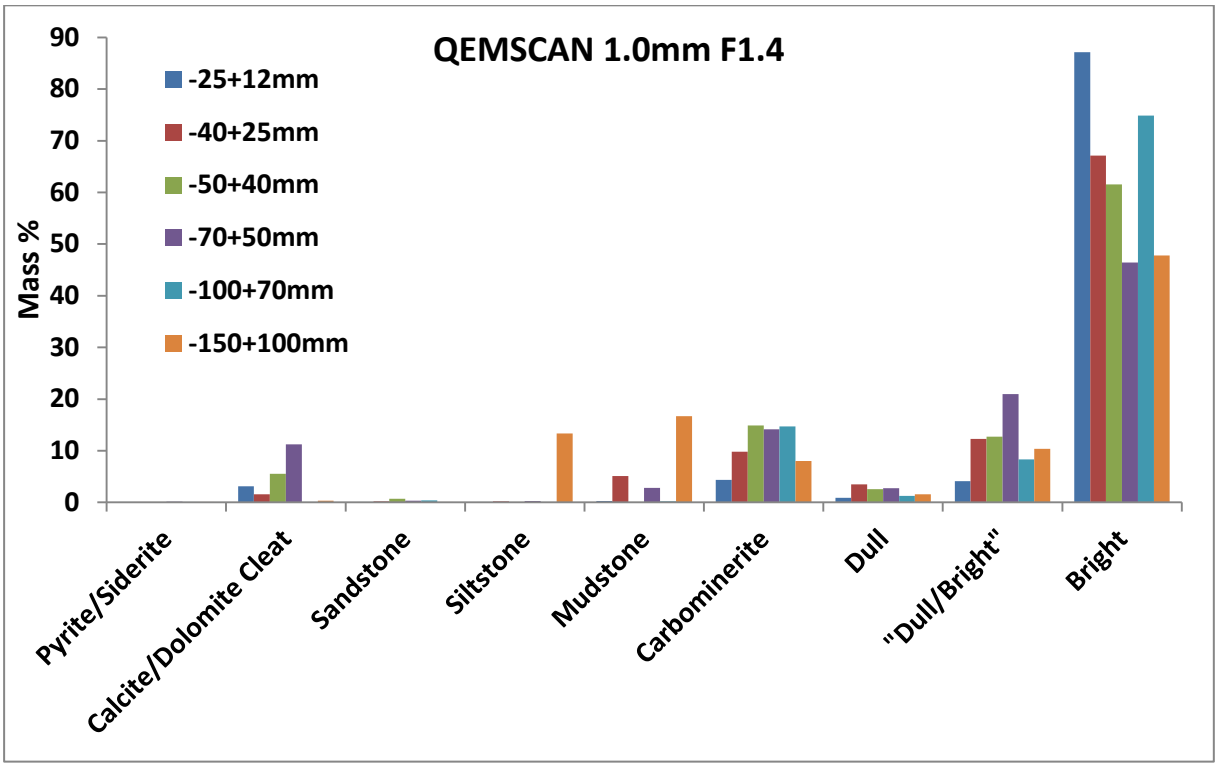

Figure 25. Particle characterisation graph for the QEMSCAN 1.0mm crushed 1.4g.cm^{-3} float fractions.

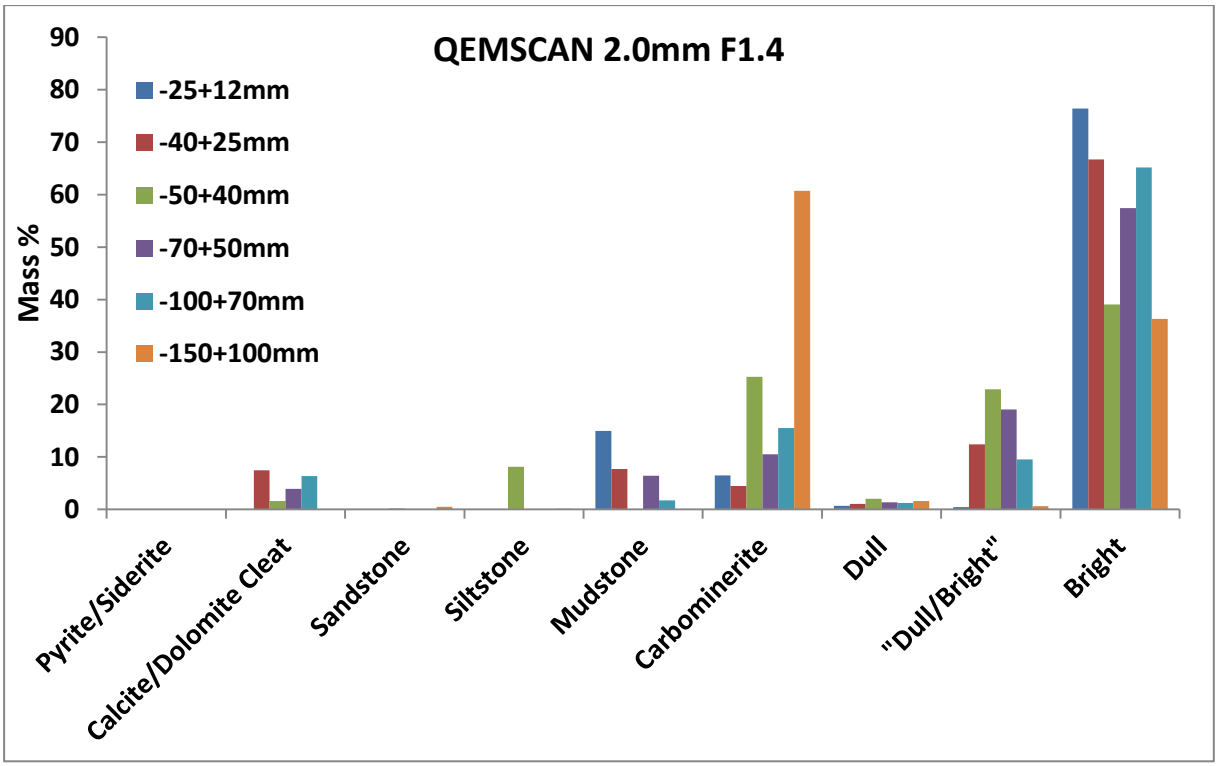

Figure 26. Particle characterisation graph for the QEMSCAN 2.0mm crushed 1.4g.cm^{-3} float fractions.

1.4g.cm^{-3} float fractions were not received for the -12+0.5mm and +150mm size fractions. The -150+100mm has an ash double the average of the other ash values (Table 8). The elevated ash is due to a lower proportion of bright and elevated mudstone and siltstone in the 0.5mm and 1.0mm samples, and a high proportion of carbominerite in the 2.0mm samples

(Figure 24, Figure 25 and Figure 26). The -150+100mm 1.4g.cm^{-3} float fraction is suspected to be an outlier because it had less than 10 particles present (poor particle statistics), it was a misfit in terms of particle characteristics and had a significantly higher ash%.

Table 8: Dry base ash % as determined by QEMSCAN analysis on the 1.4g.cm^{-3} floats across size fraction (suspected outliers highlighted in red).

Size (mm)	0.5mm ash% (DB)	1.0mm ash% (DB)	2.0mm ash% (DB)
-25+12	11.47	8.23	11.68
-40+25	13.15	13.01	17.19
-50+40	16.66	15.87	17.49
-70+50	19.58	19.00	16.70
-100+70	20.98	13.52	14.65
-150+100	31.70	31.97	31.89
Average (incl. outlier)	18.92	16.93	18.27
Average (excl. outlier)	16.37	13.93	15.54

The false colour image (Figure 27) is a representation of the proportions of the particle characterisation histogram. As expected, bright, dull/bright and carbominerite particles are predominant.

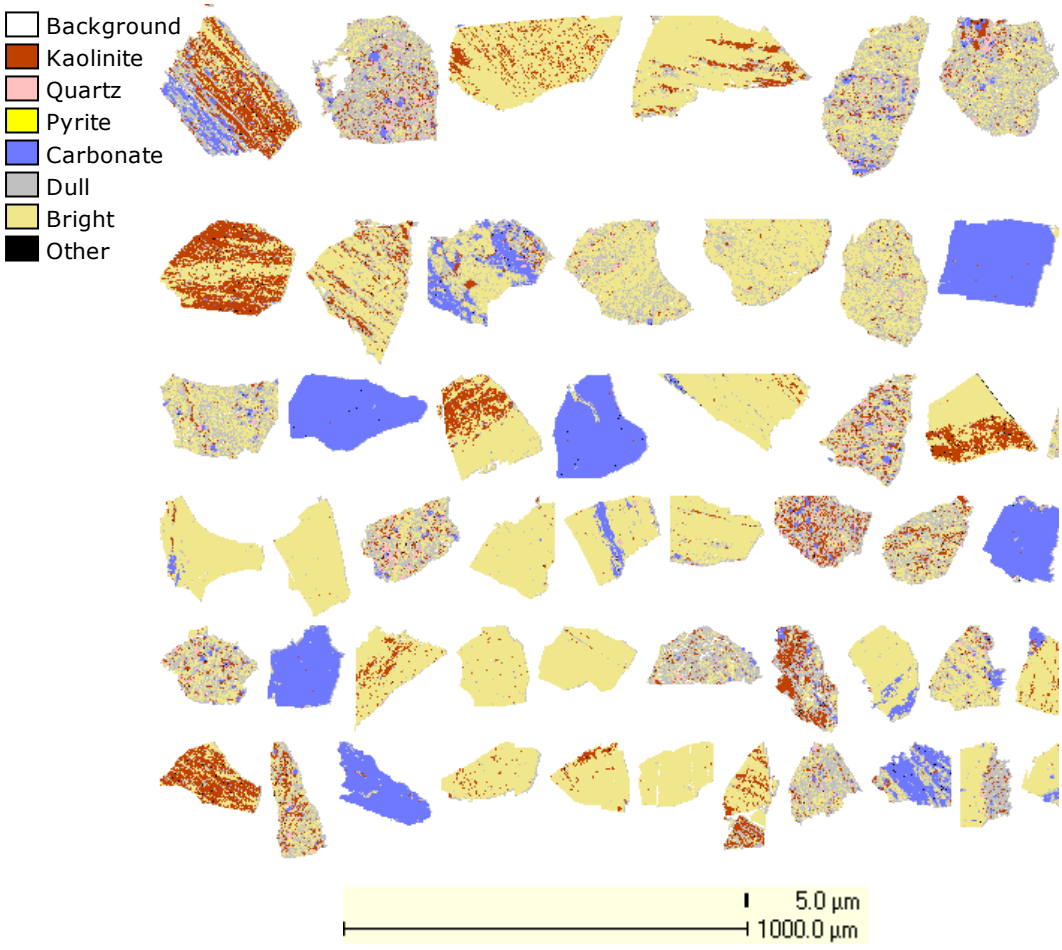

Figure 27. False colour image of particles present in the 1.4 g.cm^{-3} float fraction, -70+50mm size fraction, 0.5mm QEMSCAN sample.

As previously discussed in sub-chapter 2.2.2 (Maceral and microlithotype classification), a carbominerite particle is defined as an association of coal with a specific proportion of mineral or mineral grouping (Falcon and Snyman, 1986). Carbominerite (density range of 1.55-1.95g.cm^{-3}, Falcon and Snyman, 1986) particles commonly found in the 1.4g.cm^{-3} float of various size fractions are illustrated in Figure 28. The carbominerite in the 1.4g.cm^{-3} float is mostly carbargillite and carbankerite. Carbopolyminerite particles were only found to be abundant in the -150+100mm, 0.5mm QEMSCAN sample, which has an unusually high ash%. A couple of carbopyrite particles were found in the -70+50mm size fraction, 0.5mm QEMSCAN sample (Figure 24 and Figure 28). Carbosilicate particles were not present.

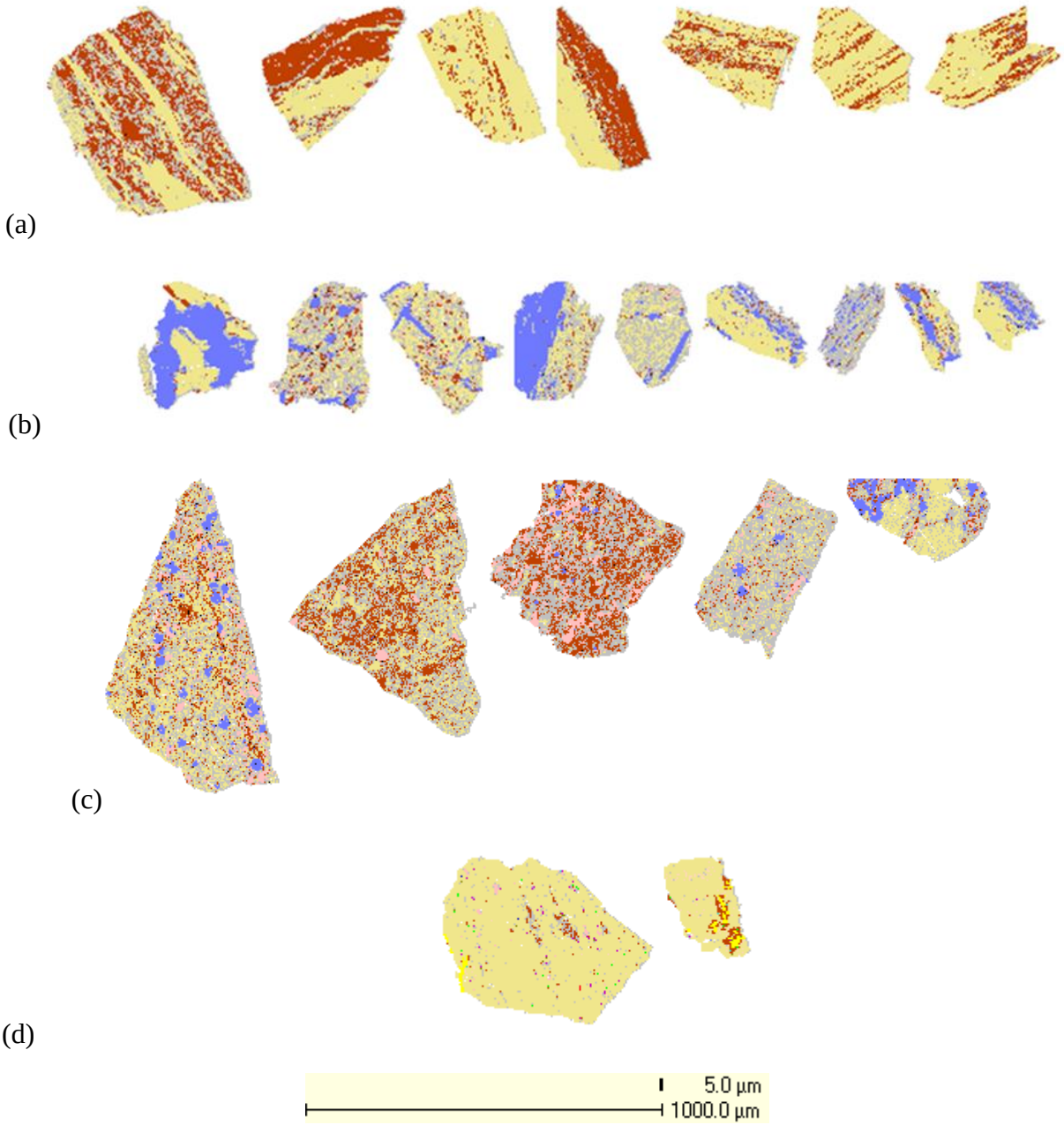

Figure 28. False colour image of various carbominerite particles of the 1.4g.cm^{-3} floats from different size fractions. (a) Carbargillite from the -25+12mm, 0.5mm QEMSCAN sample, (b) carbankerite from the -100+70mm, 0.5mm QEMSCAN sample, (c) carbopolyminerite from the -150+100mm, 0.5mm QEMSCAN sample and (d) carbopyrite from the -70+50mm, 0.5mm QEMSCAN sample.

The bright, dull/bright and some carbominerite phases have densities appropriate for the size fraction into which they were separated (≤1.4 g.cm^{-3}). However, liberated carbonate/pyrite cleat particles and mudstone particles have densities higher than 2.65g.cm^{-3}. Thin mudstone laminae and carbonate cleats are common in bright coal (Figure 28). The high proportion of mudstone particles and carbonate cleats in the 1.4 g.cm^{-3} density fraction would suggest that the cleats and lamellae act as cleavage planes during crushing and pulverisation. These cleavage planes will enhance the liberation of kaolinite and carbonate/pyrite cleat fragments.

5.2.2 Particle characteristics – 1.5g.cm^{-3} floats.

As per Figure 29, Figure 30 and Figure 31, the 1.5g.cm^{-3} density fraction has an increase in proportion of carbominerite and dull/bright particles relative to the 1.4g.cm^{-3} density fraction, which has the highest proportion of bright particles. The average bright, bright/dull and carbominerite proportions are 39.95%, 21.33% and 22.23% respectively. Carbonate cleat proportions have increased compared to the 1.4g.cm^{-3} float samples and are highest in the 1.5 floats compared to higher float/sink fractions.

The average proportions of total cleat material liberated for the 0.5mm, 1.0mm and 2.0mm were 9.97%, 4.81% and 2.67% respectively. Once again, more cleat material reporting to the finest crushed fraction (0.5mm) indicates preferential cleavage along cleat/coal boundaries. The occurrence of mudstone particles are attributed to preferential liberation along kaolinite/coal boundaries. Mudstone, cleats and carbominerite remain the predominant contributors to ash.

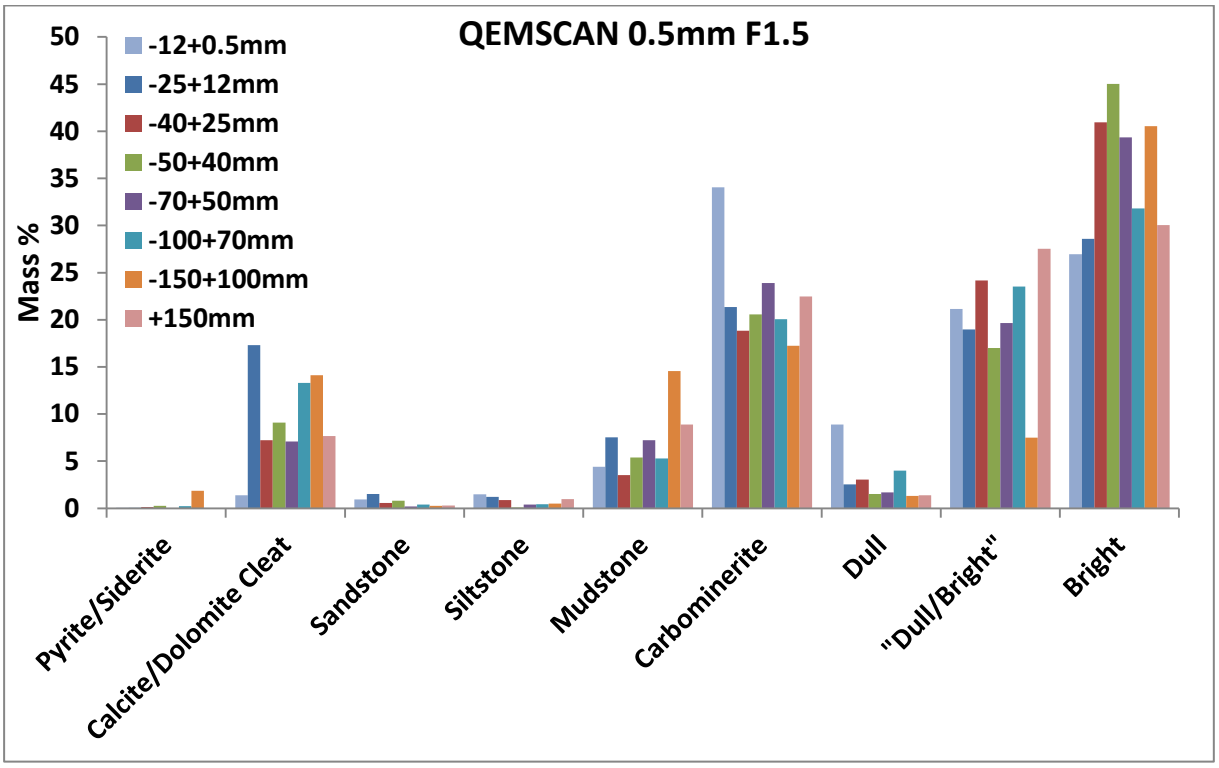

Figure 29. Particle characterisation for the QEMSCAN 0.5mm crushed 1.5g.cm^{-3} float fractions.

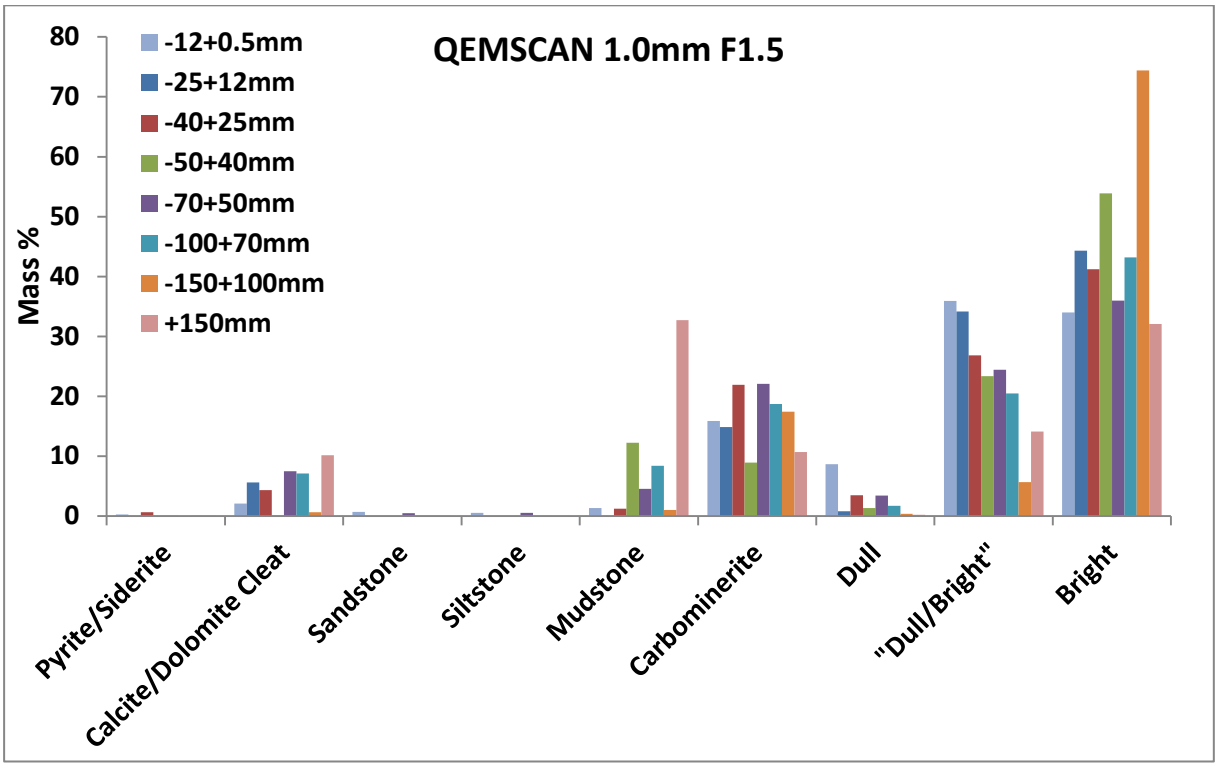

Figure 30. Particle characterisation for the QEMSCAN 1.0mm crushed 1.5g.cm^{-3} float fractions.

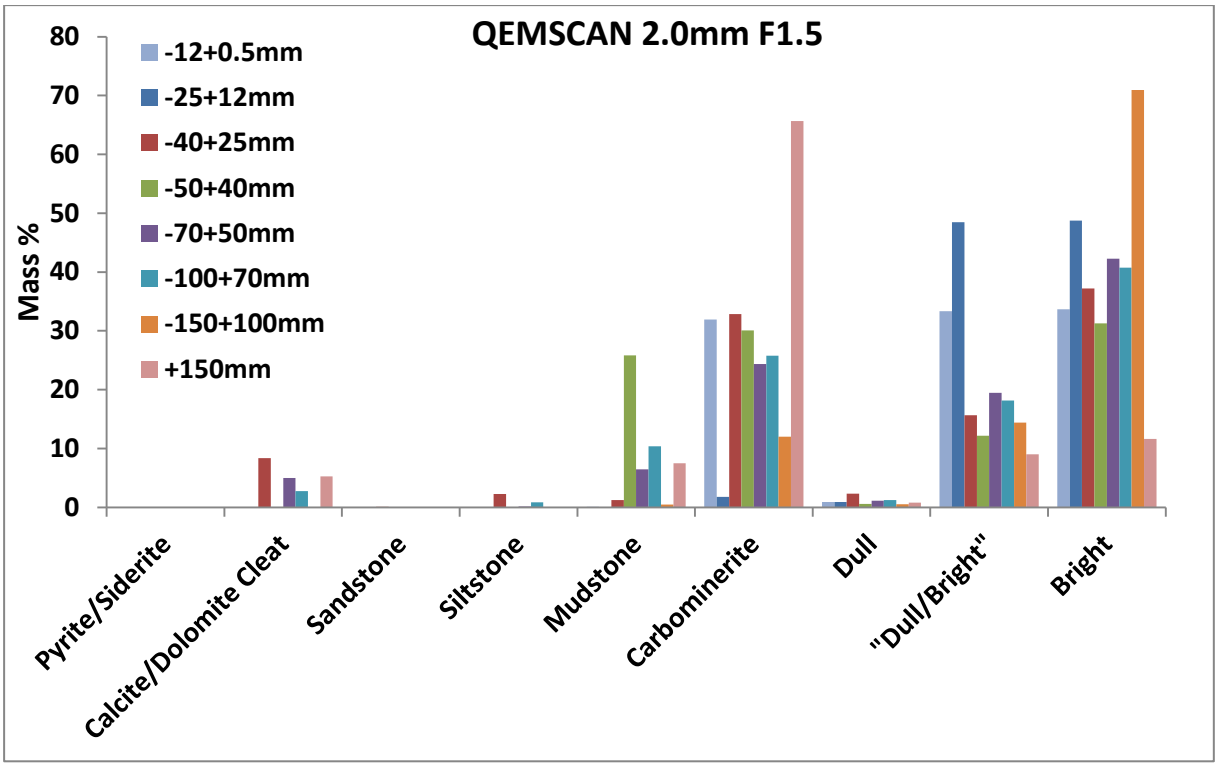

Figure 31. Particle characterisation for the QEMSCAN 2.0mm crushed 1.5g.cm^{-3} float fractions.

Particularly high mudstone (1.0mm) and carbominerite (2.0mm) proportions attribute to elevated ash values in the +150mm size fraction (Table 9).

Table 9: Dry base ash % as determined by QEMSCAN analysis on the 1.5g.cm^{-3} floats across size fractions (potential outliers highlighted in red).

Size (mm)	0.5mm ash% (DB)	1.0mm ash% (DB)	2.0mm ash% (DB)
-12+0.5	25.32	16.54	19.78
-25+12	26.94	15.01	17.84
-40+25	19.54	16.63	22.04
-50+40	21.25	16.82	16.04
-70+50	23.21	21.08	21.5
-100+70	23.25	22.57	25.05
-150+100	29.51	16.76	16.98
+150	24.99	39.68	32.2
Average (incl. outlier)	24.25	20.64	21.43
Average (excl. outlier)	24.15	17.92	19.89

The particle proportions in the false colour image (Figure 32) correspond to the particle characteristic histograms (Figure 29, Figure 30 and Figure 31). There is a decrease in proportion of bright coal particles, while dull/bright and carbominerite particles have increased. The carbominerite particles are still predominantly carbargillite, carbankerite, and carbopolyminerite, although there is more carbankerite and carbopolyminerite in the 1.5g.cm^{-3} than the 1.4g.cm^{-3} floats. Carbopyrite and carbosilicate were not present.

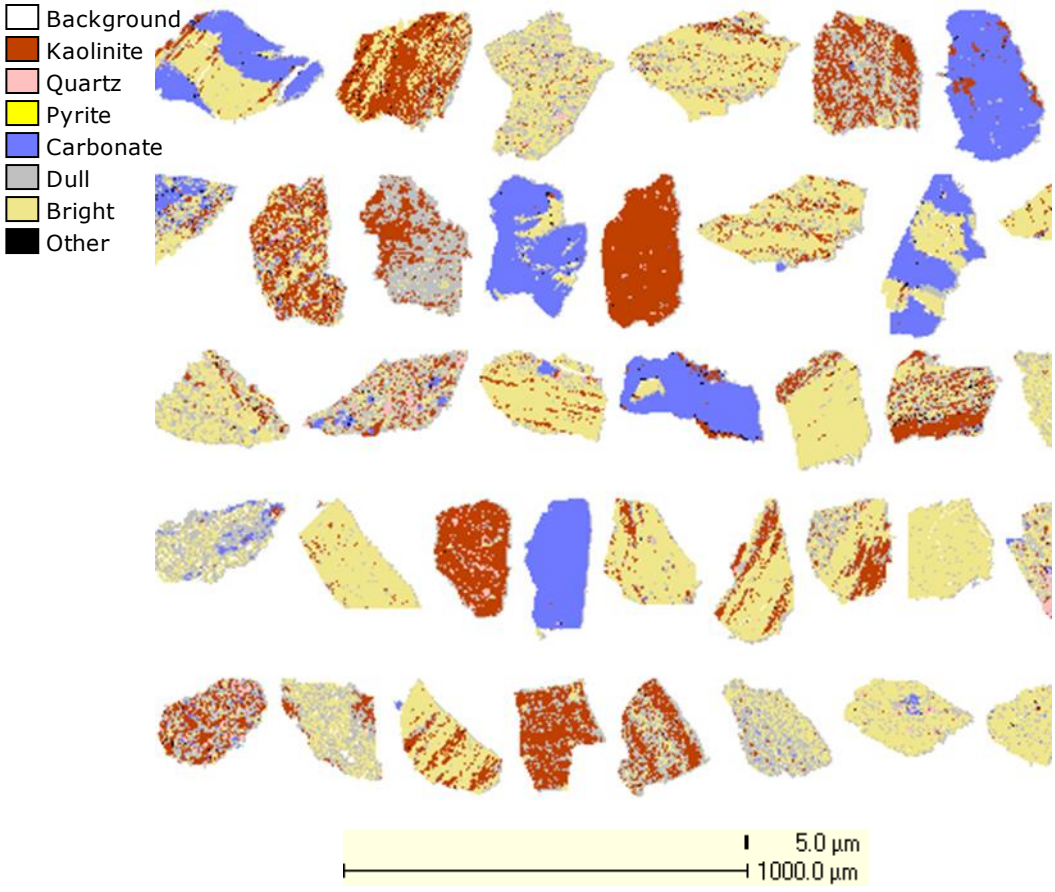

Figure 32. False colour image of particles present in a typical 1.5g.cm^{-3} float fraction, -25+12mm size fraction, 0.5mm QEMSCAN sample.

5.2.3 Particle characteristics – 1.6g.cm^{-3} floats

As per Figure 33, Figure 34 and Figure 35 , carbominerite (45.08%), dull/bright (26.40%) and bright (13.25%) are the predominant components. The increase in carbominerite and bright/dull of the 1.6 floats compared to the 1.5 float fractions are expected as carbominerite (~1.67g.cm^{-3}) has a higher density than bright (~1.3g.cm^{-3}) or dull (-1.55g.cm^{-3}) coal.

Similar to the 1.4 float and 1.5 float samples, the 1.6 float 0.5mm QEMSCAN samples have the most consistent proportions of carbonate cleats. There is a significant decrease in bright particles, and corresponding increase in bright/dull and carbominerite particles for the 2.0mm samples. Mudstone, cleats and carbominerite remain the predominant contributors to ash.

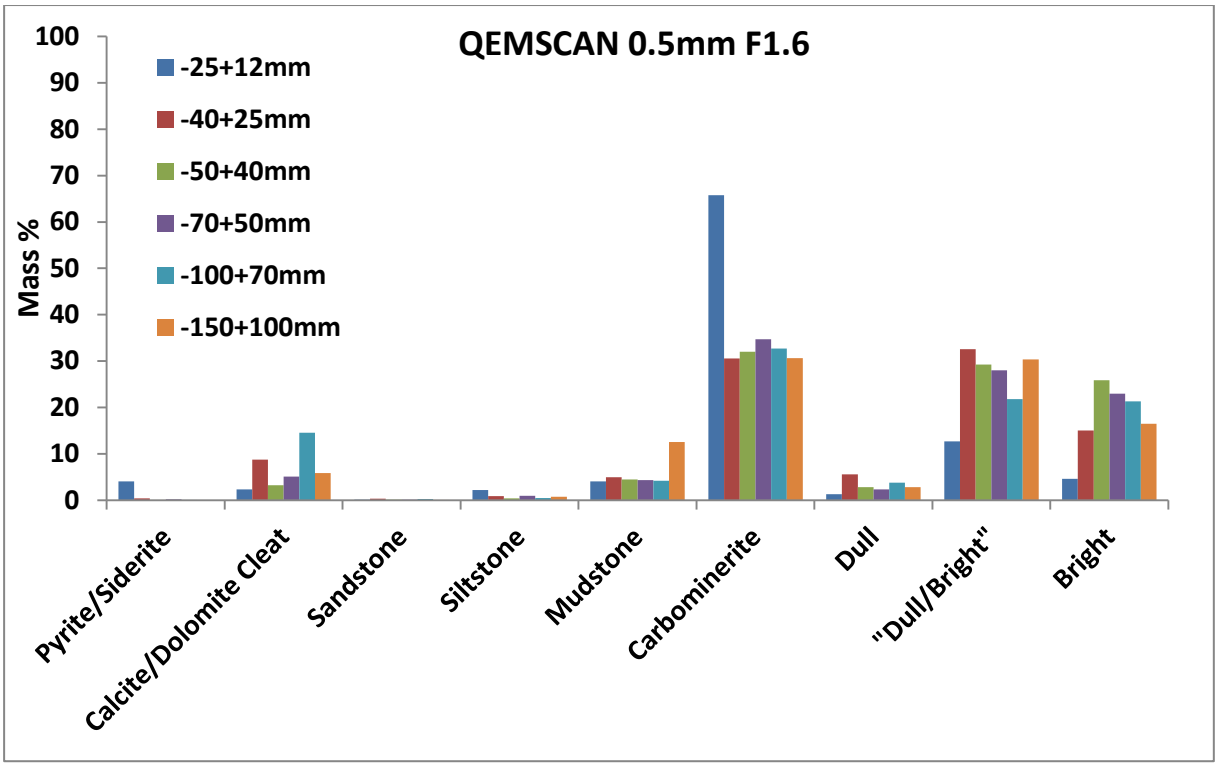

Figure 33. Particle characterisation for the QEMSCAN 0.5mm crushed 1.6g.cm^{-3} float fractions.

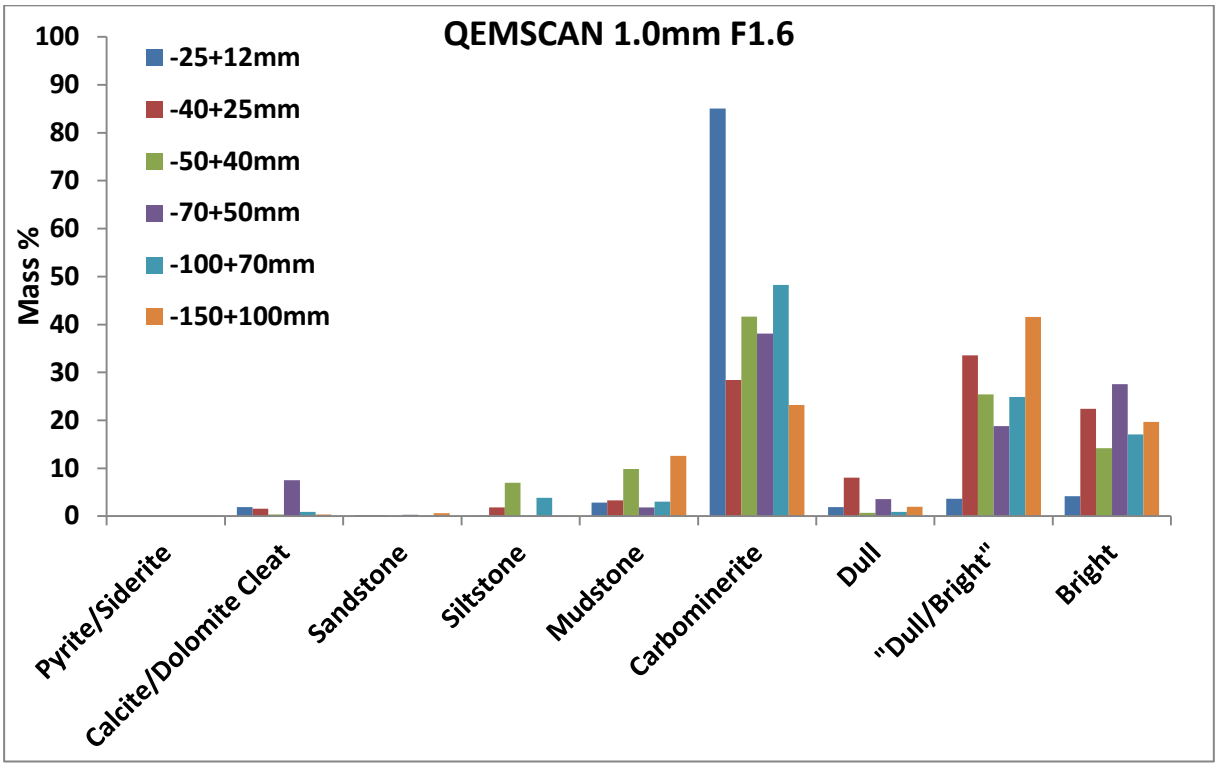

Figure 34. Particle characterisation for the QEMSCAN 1.0mm crushed 1.6g.cm^{-3} float fractions.

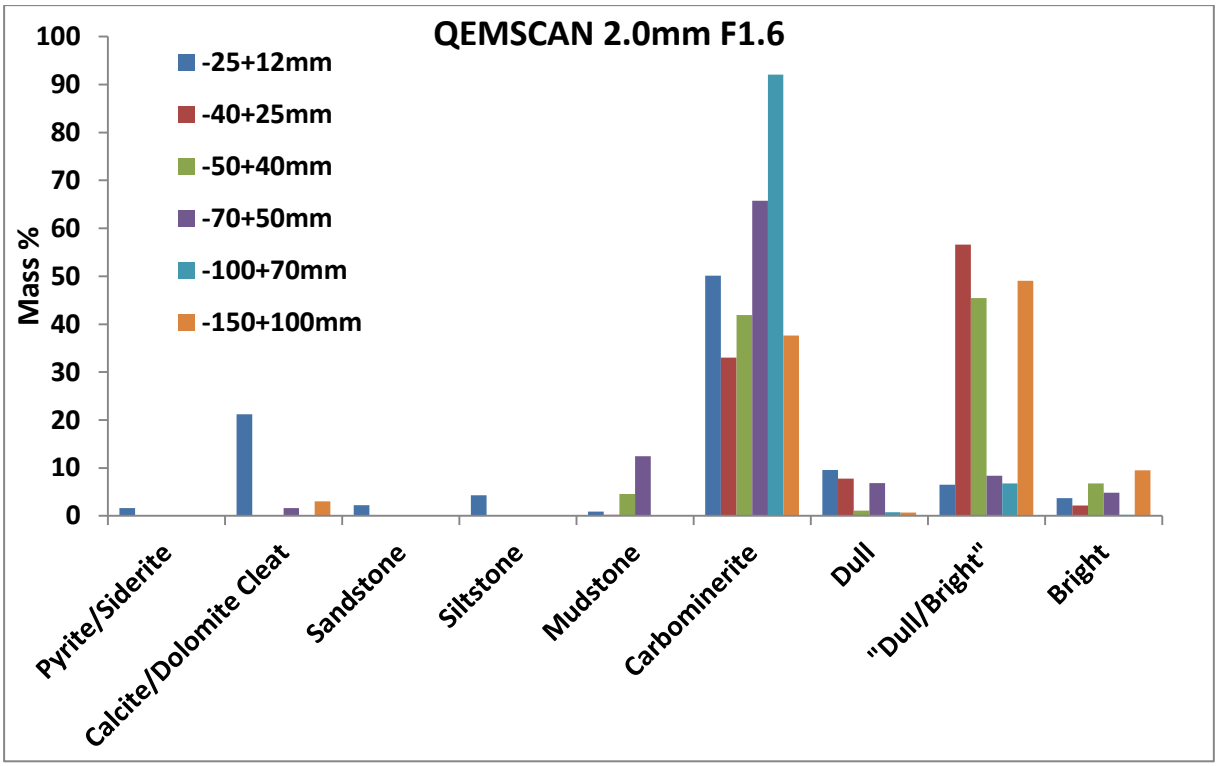

Figure 35. Particle characterisation for the QEMSCAN 2.0mm crushed 1.6g.cm^{-3} float fractions.

The 1.6g.cm^{-3} density fraction was not present for the -12+0.5mm and +150mm size fractions. The 0.5mm and 1.0mm samples in the -25+12mm size fraction have double the carbominerite than the 2.0mm sample. The 2.0mm QEMSCAN sample of the -25+12mm size fraction has 20% carbonate cleat material. This explains its elevated ash values in comparison to the other size fractions (Table 10).

Table 10: Dry base ash % as determined by QEMSCAN analysis on the 1.6g.cm^{-3} floats across size fraction (potential outliers highlighted in red).

Size (mm)	0.5mm ash% (DB)	1.0mm ash% (DB)	2.0mm ash% (DB)
-25+12	39.45	38.95	49.31
-40+25	26.27	25.09	26.92
-50+40	24.86	33.59	25.87
-70+50	26.59	26.34	37.76
-100+70	25.96	26.81	30.53
-150+100	31.46	21.93	20.57
Average	29.10	28.79	31.83

The false colour image (Figure 36) correlates to the particle proportions as depicted in the 1.6g.cm^{-3} float particle characterisation histograms (Figure 33, Figure 34 and Figure 35). Bright/dull particles are more abundant than bright particles, while carbominerite particles comprise about half of the total particles present.

The carbominerite particles are still predominantly carbankerite, carbargillite, and carbopolyminerite, although there is more carbankerite and carbopolyminerite in the 1.6g.cm^{-3} than the 1.5g.cm^{-3} floats. Carbopyrite and carbosilicate were not present.

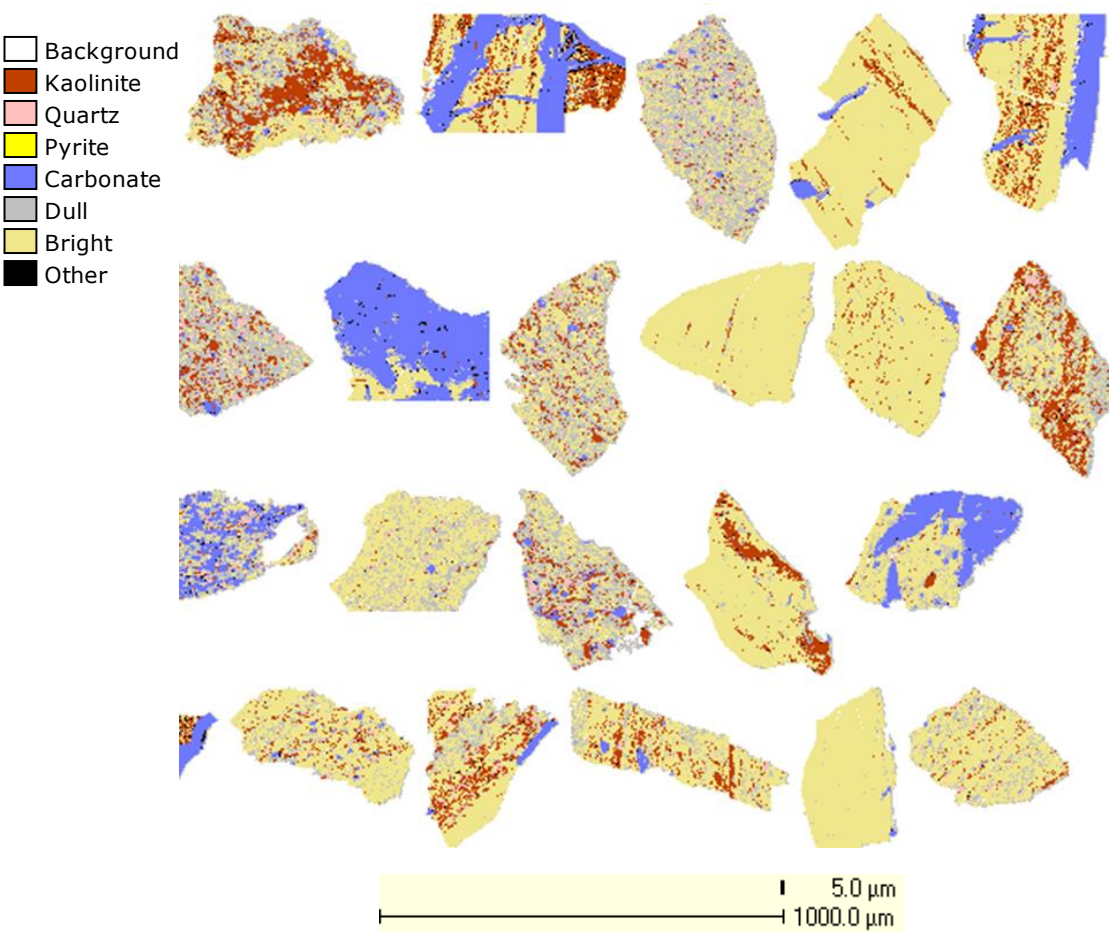

Figure 36. False colour image of particles present in a typical 1.6g.cm^{-3} float fraction , -50+40mm size fraction, 0.5mm QEMSCAN sample.

5.2.4 Particle characteristics – 1.7g.cm^{-3} floats

As per Figure 37, Figure 38 and Figure 39 the average carbominerite is 53.86%, while average dull/bright (20.47%) is double that of average bright coal (10.72%). The 1.7 floats comprise predominantly carbominerite particles, which is expected since the relative density of carbominerite is ~1.67g.cm^{-3}. The 0.5mm sample still has the highest quantity of cleats. Mudstone, siltstone and sandstone comprise 5.72%. Mudstone, cleats and carbominerite are the predominant contributors to ash.

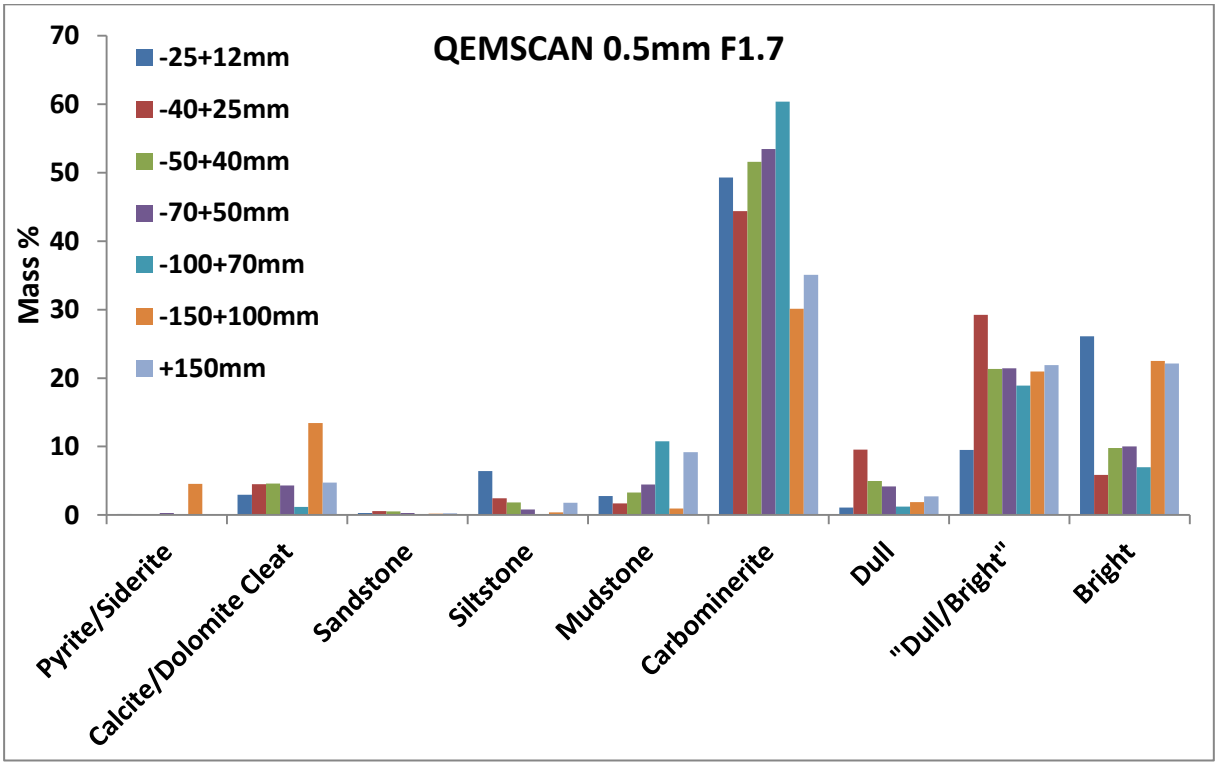

Figure 37. Particle characterisation for the QEMSCAN 0.5mm crushed 1.7g.cm^{-3} float fractions.

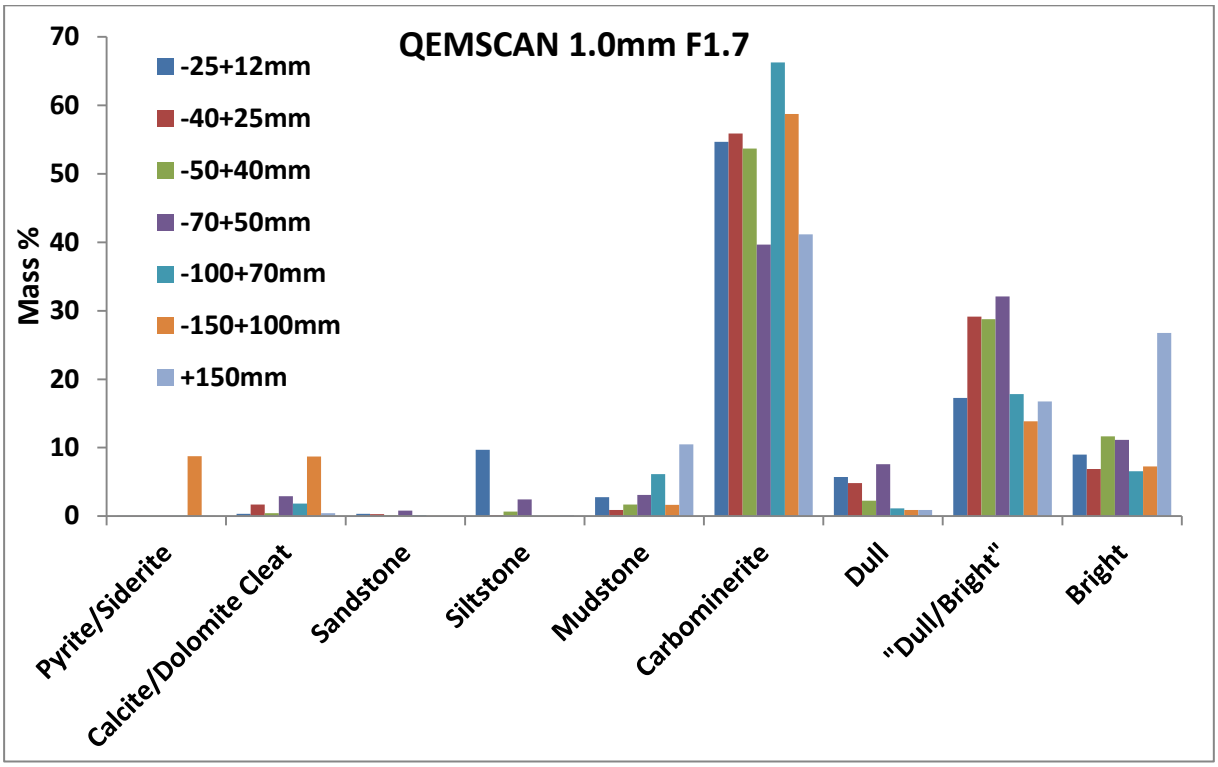

Figure 38. Particle characterisation for the QEMSCAN 1.0mm crushed 1.7g.cm^{-3} float fractions.

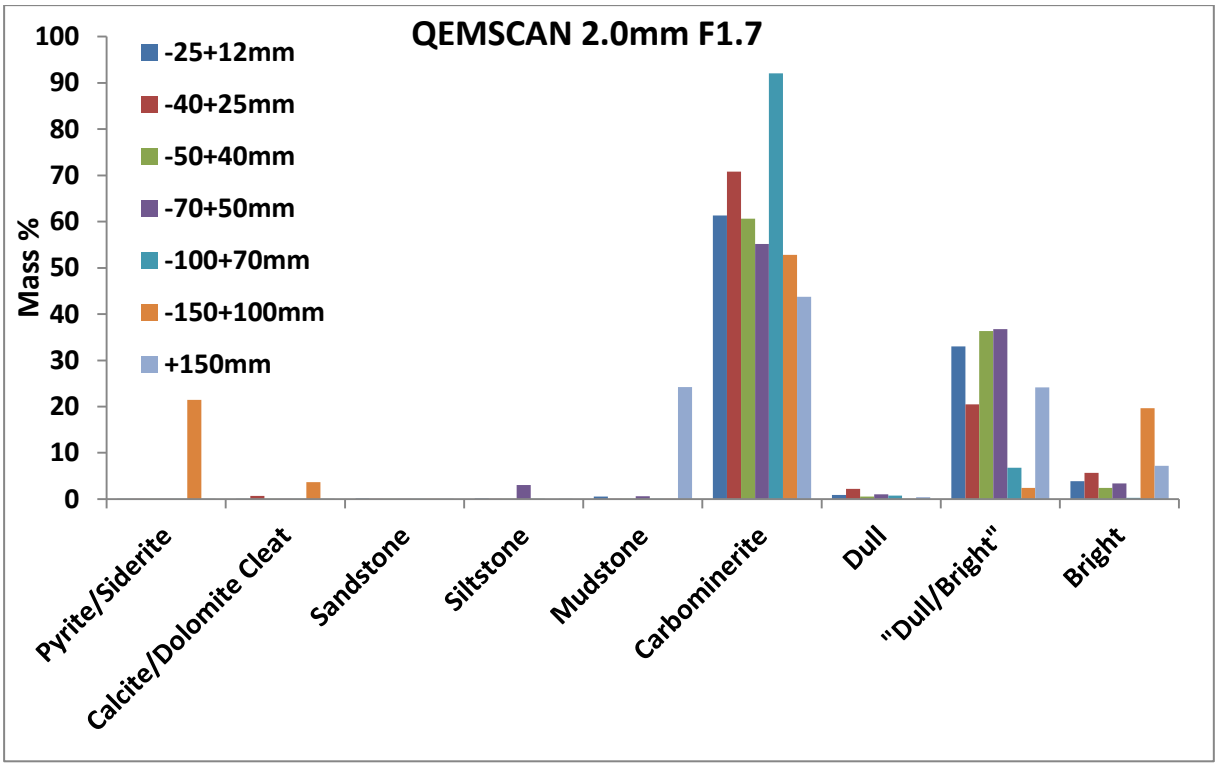

Figure 39. Particle characterisation for the QEMSCAN 2.0mm crushed 1.7g.cm^{-3} float fractions.

The 1.7g.cm^{-3} float was not received for the -12+0.5mm size fraction. The elevated ash value in the -100+70mm, 1.0mm sample was due to a high proportion of carbominerite and mudstone, while the +150mm, 2.0mm sample had an especially high quantity of mudstone (Table 11).

Table 11: Dry base ash % as determined by QEMSCAN analysis on the 1.7g.cm^{-3} floats across size fraction.

Size (mm)	0.5mm ash% (DB)	1.0mm ash% (DB)	2.0mm ash% (DB)
-25+12	26.11	21.47	35.36
-40+25	29.93	25.39	30.79
-50+40	30.00	30.77	28.48
-70+50	32.39	28.02	32.56
-100+70	34.42	37.77	29.77
-150+100	28.48	30.26	25.12
+150	29.08	28.04	39.96
Average	30.06	28.82	31.72

It is observed in Figure 41 that there are very few liberated bright particles compared to lower float fractions. Bright/dull particles predominate over bright. Pyrite becomes a significant liberated cleat phase in the -150+100mm size fraction (Figure 40). The carbominerite present is now more carbopolyminerite and carbosilicate, rather than carbargillite and carbankerite as the lower density float fractions. A higher proportion of quartz is present within the carbominerite particles. The carbonates are now also present as nodules within dull/bright coal particles, as well as cleats attached to bright coal particles (Figure 41).

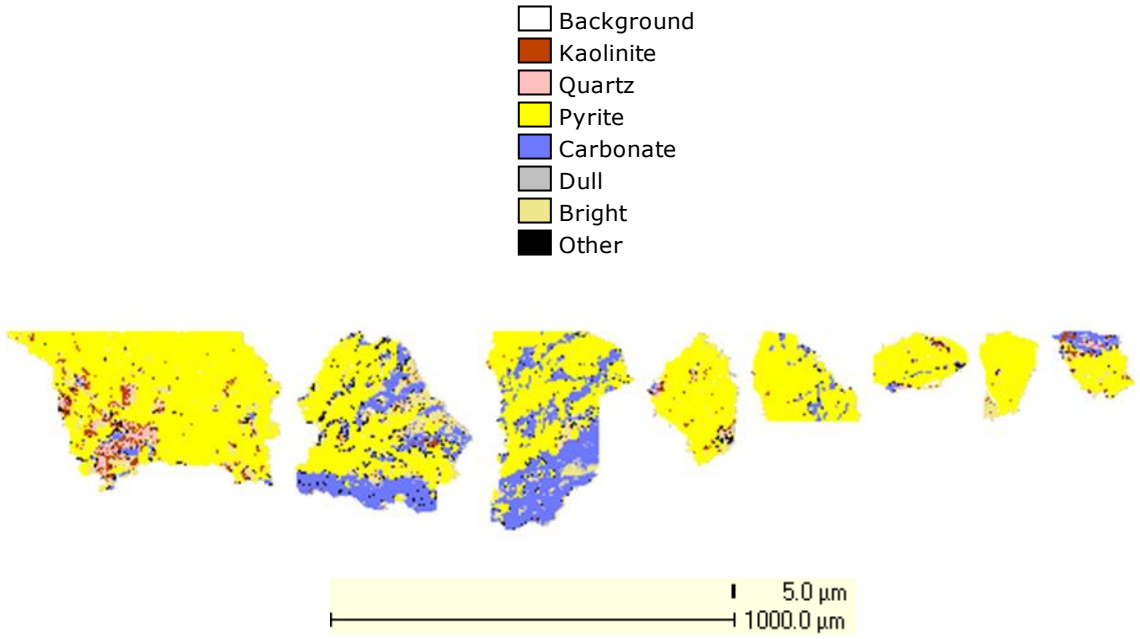

Figure 40. False colour image of liberated pyrite cleat particles within the -150+100mm size fraction, 0.5mm QEMSCAN sample.

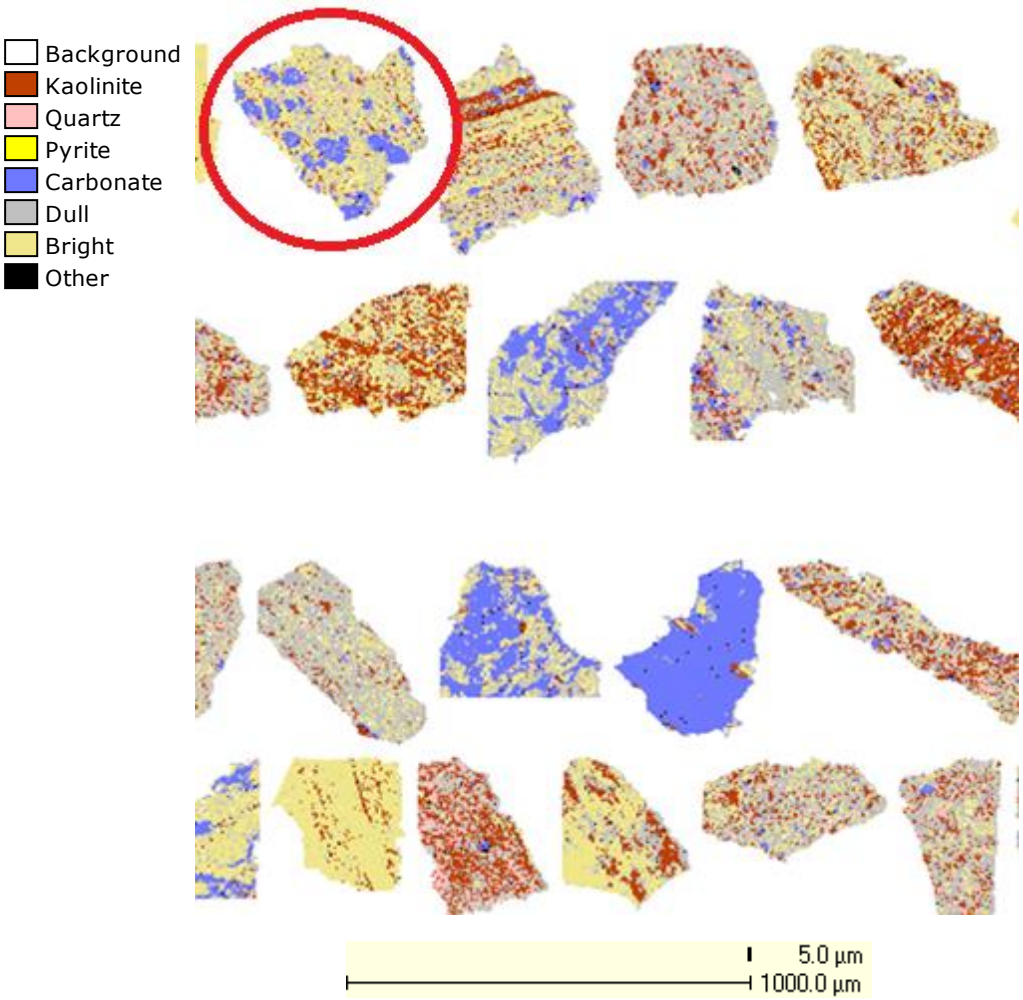

Figure 41. False colour image of particles present in the 1.7g.cm^{-3} float ,-100+70mm size fraction, 0.5mm QEMSCAN sample. Carbonate nodules present in a dull/bright coal particle circled in red.

5.2.5 Particle characteristics – 1.8g.cm^{-3} floats

As per Figure 42, Figure 43 and Figure 44 carbominerite (52.03%) is the predominant phase, while bright and bright/dull comprise 29.78%. Pyrite has increased as a cleat phase across all size fractions compared to the 1.7 floats, and is especially consistent in the 0.5mm crushed samples. Mudstone, siltstone and sandstone have doubled from 5.27% in the 1.7 floats to 10.33% in the 1.8 floats. More mudstone (6.53%) is present in comparison to siltstone (3.54%). Increased proportions of stone result in an overall increase in ash content (Table 12). It seems that the proportion of mudstone increases for larger size fractions (Figure 42). The trend is most clear for the 0.5mm samples, less for the 1.0mm samples, while the 2.0mm particle characterisation histogram shows somewhat random results.

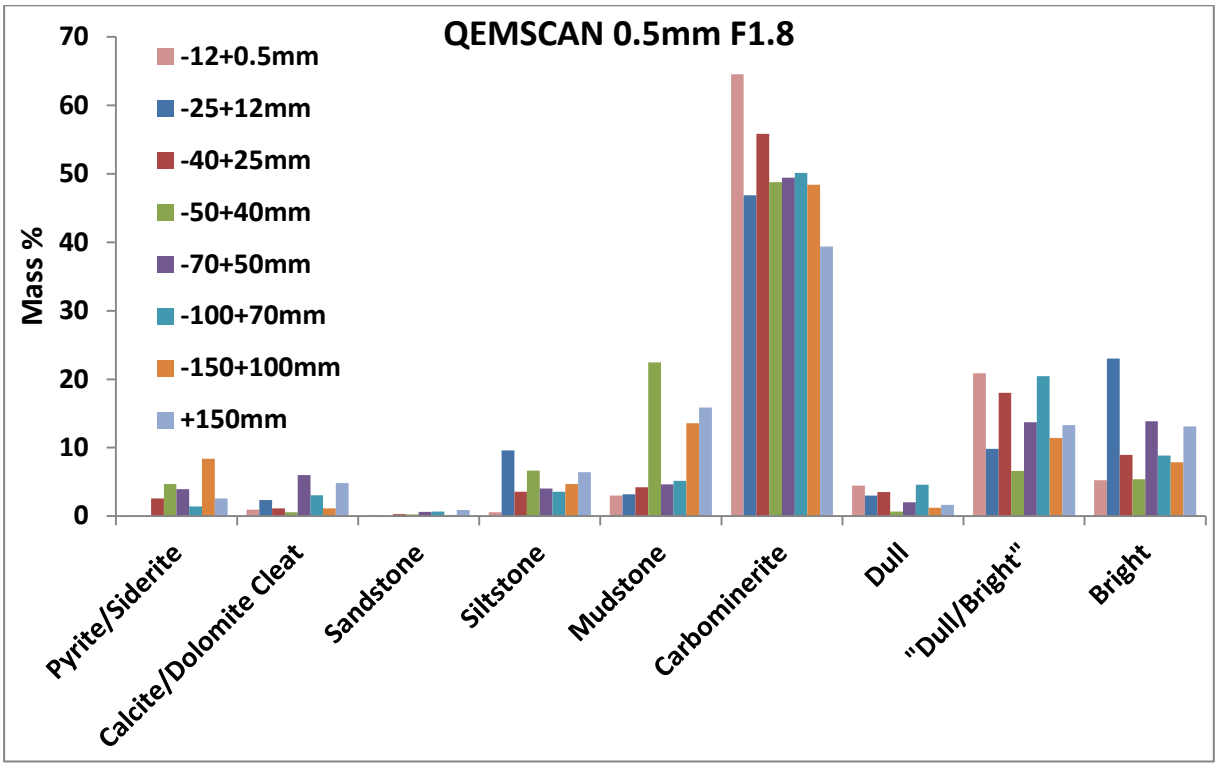

Figure 42. Particle characterisation for the QEMSCAN 0.5mm crushed 1.8g.cm^{-3} float fractions.

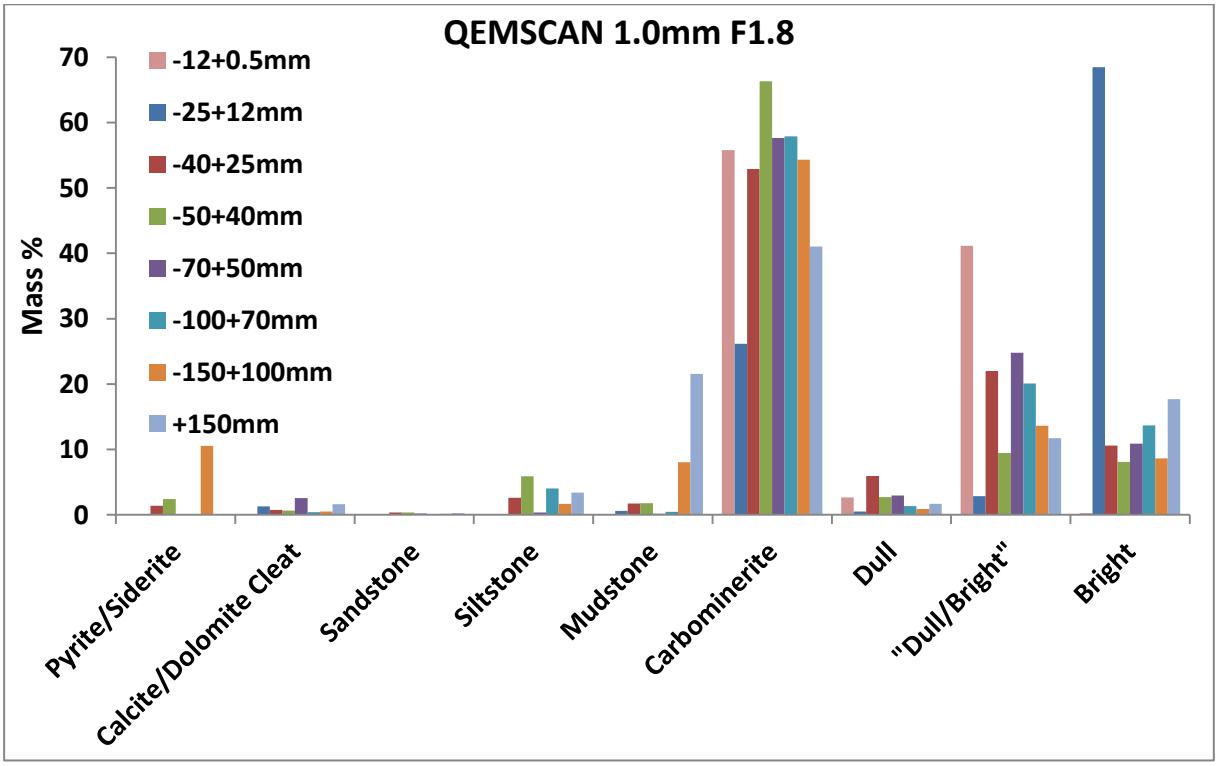

Figure 43. Particle characterisation for the QEMSCAN 1.0mm crushed 1.8g.cm^{-3} float fractions.

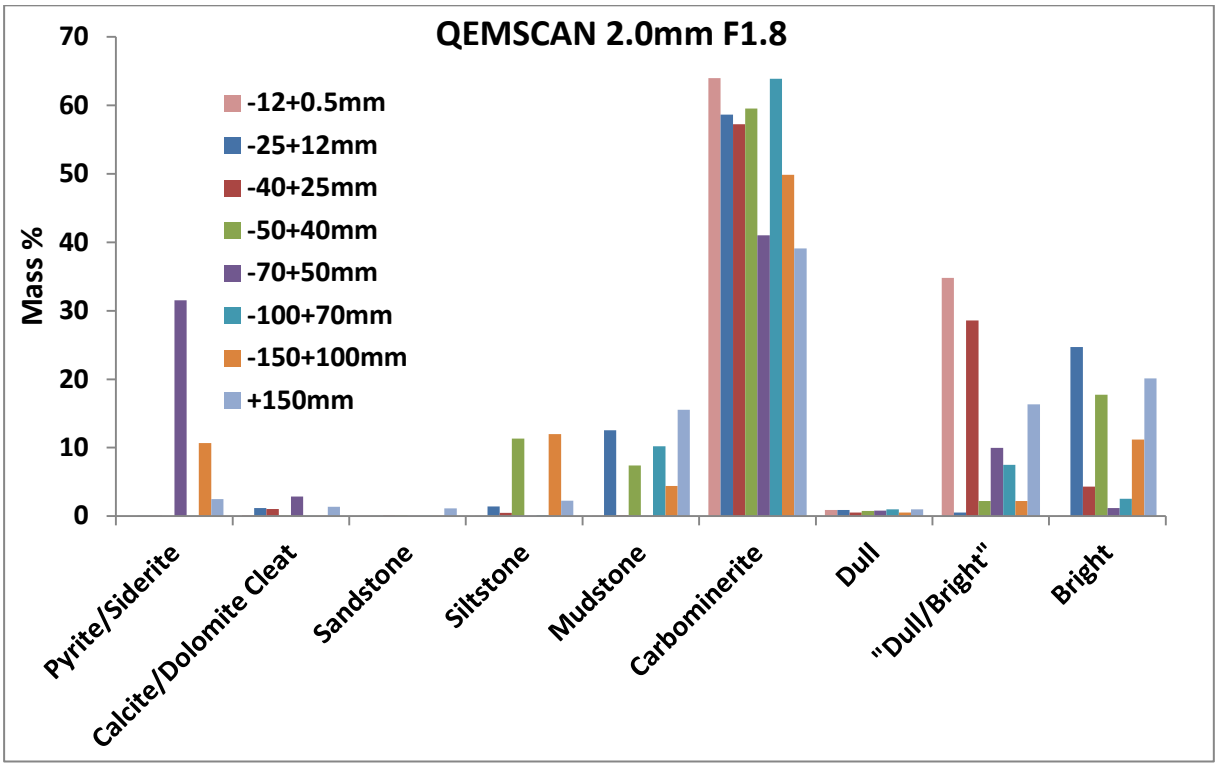

Figure 44. Particle characterisation for the QEMSCAN 2.0mm crushed 1.8g.cm^{-3} float fractions.

The 2.0mm sample has higher carbominerite (54.16%) compared to the 1.0mm (51.50%) and 0.5mm (50.43%) samples. This is reflected in the ash values as the 2.0mm samples have the highest average ash value (Table 12). The 0.5mm sample has more consistent phases present per size fraction than the 1.0mm and 2.0mm samples (dull, bright, mudstone, siltstone and cleats). Similar to the cleat trend observed in the 1.7g.cm^{-3} floats of the -150+100mm size fraction, the 1.8g.cm^{-3} floats have a high proportion of pyrite cleats. The 0.5mm, 1.0mm and 2.0mm samples from the -150+100mm size fraction have ashes higher than the average for all size fractions. The -70+50mm size fraction has a particularly high proportion of carbonate cleats (0.5mm, 1.0mm and 2.0mm samples) and pyrite cleats (0.2mm sample with 41.39% ash).

Table 12: Dry base ash % as determined by QEMSCAN analysis on the 1.8g.cm^{-3} floats across size fraction.

Size (mm)	0.5mm ash% (DB)	1.0mm ash% (DB)	2.0mm ash% (DB)
-12+0.5	31.08	28.92	27.87
-25+12	33.18	36.27	36.84
-40+25	35.67	29.59	37.14
-50+40	40.01	40.54	40.11
-70+50	34.02	30.43	41.39
-100+70	35.62	33.30	46.90
-150+100	42.26	38.94	39.96
+150	43.01	43.57	38.46
Average	36.86	35.20	38.58

Bright coal, pyrite and dull/bright coal that occurs as laminae between clay and stone, is liberated when crushed. As a result, pyrite cleats, bright and dull/bright are now liberation products. It is observed in Figure 45 that the bright particle and carbankerite particles present have likely been liberated due to their cleat/coal boundary. Carbonates are present both as cleats in bright coal and nodules within dull/bright and carbominerite particles. The carbominerite particles have more quartz incorporated into their 'speckled' textures than the 1.7 floats.

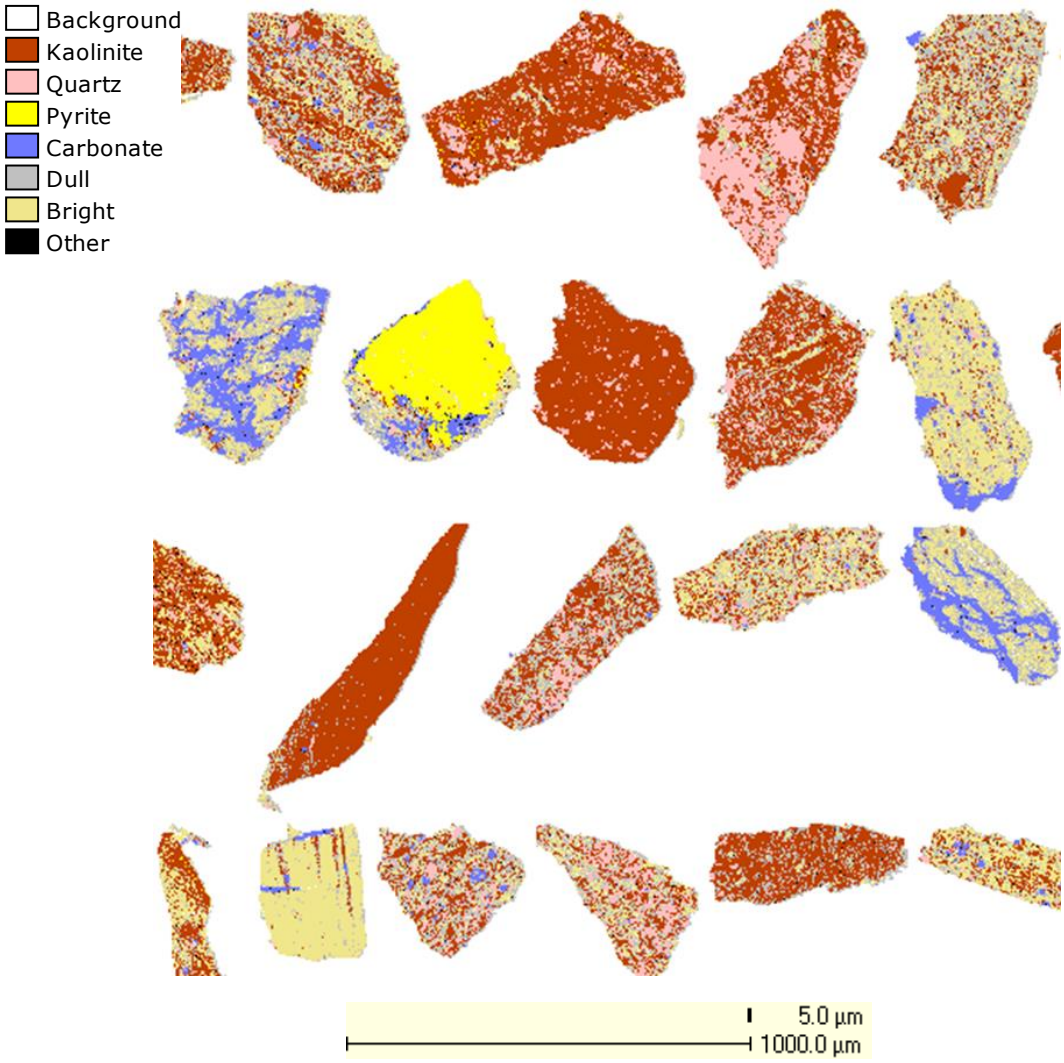

Figure 45. False colour image of particles present in the 1.8g.cm^{-3} float ,-150+100mm size fraction, 0.5mm QEMSCAN sample.

5.2.6 Particle characteristics – 1.9g.cm^{-3} floats

Figure 46, Figure 47 and Figure 48 reveal that carbominerite increases from 46.72% in the 0.5mm sample to 55.70% in the 1.0mm sample and further increases to 60.19% in the 2.0mm sample. Dull, dull/bright and dull decrease from 17.48% and 17.06% in the 0.5mm and 1.0mm samples to 10% in the 2.0mm sample. Pyrite and carbonate cleats comprise 3.93% in

the 0.5mm sample, 1.65% in the 1.0mm sample and 0.52% in the 2.0mm sample. The higher proportion of cleat material, bright and dull/bright coal in the 0.5mm and 1.0mm samples indicates liberation of these phases to be higher than the 2.0mm sample. The quantities of siltstone (14.33%) is higher than that of average mudstone (11.68%)

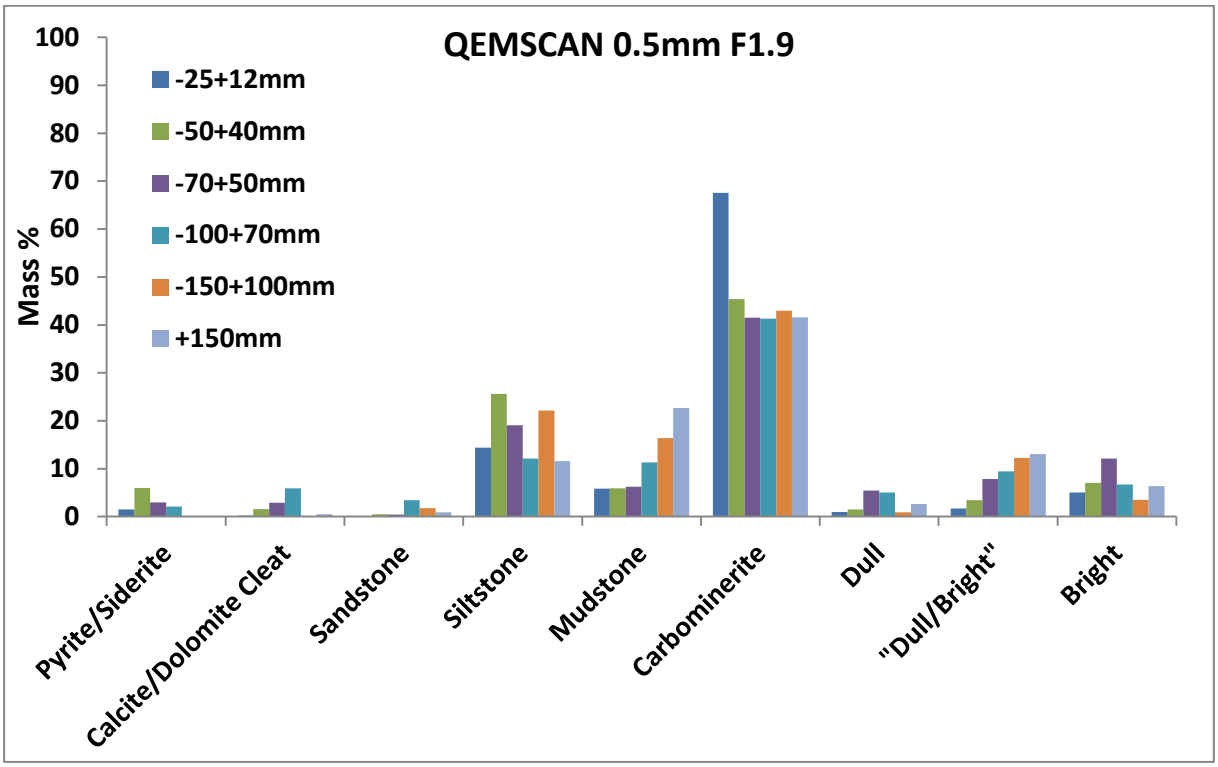

Figure 46. Particle characterisation for the QEMSCAN 0.5mm crushed 1.9g.cm^{-3} float fractions.

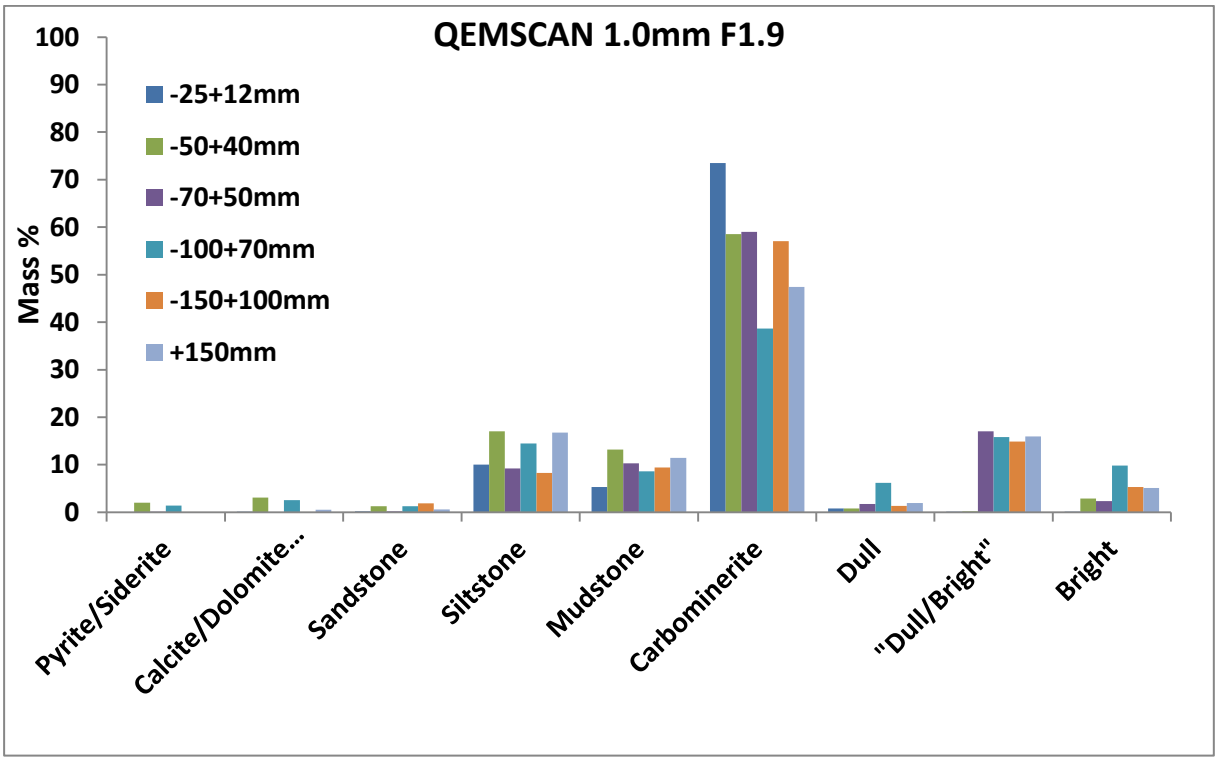

Figure 47. Particle characterisation for the QEMSCAN 1.0mm crushed 1.9g.cm^{-3} float fractions.

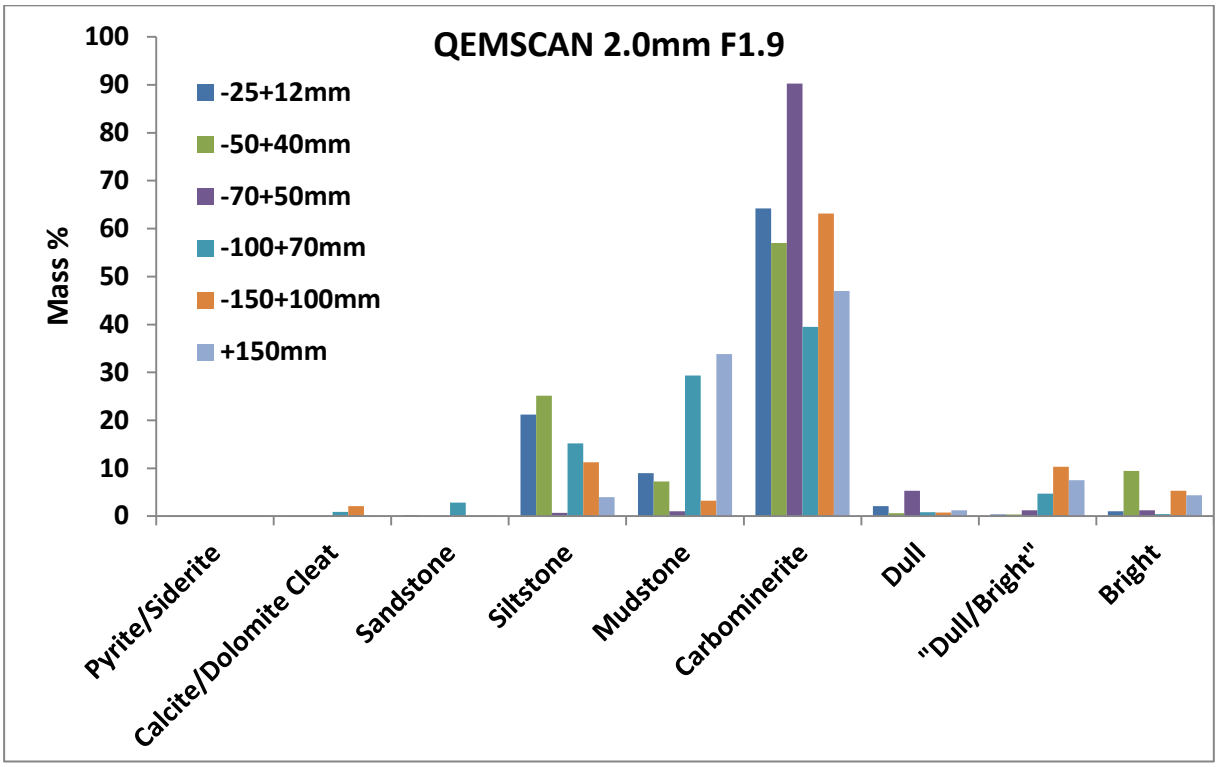

Figure 48. Particle characterisation for the QEMSCAN 2.0mm crushed 1.9g.cm^{-3} float fractions.

The 1.9g.cm^{-3} float for the -12+0.5mm and -40+25mm size fractions were not received. Mudstone and siltstone are consistent in all size fractions for the 0.5mm, 1.0mm and 2.0mm. The exception was the 2.0mm QEMSCAN sample in the -70+50mm size fraction, which has a low proportion of mudstone and elevated carbominerite. The average ash values across size fractions are similar (Table 13).

Table 13: Dry base ash % as determined by QEMSCAN analysis on the 1.9g.cm^{-3} floats across size fraction.

Size (mm)	0.5mm ash% (DB)	1.0mm ash% (DB)	2.0mm ash% (DB)
-25+12	53.70	57.57	56.06
-50+40	52.27	54.90	58.32
-70+50	47.56	41.09	48.84
-100+70	50.48	42.49	62.08
-150+100	54.92	46.70	43.63
+150	50.59	47.19	52.76
Average	51.59	48.32	53.62

The false colour image (Figure 49) shows that the carbominerite particles are incorporating more carbonate nodules, pyrite nodules and quartz into its texture than lower floats. The presence of high proportions of carbominerite is anticipated due to its density range being 1.55-1.95g.cm^{-3}. Less coal occurs as laminae within the 1.9 float than lower density floats. Kaolinite particles with lamellae of quartz are seen for the first time (Figure 49). The

proportions of mineral to coal in the carbominerite particles begin to exceed the minimum proportion of coal to be qualified as carbominerite.

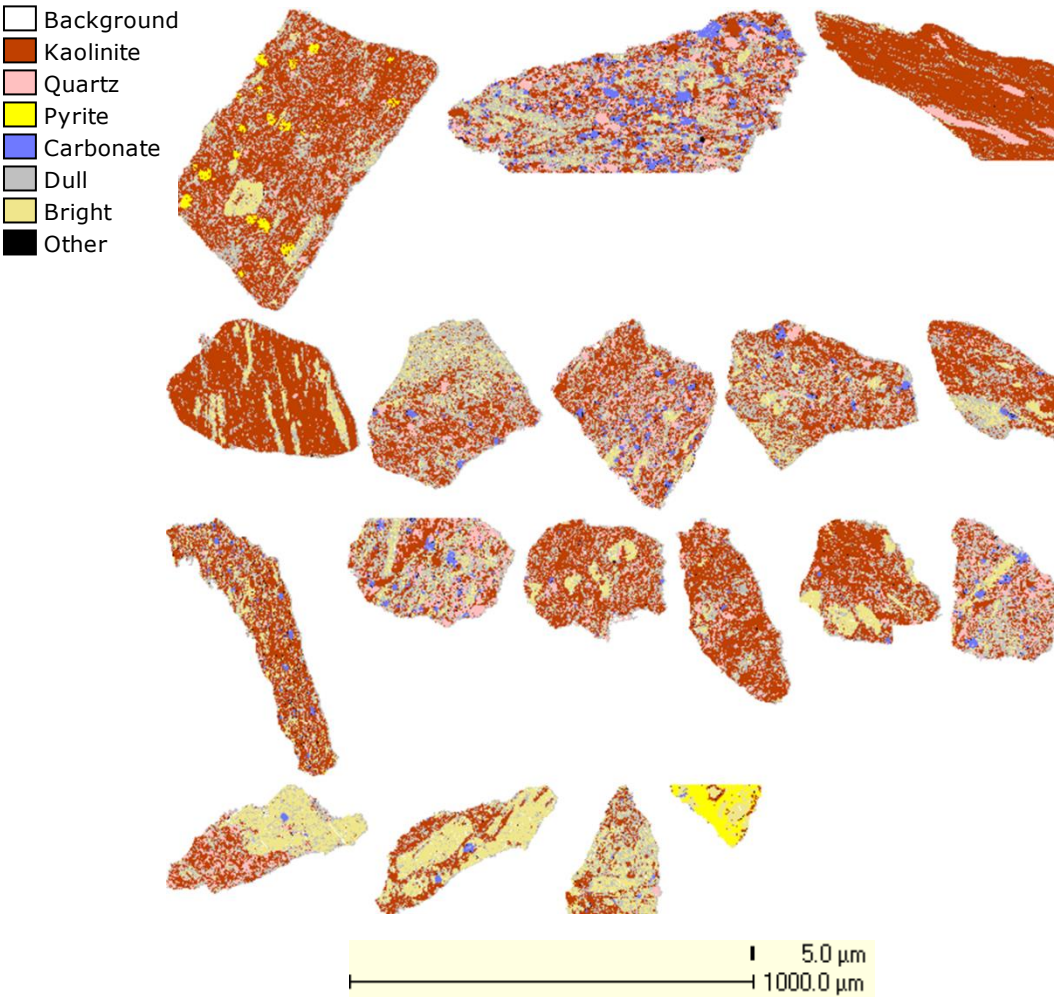

Figure 49. False colour image of particles present in a typical 1.9g.cm^{-3} float fraction,-25+12mm size fraction, 0.5mm QEMSCAN sample.

5.2.7 Particle characteristics – 2.0g.cm^{-3} floats

Figure 50, Figure 51 and Figure 52 reveal that the carbominerite proportions decreases to 41.29%, while the coal particles are similar in quantity to 1.9g.cm^{-3} floats. There is 16.16% average bright, dull/bright and dull coal. There is significantly more siltstone (21.31%) than mudstone (16.12%). Pyrite cleats are most consistently present in the 0.5mm samples.

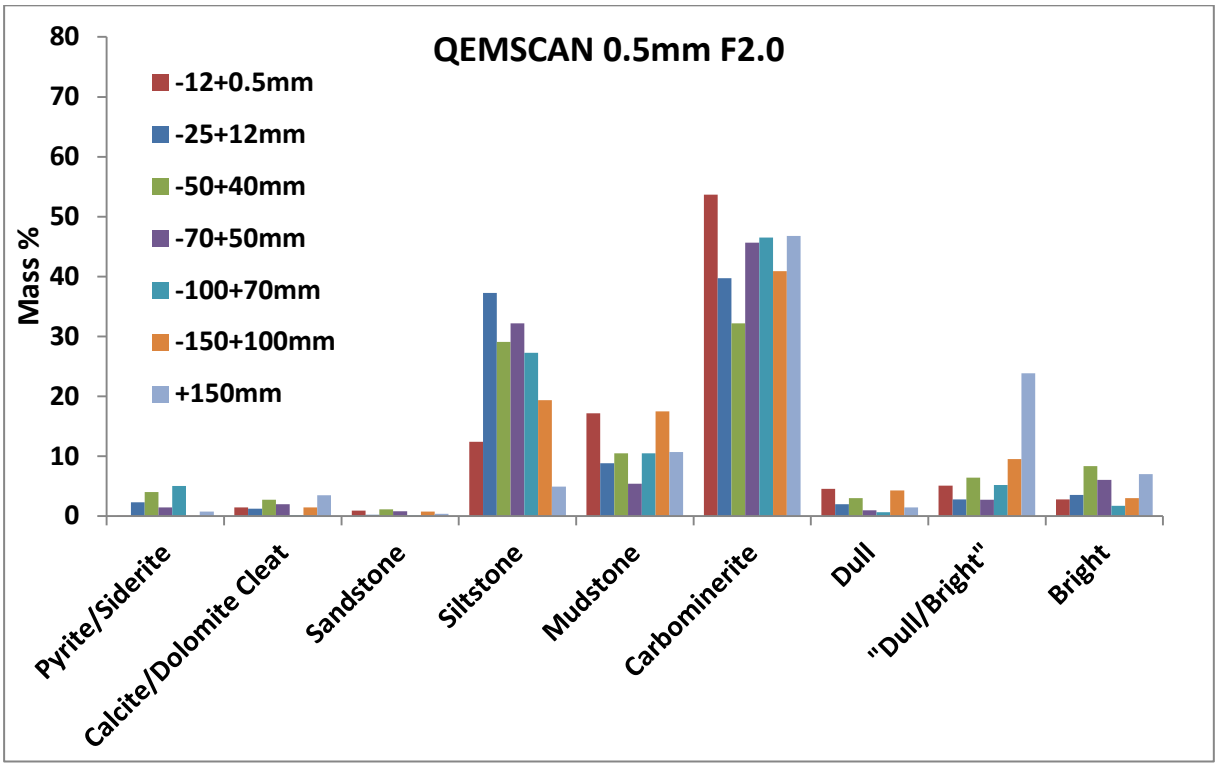

Figure 50. Particle characterisation for the QEMSCAN 0.5mm crushed 2.0g.cm^{-3} float fractions.

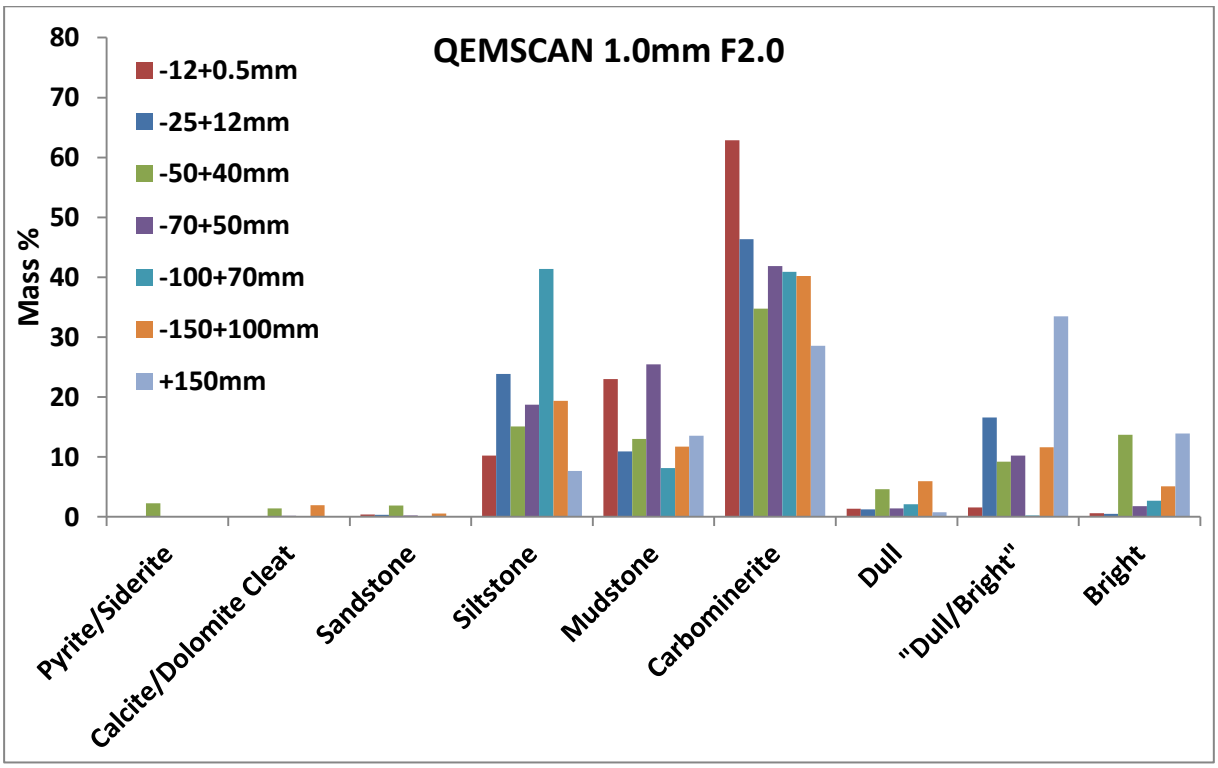

Figure 51. Particle characterisation for the QEMSCAN 1.0mm crushed 2.0g.cm^{-3} float fractions.

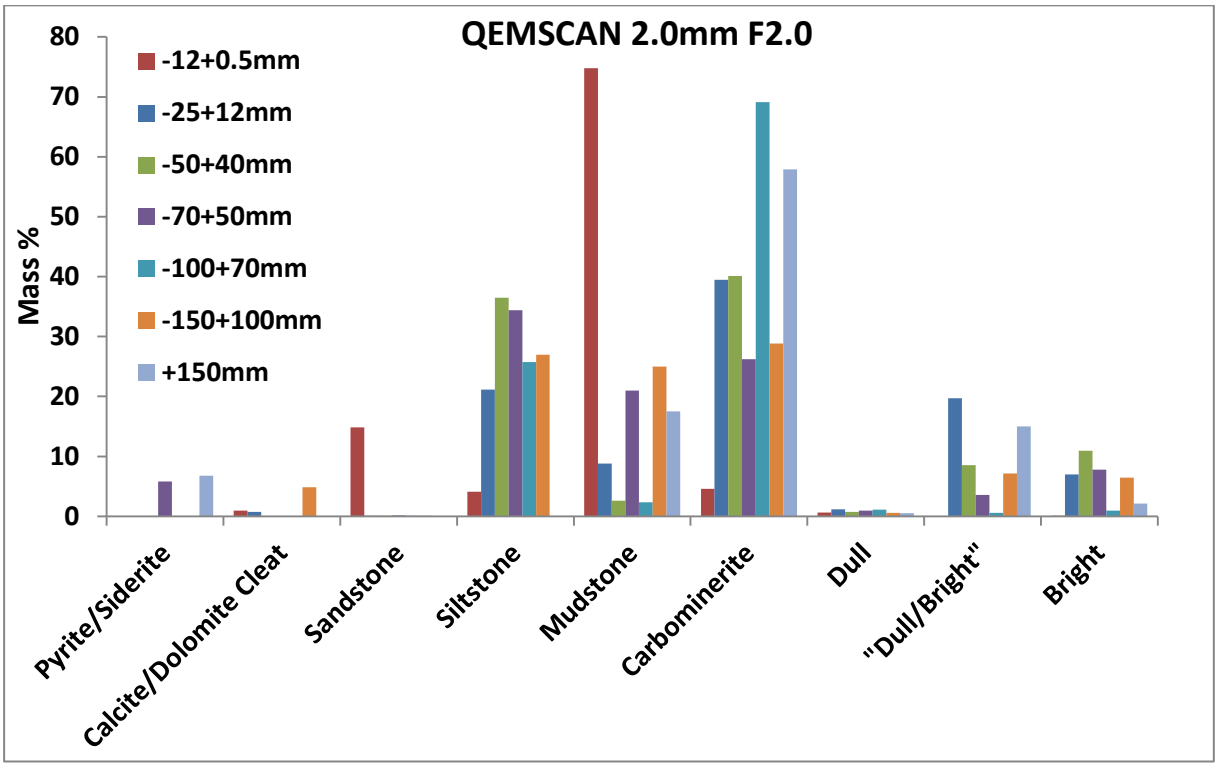

Figure 52. Particle characterisation for the QEMSCAN 2.0mm crushed 2.0g.cm^{-3} float fractions.

The 2.0g.cm^{-3} float for the -40+25mm size fraction was not received. The +150mm size fraction has unusually high bright and dull/bright in the 0.5mm and 1.0mm samples, while the 2.0mm sample has elevated dull/bright. This is reflected in the ash values of these samples having a lower than average ash value (Table 14). The high sandstone and carbominerite proportions present in the -12+0.5mm size fraction, 2mm QEMSCAN sample results in the sample having an elevated ash of 58.92%. The -100+70mm, 1.0mmQEMSCAN sample has almost double the proportion of siltstone compared to other size fractions, resulting in an elevated ash of 61.30%.

Table 14: Dry base ash % as determined by QEMSCAN analysis on the 2.0g.cm^{-3} floats across size fraction.

Size (mm)	0.5mm ash% (DB)	1.0mm ash% (DB)	2.0mm ash% (DB)
-12+0.5	51.21	55.99	58.92
-25+12	58.51	52.30	47.78
-50+40	54.26	45.90	47.87
-70+50	58.36	59.00	65.58
-100+70	56.83	61.30	53.47
-150+100	52.75	48.26	57.11
+150	38.10	44.37	41.64
Average	52.86	52.45	53.20

The false colour image of 2.0g.cm^{-3} float particles comprises more mudstone and siltstone than carbominerite (Figure 53). Coal is only present as laminations within mudstone or siltstone particles. The bottom right particle in Figure 53 comprises ~60% coal and ~40% kaolinite. The density of this particle would theoretically be 1.84g.cm^{-3} according to the calculations for the validation model. Particles such as these have been liberated to smaller particles that no longer are the same density of the original particle.

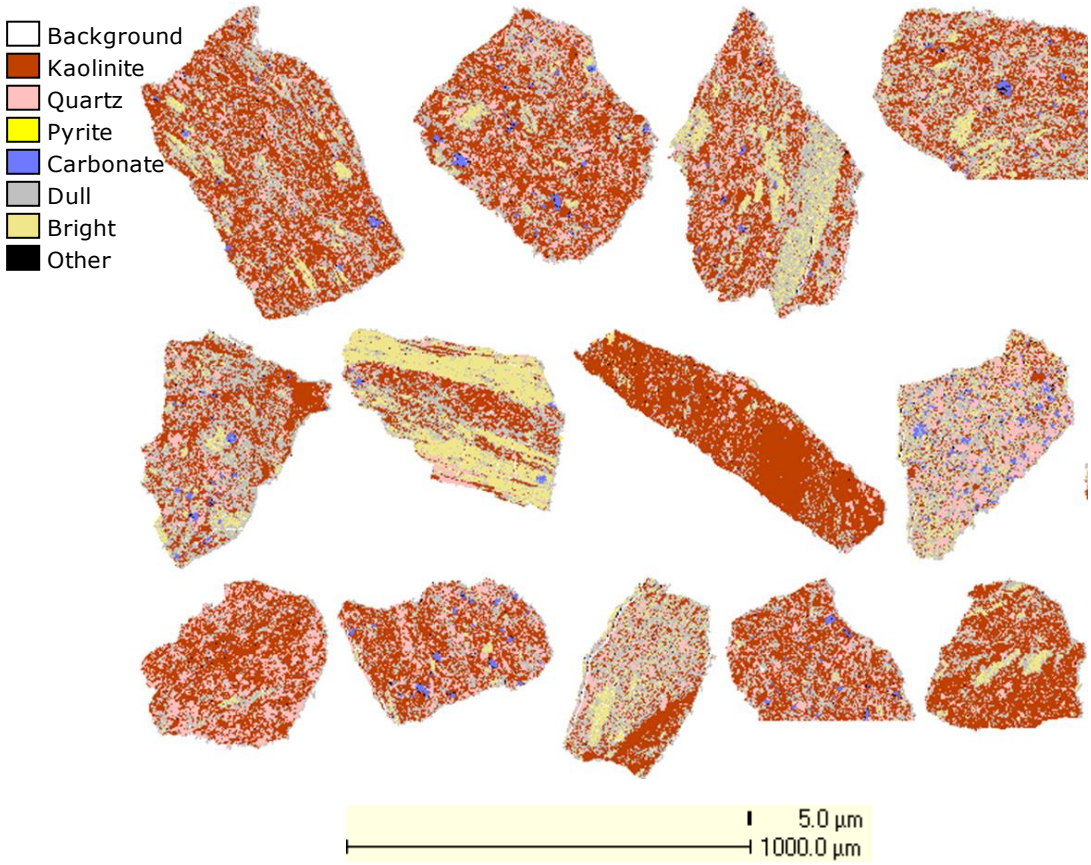

Figure 53. False colour image of particles present in a typical 2.0 float fraction, ,-100+70mm size fraction, 0.5mm QEMSCAN sample.

5.2.8 Particle characteristics – 2.0g.cm^{-3} sinks

Figure 54, Figure 55 and Figure 56 reveal that the predominant phases are mudstone (55.61%) and siltstone (16.99%). The carbominerite proportion has dropped to 14.48% from 41.29% in the 2.0 float. Coal present totals 7.72%. The cleat proportions are 2.46% for the 0.5mm samples, 1.19% for the 1.0mm samples and 0.84% for the 2.0mm samples. The low density phases (coals) are present due to liberation. The +150mm size fraction has particle characteristics that are a misfit to the proportions of all other size fractions.

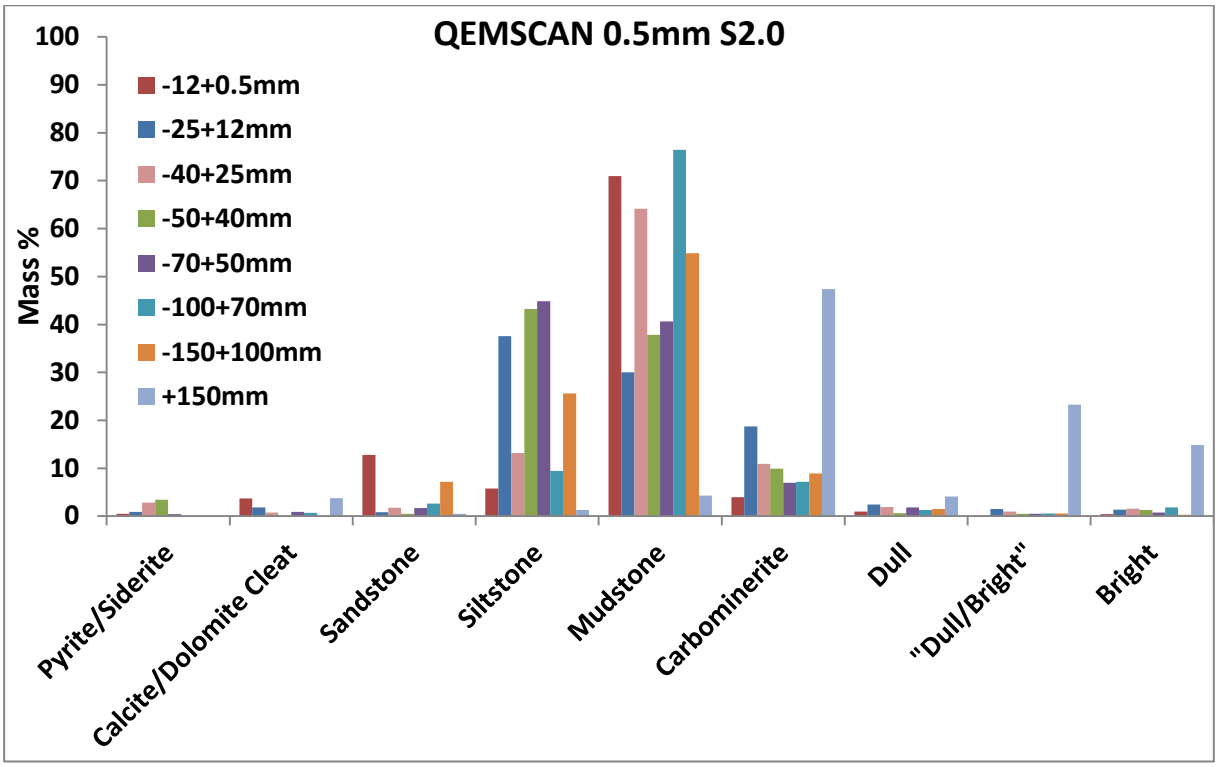

Figure 54. Particle characterisation for the QEMSCAN 0.5mm crushed 2.0g.cm^{-3} sink fractions.

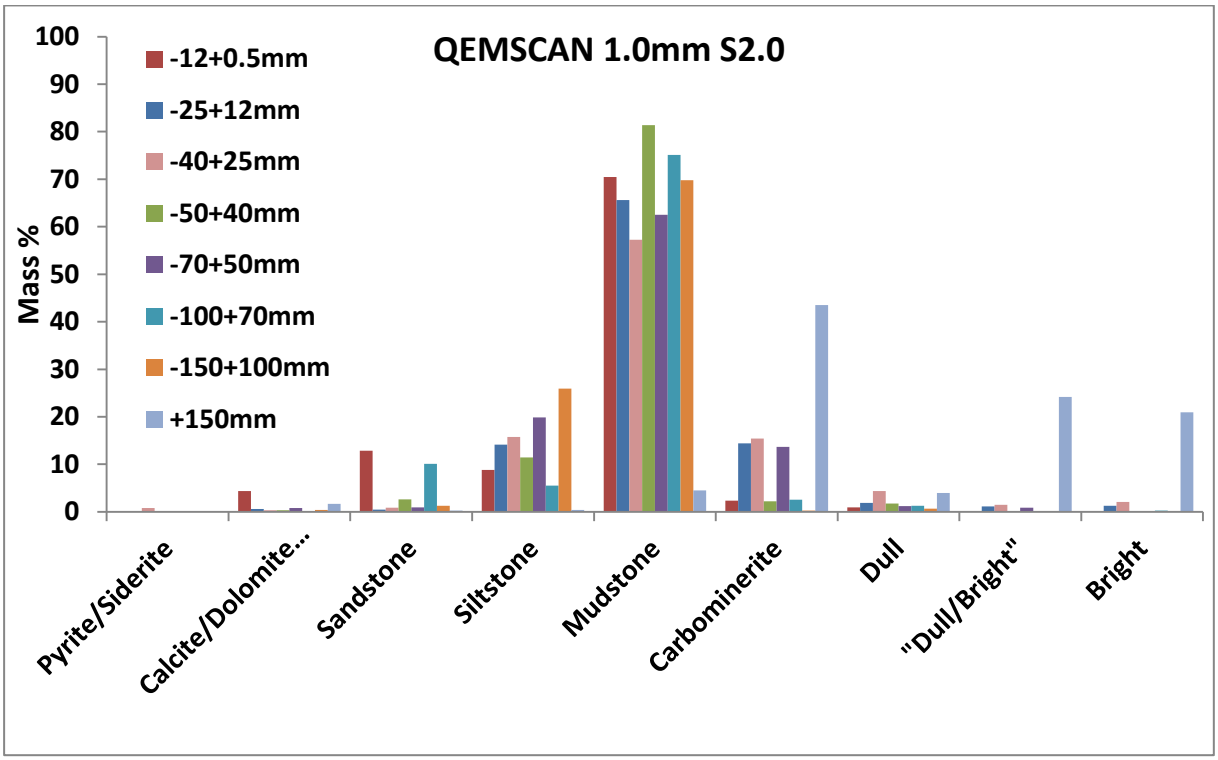

Figure 55. Particle characterisation for the QEMSCAN 1.0mm crushed 2.0g.cm^{-3} sink fractions

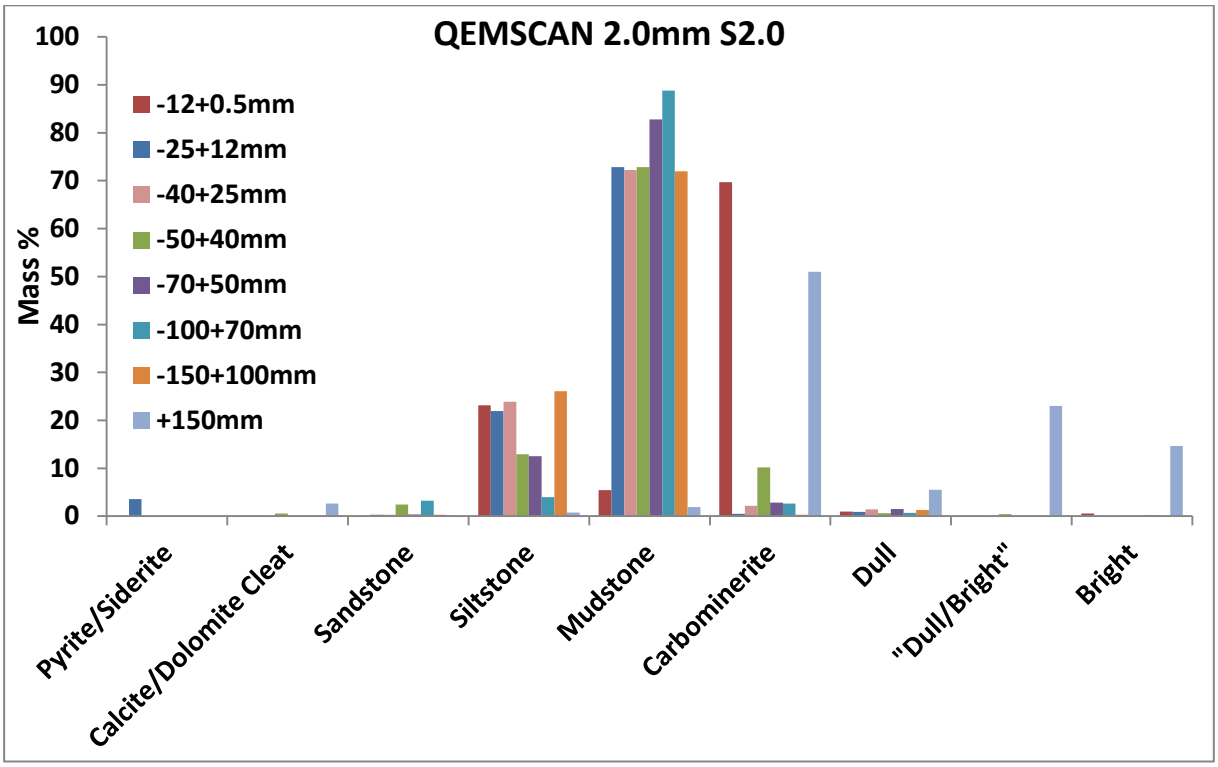

Figure 56. Particle characterisation for the QEMSCAN 2.0mm crushed 2.0g.cm^{-3} sink fractions.

The +150mm sample is identified as an outlier due to its consistent low ash and unusual particle characteristics (Table 15 and Figure 57). The sink in the +150mm size fraction was observed to be rich in bright coal bands in hand specimen. There were only two +150mm particles present in the sink fraction available for analysis. Once crushed, the coal particles were liberated and made up the predominant composition of the sample, as seen in the false colour image in Figure 57. The particles in the sample looks more like a low ash 1.5 float fraction (Figure 57) than a high ash sink fraction (Figure 58). This example illustrates the importance of having sufficient samples to provide for a representative analysis.

Table 15: Dry base ash % as determined by QEMSCAN analysis on the 2.0g.cm^{-3} sink across size fraction (suspected outliers highlighted in red).

Size (mm)	0.5mm ash% (DB)	1.0mm ash% (DB)	2.0mm ash% (DB)
-12+0.5	79.55	77.73	81.12
-25+12	66.31	73.71	78.05
-40+25	72.31	66.73	79.18
-50+40	77.25	80.66	77.99
-70+50	73.31	76.86	78.49
-100+70	76.71	80.81	81.36
-150+100	78.54	81.50	80.00
+150	29.2	26.16	26.71
Average (incl. outlier)	69.15	70.52	72.86
Average (excl. outlier)	74.85	76.86	79.46

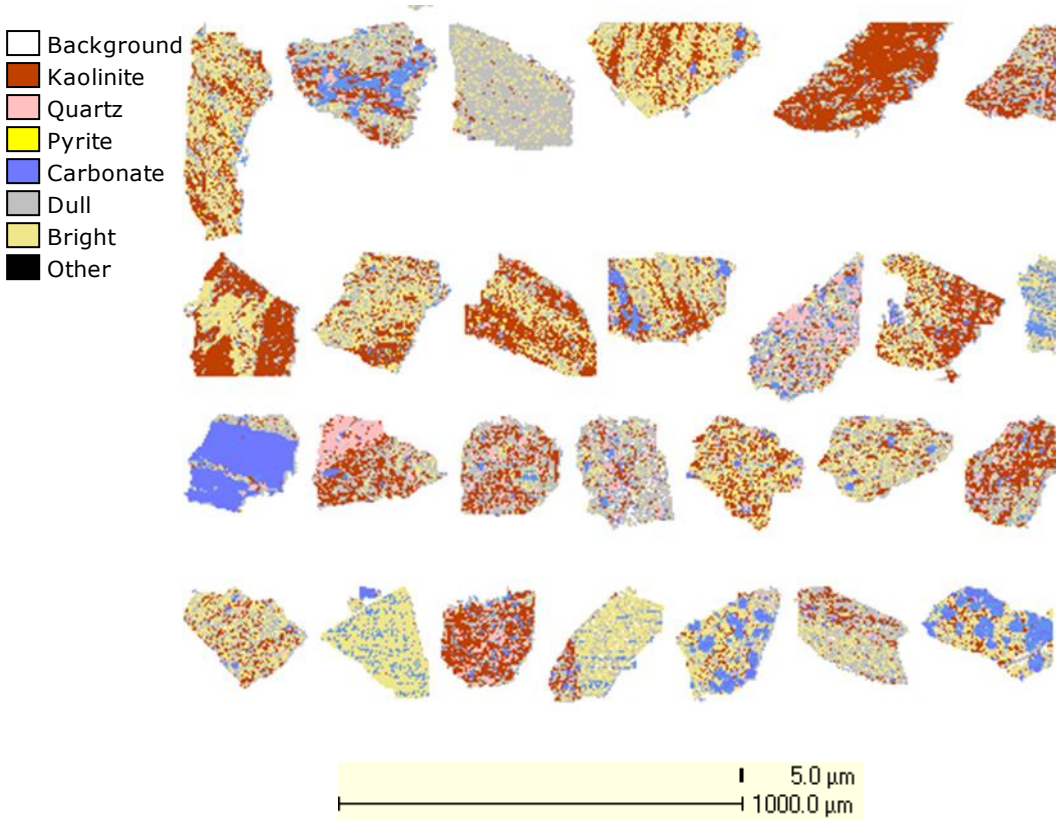

Figure 57. False colour image of particles in the +150mm size fraction, 0.5mm QEMSCAN sample.

It is observed in Figure 58 that there is mostly stone present with a few dull/bright and carbominerite liberated grains. As is observed with prior particle characterisation graphs, liberation appears random with respect to size fraction. The kaolinite-rich particles frequently have bright coal laminae, which serve as cleavage planes. Liberated pyrite particles and pyrite nodules are observed within mudstone particles.

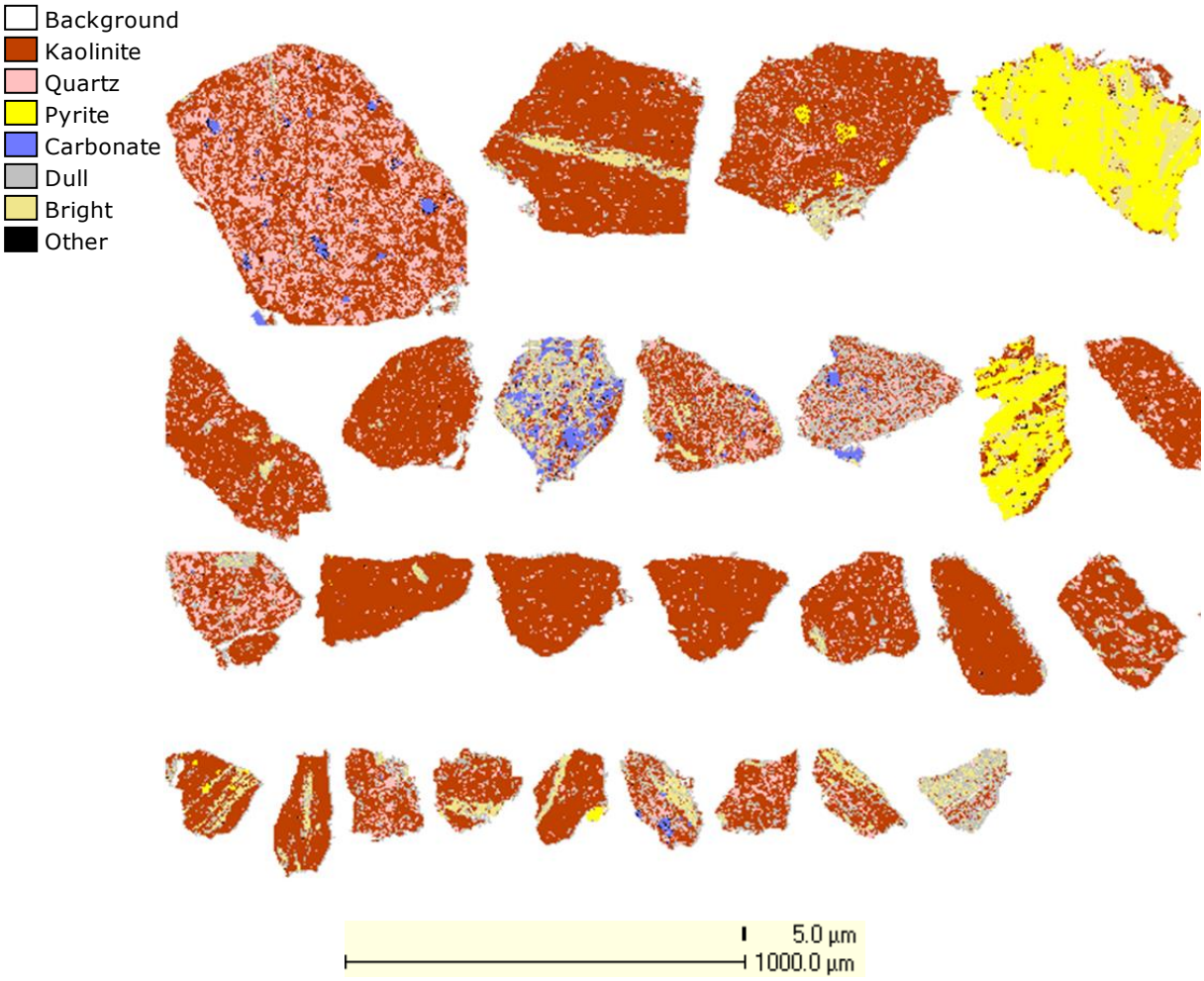

Figure 58. False colour image of particles present in the 2.0g.cm^{-3} sink, -40+25mm size fraction, 0.5mm QEMSCAN sample.

5.2.9 Particle characteristics – Average relative density per size fraction

The average particle distribution across the density fractions are illustrated in Figure 59. There is a general trend of increasing sandstone, siltstone and mudstone with increasing size fraction. Bright coal decreases in proportion for increasing relative density fraction.

Carbominerite is present in low proportions in the low density fractions (1.4-1.5g.cm^{-3}), highest for the middle to higher density fractions (1.6-2.0g.cm^{-3}), and drops significantly in the sink fraction. There is a low proportion of dull coal across all density fractions, indicating that this specific coal has particularly low proportions of dull coal.

Carbonate cleats are most abundant in the 1.4g.cm^{-3} floats and decrease in proportion with decreasing size fraction. Pyrite cleats are highest in the 1.8g.cm^{-3} float, and decrease in proportion as relative density increases.

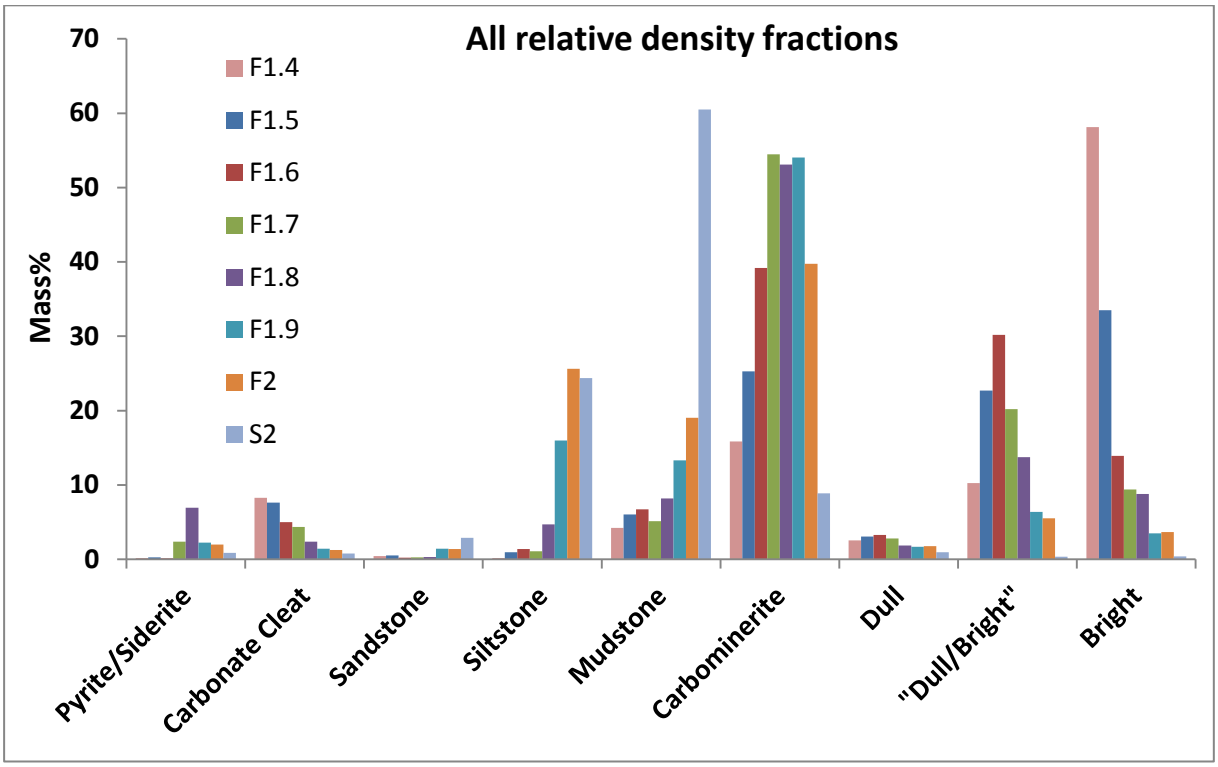

Figure 59. Particle characterisation graph of the average phase proportion per relative density fraction.

5.3 Density categorizer

A density categorizer created with iDiscover software on QEMSCAN was used to calculate the yield per density fraction. A density value is input for each distinguishable mineralogical phase present. The software utilizes a categoriser to separate particles by their density, calculated by an average volume weighting of individual minerals making up the particle. QEMSCAN measures the volume percent proportion and densities per individual mineral/coal are input to then calculate mass%, which is compared to the yield mass% determine using float and sink analysis.

Figure 60 illustrates the efficacy of the QEMSCAN density categoriser – less than 45% of the average 1.4g.cm^{-3} float particles were correctly allocated into the 1.3-1.4g.cm^{-3} density. ~20% of particles reported to the 1.4-1.5g.cm^{-3} density, ~16% to the 1.5-1.6g.cm^{-3} density and smaller proportions to higher density ranges. The reason for high proportions of particles with a density higher than 1.4g.cm^{-3} is due to liberation of smaller particles along cleat/coal and clay/coal boundaries (Figure 61).

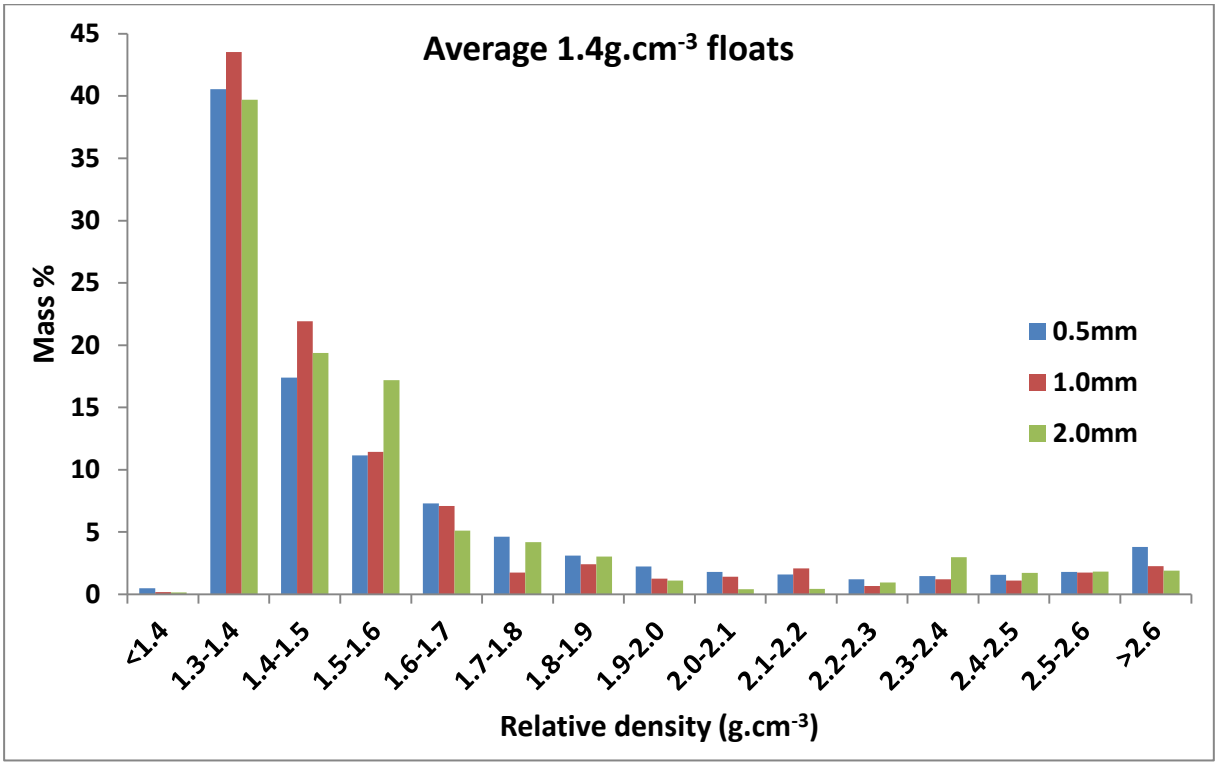

Figure 60. Density allocation of the average 1.4g.cm^{-3} floats from the -25+12mm, -40+25mm, -50+40mm, -70+50mm and -100+70mm size fractions.

As illustrated in the example in Figure 61, assuming a particle has 97% bright coal and 3% kaolinite by volume, the total particle density would be 1.34g.cm^{-3}. If the coal had to break along a kaolinite lamination during crushing, a number of smaller particles would be generated. These smaller liberated particles would have different proportions of coal to mineral, thus the densities of the liberated particles will be different from that of the original particle. Very fine kaolinite would generate many small particles with relative densities above 2.0g.cm^{-3}. When a large particle is crushed, 'puzzle pieces' of the original particle are created.

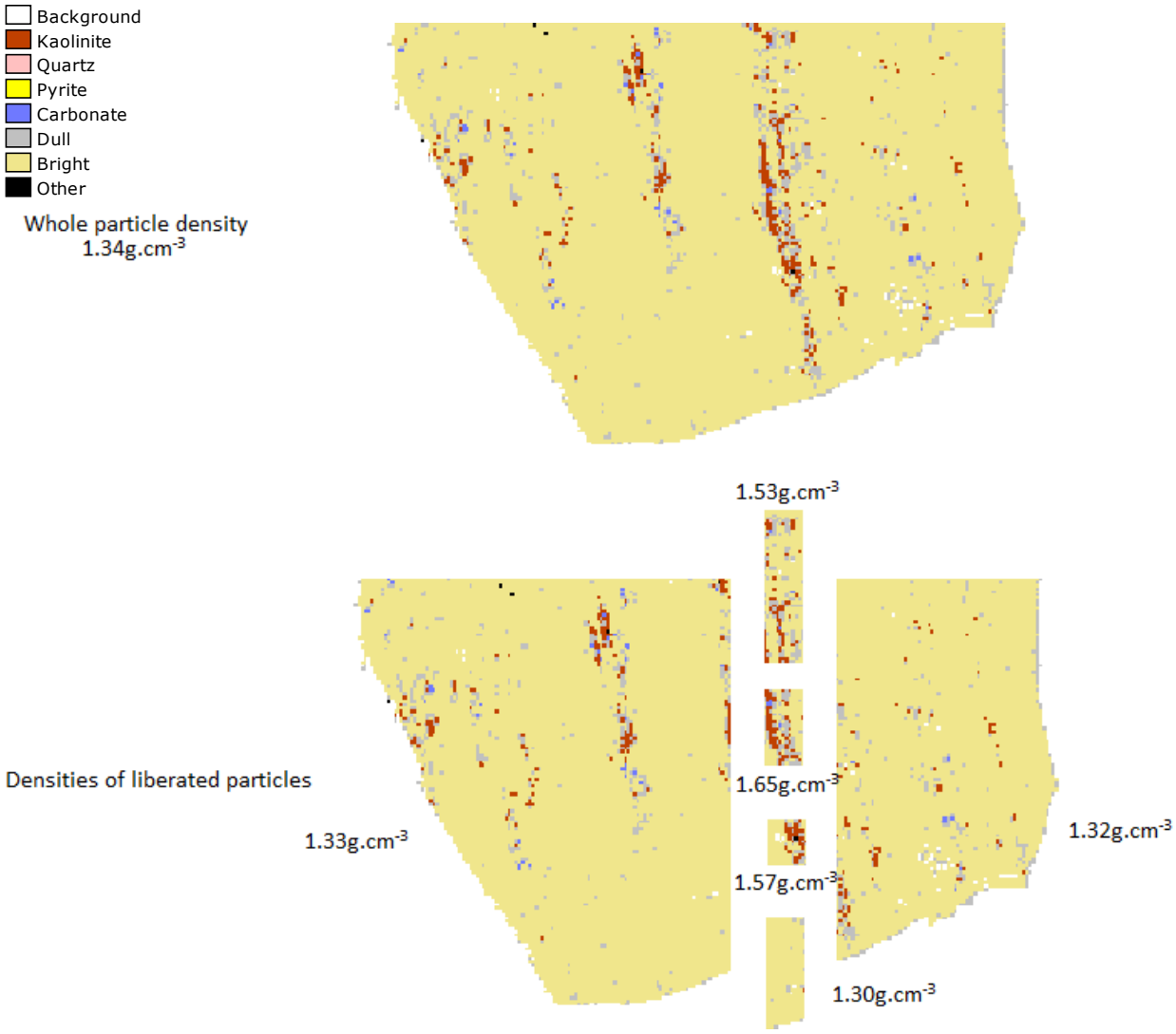

Figure 61. False colour image of a bright coal particle with clay laminations to illustrate the effect of liberation on particle density in the 1.3-1.5g.cm^{-3} range. The particle is from the -25+12mm size fraction, 1.4g.cm^{-3} float, 2.0mm QEMSCAN sample.

The particles with densities higher than 2.6g.cm^{-3} present in the lower density fractions are a result of liberated pyrite and carbonate cleat material (Figure 32). The proportion of cleat material was between 1.9-3.8% in the 1.4g.cm^{-3} floats, was the highest for the 1.5g.cm^{-3} floats (1.2-8.1%, Figure 61) and again decreases for increasing density fraction (1.6-5.7% for the 1.6g.cm^{-3} floats and 0.5-5.5% for the 1.7g.cm^{-3} floats) (Figure 62 and Figure 63).

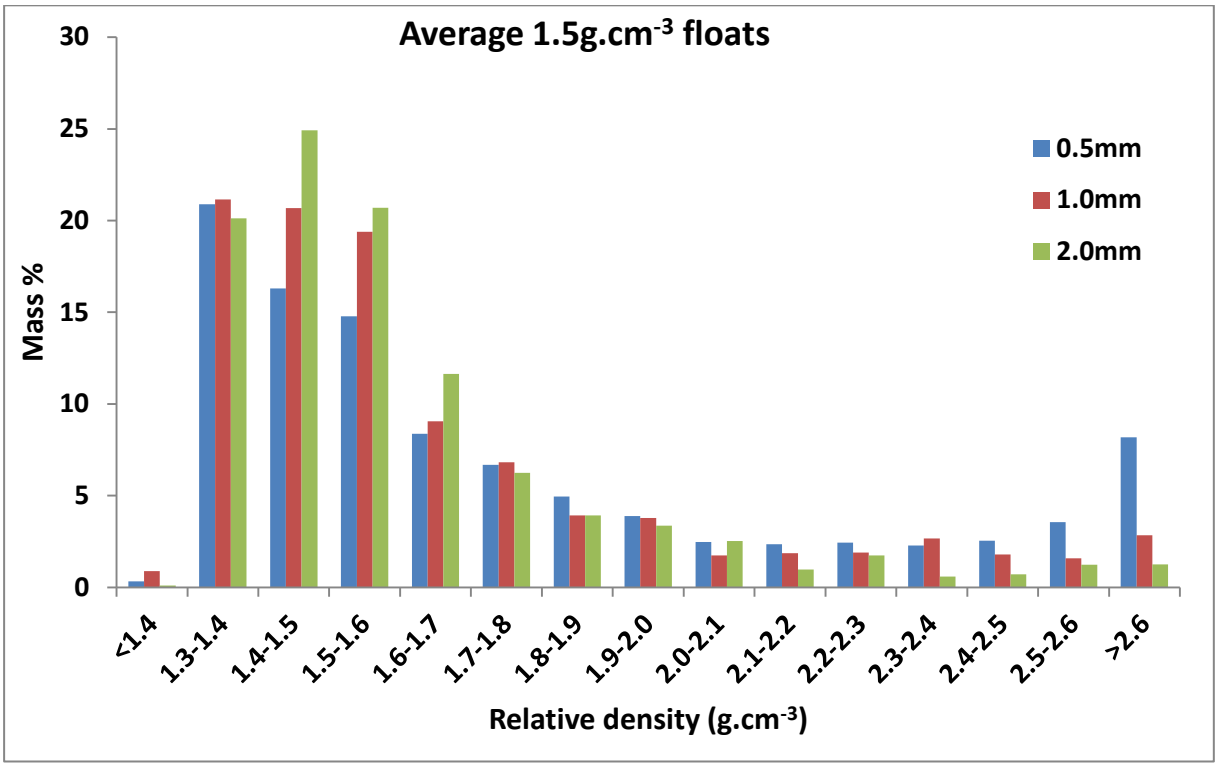

Figure 62. Density allocation of the average 1.5g.cm^{-3} floats from the -12+0.5mm, -25+12mm, -40+25mm, -50+40mm, -70+50mm, -100+70mm and -150+100mm size fractions.

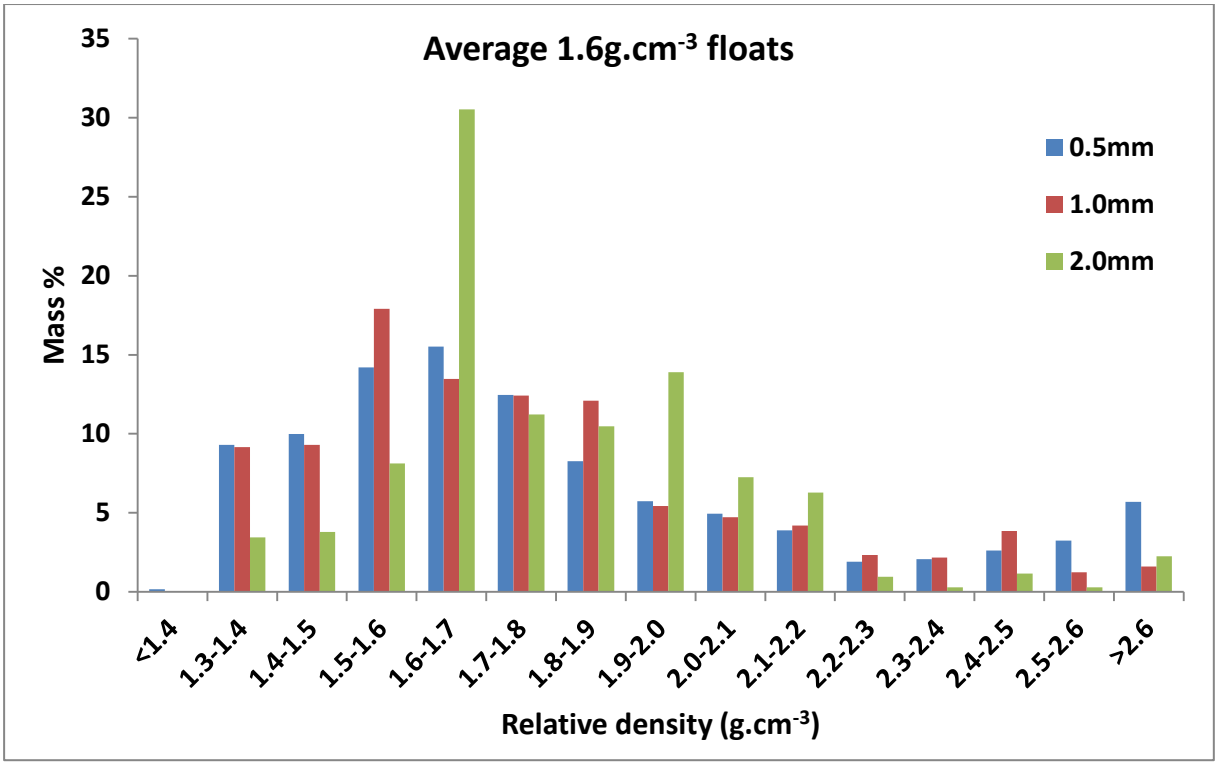

Figure 63. Density allocation of the average 1.6g.cm^{-3} floats from the -25+12mm, -40+25mm, -50+40mm, -70+50mm, -100+70mm and -150+100mm size fractions.

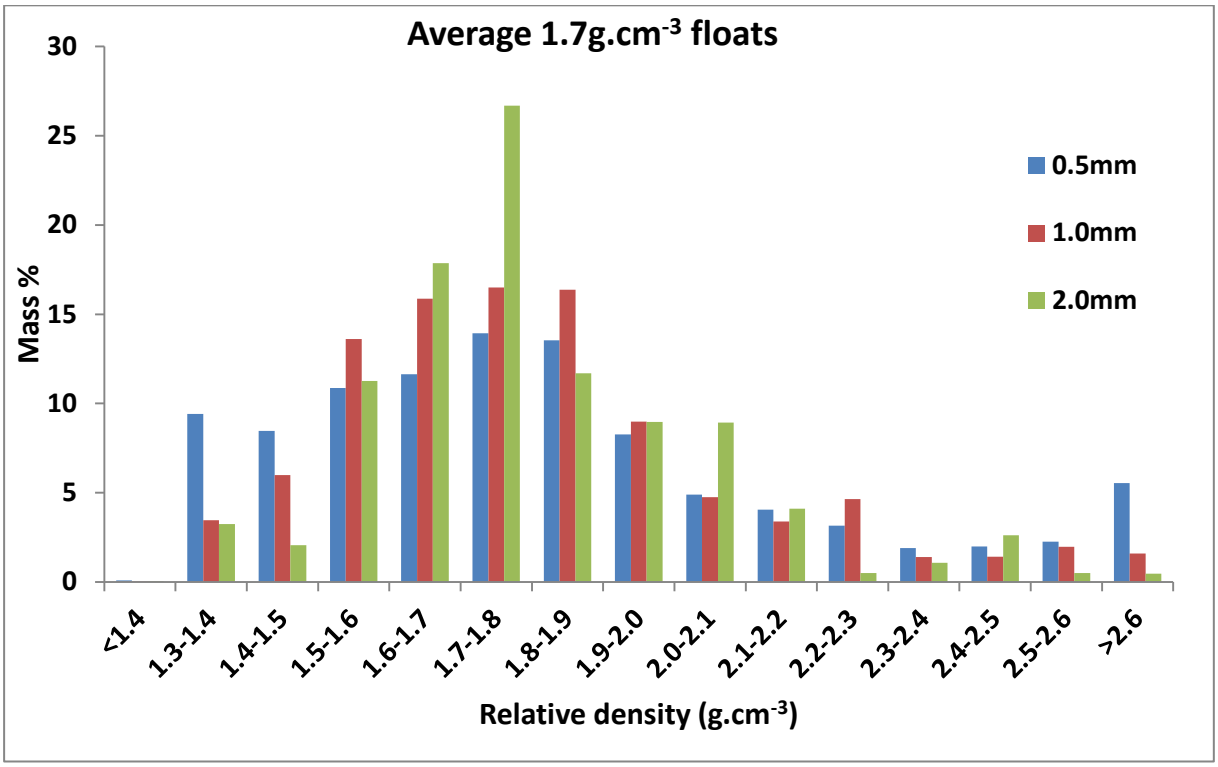

Figure 64. Density allocation of the average 1.7g.cm^{-3} floats from the -25+12mm, -40+25mm, -50+40mm, -70+50mm, -100+70mm, -150+100mm and +150mm size fractions.

The example below illustrates the wide density distribution of particles that are liberated in the floats (Figure 65). Assuming bright coal breaks along fine fractures and the carbopolyminerite-carbargillite boundary, a number of smaller particles are generated in the 1.3-1.8g.cm^{-3} range with various ratios of bright coal to kaolinite. A few larger particles within a smaller density range (1.7-2.0g.cm^{-3}) are also generated. The liberation of bright coal laminations can be seen as the high proportion of 1.3-1.4g.cm^{-3} particles in Figure 62, Figure 63 and Figure 64 for the 1.5, 1.6 and 1.7 floats respectively.

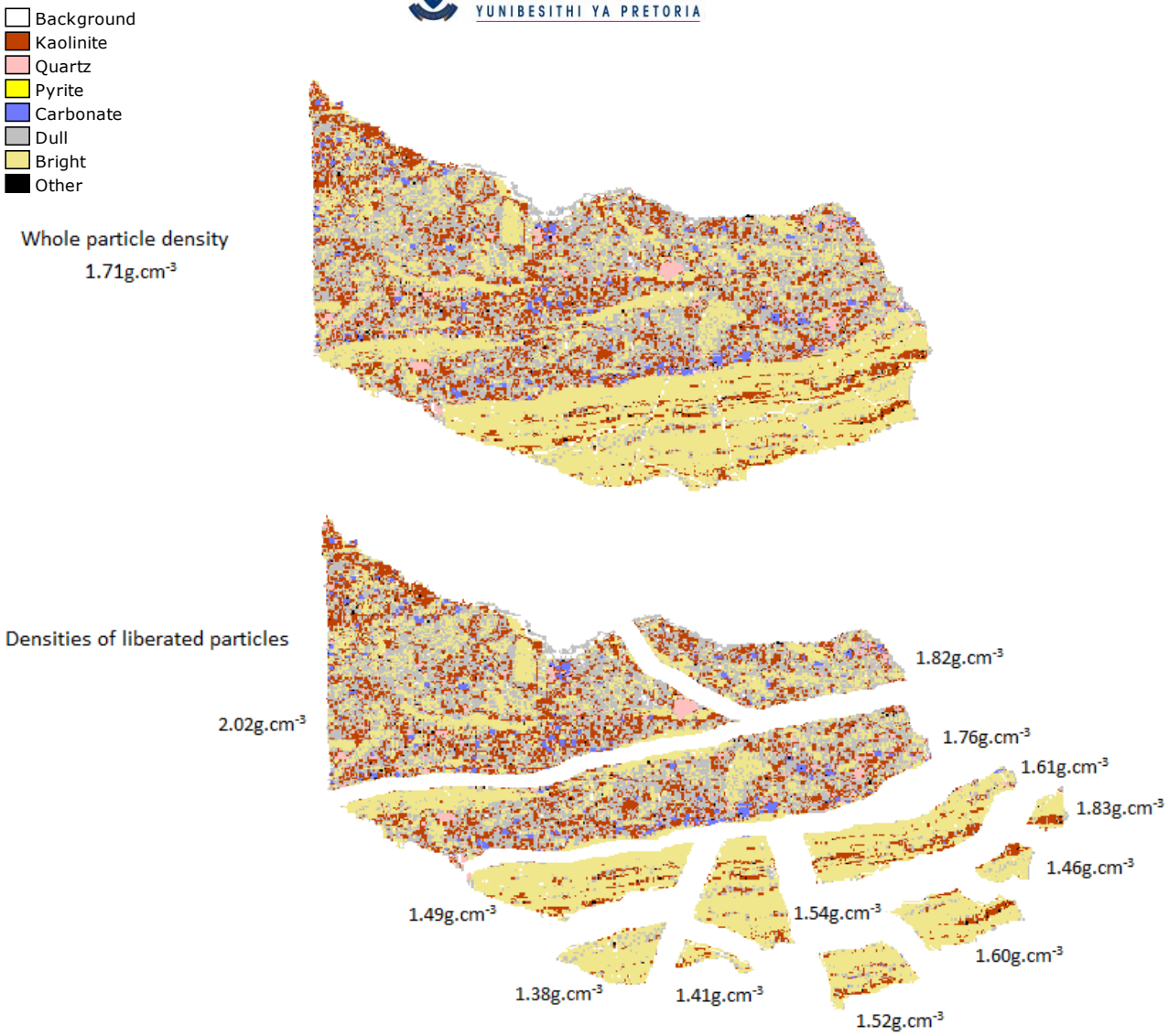

Figure 65. False colour image of a carbominerite coal particle (carbopolyminerite) with a high proportion of bright coal (with kaolinite laminations) to illustrate the effect of liberation on particle density distributions. The particle is from the -50+40mm size fraction, 1.7 float, 2.0mm QEMSCAN sample.

The particle in Figure 66 is from the same sample as the particle in Figure 65. An important difference in the two particles is that when the particle in Figure 65 is crushed, particles with a large range of densities are created. When a particle has a texture that allows for a more uniform proportion of macerals to minerals, such as the 'speckled' texture as the particle in (Figure 66), the liberated particles are of a density similar to the original particle. The higher density fractions (>1.6g.cm^{-3}) have higher proportions of particles with more uniform 'speckled' textures, although the proportion of mineral to maceral increases as density increases. Figure 66, Figure 67 and Figure 68 display the allocation of the 1.8, 1.9 and 2.0 floats respectively.

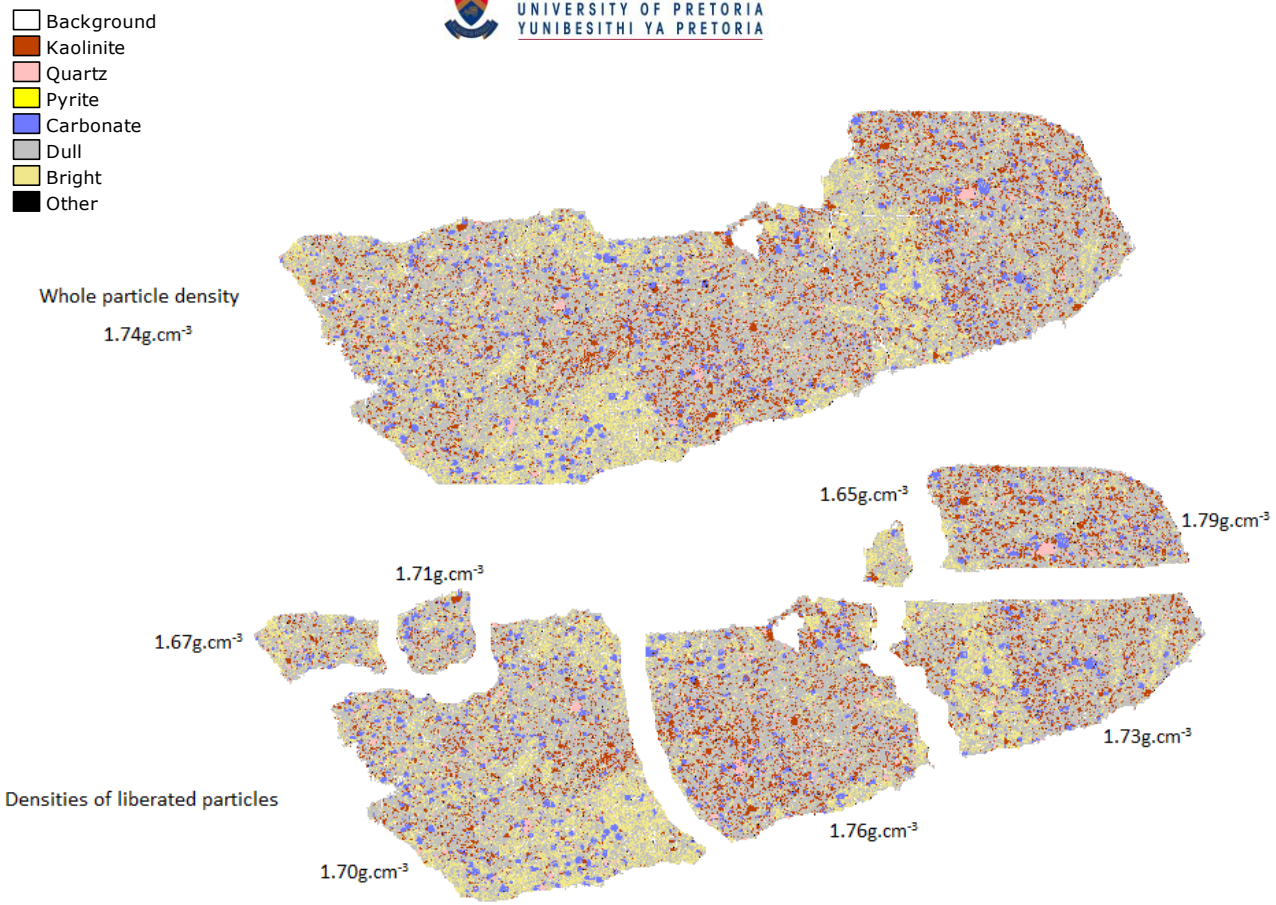

Figure 66. False colour image of a carbominerite coal particle (carbopolyminerite) with a more consistent 'speckled' texture to illustrate the effect of liberation on particle density distributions. The particle is from the -50+40mm size fraction, 1.7 float, 2.0mm QEMSCAN sample.

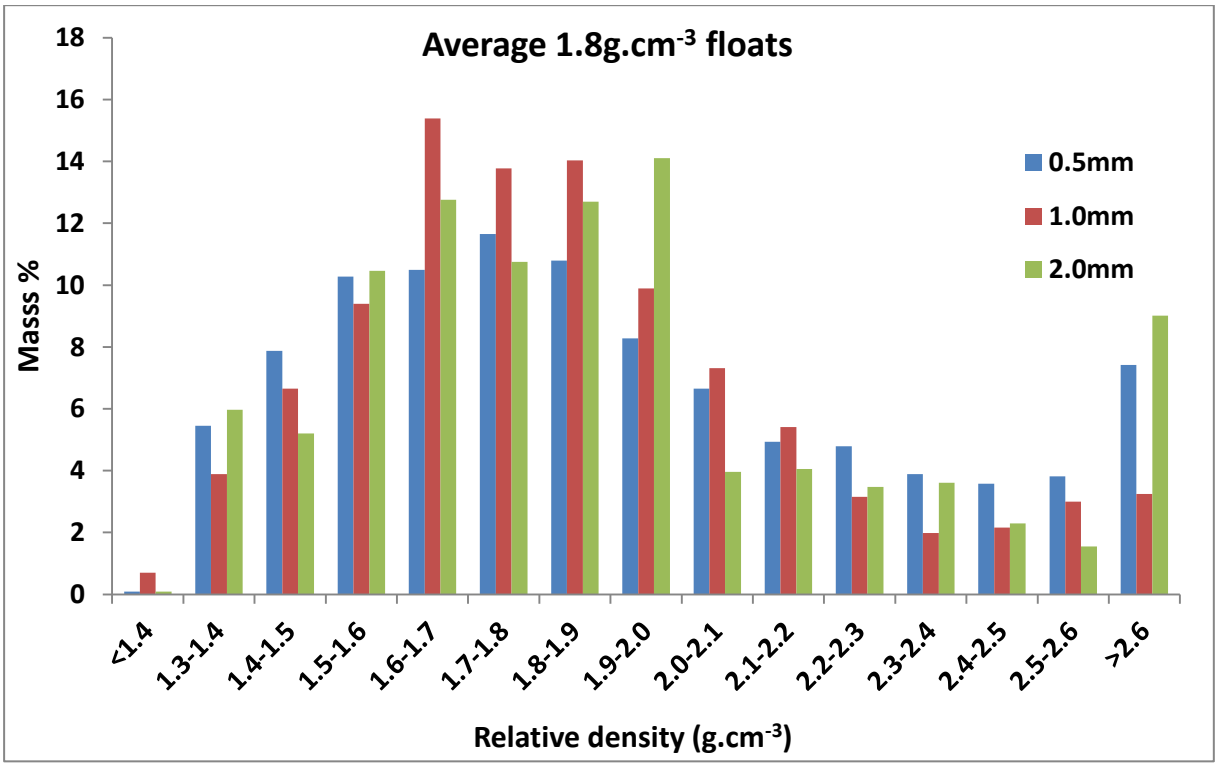

Figure 67. Density allocation of the average 1.8g.cm^{-3} floats from the -12+0.5mm, -25+12mm, -40+25mm, -50+40mm, -70+50mm, -100+70mm, -150+100mm and +150mm size fractions.

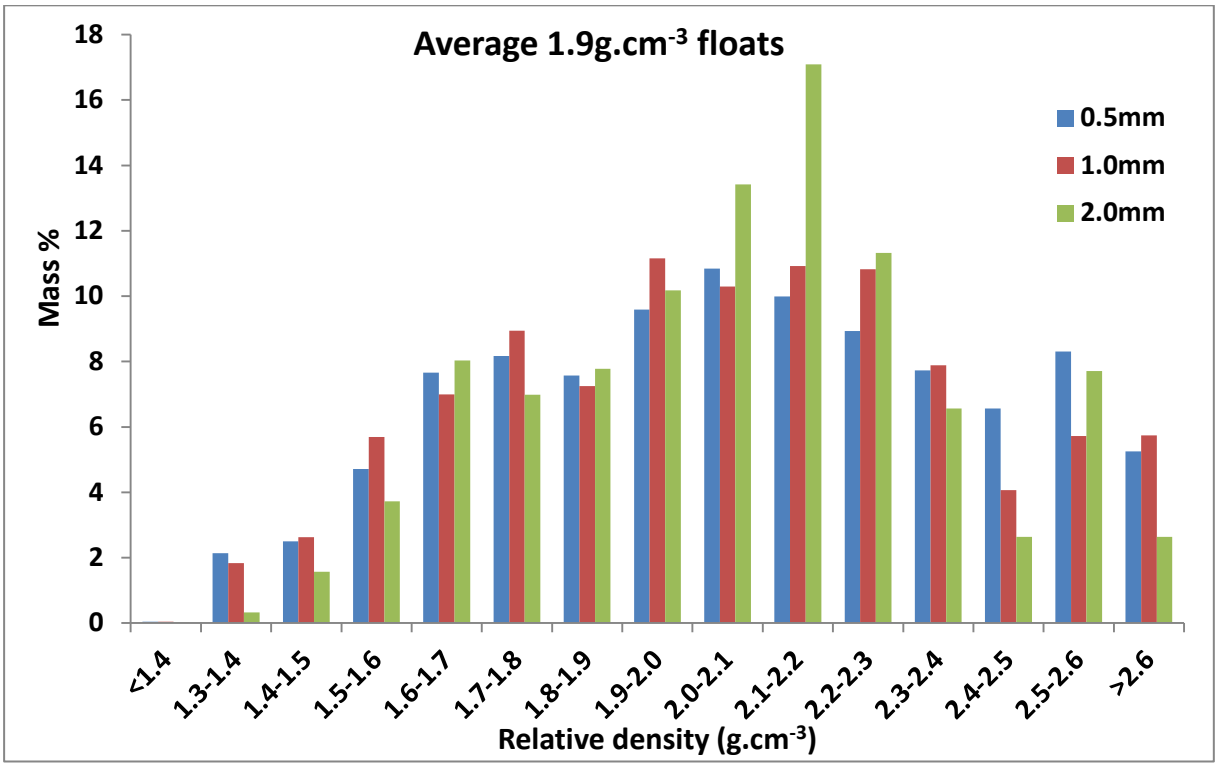

Figure 68. Density allocation of the average 1.8g.cm^{-3} floats from the -25+12mm, -50+40mm, -70+50mm, -100+70mm, -150+100mm and +150mm size fractions.

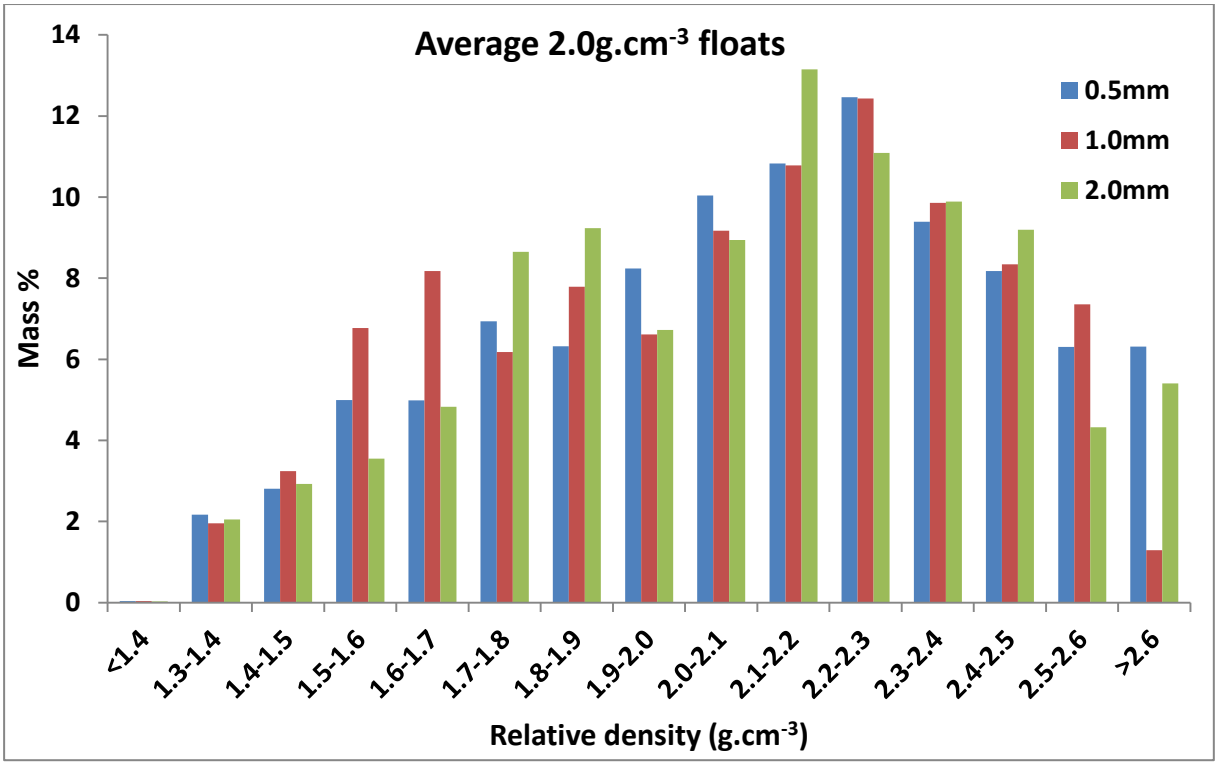

Figure 69. Density allocation of the average 1.9g.cm^{-3} floats from the -12+0.5mm, -25+12mm, -50+40mm, -70+50mm, -100+70mm, -150+100mm and +150mm size fractions.

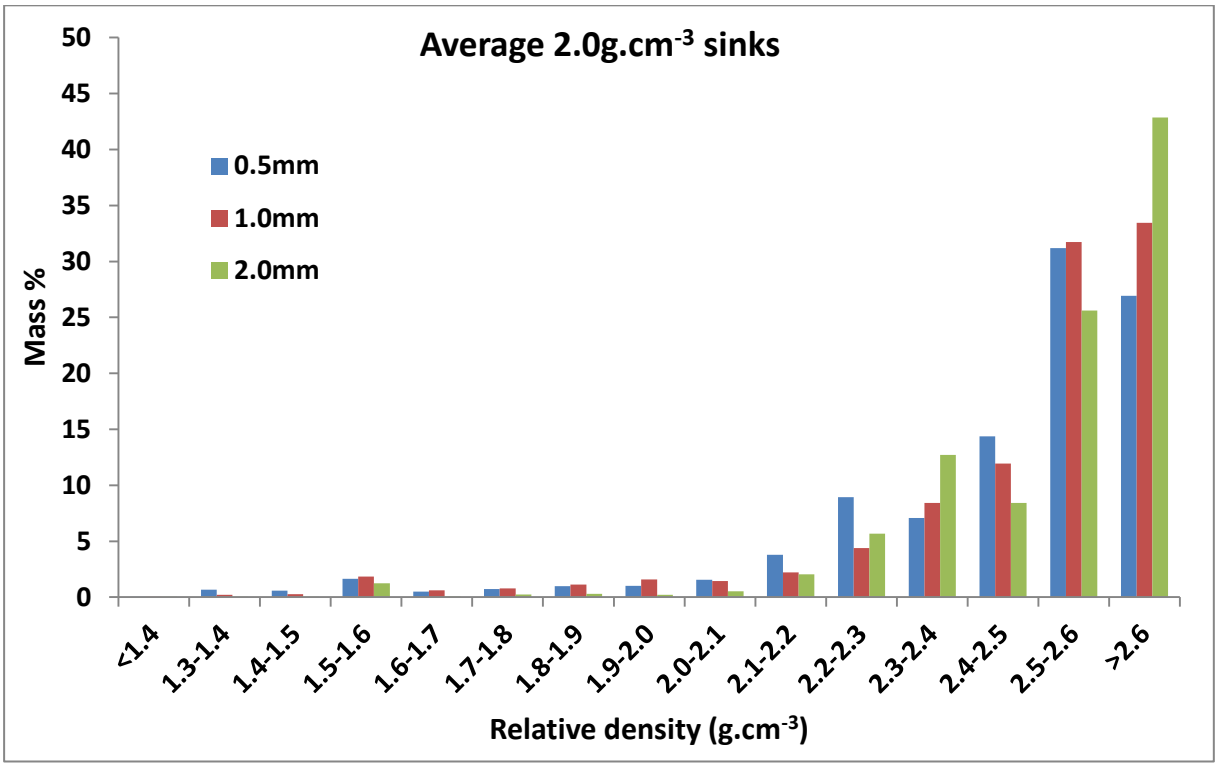

Figure 70. Density allocation of the average 2.0g.cm^{-3} sinks from the -12+0.5mm, -25+12mm, -40+25mm, -50+40mm, -70+50mm, -100+70mm, -150+100mm and +150mm size fractions.

The sink fraction comprises of a range of densities below 2.65g.cm^{-3}, due to mineral and coal material forming an intricate texture and much varied proportion of coal to mineral matter. Figure 71 illustrates the liberation of an elevated proportion of 1.4-1.6g.cm^{-3} particles as observed in Figure 70.

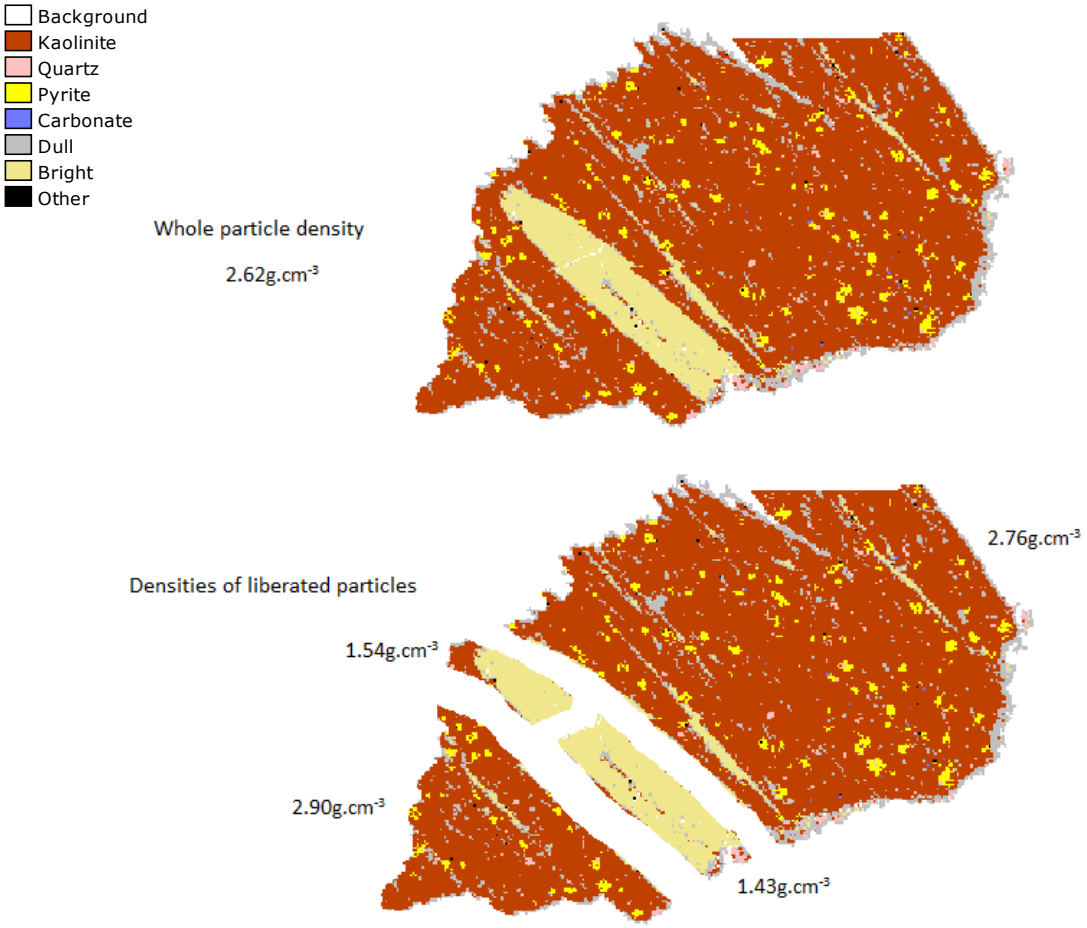

Figure 71. False colour image of a mudstone with pyrite nodules and a kaolinite lamination to illustrate the effect of liberation on particle density distributions. The particle is from the -70+50mm size fraction, 2.0 sink, 2.0mm QEMSCAN sample.

In summary, the significant proportion of misplaced particles (in terms of density) in the QEMSCAN density allocation is due to significant liberation of particles. In fact, the float and sink data is less accurate due to lock/non-liberated components. When a large particle is crushed, 'puzzle pieces' of the original particle are created. The smaller, liberated particles have densities different to the original particle. Layers/laminations of bright coal liberate smaller particles that have a wide range of densities when crushed. Crushing a carbominerite particle with a 'speckled' inertodentritic texture creates smaller particles of a smaller density range that are similar to the original particle. Most of the liberated particles have densities either higher or lower than the fraction from which it originated, resulting in a wide density range of particles. At first pass, it seems that QEMSCAN cannot correctly predict yields.

5.4 Yield prediction using QEMSCAN

The original coal feed sample is screened into a number of size ranges, on which float and sink is performed. From the eight size ranges, QEMSCAN predicted density fraction mass yields were determined for the five complete sets (Table 16). The -150+100mm size fraction with 1.4 float outlier was included. The individual floats and sinks were crushed to 0.5mm,

1.0mm and 2.0mm samples for QEMSCAN analysis, where the particles are allocated densities using a categoriser.

The QEMSCAN mass% per density is summed up across density fractions (e.g., sum of mass% 1.4g.cm^{-3} particles for the 1.5, 1.8, 2.0 floats and 2.0 sink) for a given size fraction. The newly determined mass % per density is used to calculate the QEMSCAN predicted yield. The difference between the yield as determined by float and sink analysis, and the QEMSCAN predicted yield will be error due to liberation.

The float and sink yields are summarized in Table 16, and the corresponding cumulative yields are plotted in Figure 72 for each size fraction that had undergone float and sink testing. Theoretically, the larger original sized particles show more liberation than the smaller original sized fractions, but Figure 72 shows that the coarse fractions display similar results to each other, while the -12+0.5mm fraction is observably different. Table 17, Table 18 and Table 19 are summaries of the QEMSCAN yields calculated per crushed fraction (0.5mm, 1.0mm and 2.0mm respectively).

Table 16: Yields determined using float and sink analysis.

Density (g.cm^{-3})	-12+0.5mm	-50+40mm	-70+50mm	-100+70mm	-150+100mm
1.4		1.9	3.1	2.3	0.3
1.5	19.9	10.1	8.3	8.3	5.0
1.6		23.6	22.5	26.5	36.0
1.7		27.1	27.3	24.6	25.0
1.8	37.0	6.4	5.6	7.3	3.8
1.9		4.4	3.6	5.1	5.3
2	9.0	3.4	3.7	4.4	0.9
S2.0	34.0	23.1	26.0	21.5	23.7

It is important to note that the finest size fraction (-12+0.5mm) has a higher yield for the 1.5 float (~8 mass% by difference), while the coarsest size fraction (-150+100mm) has the lowest yield for the 1.5 float (~5 mass% by difference). The -12+0.5mm size range has overestimated yield in the 1.5 float, while underestimating the 1.8 and 2.0 floats. The -150+100mm size range displays the opposite trend, slightly underestimating the 1.4 and 1.5 floats while overestimating the 1.6, 1.7 and 1.8 floats. The -50+40mm, -70+50mm and -100+70mm size ranges have similar yields, although the -70+50mm size range slightly underestimated the 1.8, 1.9 and 2.0 floats more than the other size ranges (deviates from the -50+40mm and -100+70mm yields by ~4mass% for the 1.8, 1.9 and 2.0 floats).

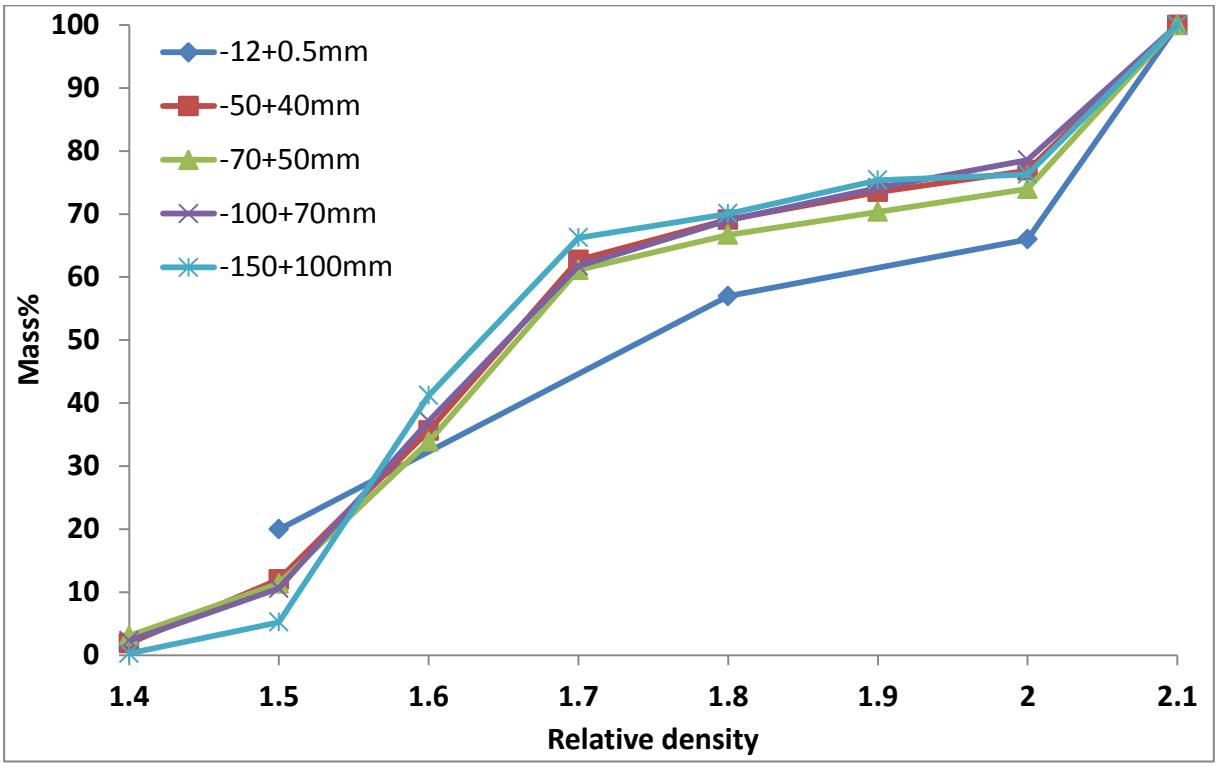

Figure 72. Cumulative float mass as determined by float and sink analysis comparing five size fractions.

Table 17: Float mass% determined using QEMSCAN software for the 0.5mm crushed samples.

Density (g.cm^{-3})	-12+0.5mm	-50+40mm	-70+50mm	-100+70mm	-150+100mm
1.4		8.9	8.3	7.0	8.0
1.5	5.9	7.9	7.4	7.4	5.6
1.6		10.5	9.3	9.4	9.6
1.7		9.4	7.8	9.0	12.0
1.8	32.0	8.3	10.2	10.1	8.6
1.9		7.2	8.4	8.6	6.0
2	15.2	4.7	6.7	4.9	3.8
S2.0	46.9	42.9	42.0	43.6	46.5

Table 18: Float mass% determined using QEMSCAN software for the 1.0mm crushed samples.

Density (g.cm^{-3})	-12+0.5mm	-50+40mm	-70+50mm	-100+70mm	-150+100mm
1.4		6.6	7.7	5.7	9.6
1.5	7.5	5.9	6.8	7.2	6.7
1.6		12.6	12.2	10.1	13.6
1.7		10.6	9.5	9.9	11.0
1.8	38.1	8.6	9.8	7.9	9.5
1.9		6.8	10.2	11.7	6.6
2	11.7	8.3	5.2	5.2	3.7
S2.0	42.7	40.6	38.7	42.3	39.3

Table 19: Float mass% determined using QEMSCAN software for the 2.0mm crushed samples.

Density (g.cm^{-3})	-12+0.5mm	-50+40mm	-70+50mm	-100+70mm	-150+100mm
1.4		5.0	5.1	7.5	4.9
1.5	5.4	6.1	3.3	4.1	5.9
1.6		7.3	7.9	7.2	14.1
1.7		19.8	10.0	8.9	17.9
1.8	38.4	11.9	14.5	15.2	11.8
1.9		11.5	5.4	8.1	14.2
2	13.7	6.3	11.9	5.3	2.1
S2.0	42.5	32.1	41.9	43.8	29.1

There is a general underestimation of QEMSCAN derived yields (Figure 73). The -12+0.5mm screened fraction is the smallest size range present in the data set. QEMSCAN and float and sink cumulative yield trends are similar in the -12+0.5mm size fraction. The only difference is QEMSCAN overestimating the proportion in the sink fraction. In the 1mm and 2mm crushed samples, QEMSCAN has overestimated the 1.5, 1.8 and 2.0 floats by ~13 mass%, ~12% and ~9% respectively. The 0.5mm fraction QEMSCAN has overestimated the proportion by ~14 mass%, ~19mass% and ~13mass% for the 1.5, 1.8 and 2.0 floats. This is expected as the 0.5mm fraction would have higher liberation of particles than the 1.0mm and 2.0mm crushed samples.

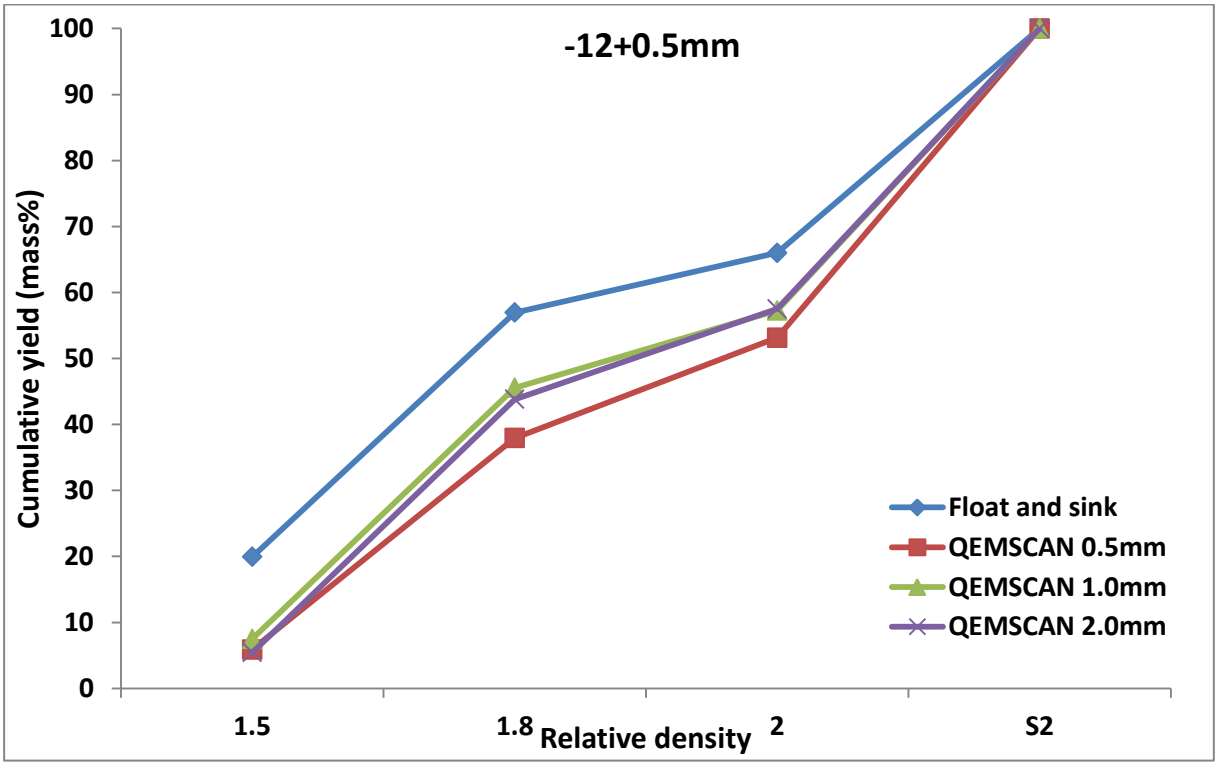

Figure 73. QEMSCAN determined cumulative float mass per crushed sample (0.5mm, 1.0mm and 2.0mm) and yield determined by float and sink analysis for the -12+0.5mm size fraction.

It is observed in Figure 74 that the QEMSCAN results deviate more from the float and sink results than in the -12+0.5mm fraction (Figure 73).

In the -50+40mm fraction, preferential cleavage and the liberation of bright coal, kaolinite lamellae and carbonate cleats has occurred. The liberated bright coal has marginally increased the proportion in the 1.4g.cm^{-3} and 1.5g.cm^{-3} density fractions, and the liberated stone and carbonate cleats has significantly increased the proportion in the sink. This is noted in the 0.5mm and 1.0mm crushed sample. In the 2mm sample, QEMSCAN has over-predicted the proportion in the sink fraction.

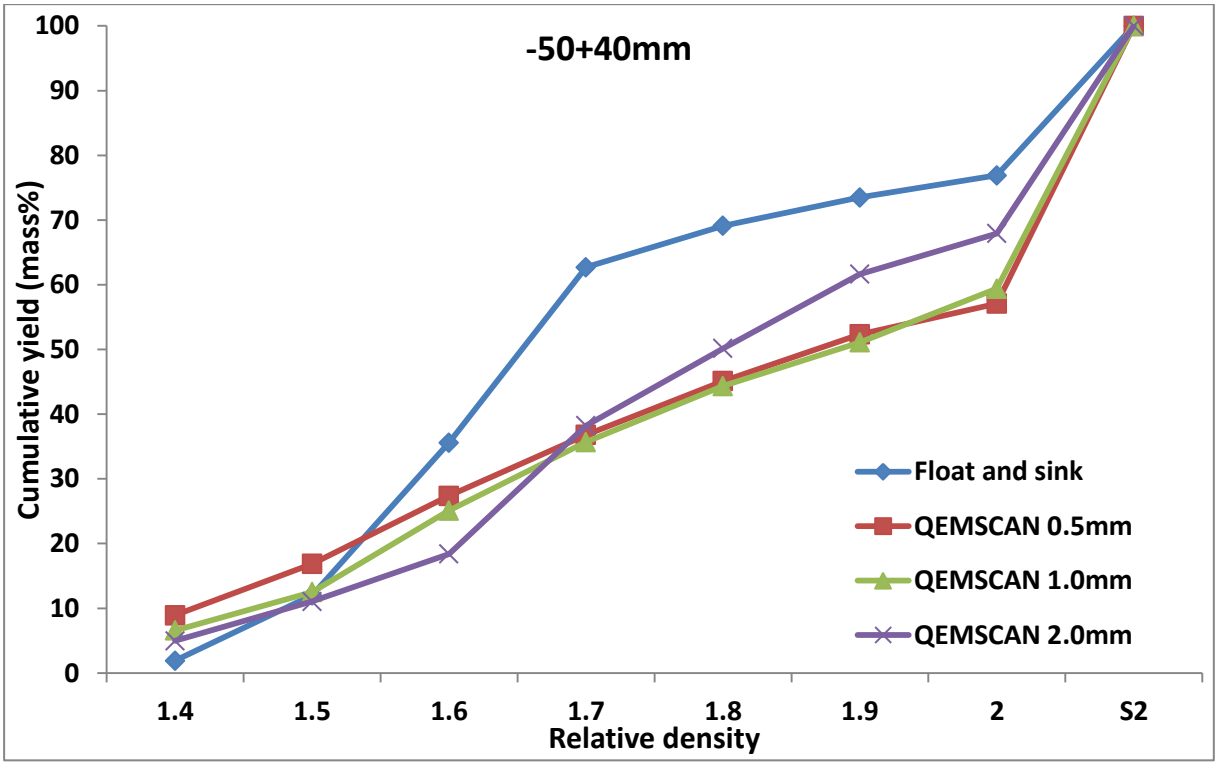

Figure 74. QEMSCAN determined cumulative float mass per crushed sample and yield determined by float and sink analysis for the -50+40mm size fraction.

It is observed from Figure 75 that QEMSCAN yields are overestimated for the 1.4 floats (4mass%) and for the 0.5mm and 1.0mm 1.5 floats (4mass% deviation and 3mass% underestimation for the 2.0mm) (similar to Figure 74). The higher yield may be caused by bright coal and cleats being liberated. Once again, the 0.5mm and 1.0mm crushed fractions have similar results (4mass% deviation).

Unlike the -50+40mm size range, the 2.0mm mass% yield for the -70+50mm size range is underestimated at both lower density and higher density ranges. The 1.0mm mass% yields follow the float and sink yields the best.

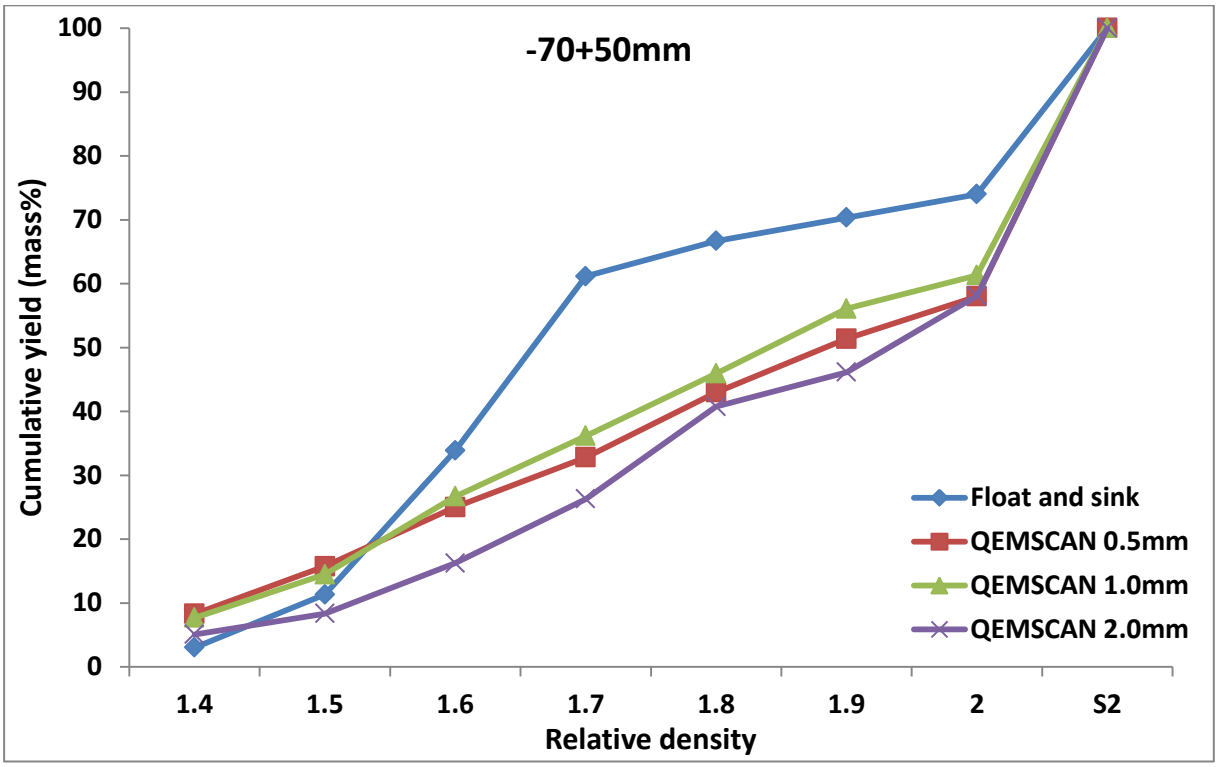

Figure 75. QEMSCAN determined cumulative float mass per crushed sample and yield determined by float and sink analysis for the -70+50mm size fraction.

Larger particles liberating bright coal and cleats may cause an elevated yield. The yields for floats higher than 1.5 are underestimated. The yields determined at floats higher than 1.5 are underestimated, similar to the -70+50mm size range. The difference to the -70+50mm size range is that the 0.5mm and 1.0mm in the -100+70mm are similar to the 2.0mm. The 2.0mm results consistently have the greatest deviation from experimental results (~35mass% in the 1.7 float), while the 1.0mm had the least deviation (~29mass% in the 1.7 float).

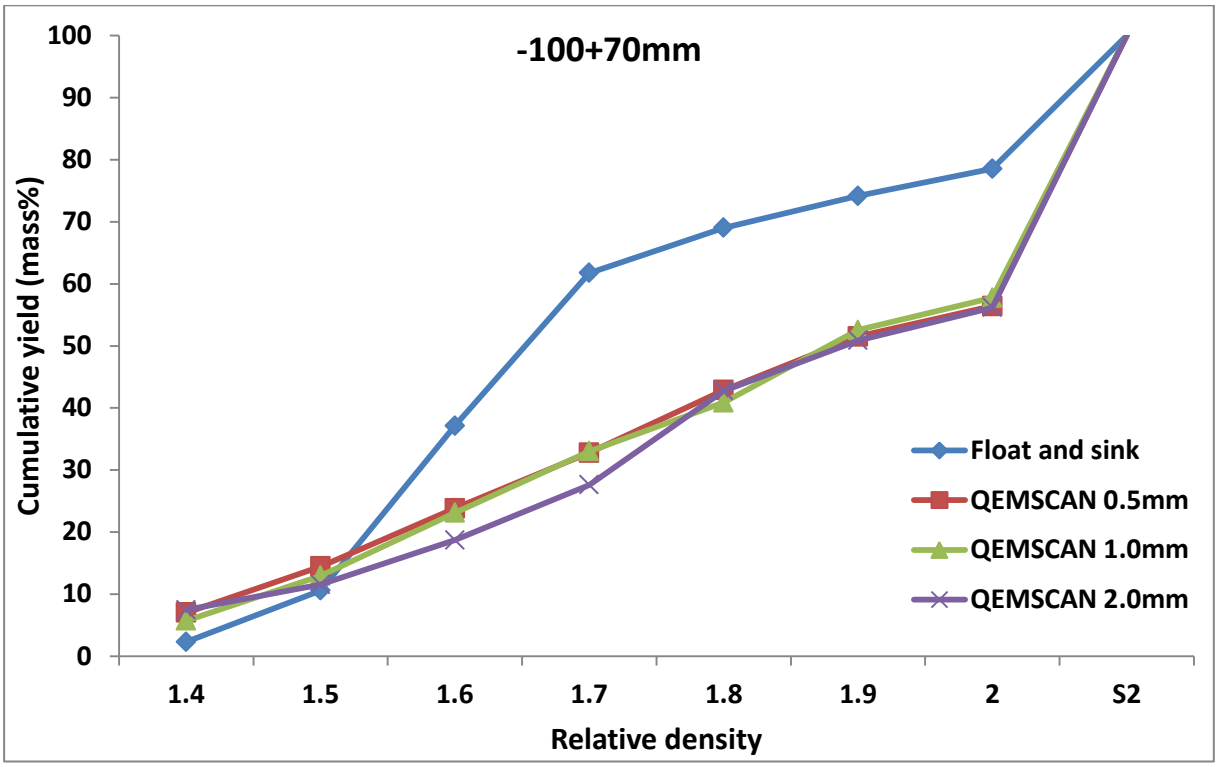

Figure 76. QEMSCAN determined cumulative float mass per crushed sample and yield determined by float and sink analysis for the -100+70mm size fraction.

A clear trend is observed illustrating that the 2.0mm QEMSCAN yield has the least deviation to the float and sink yield, while the 0.5mm QEMSCAN yield has the greatest deviation (~31mass% deviation at the 1.7 float) (Figure 77). The 2.0mm samples follow closest to the trend, similar to the -50+40mm, -70+50mm and -100+70mm trends.

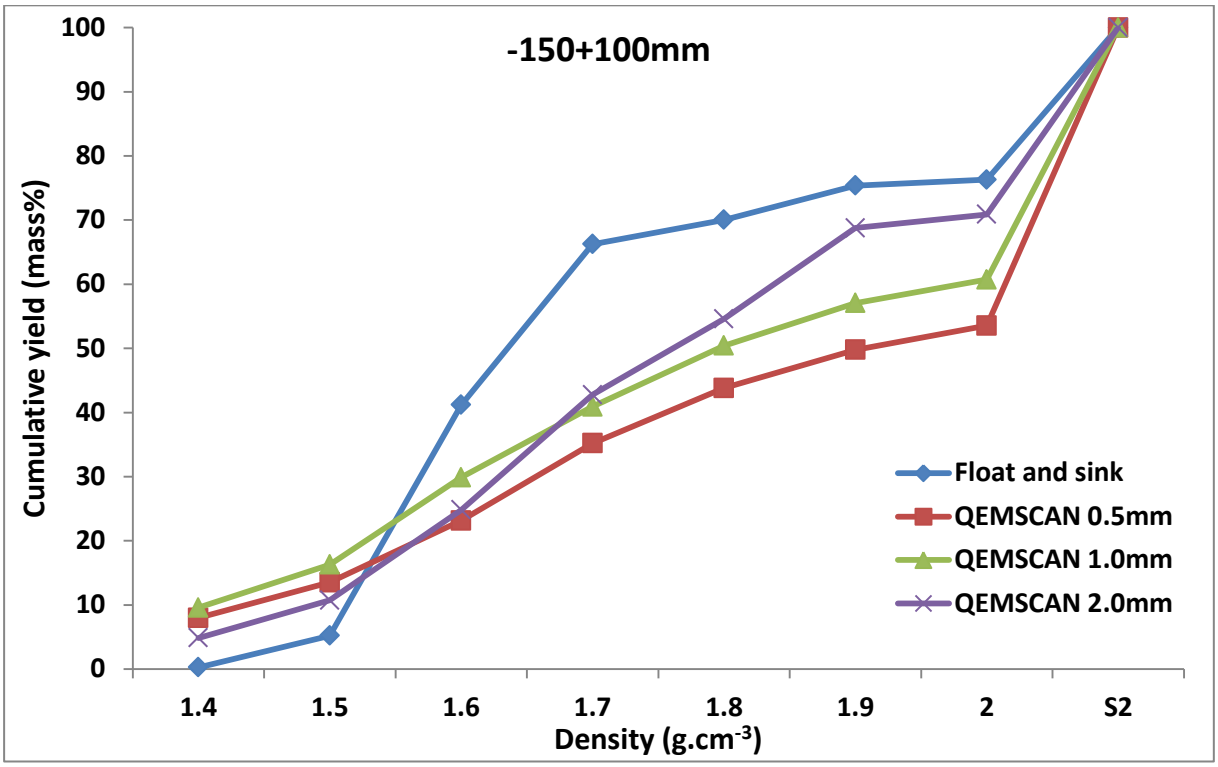

Figure 77. QEMSCAN determined cumulative float mass per crushed sample and yield determined by float and sink analysis for the -150+100mm size fraction.

5.5 Liberation analysis

The difference between the cumulative yield mass% of the experimentally determined float and sink results, and the QEMSCAN determined results are plotted in Figure 78, Figure 79, Figure 80, Figure 81 and Figure 82. The error is present due to liberation caused by crushing, as well as due to the limited density classification of organic material below a density of 1.6g.cm^{-3} on the QEMSCAN EVO50.

The 0.5mm results deviated more than the 1mm or 2mm results from experimentally derived values (Figure 78). This is expected as the 0.5mm fraction would have higher liberation of particles than the 1.0mm and 2.0mm crushed samples. The positive value with regard to error indicates there is a general underestimation of QEMSCAN derived yields.

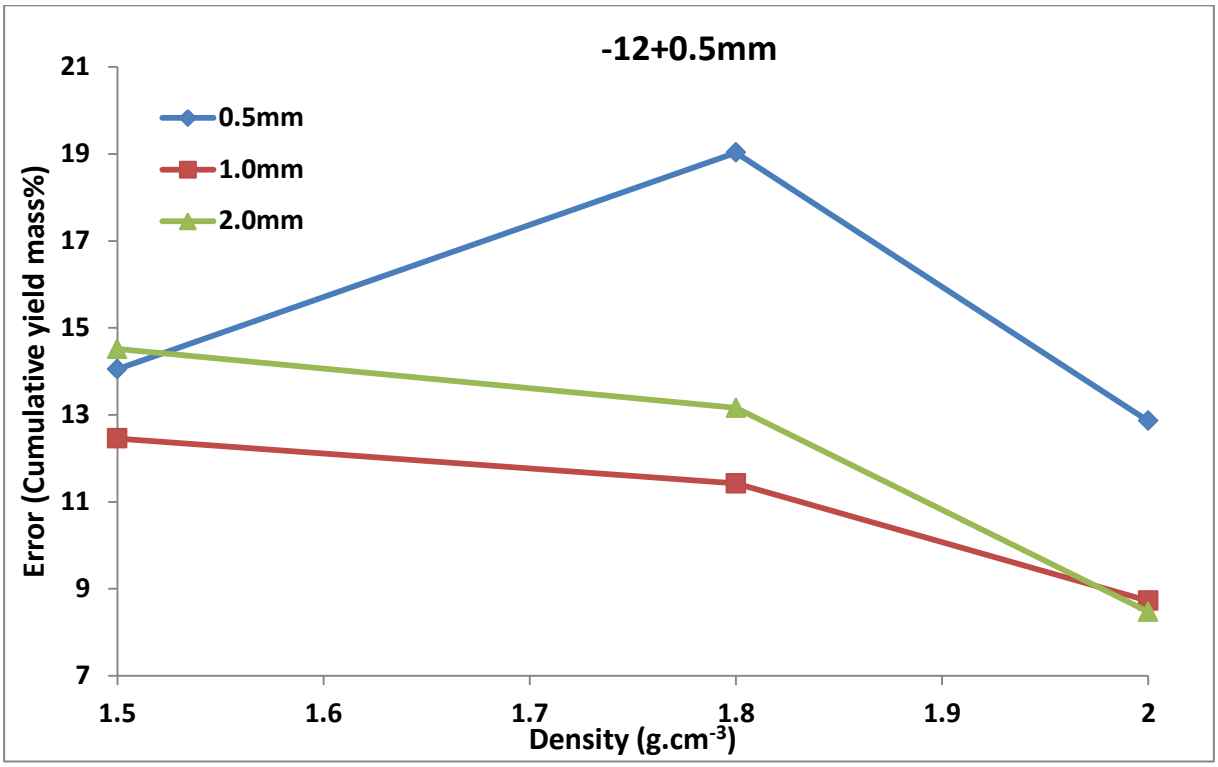

Figure 78. The difference in cumulative yield mass% between the float and sink results, and QEMSCAN derived data for the 0.5+12mm size range.

The negative error values for the 1.4g.cm^{-3} density fraction and for the 0.5mm and 1mm results for the 1.5g.cm^{-3} density fraction indicates an overestimation of cumulative yield mass%, while all positive values are underestimations. It is observed in Figure 79 that the 0.5mm and 1.0mm crushed fractions have similar results. The 'peak' at a density of 1.7g.cm^{-3} indicates the greatest discrepancy (error) between QEMSCAN and experimental results.

The QEMSCAN yield is underestimated between 3-7mass% for the 1.4 float. The 1.5 float yield values predicted for the 1.0mm and 2.0mm samples were within a percent to the float and sink yield , while the 0.5mm sample overestimated the yield by ~5mass%. The QEMSCAN yield is then underestimated for the 1.6-2.0 floats.

There is an average underestimation of 12mass% 1.6 float, 26mass% 1.7 float, 23mass% 1.8 float, 18mass% 1.9 float and15mass% 2.0 float. The 2.0mm trend has a more significant deviation from the float and sink yield in the 1.6 float, after which it has better yields than the 0.5mm and 1.0mm.

Error increases with density for increasing crushed fraction (0.5mm, 1.0mm and 2.0mm respectively) up to a density of 1.7g.cm^{-3}. After 1.7g.cm^{-3}, the 0.5mm and 1.0mm results are similar, while the 2.0mm results have the smallest error when compared to experimental results.

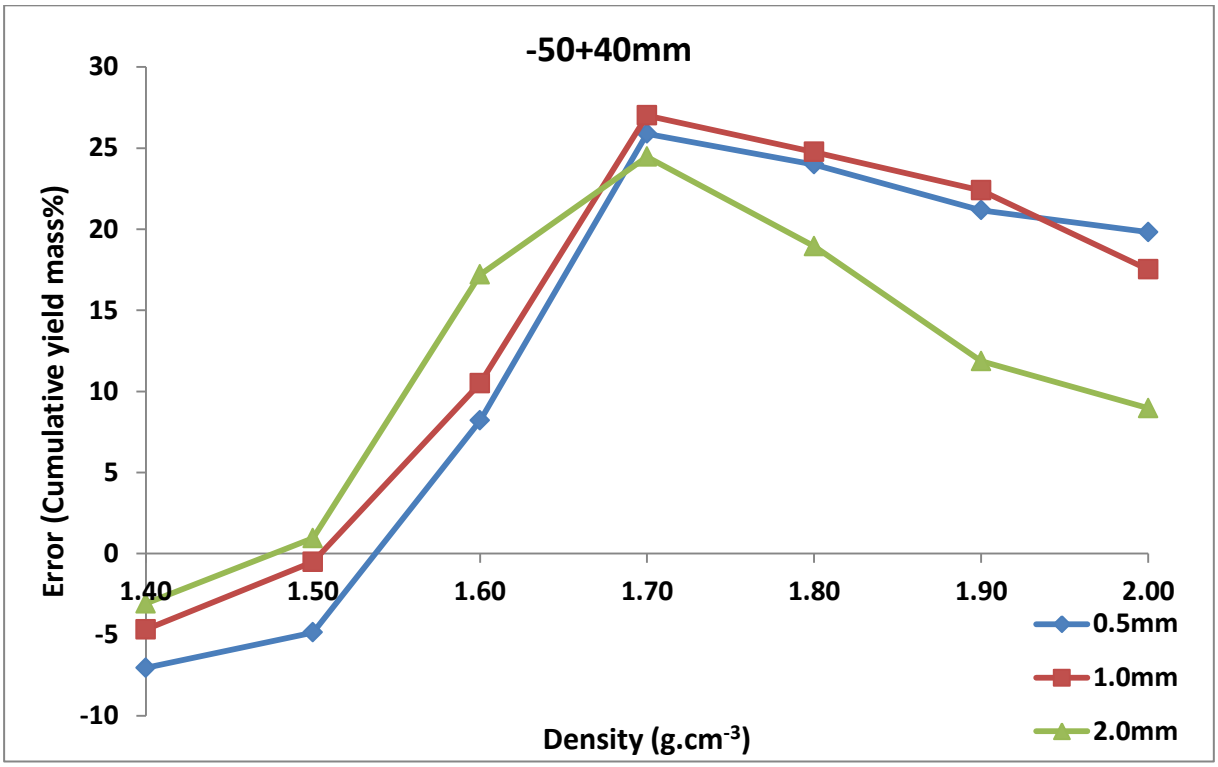

Figure 79. The difference in cumulative yield mass% between the float and sink results, and QEMSCAN derived data for the 40+50mm size range.

The -70+50mm screened sample (Figure 80) is similar to the 40+50mm screened fraction in Figure 79 with regard to the underestimation and overestimation of yield results. The 1.4g.cm^{-3} density fraction and the 0.5mm and 1mm results for the 1.5g.cm^{-3} density fraction are overestimated, while all other results are underestimated. Figure 80 illustrates that the 0.5mm and 1.0mm crushed fractions have similar results, while the 2.0mm results have the greatest error. The 0.5mm and 1.0mm results are less similar at higher densities (>1.6g.cm^{-3}).

The 2.0mm results consistently have the greatest deviation from experimental results (~35mass% in the 1.7 float), while the 1.0mm had the least deviation (~25mass% in the 1.7 float). There was an average underestimation of 11mass% 1.6 float, 29mass% 1.7 float, 23mass% 1.8 float, 19mass% 1.9 float and15mass% 2.0 float.

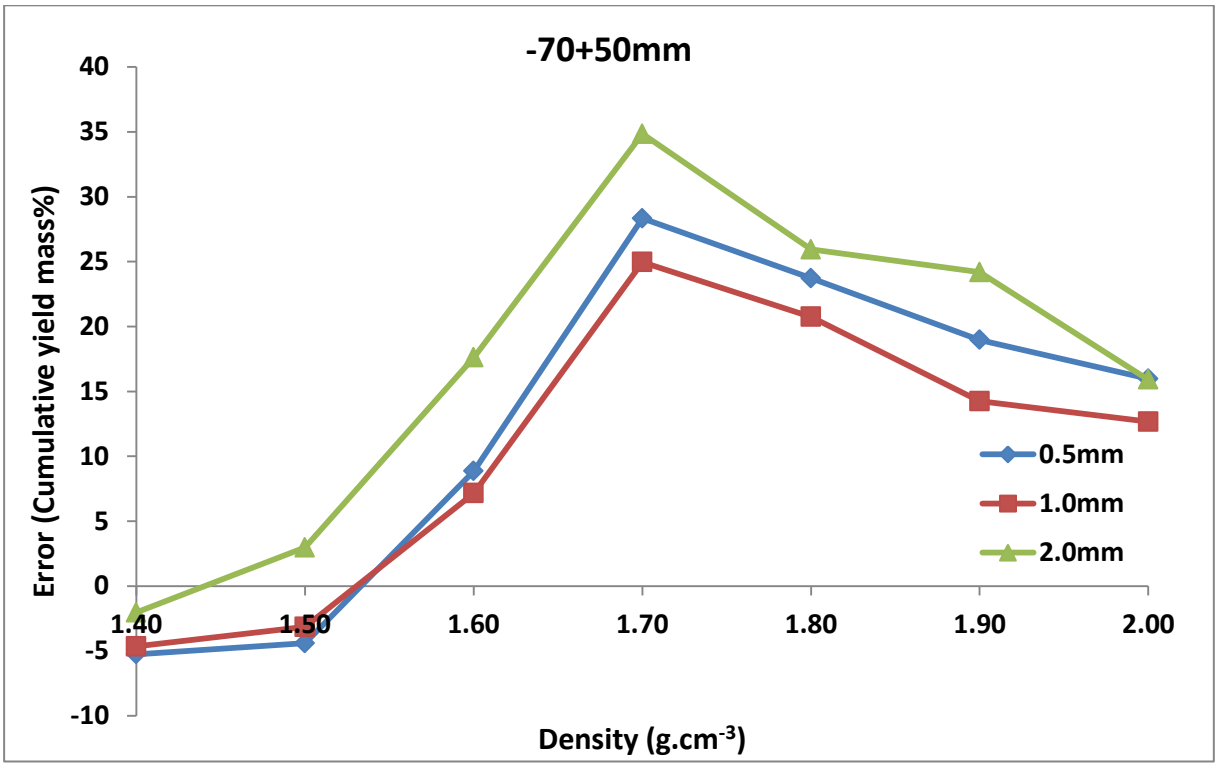

Figure 80. The difference in cumulative yield mass% between the float and sink results, and QEMSCAN derived data for the 50+70mm size range.

Observing Figure 81, the 1.4g.cm^{-3} density fraction and the 1.5g.cm^{-3} density fraction are overestimated, while all other results are underestimated. Comparable to Figure 80, Figure 81 illustrates the 0.5mm and 1.0mm crushed fractions having similar results, while the 2.0mm results have the greatest error.

It is observed from Figure 81 that QEMSCAN yields are overestimated for the 1.4 and for the 1.5 floats by an average of 4mass% and 2mass% respectively. There is an average underestimation of 15mass% 1.6 float, 31mass% 1.7 float, 27mass% 1.8 float, 23mass% 1.9 float and 22mass% 2.0 float.

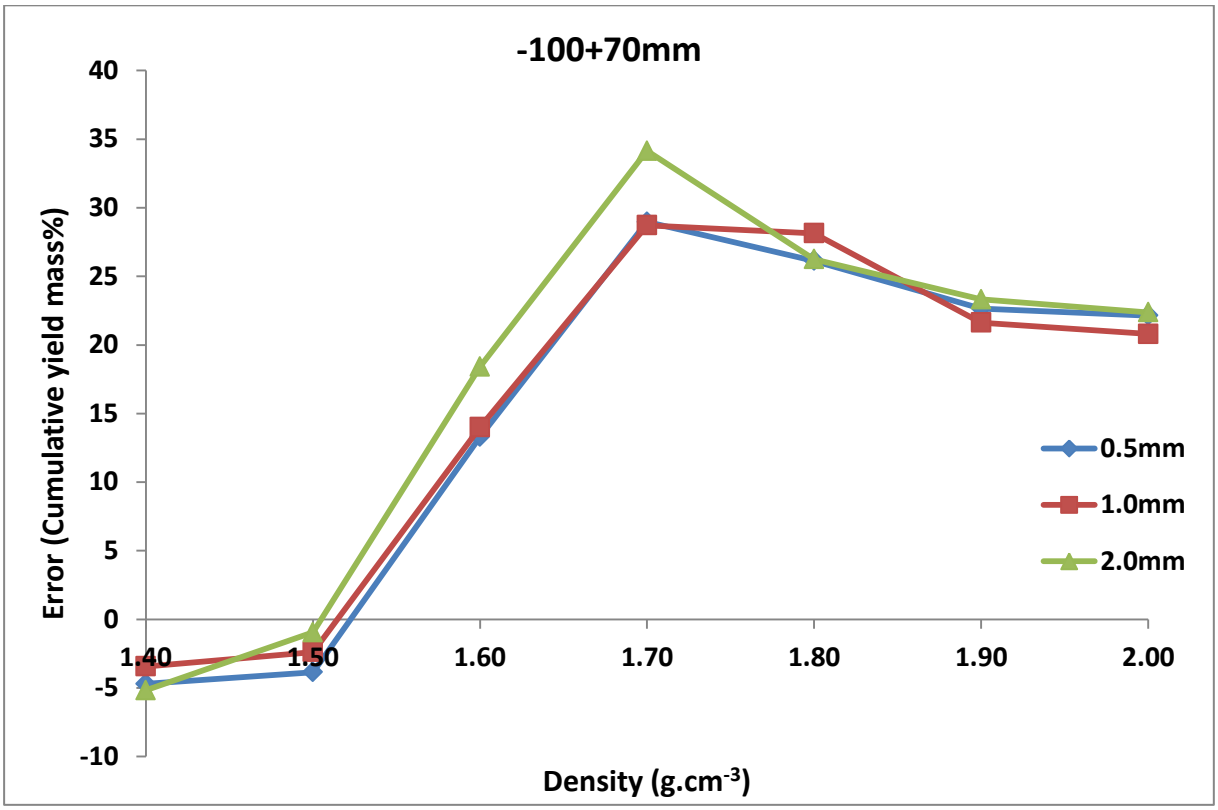

Figure 81. The difference in cumulative yield mass% between the float and sink results, and QEMSCAN derived data for the 70+100mm size range.

Figure 82 displays the results of the largest screened fraction of float and sink analysis in the data set. It is observed that that greatest overestimation of yield (~10%) occurs for the 0.5mm and 1.0mm results. The 0.5mm results display the greatest deviation to experimental results, while the 2mm displays the least.

The 0.5mm, 1.0mm and 2.0mm QEMSCAN yields are overestimated by ~5mass% for the 1.4 float, while the 1.5 float is overestimated by ~4mass% for the 2.0mm, ~2mass% for the 1.0mm and ~1mass% for the 0.5mm. There is an average underestimation of 13mass% 1.6 float, 28mass% 1.7 float, 23mass% 1.8 float, 19mass% 1.9 float and 17mass% 2.0 float.

As expected, the liberation is not as pronounced in the 2.0mm samples compared to the 0.5mm samples. The error is directly proportional to the amount of liberation of particles, which is most significant in the 1.7 float density fraction.

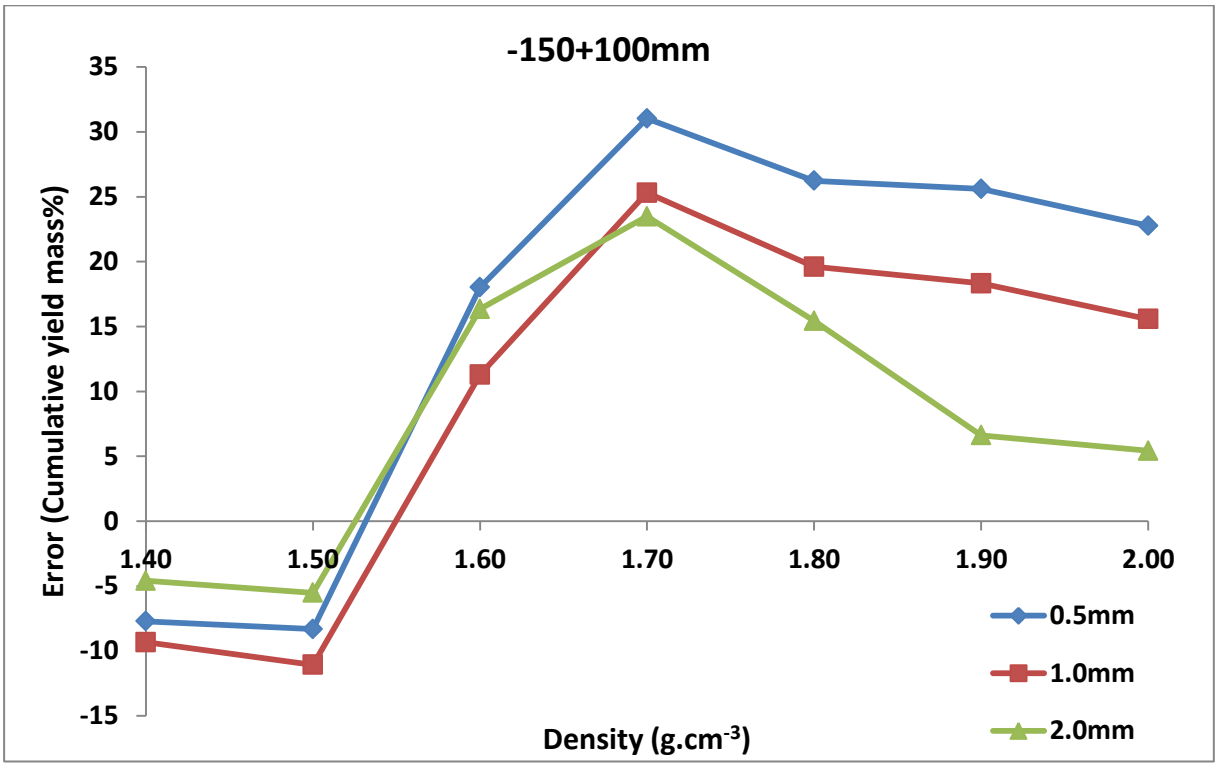

Figure 82. The difference in cumulative yield mass% between the float and sink results, and QEMSCAN derived data for the 100+150mm size range.

Table 20 displays the average liberation error per relative density fraction across the -50+40mm, -70+50mm, -100+70mm and -150+100mm size ranges. The -12+0.5mm size range was omitted as it did not contain 7 floats and a sink like the other size ranges. As a simple correction, the mass% of overestimation/underestimation can be corrected for by adding the following values to the relative density fraction. The corrected QEMSCAN yields are included in Figures 83-87. It was expected that there would be more of a variation between the -12+0.5mm size fraction (up to 12mass %) QEMSCAN corrected yields to float and sink yields compared to the larger size fractions (up to 9mass%), due to only three floats present in the -12+0.5mm size fraction. For this reason, the -12+0.5mm results were excluded in the calculation of the liberation corrections.

Table 20 Average liberation correction per relative density fraction.

RD	0.5mm	1mm	2mm	Average liberation correction
	Mass%	Mass%	Mass%	Mass%
1.40	-6.18	-5.52	-3.72	**-5.14**
1.50	-5.36	-4.28	-2.37	**-4.00**
1.60	12.10	10.74	17.40	**13.41**
1.70	28.55	26.50	29.24	**28.10**
1.80	25.02	23.31	21.64	**23.33**
1.90	22.10	19.15	16.50	**19.25**
2.00	20.17	16.64	13.17	**16.66**

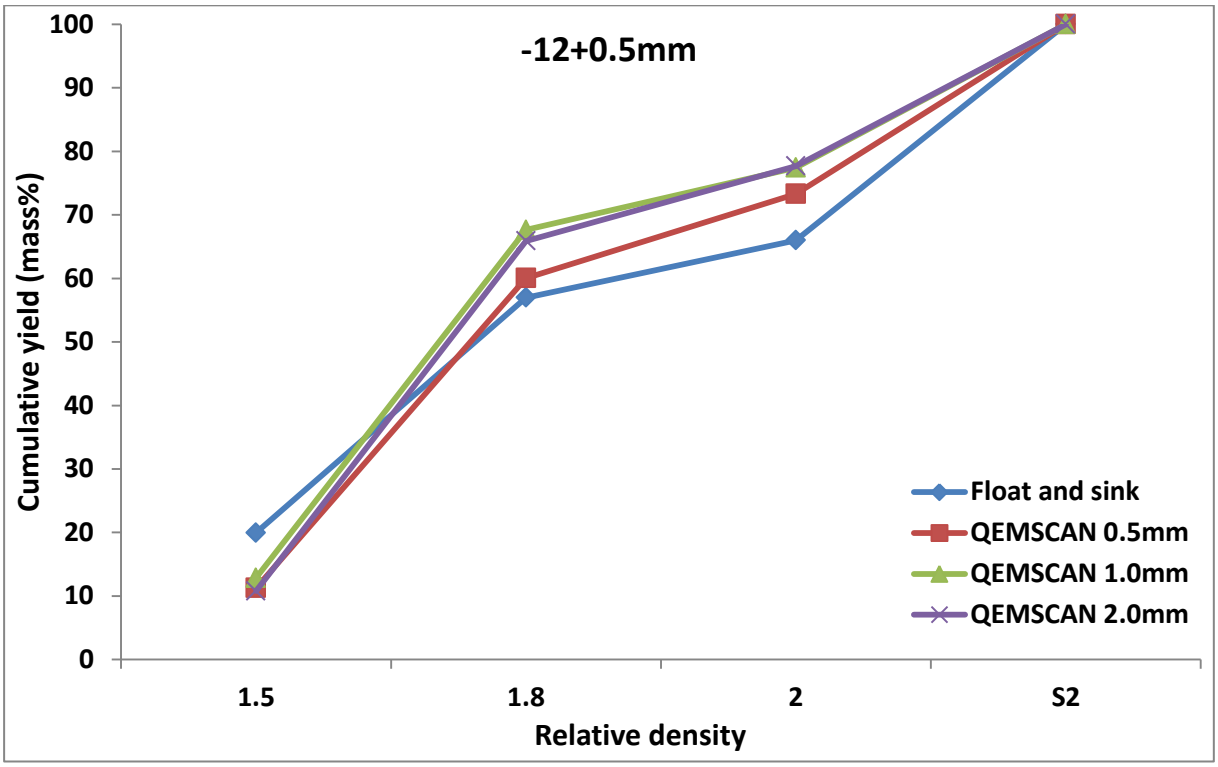

Figure 83: QEMSCAN yield corrected for liberation per crushed sample and yield determined by float and sink analysis for the -12+0.5mm size fraction.

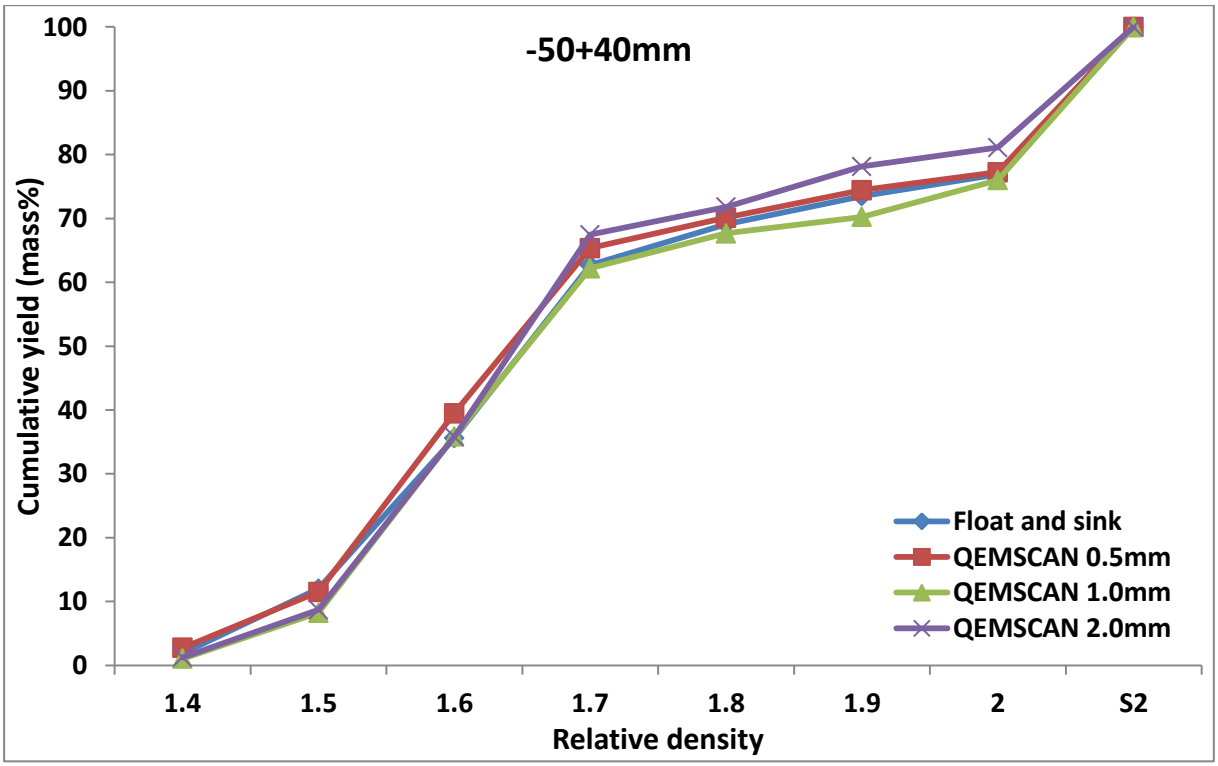

Figure 84: QEMSCAN yield corrected for liberation per crushed sample and yield determined by float and sink analysis for the -50+40mm size fraction.

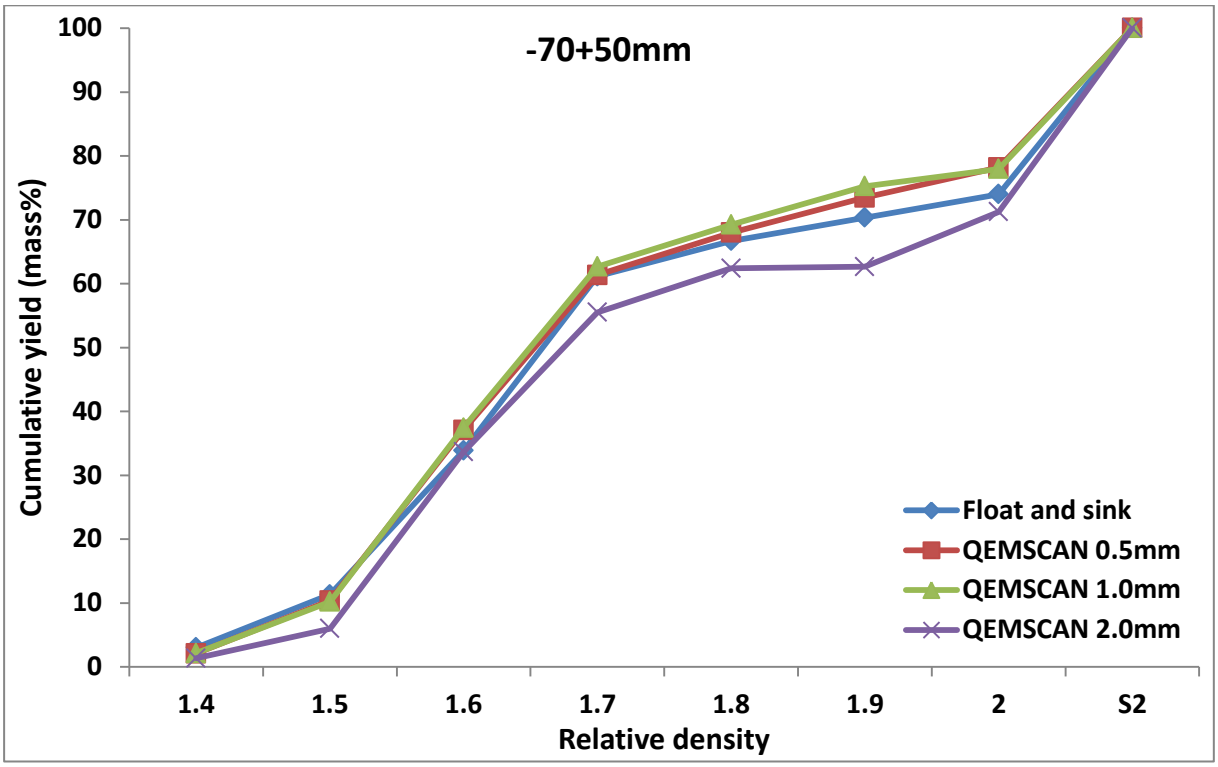

Figure 85: QEMSCAN yield corrected for liberation per crushed sample and yield determined by float and sink analysis for the -70+50mm size fraction.

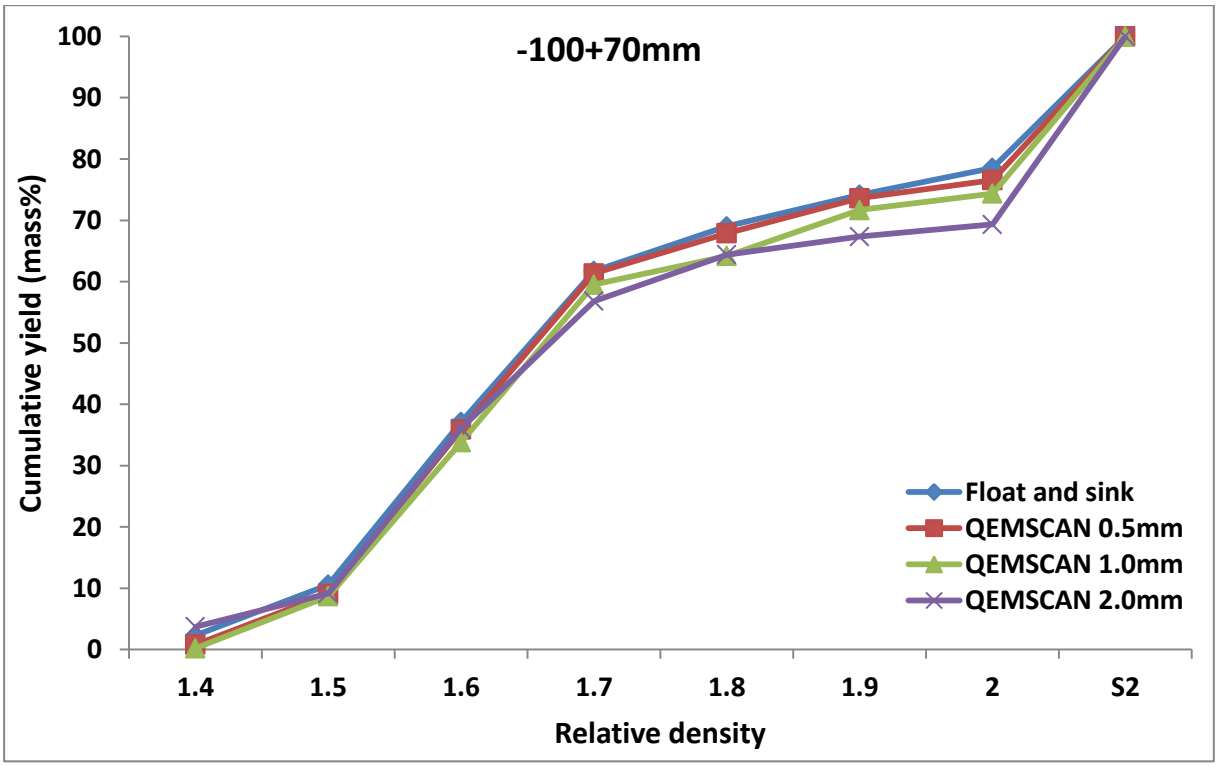

Figure 86: QEMSCAN yield corrected for liberation per crushed sample and yield determined by float and sink analysis for the -100+70mm size fraction.

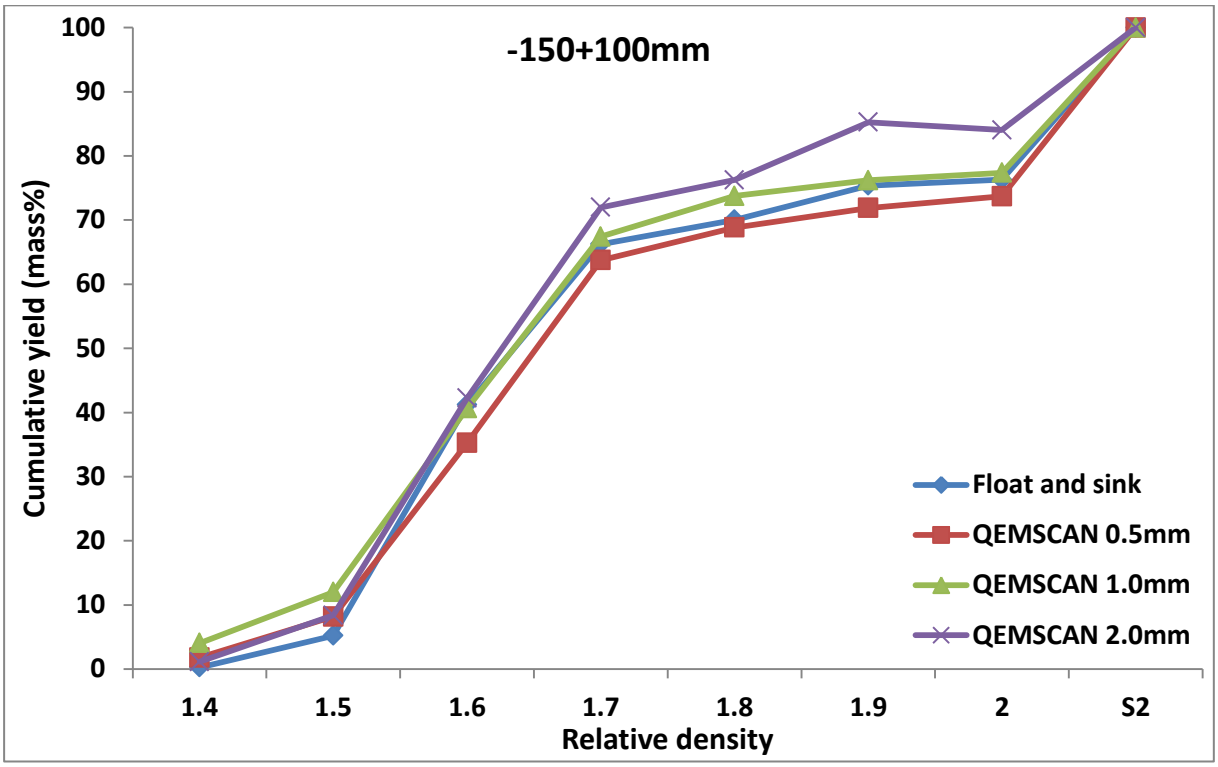

Figure 87: QEMSCAN yield corrected for liberation per crushed sample and yield determined by float and sink analysis for the -150+100mm size fraction.

6. Discussion

6.1 Data set validation

The QEMSCAN data was validated by comparing QEMSCAN calculated ash% against chemically derived proximate ash%. The float and sink data was validated using the SANS 7936 standard of a minimum of 20g and 10 particles present per density fraction. Secondly, a mineralogical density validation model was developed to validate the float and sink analysis. Suspected outliers were determined due to a combination of insufficient sample to provide for minimum masses required, deviant ash values from the average ash of the density fraction and a misfit in term of particle characteristics.

The validity of the QEMSCAN results is verified in the strong linear correlation between ash% results as determined by QEMSCAN with the ash% results determined using chemical analysis (Figure 17). It is important to take into consideration that many minerals that occur in coal have a volatile component (Falcon and Snyman, 1986).

The QEMSCAN determined ash% vs. experimentally determined ash% (Figure 16) indicates that there is a greater error for larger size fractions. The ash values determined for the float and sink dataset from both chemical analysis and QEMSCAN analysis fit into the ranges determined by the density mineralogical model (Figure 20, Figure 21, Figure 22 and Figure 23). The data set deviates from the range determined by the model at low float fractions due to the liberation of smaller bright particles with kaolinite laminations (Figure 61). The 2mm fraction had the worst correlation to chemical results due to low quantities of particles analysed, compromising statistical validity by having large error margins.

The average chemical data follows a kaolinite/vitrinite trend in the lower density fractions ($<1.7 g.cm^{-3}$) and shifts over to a quartz/inertinite trend at higher densities ($>1.7 g.cm^{-3}$). This is due to the nature of the particles present in different density fractions. At low densities, vitrite particles liberate cleats and kaolinite laminae when crushed. Kaolinite is typically present as laminae in bright coal, whereas quartz is more commonly present as either free grains or in an 'inertodentritic' particles present at higher density fractions.

The model allows for errors to be picked up, as values should be questioned if not within the calculated range. It is important to note that the model predicts that a coal with an ash value of 20% can have a density anywhere between $1.45 g.cm^{-3}$ and $1.8 g.cm^{-3}$. Similarly, a coal with a density of $1.8 g.cm^{-3}$ can have an ash value varying between 20-50%. The model supports the change in mineralogy observed around the 1.8-1.9 float fractions, changing from predominantly rich in bright coal and kaolinite, to coal that is predominantly rich in bright/dull coal, kaolinite and quartz.

Outliers were determined using a box plot calculation (Appendix E). The sink in the +150mm size fraction was observed to be rich in bright coal bands in hand specimen with two particles present. It is likely that the sample was incorrectly labelled and/or sampled.

6.2 Organic–inorganic textural associations – specific to density fraction

Figure 88(a) illustrates that vitrinite rich coal has carbonate cleats and fine lenses of kaolinite present, while Figure 88(b) displays a high mineral matter content associated with inertinite rich (dull) coal. The cleats serve as a plane of cleavage with preferential breakage taking place along the cleat/clay boundary.

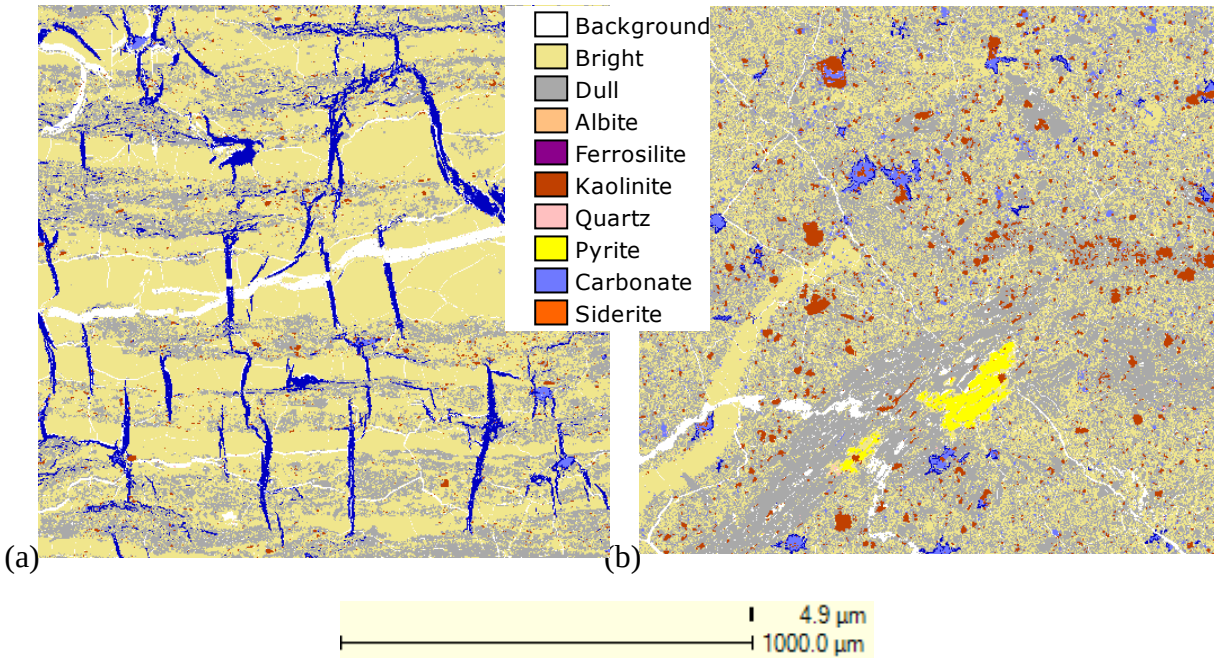

Figure 88. (a) False colour image of carbonate cleats in a predominantly vitrite rich coal (b) false colour image of carbonate nodules in a predominantly inertinite rich coal.

It is interesting to note that the carbonate cleats observed in predominantly bright coal frequently occurs perpendicular to the bedding plane of the coal seam (Figure 88(a)). Layers of vitrinitic/bright coal have very little mineral matter associated with its texture. The layers have planes of weakness perpendicular to the bedding plane through which the carbonates infiltrate and develop cleats. Carbonates mobilize parallel to the bedding plane between layers of bright, dull and mineral phases, eventually forming carbonate cleats.

Carbonate nodules present in dull coal frequently have a dolomite rim and calcite infilling (Figure 88(b)). The zonation of mineralogy and variance in occurrence of cleats is indicative of formation conditions and/or chemical reactions taking place during/after coal formation. The dolomite rim may have been due to element mobilization due to an increase in temperature and pressure during the metamorphic process. Bright and dull coals are formed from the same parts of plants, but under varying conditions of formation. The coal in Figure 88(a) was formed in a stagnant, anaerobic swamp environment.

An anaerobic environment allowed for the formation of bright coal, as the volatile component (including organically bound sulphur) was not compromised due to oxidation. The bedding plane is clearly visible with only very finely disseminated clay particles/lenses/beds present. The carbonate cleats in Figure 88(a) predominantly occur perpendicular to the bedding plane, much like the carbonate cleats observed in bright coal in hand specimen (Figure 89). In hand

sample, the carbonate cleats are observed as thin, light grey, opaque ‘sheets’ occurring within the bright phase.

In summary, vitrinite-rich coal texture is characterised by predominantly bright layers with lesser dull layers and interspersed kaolinite laminations. Inertinite-rich coal texture is characterised by a complex mix of bright coal, dull coal and minerals in a ‘speckled’ texture with fine beds of mineral matter and/or coal occurring. It is important to note that petrography classifies microlithotypes of coal per 50x50micron graticule, while QEMSCAN classifies microlithotypes of individual particles.

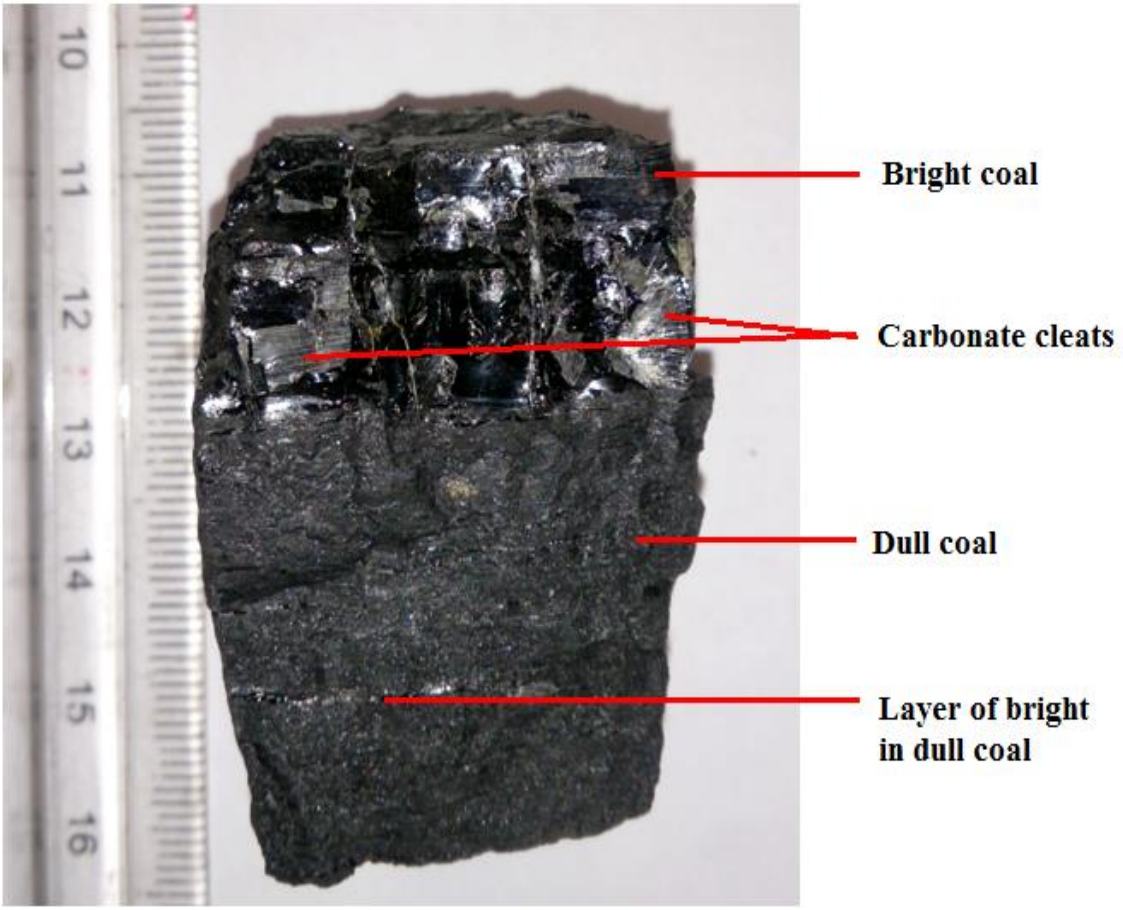

Figure 89. A piece of coal with carbonate cleats predominantly present perpendicular to the bedding plane of the bright phase.

Assuming that the particle in Figure 89 has 15% kaolinite, 5% carbonate, 50% dull and 30% bright coal by volume, the density of the particle would be 1.7g.cm^{-3}.When this particle is crushed down to <2.0mm, a number of smaller particles are generated. These smaller particles have proportions of mineral to maceral (and thus densities) that are different from the original particle (Figure 61, Figure 65, Figure 66 and Figure 71).

A density categoriser created using QEMSCAN was used to determine the densities of these smaller particles. The categoriser is created by inputting a density value is for each distinguishable mineralogical phase present. The software utilizes a categoriser to separate

particles by their density, calculated by an average volume weighting of individual minerals making up the particle.

As expected, their densities comprise a wide range of particle densities that frequently vary from the original particle density. Figure 60, Figure 62, Figure 63, Figure 64, Figure 67, Figure 68, Figure 69 and Figure 70 illustrates that most of the smaller crushed particles fall outside the density range of the original larger particles.

The first pass attempt of QEMSCAN yield determination illustrates that most of the particles fall outside the expected density range. This is due to one particle liberating many smaller particles with a wide range of densities varied from the original particle. The QEMSCAN categorised particles separated by density reveal that there are particles with textures specific to density ranges. Particle texture is indicative of coal and mineral proportions, which in turn is indicative of density. The various particle textures found in various density ranges was explored using particle characterisation histograms.

6.3 Particle characterisation per float and sink fraction.

Subchapter 5.1.4 describes the typical mineralogy of particles per relative density fraction. Figure 59 displays the average density values across size ranges which reveals a general trend of increasing sandstone, siltstone and mudstone with increasing size fraction. Bright, bright/dull and dull coal decreases in proportion for increasing relative density fraction. This results in increasing ash% as relative density fraction is increased.

The 1.4 floats comprise the largest proportions of bright coal (density of bright coal is ~1.3g.cm^{-3}) and have an average of 15.14% ash. The 1.4 and 1.5 floats predominantly comprise bright coal with fine kaolinite laminations. The particles with bright and kaolinite interlayers display indications of the particles preferentially cleaving along the bedding plane – the individual particles have straight edges parallel to the bedding plane (Figure 21, Figure 22, Figure 23 and Figure 27).

Carbonate cleats are most abundant in the 1.5g.cm^{-3} floats (average 20.65% ash) and decrease in proportion with decreasing size fraction thereafter. Carbominerite is present in low proportions in the low density fractions (15.67% 1.4 floats and 22.23% 1.5 floats), are highest for the middle to higher density fractions (45.08% 1.6 floats, 53.86% 1.7 floats, 52.03% 1.8 floats, 54.20% 1.9 floats and 41.29% 2.0 floats), and drops significantly in the sink fraction (14.48%). The carbominerite coal and mineral proportions are different for various density ranges. The predominant carbominerite in the 1.4 and 1.5 floats are carbankerite and carbargillite (bright coal with kaolinite laminations and cleats are common).

The 1.5 floats have less bright and an increase in dull/bright compared to the 1.4 floats, due to the density of dull coal being ~1.55g.cm^{-3}. The 1.6 floats, with an average 29.90% ash, have the largest increase in carbominerite (~23% more than the 1.5 float) and a further increase in

dull/bright (10% more than the 1.5 float), due to the average density of carbominerite being 1.67g.cm^{-3}. The carbominerite particles in the 1.6 and 1.7 floats have 'speckled' textures that begin to incorporate quartz. Carbosilicate, carbopolyminerite and carbopyrite increase in proportion. The average ash values for the 1.7 and 1.8 floats are 31.20% and 36.88% respectively.

The carbominerite particles in the 1.8, 1.9 and 2.0 float fractions have increasingly more nodular carbonate and pyrite, fine kaolinite and quartz in their textures, making them particularly carbopolyminerite-rich. Both nodules and cleats of carbonate are observed, with the cleats forming in a predominantly bright coal particles and nodules forming in predominantly dull coal particles (Figure 41).

Pyrite cleats are highest in the 1.8g.cm^{-3} float, and decrease in proportion as density fraction increases. The average ash values for the 1.9 float, 2.0 float and 2.0 sinks are 51.18%, 52.83% and 77.06% respectively. There is a low proportion of dull coal across all density fractions, indicating that this specific coal has particularly low proportions of dull coal.

The proportions of stone (mudstone, siltstone and sandstone) increases as density fraction is increased. The stone in the 1.4 and 1.5 floats is mostly mudstone (~5 and 7% respectively. Mudstone comprises ~5% in the 1.6 and 1.7 floats, and increases to ~7% in the 1.8 float. Siltstone and sandstone proportions for densities below 1.8g.cm^{-3} have been <2%, while it is ~4% in the 1.8 float. The proportion of siltstone (~14%) is more than mudstone (12%) in the 1.9 float. Similarly, siltstone increases to 21% and mudstone to ~16% in the 2.0 floats. The sink has the highest proportions of mudstone and siltstone (56 and 17% respectively). The sink fraction is the first density fraction to have carbominerite as a significant liberation product.

The 0.5mm samples have the most consistent cleat phases for the lower density fractions and liberated coal phases at higher density fractions. Liberation trends are observed from the 0.5mm samples across size ranges, while the 1.0mm and 2.0mm data looks more scattered due to poor particle statistics.

6.5 QEMSCAN yield determination

The QEMSCAN determined density distribution of particles observes the change in particle mineralogy/density when samples are crushed and liberation occurs. Coarse samples undergoing float and sink analysis separate particles according to their density, which is linked to their mineralogy. Coarse particles present in the low float fractions <1.6g.cm^{-3} comprise predominantly bright coal with fine beds of kaolinite, while the higher float fractions (>1.6-1.9g.cm^{-3}) comprise dull coal incorporated into an 'inertodetrinite' texture. The proportions of organic to inorganic matter change for each density fraction. As density

fraction increases, less organic material and more inorganic material is incorporated into the carbominerite texture.

The plots of yields as determined by float and sink analysis comparing the various size fractions (Figure 72) illustrates that there is only a significant liberation effect when particles are crushed to a much finer size fraction. The finest size fraction (-12+0.5mm) inflates the lower density floats (1.5 float) while the coarsest fraction (-150+100mm) underestimates the yield compared to the -50+40mm, -70+50mm and -100+70mm size fractions.

At higher floats than 1.5, the finest size fraction underestimates yield while the coarsest size fraction underestimates yield compared to the -50+40mm, -70+50mm and -100+70mm size fractions. The variance of yields between size fractions of float and sink data implies that the yield can be affected (up to ~8mass% yield error) if the feed to plant is crushed to size fractions that have large error margins (Figure 72).

It is observed in the plots of the various size fractions (Figure 73, Figure 74, Figure 75, Figure 76 and Figure 77) that the 1.4 and 1.5 float fractions have higher yields for the crushed fractions than the float data. Large particles in the 1.4 and 1.5 float fractions would have broken along cleat and kaolinite planes, liberating a greater quantity of clean vitrinite particles.

The intermediate float fractions (1.6-2.0) are predominantly ‘speckled’ organic and inorganic material that, when crushed, liberates laminations of coal. The resultant yields for these intermediate float fractions are lower for the crushed fraction than the experimentally determined yields. The relation of organic to inorganic matter in the high and low density fractions plays a significant role in the change of particle mineralogy when a particular coal is crushed to a smaller size.

Figure 88 illustrates the difference between vitrinitic and inertinitic coal textures, both as individual particles and as in a large coal particle respectively. Vitrinite particles are clean organic particles with fine lenses/beds of kaolinite, while inertinite particles have an ‘inertodentrite’ texture. When vitrinite rich coal is crushed, grains of vitrinite, liberated kaolinite and cleats are produced as a result of preferential breakage along cleavage planes. When inertinitic coal is crushed down, the smaller particles have the same texture as the larger particles i.e. there are no significant liberation of phases.

Figure 90 shows the density separation of handpicked bright and dull coal particles analysed on QEMSCAN and processed using iDiscover density categorisers. Vitrinitic and inertinitic coal have a normal distribution with predominant particle densities of 1.40g.cm^{-3} and 1.85g.cm^{-3} respectively.

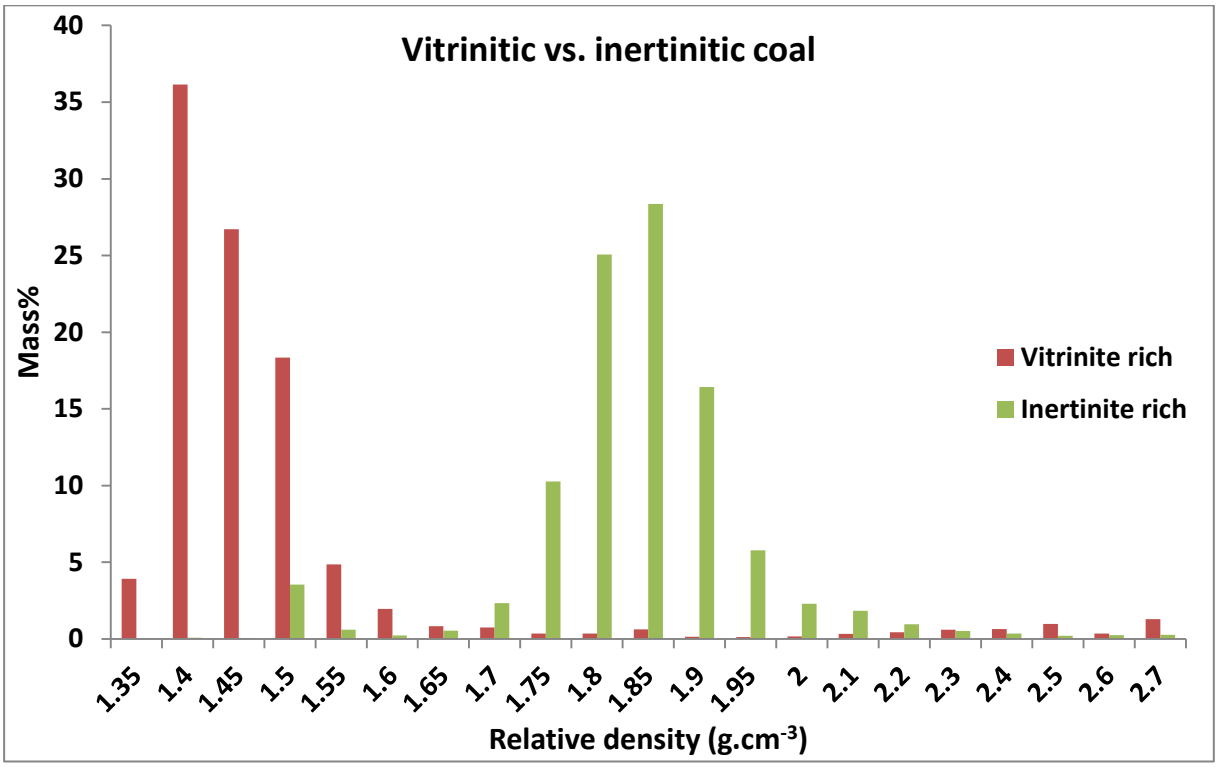

Figure 90. QEMSCAN derived density separation of handpicked bright and dull coal.

Eskom had replaced their QEMSCAN EVO50 with a QEMSCAN 650F in August 2014. The decision to upgrade the instrument was made due to strides being made in the advancement of detector, vacuum and filament technology, while the existing system was older than eight years old. The detectors on the new system have a larger total window area (60mm^2) as compared to the older instrument (40mm^2). The increased window area allows for better detection of light elements and improved acquisition times.

Figure 91 and Figure 92 are corresponding false colour images of a piece of whole coal analysed using the SIP files created on the EVO50 and 650F respectively. The EVO50 detected mostly bright coal, while it is possible to discriminate between vitrinite, fusinite, reactive semifusinite and liptinite using the new SIP developed on the 650F. Improved discrimination of maceral types are due to increasing the X-ray count rate from 1000 counts on the EVO50 to 5000 counts on the 650F. Analysing at 5000 counts on the EVO50 system would be impractical due to the long acquisition times, but it is possible on the 650F system due to an upgrade of the processing boards (90kcps to 275kcps) that has improved analysis acquisition times.

The lower float fractions analysed using the EVO50 were predominantly bright and dull coal with relative densities of 1.3g.cm^{-3} and 1.55g.cm^{-3}, while it would now be possible to discriminate between vitrinite and reactive semifusinite in bright coal (1.3g.cm^{-3} and 1.35 g.cm^{-3} respectively), and fusinite and secretinite (1.45 g.cm^{-3} and 1.55 gcm^{-3} respectively) in dull coal.

The current study based on EVO50 data is only able to quantify general ‘bright’ and ‘dull’ components per density fraction, while the new SIP based on 650F data will allow for quantification of macerals similar to those in petrographic analyses. The maceral phases are discriminated by their oxygen, carbon and organically bound sulphur compositions. It is recommended that the current washability research be continued using the QEMSCAN 650F for improved examination of the macerals present per density fraction.

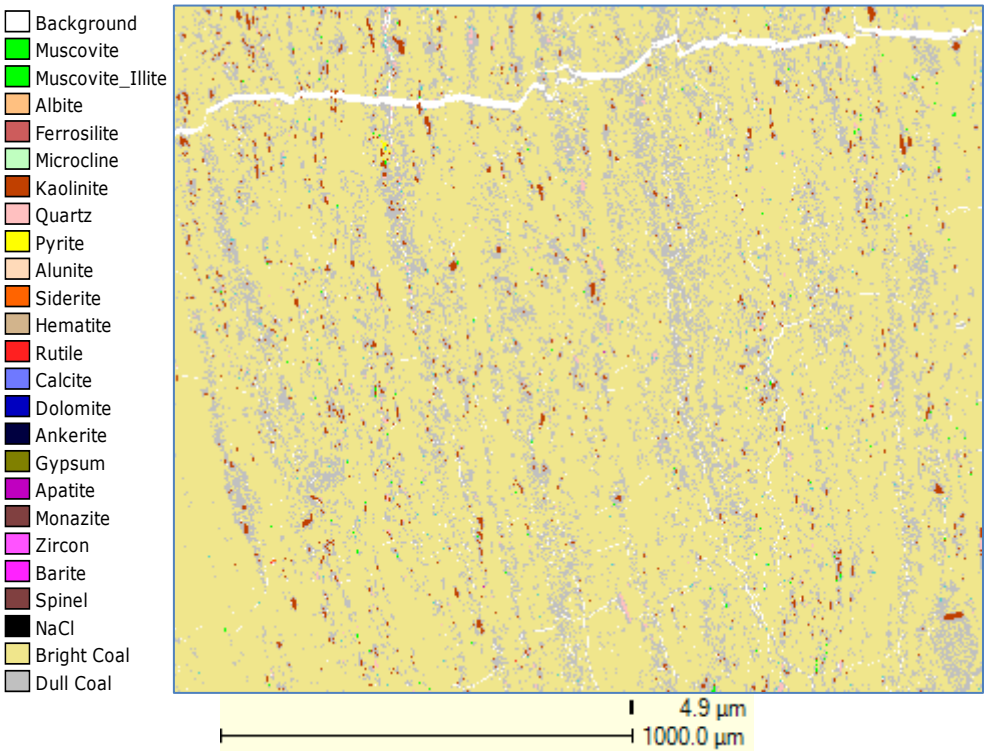

Figure 91. False colour image of a piece of coal processed using the old mineralogical calibration files (QEMSCAN EVO50, old SIP).

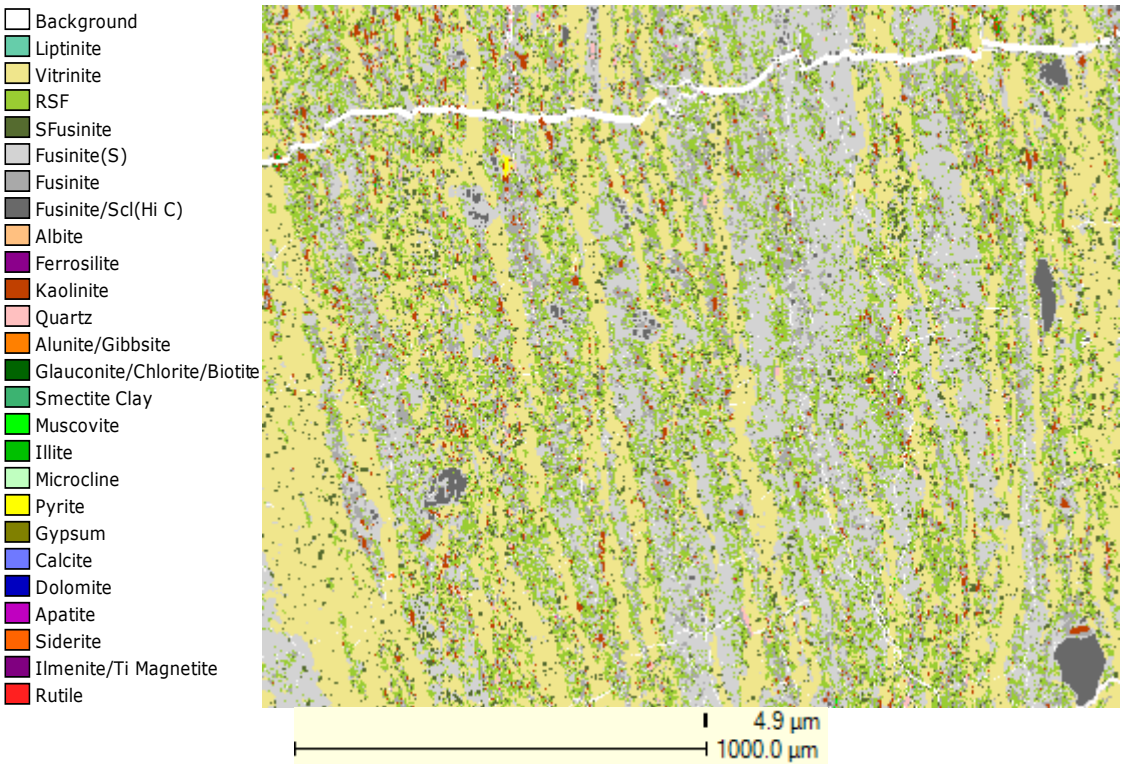

Figure 92. False colour image of a piece of coal processed using the new mineralogical calibration files (QEMSCAN 650F, new SIP).

6.6 Liberation analysis

The discrepancy between the cumulative yield mass% of the experimentally determined float and sink results, and the QEMSCAN determined yields are due to liberation caused by crushing, as well as due to the limited density classification of organic material below a density of 1.6g.cm^{-3} on the QEMSCAN EVO50. From all the density fractions, The 1.7 float fraction has been the least affected by liberation due to the particles predominantly having a more homogenous ‘speckled’ texture compared to the 1.4, 1.5 and 1.6 float fractions, which tend to have many cleats and kaolinite laminae in vitrinite-rich particles. The float fractions higher than the 1.7 float and the sink have textures that are either ‘speckled’ with coal laminae or predominantly kaolinite/quartz with coal laminae. The coal laminae serve as planes of cleavage, which then allow for greater variations in the density of particles generated when crushed.

The variance in ash value for each of the density fractions is an indication of liberation. The variance is well illustrated in Appendix E where the ash range is the smallest for the 1.7 float (other than the sink fraction) and starts to increase on either side towards the lowest density fraction and the sink. The ranges are also smallest for the PF chemical ash value, and are larger for the 0.5mm. The 1mm has slightly smaller ranges than the 2mm.

Utilizing the average difference in yield between the QEMSCAN and float and sink data as a correction factor, the corrected yields (Figures 83-87) vary from the float and sink yield more

for the 2.0mm QEMSCAN samples than the 0.5mm or 1.0mm samples. Generally, the 0.5mm and 1.0mm results are similar, while the 2mm results deviate more from experimental results.

QEMSCAN yields are overestimated for the 1.4g.cm^{-3} and 1.5g.cm^{-3} density fractions due to liberation of fine kaolinite, cleat phases, and vitrite particles, while higher density fractions are underestimated due to the liberation of carbominerite, bright and dull/bright coal laminations within mudstone/siltstone particles. The discrepancy between the cumulative yield mass% of the experimentally determined float and sink results, and the QEMSCAN determined results was corrected for, once the discrepancy was established for the mineralogy of this specific coal.

7. Conclusions

QEMSCAN can identify 'bright' and 'dull' coal based on organically bound sulphur present in 'bright' coal, as well as the elemental ratios of carbon and sulphur. Bright coal is vitrinite-rich and preferentially cleaves along kaolinite laminations, carbonate cleats and pyrite cleats. Bright coal is formed in a stagnant, anaerobic swamp environment. Dull coal is inertinite rich and preferentially breaks along bright and dull/bright coal lamination. Dull coal is formed in a sub-aerobic environment and has a 'speckled' texture with pyrite and carbonate present as spherical nodules. There are therefore controls on liberation which can be linked back to coal formation conditions.

Results correspond better to chemical results the smaller the particle size analysed. The 0.5mm samples followed more closely to the float and sink ash% determined by proximate analysis compared to the 1.0mm and 2.0mm samples, which were similar to each other. The finer the sample analysed, the better the particle statistics. The problem with finely crushed samples is that the effect of liberation is greater. There is a fine balance between sample size and acquisition time.

Float and sink data were validated by comprising the minimum amount of sample as per SANS7936:2010. A new mineralogically based ash density validation model predicts the density of volumetric ranges of theoretical particles of the most common phases found in coal - vitrinite, inertinite, kaolinite and quartz. The model allows an estimated range of ash values per density fraction to be determined. Additionally, the model illustrates that a sample with a specific ash% can have a range of densities (indicating mineralogy).

The theoretically calculated ash values of the data set were input into the validation model to establish if the mineralogical trend could be confirmed by QEMSCAN analysis. The data set fits into the range determined by the model, except at low float fractions due to bright and kaolinite particles liberating smaller particles with higher densities to the original particle, causing elevated ash values (Figure 61). The data set follows a kaolinite/vitrinite trend in the lower density fractions and shifts over to a quartz/inertinite trend at higher densities (>1.7g.cm^{-3}). Vitrite particles liberate cleats and kaolinite laminae when crushing low density fractions and inertite particles while quartz is more commonly present as either free grains or in 'speckled' particles present at higher density fractions. The coal used in this project had particularly low proportions of dull coal, although it had up to ~26mass% dull/bright coal in the 1.6 floats.

The change in mineralogy as indicated by the validation model is further substantiated by particle characterization histograms and their corresponding false colour images. Particle characterization plots represents the quantities of the most common particles present in coal i.e. pyrite, carbonates, sandstone, siltstone, mudstone, carbominerite, dull, dull/bright and bright coal. The density ranges of bright coal, dull coal and carbominerite are 1.22-1.40g.cm^{-3}, 1.36-1.74g.cm^{-3} and 1.55-2.0g.cm^{-3} respectively while the density of kaolinite and quartz is

2.65g.cm^{-3} (Falcon and Snyman, 1986). The particle characterisation histograms per relative density fraction reveals that the theoretical predictions of particles reporting to density allocations are as one would expect.

The largest proportion of bright coal is in the 1.4 float. Bright/dull coal and carbominerite increase in the 1.5 float, while bright and bright/dull decrease for increasing relative density fraction henceforth. Carbominerite increases further in the 1.6 float and is highest in the 1.7 float, after which carbominerite decreases in proportion. Stone increases as relative density increases. Carbonate cleats are predominant in the lower density fractions and highest in the 1.5 floats (~6mass%). Carbonate is present as nodules and less as cleats in the higher density fractions (>1.7 float). Pyrite also occurs as cleats in the lower density fractions and nodules in the higher float fractions. Pyrite proportions increases as relative density increases, is highest for the 1.8 float (~3mass%) and decreases in proportion for higher density fractions.

A QEMSCAN derived yield was calculated and compared to experimentally derived yields per density separated fraction. There is a significant difference in values due to the bulk particle mineralogy changing when crushed. When a large particle is crushed, 'puzzle pieces' of the original particle are created.

Coarse particles in the low float fractions (<1.6g.cm^{-3}) comprise predominantly bright coal with fine beds of kaolinite. The textural association of kaolinite beds/lenses present in volatile rich bright coal is explained by the depositional environment. Stagnant (low energy) water conditions allow only fine clay to be transported. The fine clay eventually is present as kaolinite laminations in bright coal. Calcite, dolomite and pyrite cleats form in bright coal. The cleats and kaolinite beds serve as preferential cleavage planes, which is observed by particles in the false colour images of the low density float fractions – particles of bright with kaolinite laminations have straight edges/corners illustrating the cleavage plane (Figure 27). The carbominerite particles formed are predominantly carbargillite and carbankerite in the 1.4 and 1.5 floats. Particles with a wide range of densities are generated when a bright coal particle is crushed.

The higher float fractions (1.6-2.0 floats) comprise dull/bright coal incorporated into a 'speckled' texture. Particles with densities close to that of the original particle are generated when the original particle has a 'speckled' texture. The proportions of organic to inorganic matter change for each density fraction. As density fraction increases, less organic material and more inorganic material is incorporated into the carbominerite texture. The carbominerite texture is formed as a result of macerals and minerals in a turbulent swamp environment (e.g. due to flooding).

Lenses and beds of bright and dull/bright coal are observed within the texture, which serve as preferential planes of breakage when crushed – particles with straight edges indicative if preferential cleavage are observed in false colour images of the higher density fractions (Figure 58). Carbonates and pyrite occur as nodules within the dull coal texture. The dolomite

rim on carbonate nodules may have been due to element mobilization due to metamorphic conditions. The composition of the carbominerite becomes more mineral enriched as density is increased. Predominant carbominerite particles are carbopolyminerite, carbargillite, carbankerite with some carbopyrite and carbosilicate.

The QEMSCAN yields are an attempt to put the 'puzzle pieces' back together. The difference between QEMSCAN yield and float and sink yield is due to the effect of liberation due to crushing. This difference can be quantified and applied as a correction to the original data. It is important to note that the correction is specific to the coal in this study, which comprises particularly low proportions of dull coal.

The QEMSCAN yields are overestimated for the 1.4 and 1.5 floats due to the presence of kaolinite, carbonate and pyrite cleats. QEMSCAN yields are underestimated in the middle to higher densities (>1.5 floats and sink) due to the carbomineritic texture of particles with large proportions of coal as 'speckled' laminations/bands that are liberated from the mudstone particles when crushed.

In conclusion, washability can be determined using QEMSCAN since the significant effect of liberation can be calculated and corrected for specific coal types. A particularly important limitation of QEMSCAN analysis is that samples crushed to <1mm have minimal error compared to larger size fractions, as a function of particle statistics. The coal in this study had particularly low proportions of dull coal. There is evidence to support that liberation of minerals have controls that can be identified and therefore corrected for. Vitrinite-rich coal tends to liberate carbonate cleat and fine kaolinite material when crushed, while inertinite-rich coal (carbominerite textures) tends to liberate smaller particles that are texturally the same as the original particle from which it liberated.

8. Recommendations for future research

- A coal that has undergone density separation at a fine size fraction (<2mm) by means of a spiral, reflux classifier or any other acceptable means of separating fine coal should be analysed on QEMSCAN. It would be interesting to test the accuracy of the density categoriser without the effects of liberation/crushing the particles down.

- The existing samples should be analysed using the new QEMSCAN 650FEG. The enhanced organic matter classification available with the new technology allows for more in depth investigation of proportions of reactive and less reactive organic components present in the lower float fractions (<1.6g.cm^{-3}). The EVO50 could distinguish bright from dull coal while the 650FEG can distinguish vitrinite, reactive semi-fusinite, semi-fusinite, fusinite and secretinite.

- Investigations should be conducted on the liberation effect with regard to the combustion, abrasiveness and Hardgrove Index (HGI) when the coal is pulverized from its original coarse size.

- It is important that the washability research be carried out on the new QEMSCAN 650F to better establish the various maceral layers present in bright coal, as well as the proportions of macerals present in the carbominerite texture as density fraction increases.

9. Acknowledgments

I would like to thank Coaltech for funding my research and a great thanks to Eskom for allowing me to base my research with them at their Research, Testing and Innovation Centre. I would especially like to thank Dr. Chris van Alphen and Professor Roland W. Merkle for their guidance and support.

10. References

1. Albrecht, M.C. (1980). Coal Preparation Processes. Unit and Bulk Materials Handling, ASME Annual Meeting, San Francisco, CA, August 1980. 279-288pp.
2. Callen, A.M., Patel, B., Zhou, J. And Galvin, K.P. (2008). Development of water-based methods for determining coal washability data. International journal of coal preparation and utilization, 28, 33-50pp.
3. Callen, A.M., Pratten, S.J., Belcher, N., and Galvin, K.P. (2002). An alternative method for float-sink analysis of fine coal samples using water fluidisation. International journal of coal preparation and utilization, 22, 293-310pp.
4. Davis, J. J., Wood, C. J. And Lyman, G. J. (1995). Density tracers can improve coal preparation plant yield. Australian Coal Miner, Australia, July edition, 9-11pp.
5. Davis, J. J., Wood, C. J. And Lyman, G. J. (1995). The use of density tracers for the determination of dense medium cyclone partitioning characteristics. International Journal of Coal Processing and utilization, 2(2), 107-126pp.
6. Demir, I. And Harvey, R. (1991). Variation of organic sulphur in macerals of selected Illinois Basin coals. Organic geochemistry, England, 16, 525-161pp.
7. European Food Safety Authority (EFSA). (2012). Scientific opinion on the re-evaluation of carnauba wax (E903) as a food additive. European Food Safety Authority Journal, 10(10), -23pp.
8. FEI QEMSCAN® (2007). QEMSCAN iDiscover and iMeasure version 4.2 (software). Australia Centre of Excellence for Natural Resources. FEI Australia.
9. Falcon, R and Ham, A.J. (1988 May). The Characteristics of Southern African Coals. Journal of the South African Institute of Mining and Metallurgy 88(5). 145-161pp.
10. Falcon, M.S. and Snyman, C.P. (1986). *An Introduction to Coal Petrography: Atlas of Petrographic Constituents in the Bituminous Coals of Southern Africa*. Geological Society of Southern Africa, Johannesburg. – 27pp.
11. French, D., Ward, C.R. and Butcher, A. (2008). QEMSCAN for characterisation of coal and coal utilization by-products, research report 93. © Australian Black Coal Utilization Research Limited 2008, Australia, 107pp.
12. Galbreath, K., Zygarlicke, C., Casuccio, G., Moore, T., Gottlieb, P., Argon-Olshina, N., Huffman, G., Shah, A., Vang, N., Vleeskens, J. and Hamburg, G. (1996). Collaborative study of quantitative coal mineral analysis using Computer-Controlled Scanning Electron Microscopy, Fuel, vil.75, 4. 424-430pp.
13. Galvin, K.P. and Pratten, S.J. (1999). Application of fluidization to obtain washability data. Minerals Engineering, 9, 1051-1058pp.
14. Ghosh, T., Patil, D., Honaker, R.Q., Damous, M., Boaten, F., Davis, V.L., and Stanley, F. (2012). Performance evaluation and optimization of a fullscale reflux classifier. Coal preparation society of America, 11 (2), 24-33pp.

15. Gottlieb, P., Argon-Olshina, N. And Sutherland, D.N. (1991). The characterisation of mineral matter in coal and fly ash. In: Inorganic transformations and ash deposition during combustion – Preceedings of the Engineering Foundation Conference, Benson, S.A. (Ed). The American Society of Mechanical Engineers. 135-145pp.
16. Harrison, C.H. (1990). Electron microprobe analysis of coal macerals. Organic Geochemistry, 17(4), 439-449pp.
17. Hangsubcharoen, M. (1999). A study of triboelectrification mechanisms for coal, quartz and pyrite. PhD. Thesis (unpublished), Faculty of the Virginia Polytechnic Institute and State University, Virginia, USA, 106pp.
18. Huggins, F.E., Huffman, G. and Lee, R.J. (1982). Scanning Electron Microscope-based Automated Image Analysis (SEM-AIA) and Mossbauer Spectroscopy quantitative characterization of coal minerals, ACS Symposium Series, vol.205. 239-258pp.
19. Hutton, C.A. and Gould, R.N. (1982). Cleaning Up Coal. Ballinger Publishing Company, Cambridgeshire, England. -398pp.
20. Intellection, 2007. QEMSCAN Training manual – Written by Intellection for Eskom Applications. Version: 21 December 2007. Intellection Pty Ltd 2007. Brisbane, Queensland, Australia, 350pp.
21. Klein, C., de Korte, G.J., Wotruba, H., von Ketelhodt, L. and Robben, M.R. 2012. Recent developments in dry coal sorting with X-ray transmission, XXVI International Mineral Processing Congress [IMPC]; 2012 September 24-28; New Dehli, India, 2012, 13pp.
22. Lee, R.J., Huggins, F.E. and Huffman, G.P. (1978). Scanning Electron Microscopy, vol 1. 561-571pp.
23. Laskowski, J.S. and Walters, A.D. (1987). Coal Preparation. In: R.A. Meyers (Editor), The Encyclopaedia of Physical Science and Technology, Academic Press, Britain. 79-106pp.
24. Lockhart, N.C. (1984). Dry Beneficiation of Coal. Powder Technology, 40, 17-42pp.
25. Moritomi, H., Iwasi, T. and Chiba, T.A. (1982). A comprehensive interpretation of solid layer inversion in liquid fluidized beds. Chemical Engineering Science, 37(12),1751-1757pp.
26. Mouton, J. (2006). How to succeed in your Master's and Doctoral Studies, a South African Guide and Resource book. Van Schaik Publishers, Pretoria. – 280pp.
27. Nesse, W. D. (2000). Introduction to Mineralogy. Oxford University Press, New York. – 442pp.
28. Nissen, D.A. and Greulich, F.A. (1987). Automated image analysis of coal minerals, Symposium on high temperatures materials chemistry. 494-504pp.
29. Postek, M.T., Howard, K.S., Johnson, A.H. and McMichael, K.L. (1980). Scanning Electron Microscopy – A Student's Handbook. Michael T. Postek, Jr. and Ladd Research Industries, Inc. Unites States. -305pp.

30. Rowsell, D.M. (1979). Coal in South Africa - Internal Report No. 48. Department of Mines, Minerals Bureau, Braamfontein. -53pp.
31. Ryan, B and Ledda, A. (1997). A Review of Sulphur in Coal: With Specific Reference to the Telkwa Deposit, North-Western British Columbia. Geological Fieldwork 1997, British Columbia Geological Survey Branch, Britain, 29, 1-21pp.
32. Russ, C.J. and Dehoff, R.T. (1999). Practical Stereology, 2nd edition. Plenum Press, New York. -312pp.
33. SACPS (The South Africa Coal Processing Society) (2011). Coal Preparation in South Africa. Fourth English Edition. Intrepid Printers (Pty) Ltd, Pietermaritzburg. – 298pp.
34. SANS (South African National Standard), (2011). Coal – Proximate Analysis. Edition 2. SABS Standards Division. References: SANS 17426:2011, ISO 17426:2010, 13pp.
35. SANS (South African National Standard), (2010). Hard coal – Determination and presentation of float and sink characteristics – General directions for apparatus and procedures. Edition 1. SABS Standards Division. References: SANS 7936:2010, ISO 7936:1992, 19pp.
36. SANS (South African National Standard), (2009). Hard coal – Determination of total moisture. Edition 2. SABS Standards Division. References: SANS 589:2009, ISO 589:2008, 19pp.
37. SANS (South African National Standard), (2011). Hard coal and coke – Determination of volatile matter. Edition 2. SABS Standards Division. References: SANS 50:2011, ISO 562:2010, 17pp.
38. SANS (South African National Standard), (2011). Solid mineral fuels – Determination of ash. Edition 2. SABS Standards Division. References: SANS 131:2011, ISO 1171:2010, 13pp.
39. Singh, S. (2010). The potential of the QEMSCAN instrument in identifying and quantifying coal macerals. BSc. Hons. thesis (unpublished), University of Pretoria, Pretoria, South Africa, 74pp.
40. Singh, S. (2014). Eskom internal report. Reference: RP_FUELS_QS_14_74. QEMSCAN sample preparation. Eskom Research, Testing and Development Centre, Rosherville, South Africa, 3pp.
41. Skorupska, N.M. and Couch, G. (1993). Coal characterisation for predicting ash deposition: an international perspective, In: The impact of ash deposition on coal fired plants, Williamson, J. and Wigley, F. (Eds). 137-150pp.
42. Speight, J. G. (2005). Handbook of Coal Analysis. John Wiley & Sons, Inc. New Jersey. -222pp.
43. SSA (Statistics South Africa), (2012). National Accounts, Environmental Economic Accounts – Mineral Accounts for South Africa: 1980 – 2009, SSA. Discussion report D0405.2. Available from SSA, Private Bag X44, Pretoria 0001, and/or www.statssa.gov.za.

44. Steadman, E.N., Erickson, T.A., Folkedahl, B.C. and Brekke, D.W. (1991). Coal and ash characterisation: Digital image analysis applications, In: Inorganic Transformation and Ash Deposition during Combustion. Benson, S.A. (Ed). 147-163pp.
45. Straszheim, W.E. and Markuszewski, R. (1990). Automated image analysis of minerals and their association with organic components in bituminous coals, Energy and Fuels, 4. 748-754pp.
46. Van Alphen, C. (2009) Eskom Practical Combustion Course, June 2009 (PowerPoint presentation) Coal Quality: Analysis, prediction, slagging and impact on boilers. Eskom Fuels. Private conference.
47. Van Alphen, C. (2012). Eskom Power Plant Engineering Institute, Lectures 1 and 2 (EPPEI), January 2012 (PowerPoint Presentation). Coal geology, components, mining and beneficiation. Eskom Fuels. EPPEI training.
48. Van Alphen, C. (2012). Eskom coal XRT sensor optimization report: Tomra Sorting Solutions; July 2012, South Africa, 18pp.
49. Van Alphen, C. (2005). Factors influencing fly ash formation and slag deposit formation (slagging)on combusting a South African pulverized fuel in a 200MW_e boiler. PhD. Thesis (unpublished), University of Witwatersrand, Gauteng, South Africa, 354pp.
50. Van Alphen, C. and Falcon, L. (2000). Application of CCSEM to coal processing, in: Coal – The Future, 12th International Conference on Coal Research, South African Institute of Mining and Metallurgy, 197-201pp.
51. Ward, C.R. (1984). Coal geology and coal technology. Blackwell Scientific Publications, Australia. -345pp
52. Yu, H., Marchek, J.E., Adair, N.L. and Harb, J.N. (1993). Characterization of minerals and coal/mineral associations in pulverized coal, In: The Impact of ash deposition on coal fired plants, Williamson, J., and Wigley, Y.F. (Eds). 361-371pp.
53. Zhang, B., Akbari, H., Yang, F., Mohanty, M.K. and Hirschi, J. (2011). Performance optimization of the FGX dry separator for cleaning high-sulphur coal, International Journal of Coal Preparation and Utilization, 31, 161-186pp.
54. Zou, W., Nakashima, T., Onishi, Y., Koike, A., Shinomiya, B., Morii, H., Neo, Y., Mimura, H., and Aoki, T. (2008) Atomic number and electron density measurement using a conventional x-ray tube and a CDTE detector. Japanese journal of applied physics, Japan, 47(9), 7317-7323p

APPENDIX A

Microlithotype classification tables

Table A 1: Microlithotypes present in common South African coals (Falcon and Snyman, 1986).

Microlithotype	Maceral-group composition (mineral-free)	Microlithotype group
Monomaceral - (Collinite or telite)	Vitrinite>95%	Vitrite
Sporite (Cutite or resite), Algite	Liptinite>95%	Liptite
Micrite, macroite, semifusite, fusite (secretinite), inertodentrite	Inertinite>95%	Inertite
Bimaceral – Sporoclarite, cuticlarite (resinoclarite, algoclarite)	Vitrinite + liptinite>95%	Clarite (vitrinite, liptinite)
	Vitrinite + inertinite>95%	Vitrinertinite (vitrinite, inertinite
	Inertinite + liptinite>95%	Durite
Trimaceral – Duroclarite, vitrinertoliptite, clarodurite	Vitrinite>inertinite, liptinite Liptinite>inertinite, vitrinite Inertinite>vitrinite, liptinite	Trimacerite (vitrinite, liptinite, inertinite

The vitrinite maceral group has its maceral components formed from cell wall matter, and woody tissue of plants which include trunks, branches, twigs, roots and leaf tissue (Falcon and Snyman, 1986). The inertinite maceral group contains macerals originating from plant material that has been greatly altered in oxidising conditions during the peat stage of coal formation (Falcon and Snyman, 1986).

Table A 2: Carbominerites present in common South African coals (Falcon and Snyman, 1986).

Mineral group/mineral related to coal	Composition
Carbargillite	Coal + 20-60vol.% clay minerals
Carbosilicate	Coal + 20-60vol.% quartz
Carbopyrite	Coal + 5-20vol.% sulphides
Carbankerite	Coal + 5-60vol.% carbonates
Carbopolyminerite	Coal + 20-60vol.% mineral matter

Table A 3: The individual macerals that comprise the vitrinite maceral group (Falcon and Snyman, 1986).

Macerals	Form
Telinite	Cell walls that are well-preserved
Collinite	Cell walls and cell fillings that are well-preserved
Vitrodentrite	Fragments of detrital angular material

The macerals in the inertinite group have parent material identical to that of the vitrinite group, but the oxidising conditions it is exposed to leads to aerobic decomposition and carbon enrichment during fusinitization (Falcon and Snyman, 1986).

The liptinite maceral group was previously known as the exinite maceral group in order to describe the chemically resistant exines in coal spores (Falcon and Snyman, 1986). This maceral group contains the macerals that have originated from the most resistant parts of plants, for example, the spores, cuticles, suberine cell walls, resins, polymerised waxes, fats and oils of plants (Falcon and Snyman, 1986).

Table A 4: The individual macerals that comprise the inertinite maceral group (Falcon and Snyman, 1986).

Macerals	Form
Fusinite	Cell walls that are well-preserved and have undergone extreme oxidation
Semifusinite	Preserved cell wall that has undergone partial oxidation
Secretinite	Well- preserved botanical structures surrounded by fungal or cellular matter
Micrinite	Granules <2µm
Macrinite	Amorphous groundmass >30µm
Inertodentrite	Detrital material comprising all abovementioned forms lacking woody cell cavities and are 2-30µm

The various macerals in the liptinite maceral group are named according to the specific plant (algae), part of plant (spores and cuticles), or product of plant (waxes and resins) from which the maceral originated (Falcon and Snyman, 1986).

Table A 5: The individual macerals that comprise the liptinite maceral group (Falcon and Snyman, 1986).

Macerals	Form
Sporinite	Well-preserved compressed micro-, macro, and megaspore exines
Cutinite	Well-preserved, elongated, saw-toothed botanical structures
Alginite	Well-preserved algal colonies that are rounded and semi-compressed
Resinite	Resin that filled cellular cavities and appear as globular or irregular forms
Liptodentrite	Smaller detrital fragments of the resinite form

APPENDIX B

Sample preparation and analysis procedures

B.1 Float and sink analysis procedure

When a test sample has a range of low to high relative density material with very little intermediate density material, the sample is placed in the low density medium first (SANS7936, 2010). The float is drained, washed, dried and weighed while the sink is subjected to the medium with highest relative density (SANS7936, 2010). The sink is drained, washed, dried and weighed (SANS7936, 2010). The float fraction is now of a smaller mass and can be subjected to a medium of either ascending or descending order (SANS7936, 2010). This process avoids washing large amounts of material in intermediate relative densities, thereby reducing handling and breakage (SANS7936, 2010).

Discards and middlings have a higher relative density than that of clean coal and hence the minimum masses of samples containing these phases should be increased to ensure that these samples have approximately the same number of particles as the clean coal samples, as well as similar accuracy (SANS7936, 2010).

Samples with large amounts of intermediate relative density material are first washed in a medium of intermediate relative density (SANS7936, 2010). Once the estimated split in the mass of the sample is known, the floats are tested in ascending order of density, while the sinks are tested in descending order (SANS7936, 2010).

It is important to note the following when carrying out float and sink analysis:

- The sample should carefully be placed into the separating liquid to avoid splashing as the liquid is harmful if exposed to the eyes/skin (SACPS, 2011) and sample loss may occur (SANS7936, 2010).
- Many solvent vapours are toxic therefore adequate ventilation is necessary (SANS7936, 2010).
- A large quantity of sample should not be placed into the separating liquid at once as particles may become trapped i.e. a float particle trapped under sink particles (SACPS, 2011). Float values may be underestimated if the float and sink analysis is not carried out correctly (SANS7936, 2010).
- Sufficient time must be allowed for adequate separation (SACPS, 2011) (SANS7936, 2010).
- The sample should be handled carefully to avoid breakage, as the broken off chip may float when it would otherwise sink and the result accuracy would be compromised (SACPS, 2011).

B.1.1 Sampling and screening

The minimum mass required to carry out a float and sink test is derived as per equation B.1 (SANS7936, 2010):

$$mt = mr/ms \times 100 \quad \text{(B.1)}$$

Where:

mt = total minimum mass

mr = suggested mass of coarsest fraction

ms = mass percent of coarsest size fraction

A minimum mass per float fraction can be calculated per size fraction assuming particles are somewhat spherical and that the relative density of coal is ~1.5 (SACPS, 2011). The minimum mass required may not be achievable for some plant products or bore core samples (SANS, 2010). Equation B.2 below, as given by SACPS (2011) is used to calculate the mass of the sample per size fraction:

$$M = 5.24\ D \quad \text{(B.2)}$$

Where:

M = Sample mass per float fraction (kg)

D = Mean diameter of particle (mm)

Ideally the coal sample is taken as soon as possible to minimize breakage (SANS7936, 2010). The sample is spread out to dry, after which the sample is screened into a range of size fractions (SANS7936, 2010). Samples are wet screened to ensure that smaller particles attached to larger particles are removed so that these small particles report to the correct size fraction (SANS7936, 2010). Although each size fraction requires a minimum of 1000 particles to undergo float and sink analysis, each relative density fraction is required to have a minimum mass of 20 grams and contain at least 10 discrete particles (SANS7936, 2010).

B.1.2 Washing medium

Sized coals are placed in organic liquids, aqueous solutions, or solids in aqueous suspension of various specific gravities (SANS7936, 2010). The organic liquids used to prepare the floats and sinks in the research data set were a mix of benzene ($0.88 g.cm^{-3}$), perchloroethylene ($1.62 g.cm^{-3}$) and bromoform ($2.89 g.cm^{-3}$).

The medium is chosen according to the bulk density and particle size of the coal, as well as its rank and relative density (SANS7936, 2010). After analysis, the samples are sent to the chemical laboratory to determine ash content (SACPS, 2011). The ash content, together with the density of each sample and the experimentally determined yield % are used to plot the washability curve (Galvin, 2006).

The specific density of the wash medium is achieved by mixing calculated volumes of liquids with different specific gravities, one higher and one lower, to achieve a mixture with the required specific gravity (SANS7936, 2010). The specific gravity of the mixture is then checked using a hydrometer (SANS7936, 2010). The volumes of the liquids are calculated using equation B.3 (SANS7936, 2010):

$$Vm = Vt ((\rho t - \rho p)/(\rho m - \rho p) \qquad (B.3)$$

Where:

Vm = *volume of the liquid with greater specific gravity*

Vt = *volume of mixture with required specific gravity*

ρm = *specific gravity of the liquid with greater specific gravity*

ρt = *specific gravity of mixture*,

ρp = *specific gravity of the liquid with lower specific gravity*.

B.1.3 Apparatus and test procedure

The apparatus used is dependent on the size fraction of the sample (SANS7936, 2010). It is important that the apparatus used does not react with the dense medium or suspensions utilized (SANS7936, 2010). A woven wire basket with an adjustable partition is used to keep the float and sink fractions separate while having access to both (Figure B.1) (SANS7936, 2010). The wire basket fits into a galvanised metal tank (SANS7936, 2010). The float and sink bench consists of cupboard space for the galvanised metal tanks and an air duct to extract the toxic fumes (SANS, 2010). A draining board allows for the fractions to drain of wash medium (SANS7936, 2010).

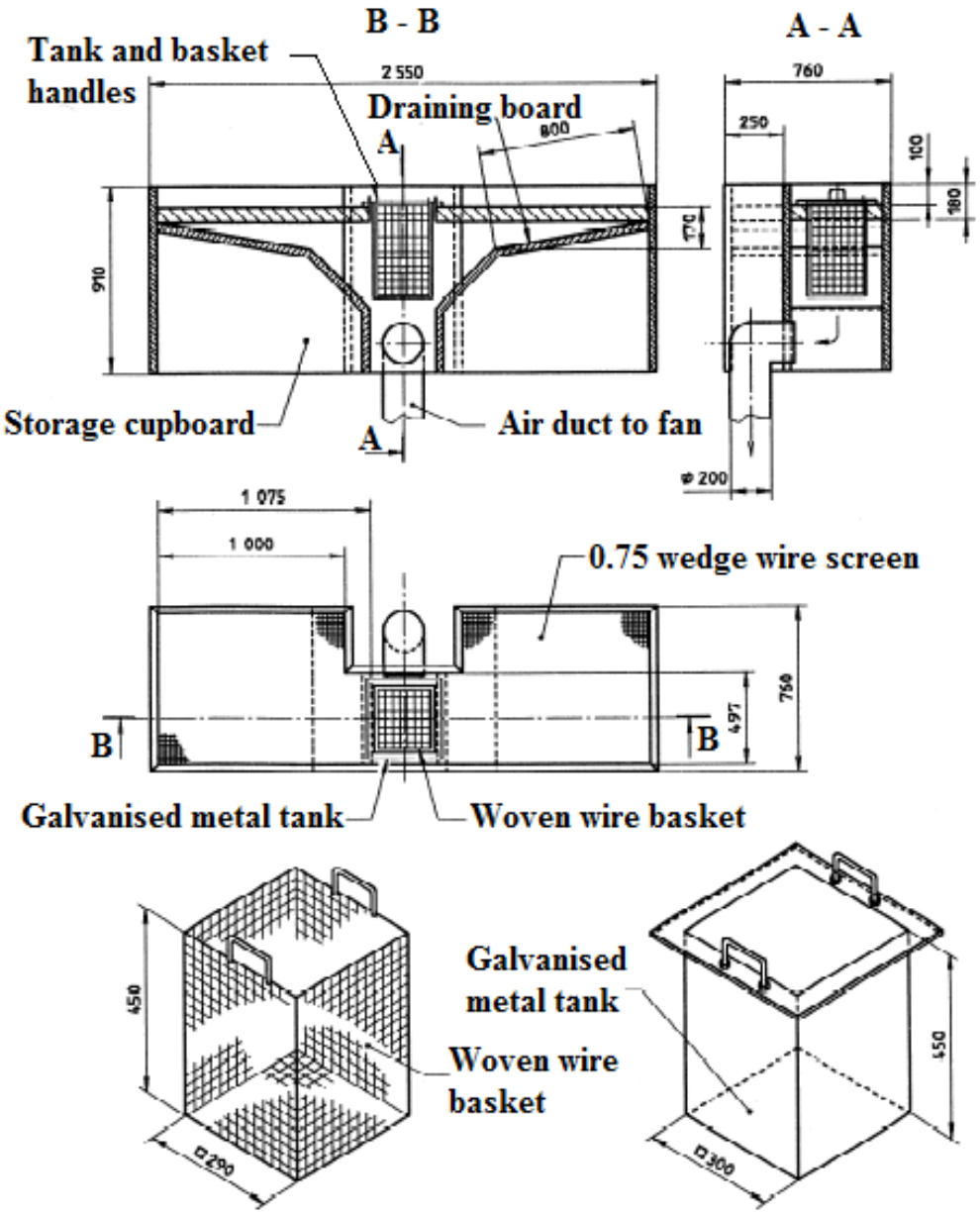

Figure B 1. Float and sink bench for analyses of coarse size fractions (Adapted from SANS7936, 2010). Dimensions are in millimetres (SANS7936, 2010).

As per Figure B.2 below, another apparatus commonly used involves a tank with a mesh base that fits into a larger tank (SANS7936, 2010). The floats are skimmed off the surface with a mesh scoop while the sinks are recovered by draining off the liquid from the base tank (SAN-S7936, 2010).

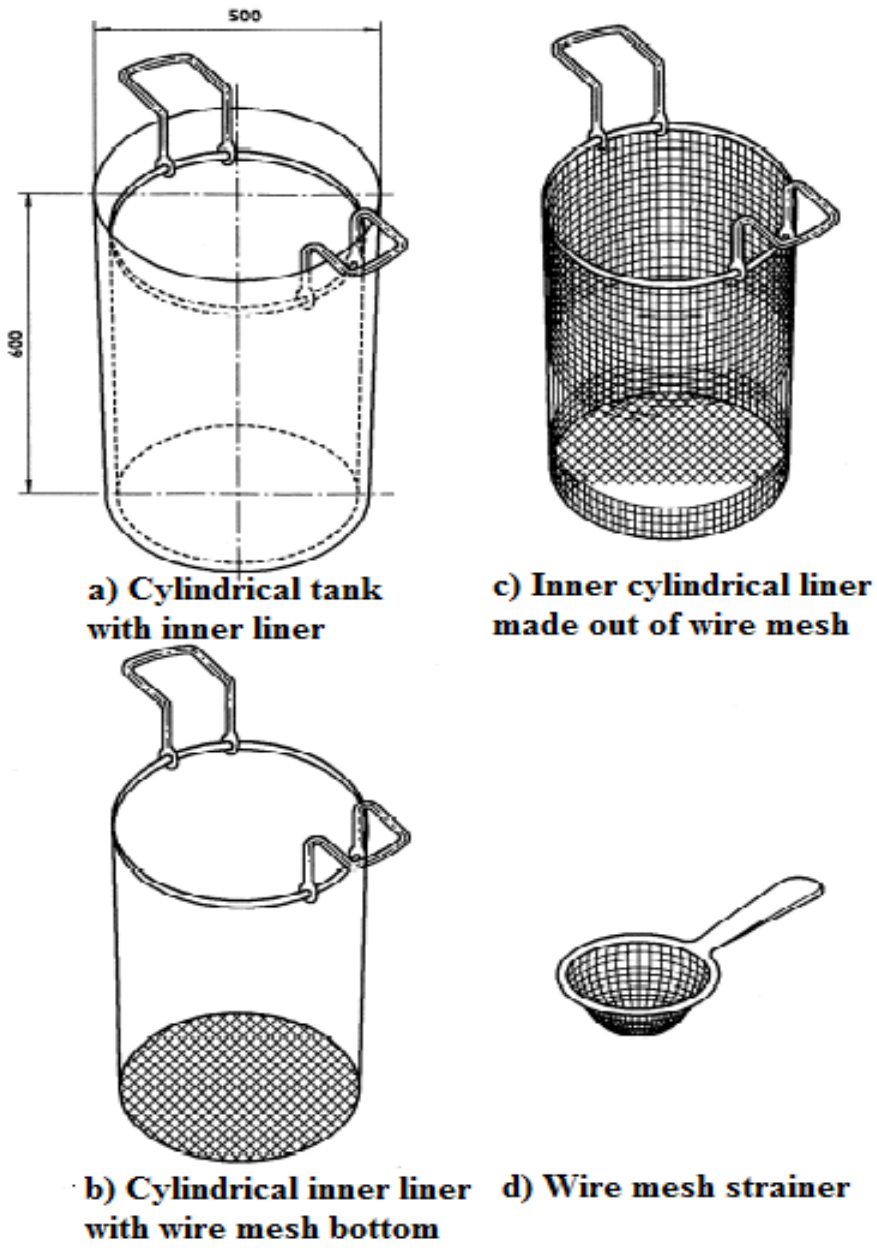

Figure B 2. Apparatus for float and sink testing of coarse coal (Adapted from SANS7936, 2010). Dimensions are in millimetres (SANS7936, 2010).

The separation vessel is partially filled with the separating medium and the density is checked using a hydrometer (SANS7936, 2010). The hydrometer is used to frequently check that the density medium stays in the ±0.002 error margin range for the duration of the test, with adjustments being made to the medium as required (SANS7936, 2010). A portion of the size fraction, large enough to form a thin layer at the apparatus base, is placed into the apparatus containing medium and gently agitated (SANS7936, 2010). Overloading the tank apparatus with sample will adversely affect separation of entrained near density material (SANS7936, 2010). Sufficient time must be allocated to allow complete separation of floats from sinks (SACPS, 2011). The time required depends on the size fraction undergoing separation, viscosity of the separating liquid and the number of near density particles (particles with a relative density similar to that of the separating liquid (SACPS, 2011).

A portion of the coal will float on the surface of the separating liquid, while the rest will sink (SANS7936, 2010). The float material is skimmed off and placed in a draining tray while the sinks are once again agitated to release trapped float particles (SANS7936, 2010). Once all float particles have been separated, the fractions are removed, washed, dried and weighed (Galvin, 2006). The sinks are then subjected to an organic liquid with an incrementally higher specific gravity (Galvin, 2006). The process is continued until all the material sinks in an organic liquid with higher specific gravity (Galvin, 2006). If the sample is of a -0.5mm fraction or smaller, a centrifuge should be used (SACPS, 2011). Float and sink testing can be carried out either in ascending or descending order of relative density, depending on the density of majority of the sample (SANS7936, 2010). A large proportion of the sample is removed from the test in the initial separation/s, which reduces handling and breakage (SANS7936, 2010).

B.2 Proximate analysis

Each sample of coal sent to the chemical laboratory is passed through a riffler or it is coned and quartered in order to get a representative split sample (van Alphen, 2011). In order to determine total moisture, the sample is air dried under ambient conditions. The mass loss due to air drying accounts for the surface moisture (SM) lost (SANS589, 2009). The air-dried sample is then crushed to a 2.8mm size fraction and dried in air between 105-110°C to determine the inherent moisture (IM) (SANS589, 2009). The inherent moisture and surface moisture make up the total moisture (TM=SM+IM) (SANS589, 2009). Excess moisture is a problem in that it causes the coal to cake and form blockages in handling equipment (van Alphen, 2011). The procedure for calculation of total moisture as per the SANS589 (2009) standard is only applicable to hard coal that is not susceptible to oxidation (SANS589, 2009).

The volatile hydrocarbons are measured by placing a gram of 212 μm sample into a furnace at 900°C for 7 minutes and measuring the resultant mass loss (SANS50, 2011). The ash value is obtained by placing a gram of 212 μm sample into a furnace and heated in air at a predetermined rate at 815±10°C until a constant mass is achieved (SANS131, 2011). The resultant weighed residue is the ash value (SANS131, 2011). The ash value is a representation of inorganic phases present in the uncombusted coal substance and associated minerals (SANS131, 2011).

The fixed carbon content is determined by difference as per equation B.4 (SANS17426, 2010):

$$C_{fix,ad} = 100 - (M_{ad} + A_{ad} + V_{ad}) \qquad (B.4)$$

Where:

M_{ad} *= moisture of air-dried sample*

A_{ad} *= ash calculated to an air dried basis and,*

V_{ad} *= volatile matter calculated to an air dried basis.*

B.3 QEMSCAN sample preparation and instrument operation

Sample preparation should be carried out carefully and as accurately as possible because inadequate sample dispersion can result in touching particles, which distort the size determination of larger samples and also makes it difficult to locate the centre of the particle (French et al., 2008).

The required amount of sample per size fraction for QEMSCAN sample preparation was determined experimentally by choosing a mass of sample that allowed for a monolayer of

particles on the bottom of the 30cm diameter sample preparation Teflon mould. These determined masses are presented in Table B.1 below.

Table B 1: Mass of sample required for QEMSCAN sample preparation per size fraction.

New size fraction (mm)	Required amount for sample preparation (g)
-0.5	0.5±0.1
-1.0	1.0±0.2
-2.0	1.5±0.2

B.3.1 Sample splitting

In order to ensure that a representative sample is acquired, the samples are riffled using a Rotary Micro Riffler as per Figure B.3 (Intellection, 2007). The prepared 0.5mm, 1mm and 2mm samples are decanted into the riffler. The rotation of the test tubes and the vibration on the riffler can be adjusted. Larger size fractions riffle quicker than smaller size fractions. As the test tube holder on the riffler rotates, coal sample pours into the test tubes. The vibration applied to the riffler ensures that there is an even distribution in terms of even mass, particle size and density distribution in the flow of coal to each of the test tubes (Intellection, 2007). Each test tube contains a representative sample of the original sample (Intellection, 2007). The coal from one of the test tubes is riffled again to obtain a representative smaller mass (Intellection, 2007). The procedure is continued until the mass required for QEMSCAN polished sections is obtained ()(Intellection, 2007). The mass is measured by means of a mass balance (Intellection, 2007). Once the required sample mass is obtained, the sample is ready for potting (Singh, 2014).

Figure B 3. Rotary micro riffler (Quantachrome Instruments) that splits the coal sample into representative samples.

B.3.2 Potting

30mm Teflon sample moulds must be coated with Silicone Oil, clearly labelled and left in the oven to dry for half an hour at 60ºC (Singh, 2014). Once dry, the moulds are topped up with carnauba wax flakes (Figure B.4) and left to melt in the oven at 120ºC for 20 minutes (Singh, 2014). The melting temperature range of carnauba wax is between 80-86 degrees Celsius (EFSA, 2012). The rifled sample must be added to the molten wax and stirred (Singh, 2014). Each Teflon pot (Figure B.5) is to be taken out individually from the oven and mixed thoroughly with sample before being returned to the oven (Singh, 2014).

Figure B 4. Flakes of carnauba wax before being decanted and melted in Teflon sample moulds.

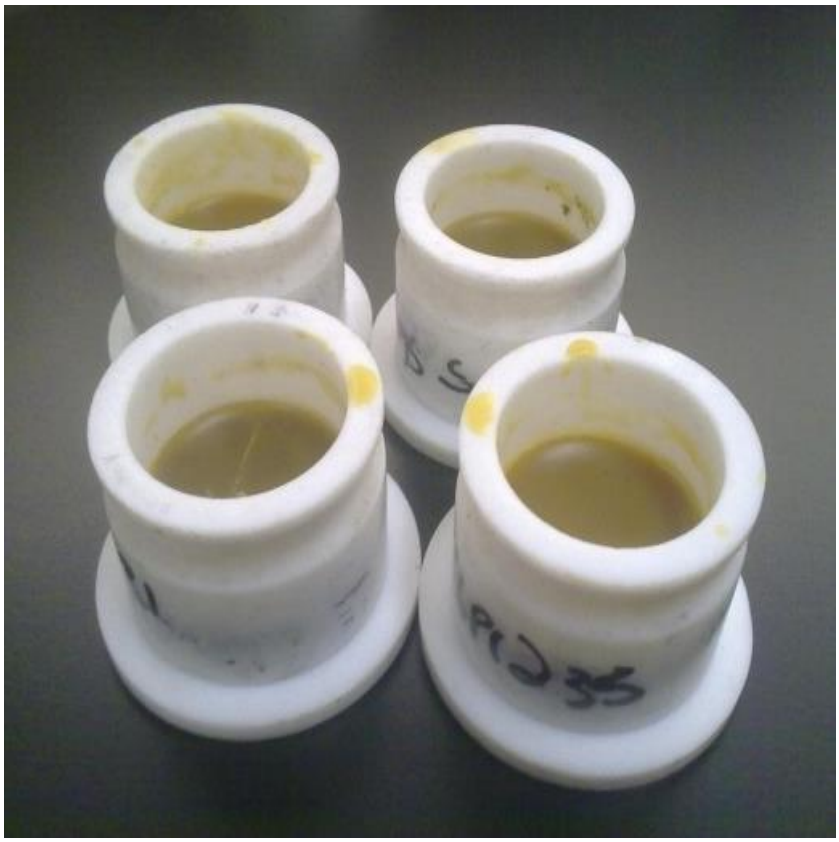

Figure B 5. Coal samples set in carnauba wax in labelled Teflon moulds.

The sample should be mixed with a bamboo stick, slowly stirring in a figure of eight motion while turning the sample mould (Singh, 2014). Coarser size fractions should be stirred gently

until the bottom of the sample mould is evenly covered (Singh, 2014). Air bubbles are easily trapped between/under larger particles if stirred vigorously (Singh, 2014). It is recommended that the sample be stirred with a bamboo stick in figures of eight and in small circles from the center of the sample toward the sample mould edge (Singh, 2014).

The samples are left in the oven for 35 minutes at 120ºC to equilibrate the temperature of the sample, wax and Teflon mould (Singh, 2014). The heat on the oven should be turned down to 60ºC to allow the samples to solidify (Singh, 2014). The samples should then be left in the oven undisturbed/unopened for 90 minutes (Singh, 2014). Once the samples are ready, they should be taken out of the oven and left to cool to room temperature (Singh, 2014). The coal samples have now securely set in the hardened carnauba wax as per Figure B.5. The samples are ready to be removed from the sample moulds and labelled with permanent markers (Singh, 2014). The samples are then ready for polishing (Singh, 2014).

Coal samples are set in carnauba wax since epoxy resin has a BSE response which is very close to that of coal (French et al., 2008). Carnauba wax has very low BSE values, thus the coal and minerals can be seen due to better contrast with the carnauba wax (French et al., 2008). This allows for the relationships between the organic and inorganic phases to be determined (French et al., 2008). Before carnauba wax was used as a sample medium for coal, epoxy resin was used by adding barium or iodine to it (heavy atoms) giving it a BSE response that is in between that of coal and other common minerals (French et al., 2008).

B.3.3 Polishing

The polishing instrument used was the Struers TegraPol-21 (Figure B.6). The ‘backs’ of the samples are polished down till a neat and even surface is reached (Singh, 2014). This is done so that even polishing of the sample surface is accomplished (Singh, 2014). The sample surface is polished with progressively finer polishing paper to prevent scratches on the final polished sample (Singh, 2014). The polishing process includes the initial polishing stage using a rough disc called MD Largo (Singh, 2014). Thereafter the samples are polished for ten seconds each using silica carbide paper with decreasing roughness for a finer polish (Singh, 2014). The papers used are 1200, 2400 and 4000 (Singh, 2014). The final polishing stage used a velvet disc called MD Chem for 60 seconds to shine and clean the sample surface (Summary Table B.2) (Singh, 2014).

Figure B 6. Struers TegraPol-21 polishing instrument used to polish carnauba and epoxy blocks.

All polishing is carried out as per procedure summarized in Table B.2 at the following settings:

Force: 10N/60N; Disc rotation speed: 300rpm; Lubricant: Water

Table B 2: Polishing process.

Polishing Step No.	Polishing Surface	Polishing Paper	Time (s)	Lubricant
1	Sample back	MD Piano 80	10	Water
2	Sample surface	1200 SiC grit	10	Water
3	Sample surface	2400 SiC grit	10	Water
4	Sample surface	4000 SiC grit	10	Water
5	Sample surface	MD Chem	60	Water

Samples must be washed with soapy water to make sure all the samples are adequately clean (Singh, 2014). The sample surfaces are now polished to a three micron finish (Singh, 2014). Samples are washed with warm soapy water, rinsed, dried and ready to be sputter carbon coated (Singh, 2014).

B.3.4 Carbon coating

The samples are placed in the carbon coater (Figure B.7) with polished sample surface facing upwards (Intellection, 2007). A carbon rod is sharpened and set in the carbon rod holder with the sharpened rod in contact with an evenly flattened rod (Intellection, 2007). The carbon rods are set up in holders located on the lid of the instrument. It is crucial that the carbon rods are securely in contact with each other (Intellection, 2007). Press the "*Start"* button to stabilize the instrument's vacuum (5 minutes) (Intellection, 2007). Press the "*Down"* button to outgas (30 seconds), after which press the "*Up"* button to evaporate (30 seconds) (Intellection, 2007). The carbon rods visibly spark during evaporation, indicating that the samples are being coated (Intellection, 2007). Press "*Stop"* to release the vacuum (1 minute) (Intellection, 2007).

Outgassing of samples decreases the time required to pump down the scanning electron microscope to the required vacuum. Samples can be coated a second time if necessary. Samples require a second coating if a visible spark was absent, the first coat was not sufficient (as indicated by the brass insert), or if the sample has holes on the surface (Intellection, 2007). The purpose of the carbon coat is to prevent a static charge forming on the sample due to the electron beam interacting with the sample surface (Intellection, 2007). Holes on the sample surface are especially susceptible to charging (Intellection, 2007). Once the samples are adequately coated, they are ready for loading into the instrument (Singh, 2014).

Figure B 7. Samples sputter coated with K950x Turbo Evaporator.

B.3.4 QEMSCAN loading and operation

The sample now displays individual particles in cross section and is inserted into the QEMSCAN instrument for analysis (Figure B.8). The accuracy of the analysis is affected by the BSE threshold level and the accelerating voltage (French et al., 2008).

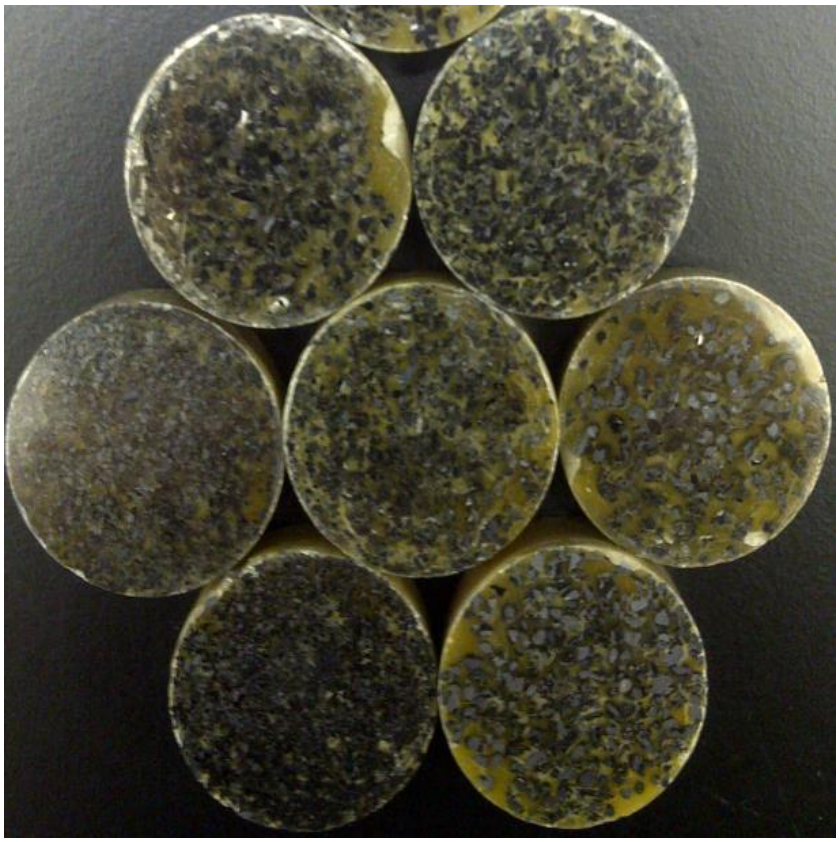

Figure B 8. Float and sink data set samples prepared in 30mm diameter carnauba wax blocks, ready for QEMSCAN analysis.

The QEMSCAN instrument is calibrated for the sample run and the sample holder is inserted into the instrument. The 0.5mm, 1.0mm and 2.0mm samples were analysed using iMeasure software, version 5.2. Once the samples were run, they were processed using iDiscover software, version 5.2. Processing allows for separation of the individual particles, determination of elemental proportions, textural data and particle size (Intellection, 2007). A Species Identification Protocol (SIP) is a list of rules/specifications used to identify the minerals from the X-ray spectrum derived elemental proportions (Intellection, 2007).

Samples can be placed into either the 9 block (Figure B.9) or 16 block holder and loaded into the instrument. The sample holder assigns each sample a number, which are labelled electronically for sample data identification using the QEMSCAN interface (Intellection, 2007).

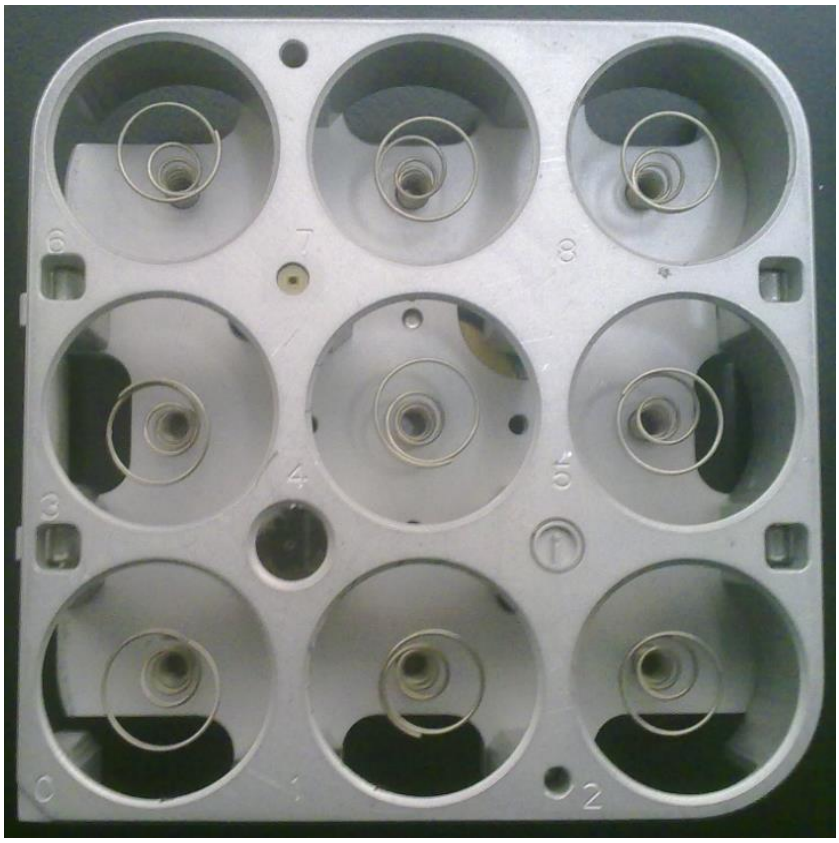

Figure B 9. 9 block sample holder used for QEMSCAN analysis.

B.3.4.1 Creation of measurements in iDiscover

A measurement is created for each sample. Each measurement describes the mode of measurement selected, target minerals, number of particles required, particle size and shape (Intellection, 2007). All samples analysed in the data set were set to Field Scan Mode. The Field Scan Mode analyses a full image per field and is used to analyse textural associations between phases (Intellection, 2007). The fields can later be stitched to produce a complete image of the sample surface analysed (Intellection, 2007).

A Species Identification Protocol (SIP) needs to be added to a new data store before a measurement can be added. The SIP file serves as the primary phase classification for QEMSCAN (French et al., 2008). The SIP file contains various entries on BSE response, information on the element present and their respective intensities (French et al., 2008). A SIP is created by analysis of standards to acquire reference spectra (French et al., 2008). The reference spectra are used to acquire simulated 1000 count spectra and the SIP is tested against it in order to correctly match the spectra with their respective mineral phases (French et al., 2008).

The primary species list is the most extensive as it contains all the possible mineral species likely to occur in a rock type and /or sample group (French et al., 2008). Secondary and tertiary species lists may be formed by grouping the entries present in the primary list to form a more compact list of phases relevant to a project (French et al., 2008). An example would be

to group all the oxides (FeO, MgO, CaO etc.) from the primary list in a grouping titled 'Oxides'.

Each sample block had an analysed field size of 1200 microns, an electron beam diameter of 5 microns and a total of 27 analysed fields per sample block. The sample block measurement settings are dragged and dropped into the appropriate locations on an image of the sample block holder (Intellection, 2007). The sample block description and name will appear on the sample block holder (Intellection, 2007). The sample block is opened up in iMeasure which creates a digital copy of the sample block holder to instruct the instrument of the sample blocks present, as well as how the measurements are to be performed (Intellection, 2007). The measurements can be reordered in terms of priority of analysis (Intellection, 2007).

B.3.4.2 Electron microscope loading and calibration

The stage is centralized and the electron beam is turned off, after which the system can be vented to air for sample exchange (Intellection, 2007). Selecting the TV mode/chamber scope mode allows for a view inside the chamber to ensure clearance between the stage and detectors (Intellection, 2007). Once the samples are loaded, the sample holder chamber is pumped up to an adequate vacuum (Intellection, 2007).

The column isolation is activated at ~3.7 x 10^{-5} Torr and a green tick appears on the vacuum tab indicating that a stable vacuum has been reached and the electron gun may now be switched on (Intellection, 2007). The tungsten filament is heated up to an accelerating voltage of 25kV producing an electron beam that is directed at the sample surface/sample holder (Intellection, 2007). A hysteresis is performed once the beam is turned on to remove residual magnetic memory from the lenses (Intellection, 2007).

The brightness and contrast settings are used to set up an image once the beam is on (Intellection, 2007). Due to the reinsertion of the sample holder with new samples, the faraday cup, gold, quartz and copper positions need to be centred and saved (Intellection, 2007). The Faraday cup is a small hole drilled into the centre of the sample holder that allows the pure strength of the beam to be measured when the electron beam is directed into it (Intellection, 2007). Gold, quartz and copper are used as their chemical compositions are constant (Intellection, 2007).

A beam optimisation is performed to automatically search for the appropriate filament current by adjusting the probe current and spot size to achieve a -5.00nA specimen current (Intellection, 2007). Alternately, the specimen current is adjusted to -5.00nA by adjusting the tilt, shift, probe current and spot size settings (Intellection, 2007). Once the beam is optimized, test spectra are acquired of the gold and quartz standards (Intellection, 2007).

The brightness and contrast settings are calibrated to allow grains to be located, identified and measured within the sample preparation medium (Intellection, 2007). A line scan is used to calibrate brightness and contrast (Intellection, 2007). The brightness is adjusted until the line

across the Faraday cup sits on the bottom of the line scan window and the contrast is adjusted until the line across gold sits approximately 1cm from the top of the line scan window (Intellection, 2007). The brightness and contrast settings are saved once the settings are stable, or else the beam requires beam optimization until the beam is stable (Intellection, 2007).

The electron beam is then calibrated at three points, which are the Faraday cup, quartz and gold (Intellection, 2007). A spot is turned on at each of the three points, repeatedly scanning the same point (Intellection, 2007). The calibrated BSE values for the Faraday cup, quartz and gold should be 5, 42 and 232 respectively (Intellection, 2007). A focus calibration is performed and saved for each individual analysis (Intellection, 2007). The specimen current is once again checked to be -5.00nA to ensure beam stability (Intellection, 2007). If the specimen current has changed, the beam need to be optimised once again, as well as the line scan and BSE calibrations repeated (Intellection, 2007). The instrument is now ready to begin analysis of the samples. Once the analysis has started, it is important to check if the beam optimises and the focus is accurate (Intellection, 2007).

B.3.4.2 QEMSCAN quantitative analysis - stereology

QEMSCAN analysis uses stereological principals in its analyses. Stereology is the study of geometric relationships between structures that are present in 3-D space, but are observed only as 2-D (Russ and Dehoff, 1999). In order to extend two-dimensional information to three-dimensional information, the principle of stereology assumes that the plane section is composed of homogenous material and that the plane sections are selected according to a random sampling method.

The sample surface is analysed in a grid-like raster pattern (Intellection, 2007). The grid area analysed by QEMSCAN can be adjusted in terms of the number of points in the grid to be analysed, the size of the grid blocks and how much of the sample surface the grid will cover (Intellection, 2007). As per equation B.5 below (the first law of stereology), the mean surface area proportion (A_a) on a two-dimensional surface are the same as the mean volume proportion (V_v) in a three-dimensional structure (Russ and Dehoff, 1999):

$$P_p = L_l = A_a = V_v \qquad (B.5)$$

Where:

P_p *= the point fraction analysed in the grid*

L_l *= the line fraction which is obtained by analysing points in a horizontal or vertical manner in the grid*

A_a *= area and,*

V_v *= volume.*

Both the point fraction and line fraction are one dimensional (Russ and Dehoff, 1999). As the point fraction forms line fractions both in a horizontal and vertical manner in the grid, an area

fraction can be determined (Russ and Dehoff, 1999). The area fraction is two dimensional and is then representative of the volume fraction which is three dimensional (Russ and Dehoff, 1999). Problems arise with elongated particles as needle-like particles may be incorrectly interpreted as plate-like particles and vice versa. Similarly, oval structures may be confused with spherical structures.

APPENDIX C

Original float and sink data

Table C 1: Float and sink data for the -12+0.5mm size fraction.

	Mass (g)		% Yield	
	Total	Fractional	Fractional	Cumulative
Sample Mass	65680			
F 1.50		11400	19.9	19.9
F 1.80		21160	37	57
F 2.00		5160	9	66
S 2.00		19440	34	100
Total		57160	100	

Table C 2: Float and sink data for the -25+12mm size fraction.

	Mass (g)		% Yield	
	Total	Fractional	Fractional	Cumulative
Sample Mass	32060			
F 1.40		1760	5.489707	5.489707
F 1.50		2660	8.296943	13.78665
F 1.60		5500	17.15533	30.94198
F 1.70		7400	23.08172	54.02371
F 1.80		3100	9.66937	63.69308
F 1.90		1400	4.366812	68.05989
F 2.00		1020	3.181535	71.24142
S 2.00		9220	28.75858	100
Total		32060	100	

Table C 3: Float and sink data for the -40+25mm size fraction.

	Mass (g)		% Yield	
	Total	Fractional	Fractional	Cumulative
Sample Mass	89780			
F 1.40		3080	3.430608	3.430608
F 1.50		9860	10.9824	14.41301
F 1.60		18080	20.13812	34.55112
F 1.70		19060	21.22967	55.7808
F 1.80		7000	7.796837	63.57763
F 1.90		3980	4.433059	68.01069
F 2.00		3020	3.363778	71.37447
S 2.00		25700	28.62553	100
Total		89780	100	

Table C 4: Float and sink data for the -50+40mm size fraction.

	Mass (g)		% Yield	
	Total	Fractional	Fractional	Cumulative
Sample Mass	188360			
F 1.40		3640	1.93247	1.93247
F 1.50		19080	10.12954	12.06201
F 1.60		44440	23.59312	35.65513
F 1.70		50960	27.05458	62.7097
F 1.80		11980	6.360161	69.06987
F 1.90		8360	4.43831	73.50818
F 2.00		6480	3.440221	76.9484
S 2.00		43420	23.0516	100
Total		188360	100	

Table C 5: Float and sink data for the -70+50mm size fraction.

	Mass (g)		% Yield	
	Total	Fractional	Fractional	Cumulative
Sample Mass	558240			
F 1.40		17040	3.052451	3.052451
F 1.50		46260	8.286758	11.33921
F 1.60		125740	22.52436	33.86357
F 1.70		152260	27.27501	61.13858
F 1.80		31000	5.553167	66.69175
F 1.90		20360	3.647177	70.33892
F 2.00		20400	3.654342	73.99326
S 2.00		145180	26.00674	100
Total		558240	100	

Table C 6: Float and sink data for the -100+70mm size fraction.

	Mass (g)		% Yield	
	Total	Fractional	Fractional	Cumulative
Sample Mass	687960			
F 1.40		15800	2.296645	2.296645
F 1.50		57000	8.285365	10.58201
F 1.60		182520	26.53061	37.11262
F 1.70		169480	24.63515	61.74778
F 1.80		50020	7.270772	69.01855
F 1.90		35420	5.148555	74.1671
F 2.00		30120	4.378162	78.54526
S 2.00		147600	21.45474	100
Total		687960	100	

Table C 7: Float and sink data for the -150+100mm size fraction.

	Mass (g)		% Yield	
	Total	Fractional	Fractional	Cumulative
Sample Mass	297760			
F 1.40		780	0.261956	0.261956
F 1.50		14740	4.950296	5.212251
F 1.60		107120	35.97528	41.18753
F 1.70		74580	25.04702	66.23455
F 1.80		11340	3.808436	70.04299
F 1.90		15880	5.333154	75.37614
F 2.00		2760	0.926921	76.30306
S 2.00		70560	23.69694	100
Total		297760	100	

Table C 8: Float and sink data for the +150mm size fraction.

	Mass (g)		% Yield	
	Total	Fractional	Fractional	Cumulative
Sample Mass	267360			
F 1.50		5900	2.206762	2.206762
F 1.60		47900	17.91592	20.12268
F 1.70		54120	20.24237	40.36505
F 1.80		24220	9.058947	49.424
F 1.90		25620	9.582585	59.00658
F 2.00		5580	2.087074	61.09366
S 2.00		104020	38.90634	100
Total		267360	100	

APPENDIX D

Washability curves: characteristic ash curve, float curve, sink curve and densimetric curve

Table D 1: Float and sink data for the -12+0.5mm size range

1		2	3	4	5	6	7	8	9	10	11	12
				Ash	RD	Cumulative Floats			Cumulative Sinks			Mass
RD	Mass (g)	Mass %	Ash%	Proportion		Mass%	Ash Prop.	Ash%	Mass%	Ash Prop.	Ash%	
									100.00	4211.88	42.12	
F 1.50	11400.00	19.94	13.85	276.22	1.5	19.94	276.22	13.85	80.06	3935.65	49.16	9.97
F 1.80	21160.00	37.02	27.40	1014.32	1.8	56.96	1290.54	22.66	43.04	2921.34	67.88	38.45
F 2.00	5160.00	9.03	48.40	436.92	2	65.99	1727.46	26.18	34.01	2484.42	73.05	61.48
S 2.00	19440.00	34.01	73.05	2484.42	2	100.00	4211.88	42.12				83.00
Total	57160.00	100.00										

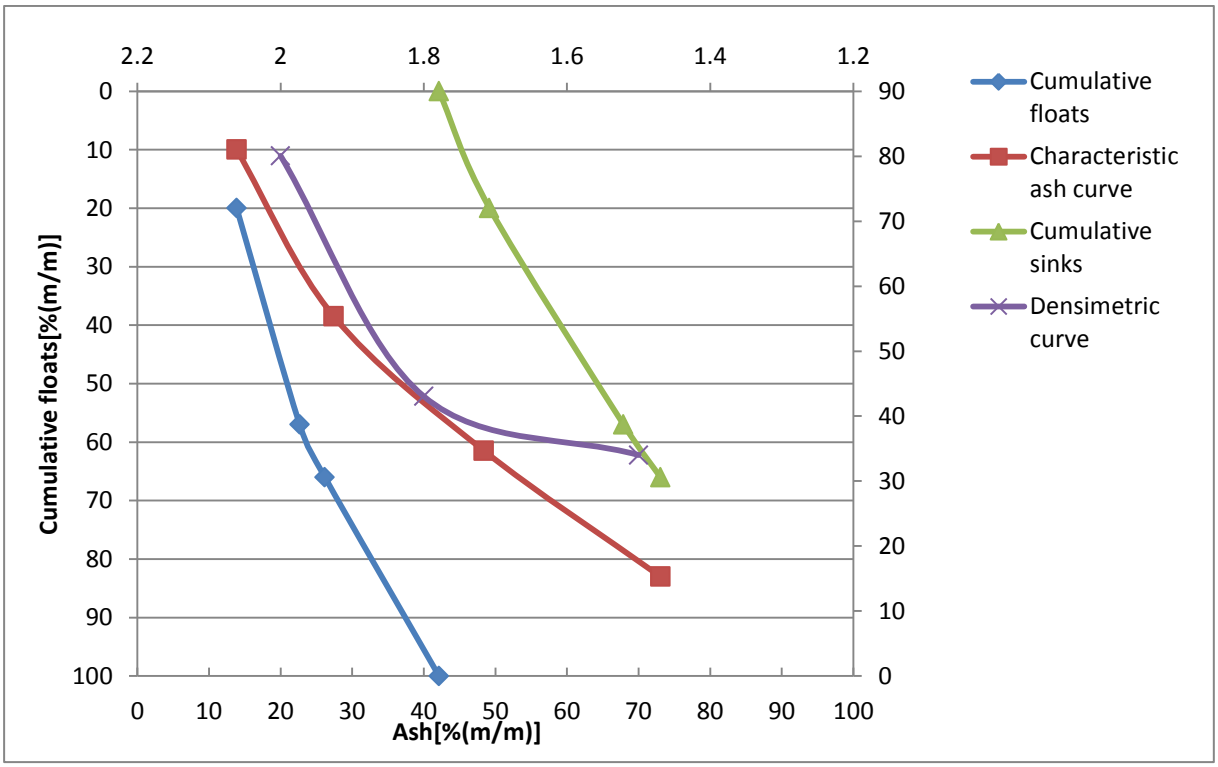

Figure D 1.. Washability curves generated from original float and sink data for the -12+0.5mm size range.

Table D 2: Float and sink data for the -25+12mm size range.

1		2	3	4	5	6	7	8	9	10	11	12
				Ash	RD	Cumulative Floats			Cumulative Sinks			Mass
RD	Mass (g)	Mass %	Ash%	Proportion		Mass%	Ash Prop.	Ash%	Mass%	Ash Prop.	Ash%	
									100.00	4015.11	40.15	
F 1.40	1760	5.49	9.9	54.35	1.4	5.49	54.35	9.90	94.51	3960.76	41.91	2.74
F 1.50	2660	8.30	15.9	131.92	1.5	13.79	186.27	13.51	86.21	3828.84	44.41	9.64
F 1.60	5500	17.16	23.6	404.87	1.6	30.94	591.14	19.10	69.06	3423.97	49.58	22.36
F 1.70	7400	23.08	28.1	648.60	1.7	54.02	1239.73	22.95	45.98	2775.38	60.37	42.48
F 1.80	3100	9.67	35.3	341.33	1.8	63.69	1581.06	24.82	36.31	2434.05	67.04	58.86
F 1.90	1400	4.37	47.8	208.73	1.9	68.06	1789.79	26.30	31.94	2225.32	69.67	65.88
F 2.00	1020	3.18	43.2	137.44	2	71.24	1927.24	27.05	28.76	2087.87	72.60	69.65
S 2.00	9220	28.76	72.6	2087.87	2	100.00	4015.11	40.15				85.62
Total	32060	100										

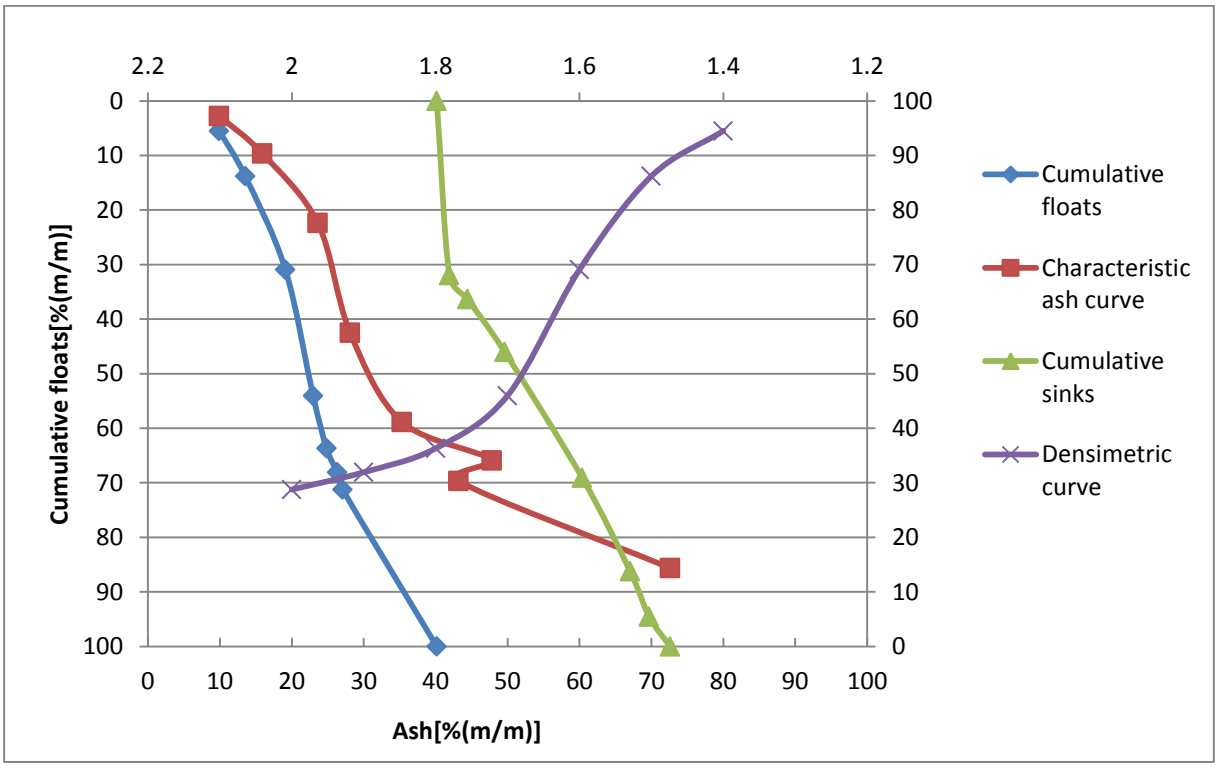

Figure D 2 Washability curves generated from original float and sink data for the -25+12mm size range.

Table D 3: Float and sink data for the -40+25mm size range.

1		2	3	4	5	6	7	8	9	10	11	12
				Ash	RD	Cumulative Floats			Cumulative Sinks			Mass
RD	Mass (g)	Mass %	Ash%	Proportion		Mass%	Ash Prop.	Ash%	Mass%	Ash Prop.	Ash%	
									100.00	4055.48	40.55	
F 1.40	3080	3.430608	10.4	35.68	1.4	3.43	35.68	10.40	96.57	4019.80	41.63	1.72
F 1.50	9860	10.9824	14.75	161.99	1.5	14.41	197.67	13.71	85.59	3857.81	45.07	8.92
F 1.60	18080	20.13812	23.2	467.20	1.6	34.55	664.87	19.24	65.45	3390.61	51.81	24.48
F 1.70	19060	21.22967	28.2	598.68	1.7	55.78	1263.55	22.65	44.22	2791.93	63.14	45.17
F 1.80	7000	7.796837	34.1	265.87	1.8	63.58	1529.42	24.06	36.42	2526.06	69.35	59.68
F 1.90	3980	4.433059	46.6	206.58	1.9	68.01	1736.00	25.53	31.99	2319.48	72.51	65.79
F 2.00	3020	3.363778	51.3	172.56	2	71.37	1908.56	26.74	28.63	2146.91	75.00	69.69
S 2.00	25700	28.62553	75	2146.91	2	100.00	4055.48	40.55				85.69
Total	89780	100										

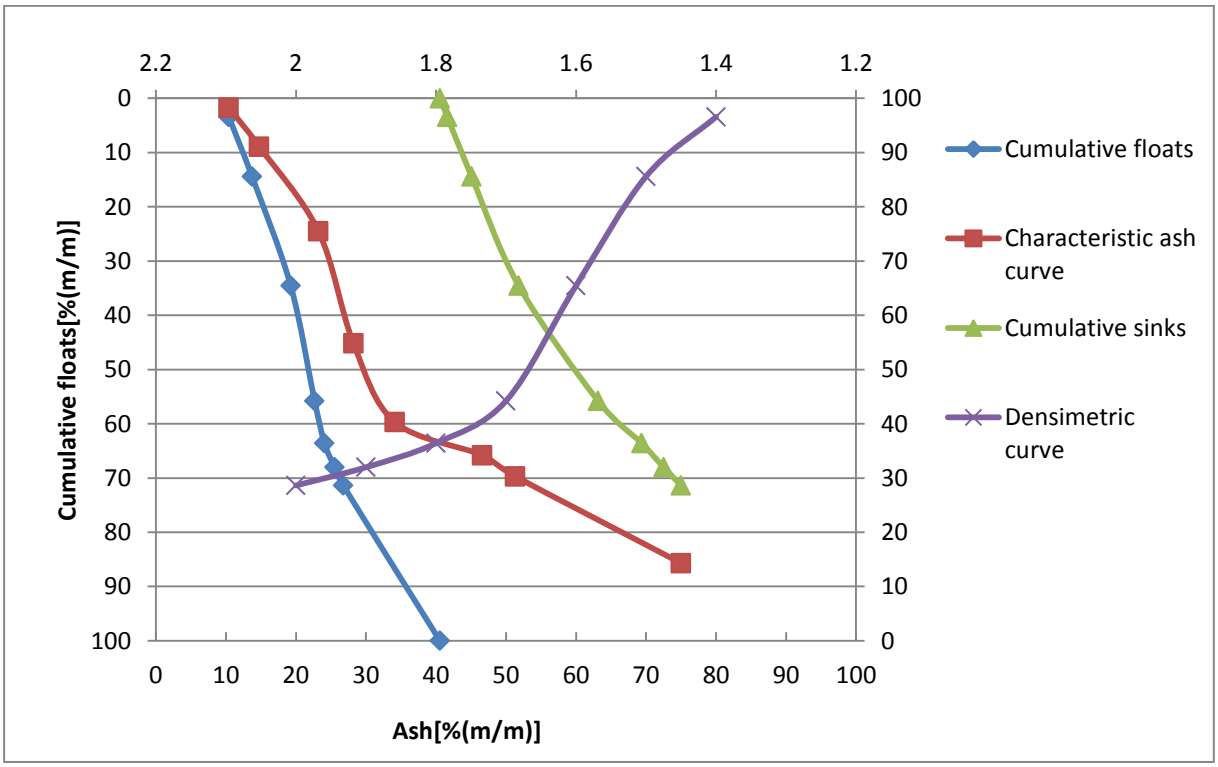

Figure D 3. Washability curves generated from original float and sink data for the -40+25mm size range.

Table D 4: Float and sink data for the -50+40mm size range.

1		2	3	4	5	6	7	8	9	10	11	12
				Ash	RD	Cumulative Floats			Cumulative Sinks			Mass
RD	Mass (g)	Mass %	Ash%	Proportion		Mass%	Ash Prop.	Ash%	Mass%	Ash Prop.	Ash%	
									100.00	3859.84	38.60	
F 1.40	3640	1.93247	12.95	25.03	1.4	1.93	25.03	12.95	98.07	3834.82	39.10	0.97
F 1.50	19080	10.12954	15.3	154.98	1.5	12.06	180.01	14.92	87.94	3679.83	41.85	7.00
F 1.60	44440	23.59312	24.1	568.59	1.6	35.66	748.60	21.00	64.34	3111.24	48.35	23.86
F 1.70	50960	27.05458	28.1	760.23	1.7	62.71	1508.84	24.06	37.29	2351.01	63.05	49.18
F 1.80	11980	6.360161	36.5	232.15	1.8	69.07	1740.98	25.21	30.93	2118.86	68.50	65.89
F 1.90	8360	4.43831	43.9	194.84	1.9	73.51	1935.82	26.33	26.49	1924.02	72.63	71.29
F 2.00	6480	3.440221	51.7	177.86	2	76.95	2113.68	27.47	23.05	1746.16	75.75	75.23
S 2.00	43420	23.0516	75.75	1746.16	2	100.00	3859.84	38.60				88.47
Total	188360	100										

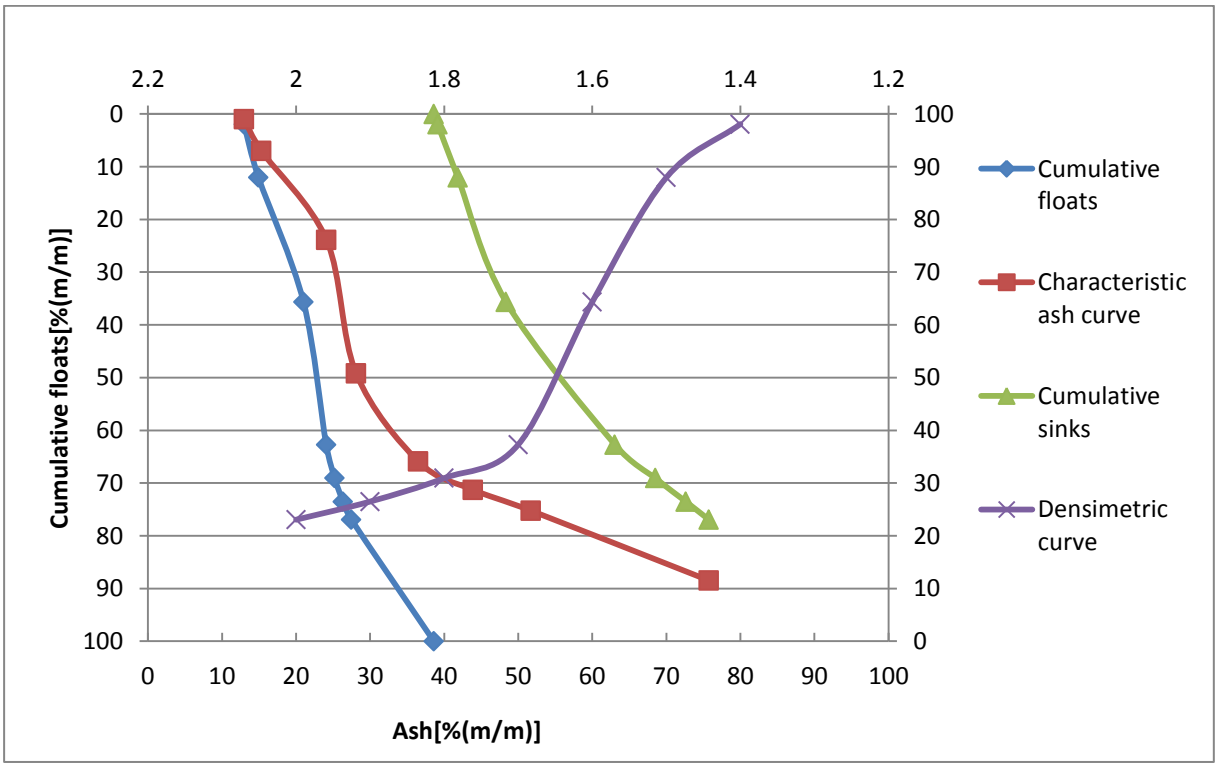

Figure D 4 Washability curves generated from original float and sink data for the -50+40mm size range.

Table D 5: Float and sink data for the -70+50mm size range.

1		2	3	4	5	6	7	8	9	10	11	12
				Ash	RD	Cumulative Floats			Cumulative Sinks			Mass
RD	Mass (g)	Mass %	Ash%	Proportion		Mass%	Ash Prop.	Ash%	Mass%	Ash Prop.	Ash%	
									100.00	3888.74	38.89	
F 1.40	17040	3.052451	14.6	44.57	1.4	3.05	44.57	14.60	96.95	3844.18	39.65	1.53
F 1.50	46260	8.286758	21.7	179.82	1.5	11.34	224.39	19.79	88.66	3664.36	41.33	7.20
F 1.60	125740	22.52436	24.9	560.86	1.6	33.86	785.25	23.19	66.14	3103.50	46.93	22.60
F 1.70	152260	27.27501	28.7	782.79	1.7	61.14	1568.04	25.65	38.86	2320.71	59.72	47.50
F 1.80	31000	5.553167	32.3	179.37	1.8	66.69	1747.41	26.20	33.31	2141.34	64.29	63.92
F 1.90	20360	3.647177	46.2	168.50	1.9	70.34	1915.90	27.24	29.66	1972.84	66.51	68.52
F 2.00	20400	3.654342	48.1	175.77	2	73.99	2091.68	28.27	26.01	1797.07	69.10	72.17
S 2.00	145180	26.00674	69.1	1797.07	2	100.00	3888.74	38.89				87.00

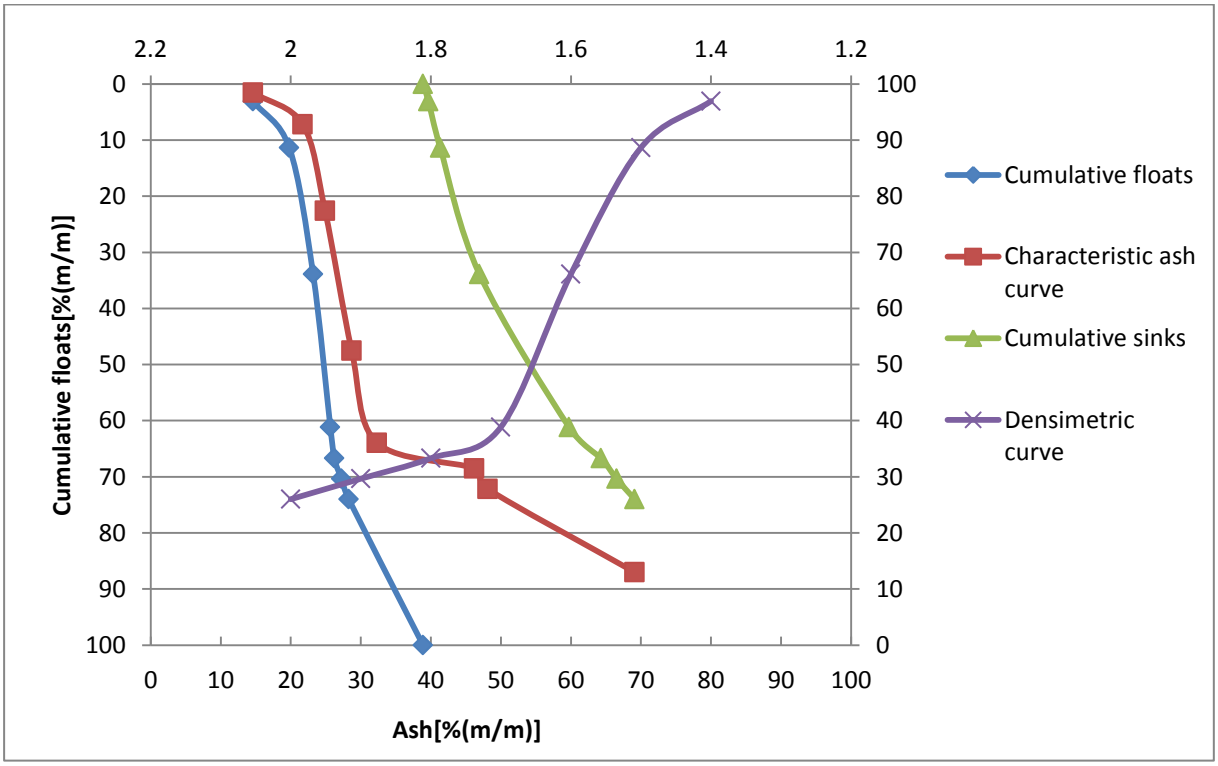

Figure D 5 Washability curves generated from original float and sink data for the -70+50mm size range.

Table D 6: Float and sink data for the -100+70mm size range.

1		2	3	4	5	6	7	8	9	10	11	12
				Ash	RD	Cumulative Floats			Cumulative Sinks			Mass
RD	Mass (g)	Mass %	Ash%	Proportion		Mass%	Ash Prop.	Ash%	Mass%	Ash Prop.	Ash%	
									100.00	3728.89	37.29	
F 1.40	15800	2.296645	15.8	36.29	1.4	2.30	36.29	15.80	97.70	3692.60	37.79	1.15
F 1.50	57000	8.285365	20.5	169.85	1.5	10.58	206.14	19.48	89.42	3522.75	39.40	6.44
F 1.60	182520	26.53061	25	663.27	1.6	37.11	869.40	23.43	62.89	2859.49	45.47	23.85
F 1.70	169480	24.63515	28.3	697.17	1.7	61.75	1566.58	25.37	38.25	2162.31	56.53	49.43
F 1.80	50020	7.270772	28.25	205.40	1.8	69.02	1771.98	25.67	30.98	1956.92	63.16	65.38
F 1.90	35420	5.148555	42.3	217.78	1.9	74.17	1989.76	26.83	25.83	1739.13	67.32	71.59
F 2.00	30120	4.378162	44.4	194.39	2	78.55	2184.15	27.81	21.45	1544.74	72.00	76.36
S 2.00	147600	21.45474	72	1544.74	2	100.00	3728.89	37.29				89.27
Total	687960	100										

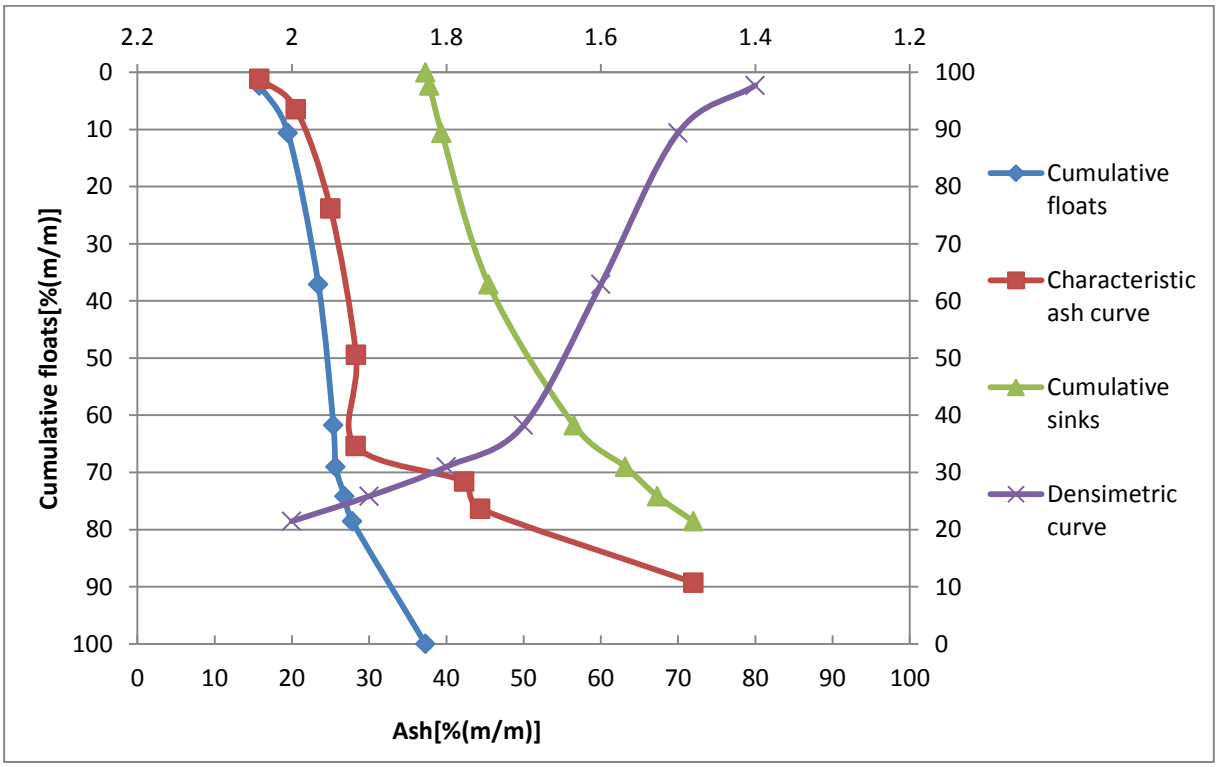

Figure D 6. Washability curves generated from original float and sink data for the -100+70mm size range.

Table D 7: Float and sink data for the -150+100mm size range.

1		2	3	4	5	6	7	8	9	10	11	12
				Ash	RD	Cumulative Floats			Cumulative Sinks			Mass
RD	Mass (g)	Mass %	Ash%	Proportion		Mass%	Ash Prop.	Ash%	Mass%	Ash Prop.	Ash%	
									100.00	3517.70	35.18	
F 1.40	780	0.261956	19.55	5.12	1.4	0.26	5.12	19.55	99.74	3512.58	35.22	0.13
F 1.50	14740	4.950296	21.5	106.43	1.5	5.21	111.55	21.40	94.79	3406.15	35.93	2.74
F 1.60	107120	35.97528	21.3	766.27	1.6	41.19	877.83	21.31	58.81	2639.87	44.89	23.20
F 1.70	74580	25.04702	28.9	723.86	1.7	66.23	1601.68	24.18	33.77	1916.01	56.74	53.71
F 1.80	11340	3.808436	34.85	132.72	1.8	70.04	1734.41	24.76	29.96	1783.29	59.53	68.14
F 1.90	15880	5.333154	39.2	209.06	1.9	75.38	1943.47	25.78	24.62	1574.23	63.93	72.71
F 2.00	2760	0.926921	54.5	50.52	2	76.30	1993.99	26.13	23.70	1523.71	64.30	75.84
S 2.00	70560	23.69694	64.3	1523.71	2	100.00	3517.70	35.18				88.15
Total	297760	100										

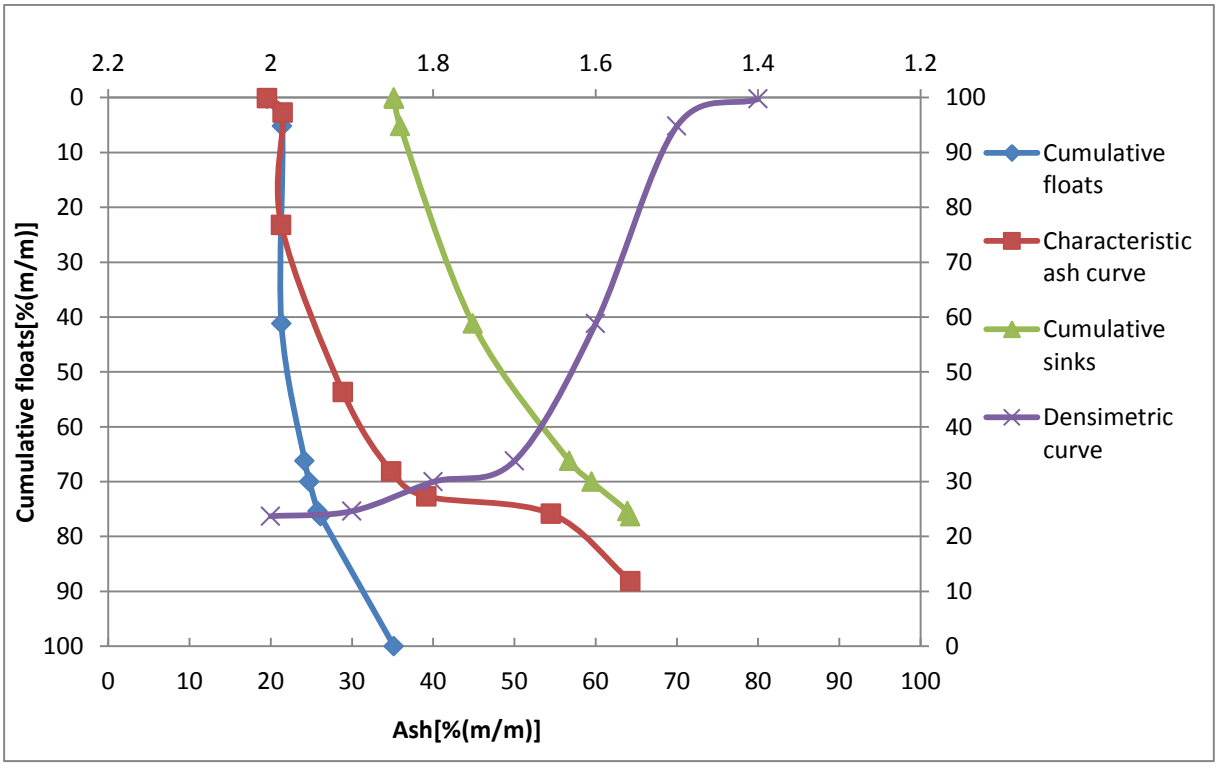

Figure D 7 Washability curves generated from original float and sink data for the -150+100mm size range.

Table D 8: Float and sink data for the +150mm size range.

1		2	3	4	5	6	7	8	9	10	11	12
				Ash	RD	Cumulative Floats			Cumulative Sinks			Mass
RD	Mass (g)	Mass %	Ash%	Proportion		Mass%	Ash Prop.	Ash%	Mass%	Ash Prop.	Ash%	
									100.00	2877.88	28.78	
F 1.50	5900	2.206762	20.2	44.58	1.5	2.21	44.58	20.20	97.79	2833.31	28.97	1.10
F 1.60	47900	17.91592	21.6	386.98	1.6	20.12	431.56	21.45	79.88	2446.32	30.63	11.16
F 1.70	54120	20.24237	25.9	524.28	1.7	40.37	955.84	23.68	59.63	1922.05	32.23	30.24
F 1.80	24220	9.058947	35.3	319.78	1.8	49.42	1275.62	25.81	50.58	1602.27	31.68	44.89
F 1.90	25620	9.582585	37.4	358.39	1.9	59.01	1634.01	27.69	40.99	1243.88	30.34	54.22
F 2.00	5580	2.087074	44.2	92.25	2	61.09	1726.26	28.26	38.91	1151.63	29.60	60.05
S 2.00	104020	38.90634	29.6	1151.63	2	100.00	2877.88	28.78				80.55
Total	267360	100										

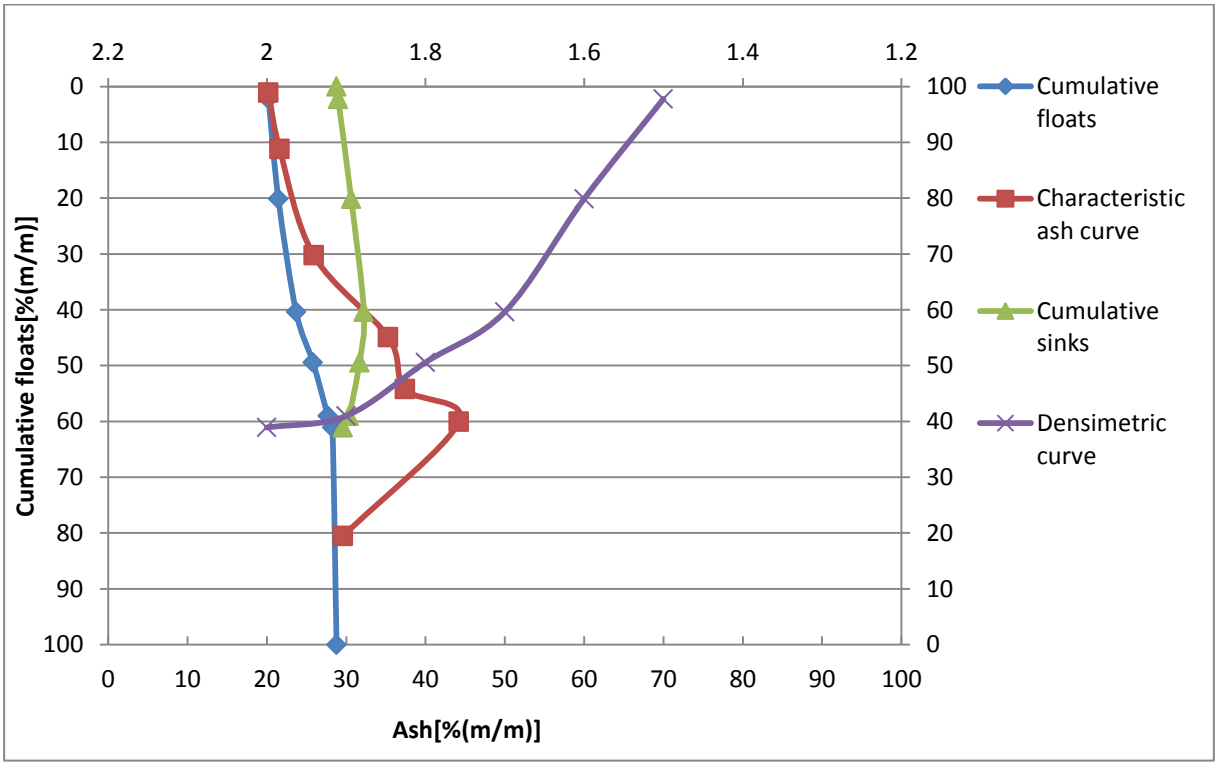

Figure D 8. .Washability curves generated from original float and sink data for the +150mm size range.

APPENDIX E

Box plot determination of outliers

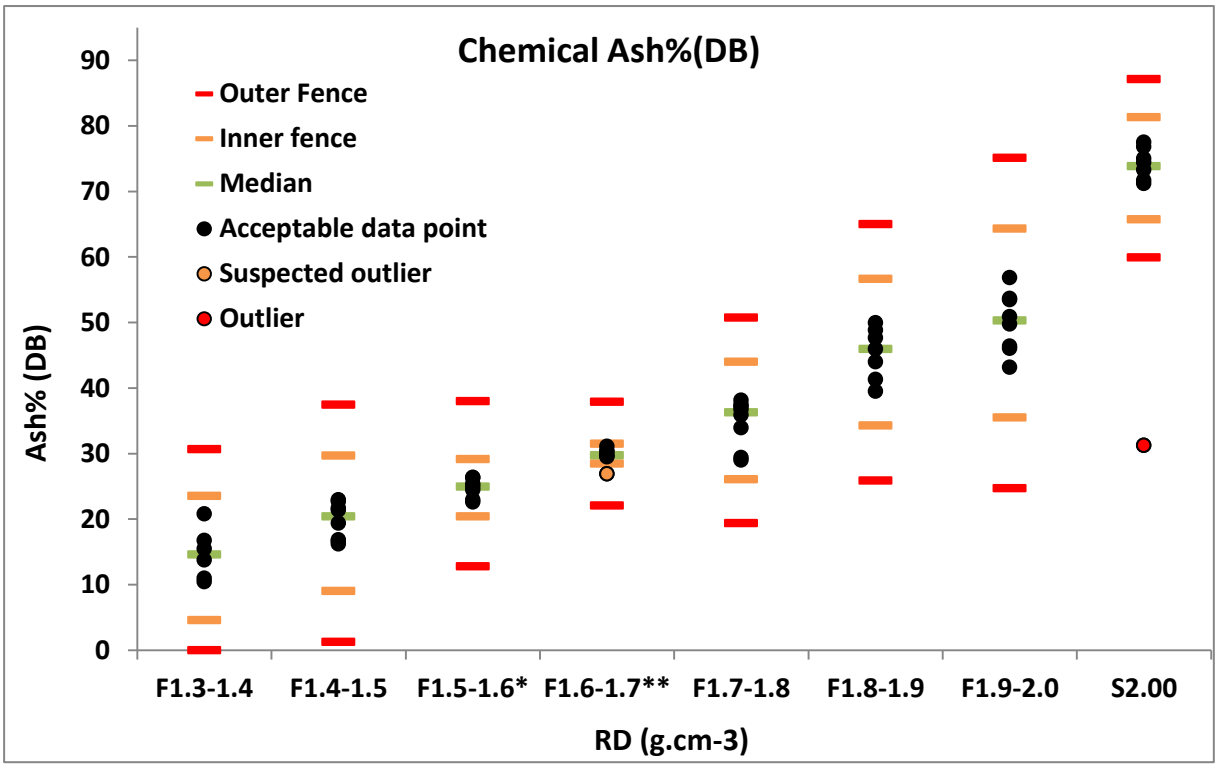

Figure E 1: Box plot outlier determination for the chemically determined ash values.

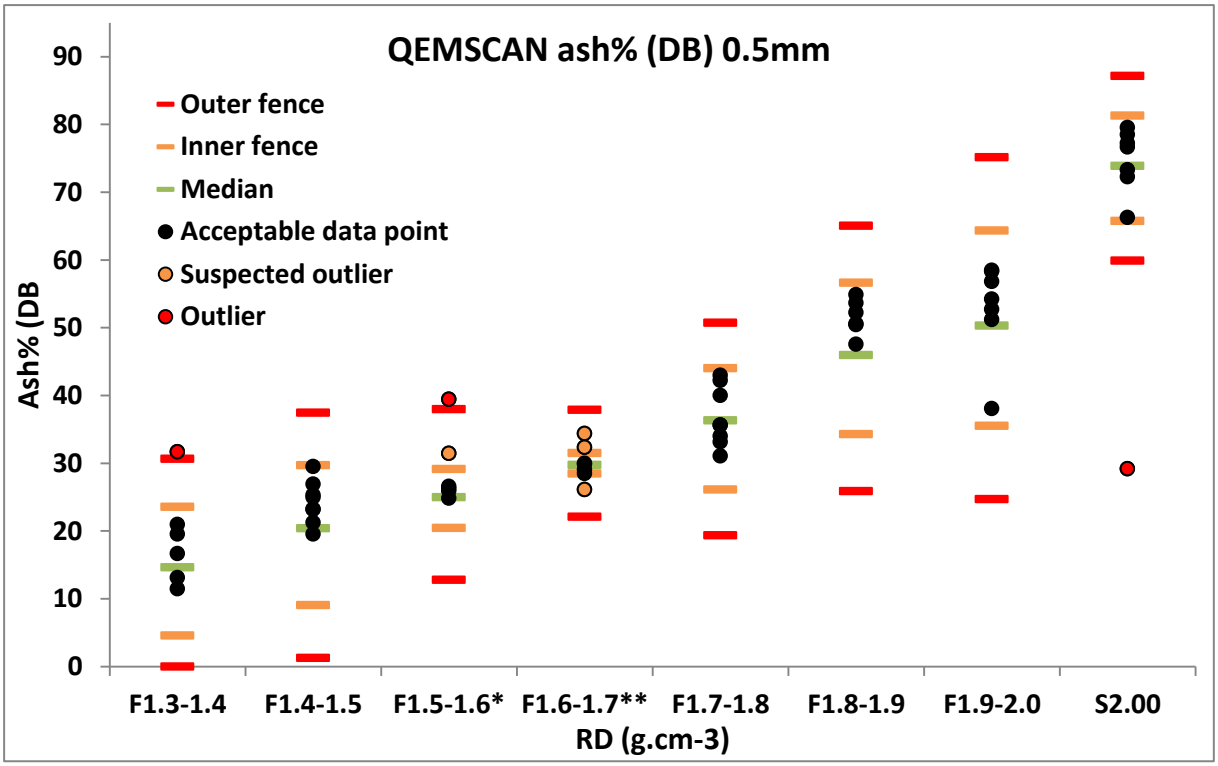

Figure E 2: Box plot outlier determination for the 0.5mm QEMSCAN determined ash values.

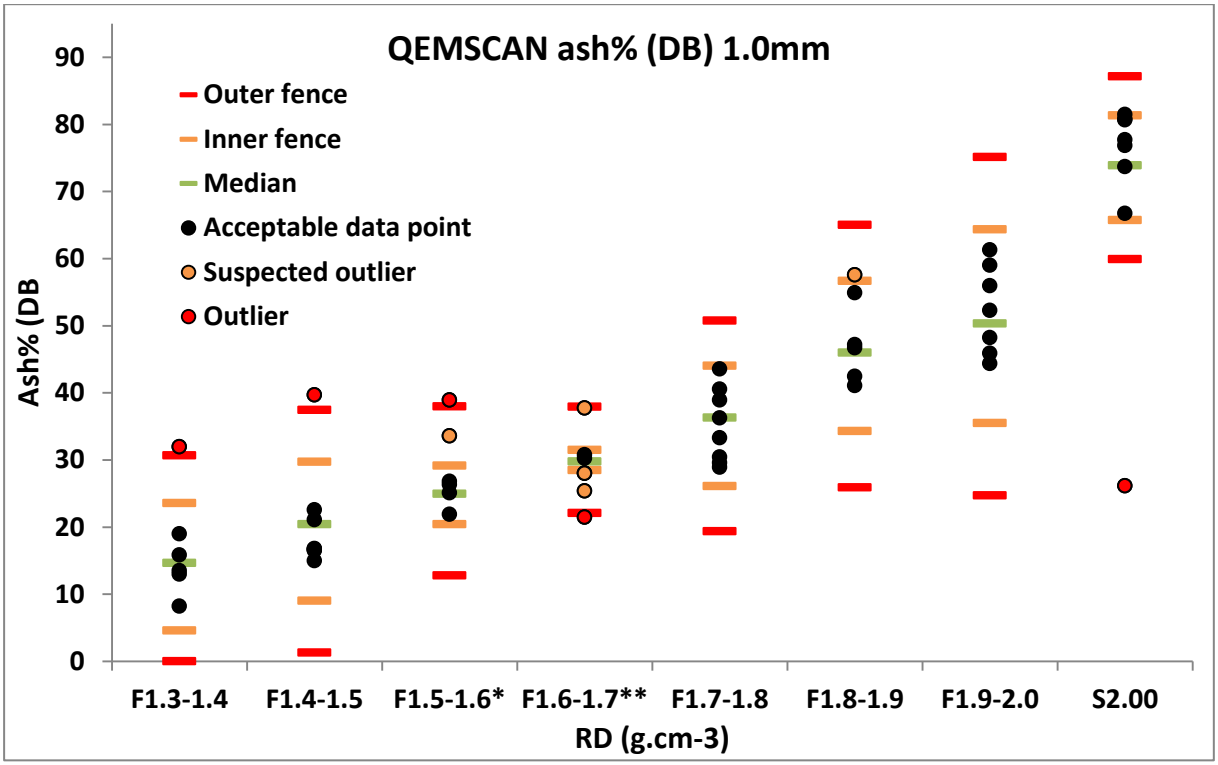

Figure E 3: Box plot outlier determination for the 1.0mm QEMSCAN determined ash values.

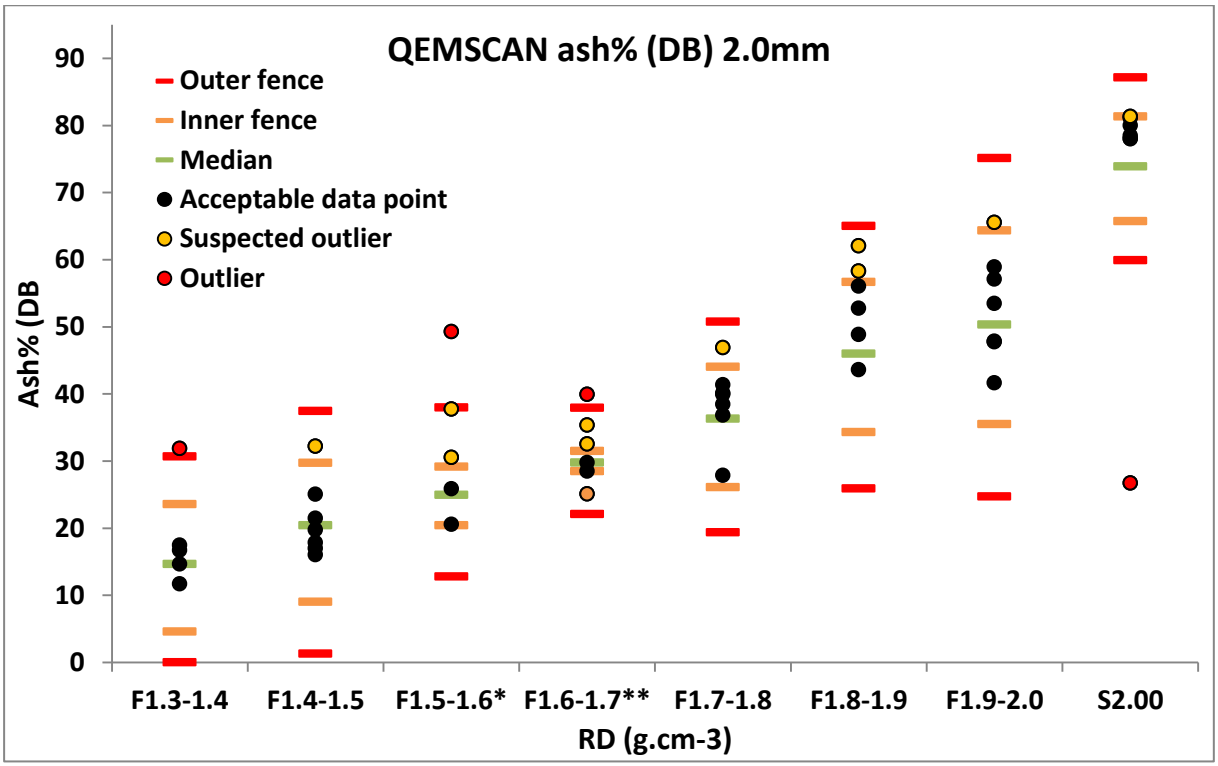

Figure E 4: Box plot outlier determination for the 2.0mm QEMSCAN determined ash values.